Design and preparations of multifunctional nanomaterials for biomedical applications

Matteo Andrea Lucherelli

UNIVERSITÉ DE STRASBOURG

***ÉCOLE DOCTORALE* DES SCIENCES CHIMIQUES**

UPR3572

THÈSE présentée par :

Matteo Andrea LUCHERELLI

Soutenue le : **26 Novembre 2019**

Pour obtenir le grade de : **Docteur de l'université de Strasbourg**

Discipline/ Spécialité : Chimie biologique et thérapeutique

Conception et préparation de nanomatériaux multifonctionnels pour des applications biomédicales

THÈSE dirigée par :

M. BIANCO Alberto	**Directeur de recherche**, CNRS

RAPPORTEURS :

M. MARTIN Nazario	Professeur, Universidad Complutense de Madrid, Spain
M. PRATO Maurizio	Professeur, Università degli studi di Trieste, Italy

AUTRES MEMBRES DU JURY :

SAMORÌ Paolo	Professeur, Université de Strasbourg, France

ACKNOWLEDGMENT

Three years of my life are hard to be summarized here in few pages. I really would like to write some words for everyone I met and with whom I spent part of my time, but probably this would require another thesis, so I will try to do my best to thank everyone, here or directly in real life. The period I have spent in Strasbourg is not only about work, is also, and I would say mostly, about new experience, friendship, emotions and discovery. Is part of my life and will surely affect the rest of it, probably in better.

At first, I want to thank my supervisor, Alberto Bianco. Without him I would have never been to Strasbourg. I want to thank him to have believe in me for this project, to have given me the opportunity to be member of his team, and more, to have always believed and take in account my suggestion and proposition about the research project, living to me the opportunity to propose new ideas. I want to also thank him for the opportunity he gave me of travelling around the world to develop the project and my knowledges. Grazie mille per aver creduto in me e in quello che ho fatto.

To don't go so far from his office, I want to thank Cécilia, for all friendly helps and suggestions she gave me, but also for the passion for science she's always sharing with us. Merci beaucoup.

I would like to thank the unit research director Hélène Dumortier and the past unit research director, prof. Sylviane Muller.

I'm grateful to Prof. Maurizio Prato, Prof. Nazario Martin and Prof. Paolo Samorì, for accepting to be member of my defense commission and reading the manuscript.

A special thank goes to Gonzalo Abellan (muchas gracias) and the Hirsch research group in Erlangen-Nuremberg University, to host and teach me many things about Germany and graphene. And to the people I met there in Erlangen and with whom I shared many experiences.

Another thank is for Eijiro Miyako, to host me in his laboratory in Tsukuba, Japan, and to Yue, who has been an unexpected awesome colleague.

I want to thank also all the researcher and teams with which I collaborate during these years, the team of Prof. Paolo Samorì (UNISTRA), the team of Prof. Kostas Kostarelos (University of Manchester), the Dr. Annette von Dem Bussche and Prof Gao Huajian (Brown University).

I also would like to acknowledge Dr. Jésus Raya for the MAS NMR, and all the people have formed and helped me for the use of instruments and performing new analysis.

A special thanks it's for Cathy of the plateforme de imagerie de l'université de Strasbourg, for the great time spent together at the TEM and for her unbeatable optimism.

I want to thank all the member of the research group, one by one. Grazie a Giacomo per avermi ospitato a casa sua nella prima crisi da appartamento tipica di Strasburgo, ma anche per avermi sempre aiutato come amico e come collega (e per le imitazioni di Nadia). Gracias a Cristina, por todas las conversaciones que hemos tenido en el despacio, por haber compartido su vida aqui y su futuros sueños conmigo. Je veux remercier Rym et Chloe, pour bavarder tous les jours ensemble, pour partager de très bon moment et rire toujours ensemble. Thanks to Dingkun and Shi, for the Chinese meal they cooked for us and for teach me the history of China. Thank to Hazel for all the agricas lunch together. I want to thank all the new members of the group, Lukas, Kim, Tenf Fei, Shiyuan, Baojin, Zheng Mei. I also want to thank the former members of the group, with whom I shared my time at the beginning of this experience, Dinesh, Rajendra, Diane, Amalia, Queyen, e un grazie speciale va ad Isabella, per avermi accolto fin da subito come un amico oltre che come un college, per

le gite in canoa, le cene insieme a Giacomo e Fengjuan e tutti gli aperitivi fatti insieme. Avec eux, je veux remercier aussi Sophia et Janina, nous avons commencé ensemble le doctorat, et plus o moins ensemble nous allons terminer, avec le stresse de la thèse e tous les autres choses. And with them I want to thank all the members of the research unit UPR3572. Thank you all for all the laught and the happy moments spended together.

Un enorme grazie va a tutte le persone che ho conosciuto o ritrovato a Strasburgo, sin dai primissimi giorni fino agli ultimi (che ancora non so se mai arriveranno), Agnese, Agostino, Alessandro, Alessia L, Alessia V, Alice, Antonella, Barbara, Camilla, Cecilia, Cosimo, Edoardo, Elenia, Elisabetta, Fabrizio, Federica, Federico, Flavio, Gianni, Giulia, Livia, Lorenzo, Lucrezia, Lukas (ormai sei italiano), Marco C, Marco R, Matilde, Matteo, Riccardo, Rosanna, Serena, Valentina. Vorrei davvero scrivere qualcosa per ognuno di voi, ma non credo che potremmo arrivare mai alla fine di questi ringraziamenti, siete tutti una grande famiglia per me, in questi anni abbiamo condiviso bellissimi momenti, siete stati il supporto nei momenti difficili, gli amici con i quali bere, fare due chiacchiere, scalare ed arrampicare montagne, cucinare e semplicemente guardare un film. Senza di voi sarebbe stata una città diversa, un dottorato diverso, ma sicuramente una vita meno piena di gioie, risate ed emozioni.

Y tambien, siempre nos hemos encontrado en Estrasburgo, quiero agradecer Paula por el entusiasmo que lleva en todas las cosas y la felicidad que esta capaz de donar a la gente. Y tambien a Anna y Nuria, por el año que se han pasado aqui y todas las postales recibida.

Toujour à Strasbourg, je veux faire merci à tous mes colocs, Alice, Coline, Adrien pour rigoler ensemble et tous le diner fait ensemble !

I want to thank all the people I met in Tsukuba, who transformed my stay in that city in something beautiful, and introduced me to Japanese culture: Christina, Toni, Vishal, Stina, Petra, Ralph, Takahiro, Luca, Valeria, Pablo.

Cambiamo adesso città e stato, e andiamo finalmente a casa, Prato.

Prima di tutto voglio ringraziare la mia famiglia, mia Mamma che mi saluta sempre con dolcezza e con gli occhi lucidi ogni volta che riparto, mio Babbo, che continua ad aver paura ogni volta che vado ad arrampicare e non riesce a farsi una ragione del perché non preferisco nuotare ed evitare di rischiare di farmi male, e Bianca, mia sorella, il nostro rapporto è cresciuto durante gli anni, forse mi sei solo riconoscente di averti lasciato camera, ma sono felice di tutte le chiacchiere, le foto, le volte che sei venuta a trovarmi. Ci sono anche i nonni, Franco e Renza, per la loro gentilezza e semplicità, per avermi chiesto più e più volte cosa facessi in Francia, per avermi spronato a cercare le parole più semplici ed efficaci per spiegare in cosa consistesse questo lavoro di tesi, e nell'accettare la lontananza del nipote preferito (Bianca fattene una ragione) perché voleva seguire i suoi sogni.

Ci siete poi voi, tutti gli amici che ancora vivono a Prato (o almeno, lì ci siamo conosciuti). Ci vediamo ogni morto di Papa è vero, ma ogni volta cerchiamo di ritagliarci del tempo insieme. Voglio ringraziare Francesca per tutto il supporto da lontano, le storie sulle molecole, i racconti della sua vita. Voglio ringraziare Claudia per gli abbracci, per le ore passate a chiacchierare, per le chiamate e i messaggi vocali. Costanza, perché anche se ci sentiamo poco cerchiamo di aggiornare un anno intero in poche parole, e in parte funziona. Pedro, Marco, Tommi, il Tempe per tutte le cene fatte insieme e quelle che faremo. Amedeo, proprio perché è Amedeo, per le foto i video e tutto quanto. Niccolò, per le risate che mi fa sempre fare. Roberto, per la sua oggettività e analisi del mondo, ma anche per preoccuparsi sempre, per essere arrivato fino a Strasburgo,

per cercare sempre di rendere il mondo un posto migliore, per aver beccato il primo palese errore della tesi. Anita, per l'entusiasmo che la contraddistingue.

E l'ultimo dei ringraziamenti va ad un posto, un concetto e un gruppo di amici, tutto raccolto in un gioco di parole, AL^3. Grazie a Sasso Masso Bessi, perché gli mancavo così tanto che a Strasburgo ci si è direttamente trasferito. Grazie a Pippo, perché nel tempo e con la distanza le amicizie si trasformano ma non si perdono, e bastano pochi gesti per capirsi sempre. Grazie a Ciccio, perché riesce sempre a fare qualcosa di nuovo per stupirci tutti quanti. Grazie a Emilio, per le chiacchiere che riusciamo ogni tanto a fare, per essere comparso gradualmente nella mia vita e per il fatto che probabilmente non se ne andrà mai. Grazie a Barto, perché malgrado i problemi di comunicazione, resta uno dei miei migliori amici. Grazie a Sara, perché mi ricorda sempre che non c'è bisogno di essere troppo preoccupati e che le cose andranno bene.

Forse cosa strana, ringrazio la mia città. Perché seppur piccola, seppur a volte particolare, Prato è, e resterà sempre, la città dove tutto è iniziato, dove ho passato la maggior parte della mia attuale vita, e che mi ha insegnato tanto. Come diceva il buon Curzio Malaparte, "io sono di Prato, m'accontento d'esser di Prato, e se non fossi nato pratese vorrei non esser venuto al mondo […]".

ABSTRACT

Doctoral thesis

By Matteo Andrea Lucherelli

Graphene and boron nitride are members of the 2D materials family, widely investigated during the last fifteen years for their interesting chemicophysical properties. These materials are characterized by hydrophobic surface, able to adsorb by π-π stacking or hydrophobic interactions organic molecules. This ability can be exploited for the targeted delivery of hydrophobic drugs or genetic materials into cells. With this aim, very important is the assessment of the biocompatibility of these materials, understanding their interactions with biological environment, their toxicity and impact with live organisms. Moreover, key point is the functionalization of graphene, for the introduction of different functionalities able to improve the drug carrier properties, and for the development of effective therapies. The purpose of this thesis work was the production of graphene and boron nitride in water, and the development of a graphene-based drug delivery platform, for the evaluation of the biological impact and the nanomedicine applications of these materials.

We therefore investigated the exfoliation of graphene and boron nitride in water, employing biocompatible surfactants for the stabilization of the sheets. Graphene was exfoliated using Riboflavin-5'-phosphate sodium salt, to obtain water dispersion with long stability and high concentration, useful for the *in vitro* and *in vivo* investigation of the toxicity of this material. The first results obtained have showed a low toxicity of graphene in HeLa cells and in mice, making graphene a promising material for biomedical applications. Moreover, I also investigated the exfoliation of this material using other family of organic molecules, discovering interesting fluorescence properties of the obtained complexes. Similarly, boron nitride was produced employing sodium cholate as surfactant. The applications of size selection techniques based on ultra-centrifugation permit to obtain dispersions with different lateral size, to explore the effect of the sheet size on cell viability.

Regarding the covalent functionalization of graphene, various reactions were explored for the modification of the surface. 1,3-Dipolar cycloaddition reaction and diazonium compound functionalization were tested. Few-layer graphene (FLG) and graphene intercalated compounds (GICs, KC_8) were employed and compared in terms of functionalization degree and quality of the obtained material, showing the high reactivity of GICs respect to FLG. We obtained multifunctional graphene (mfG) reacting KC_8 with three different diazonium compounds. The material produced presented three amino groups quasi-orthogonally protected. We selected amines as functional groups for their easy functionalization and the variety of protecting groups that allow a controlled subsequent functionalization of the material. From the obtained mfG I developed a multifunctionalities platform, constituted of a targeting agent for cancer cells, a fluorophore for the tracking of the material and a drug (doxorubicin, Dox), covalently bound by a cleavable imine bond, for the selective release in cancer cells. Finally, I investigated the anti-cancer properties of the developed platform on HeLa cells. mfG-Dox showed high cancer cell killing activity and great cell targeting properties. The same platform not functionalized with the drug showed low cytotoxicity for HeLa cells, and preliminary *in vivo* test with the starting mfG without functional groups showed no toxic effects in mice. The obtained results are promising for the application of graphene-based materials in nanomedicine.

INDEX

ACRONYMS AND ABBREVIATION

a.u.	Arbitrary units
AFM	Atomic force microscopy
ATR-IT	Attenuated total reflection IR
BAL	Bronchoalveolar lavage
Boc	Di-*tert*-butyloxycarbonil group
Cbz	Benzyloxycarbonyl group
DCM	Dichloromethane
DIPEA	N, N-Diisopropylethylamine
Dox	Doxorubicin
DS	Diazonium salt compound
EDC	N-(3-Dimethylaminopropyl)-N'-ethylcarbodiimide hydrochloride
EtOH	Ethanol
FA	Folic acid
f-G	Functionalized graphene
FLG	few-layer graphene
FT-IR	Fourier transform IR
GC	Gas chromatography
GIC	Graphene intercalated compound
GO	Graphene oxide
hBN	Hexagonal boron nitride
HR-TEM	High-resolution TEM
ICG	Indocyanine green
I_D/I_G	D/G Raman band intensity ratio
IR	Infrared spectroscopy
i.v.	Intravenous injection

m/z	Mass to charge ratio
MAS-NMR	Magic angle spinning NMR
MeOH	Methanol
mf-G/mfG	multifunctional graphene
MS	Mass spectroscopy
NHS	N-Hydroxysuccinimide
NMP	N-Methyl-2-pyrrolidone
NMR	Nuclear magnetic resonance
PEG	Polyethylene glycol
Pht	Phthalimide group
R6G	Rhodamine 6G
Rb	Rhodamine b
Rbb	Rhodamine b base
Rib	Riboflavin-5'-phosphate sodium salt
SC	Sodium cholate
SEM	Scanning electron microscopy
TEA	Triethylamine
TEM	Transmission electron microscopy
TGA	Thermogravimetric analysis
THF	Tetrahydrofuran
UV-Vis	Ultraviolet-visible spectroscopy
w/w	Weight/weight ratio
XPS	X-ray photoelectron spectroscopy

RESUME DE THESE

Chapitre 1: Introduction

Le graphène a été isolé pour la première fois en 2004[1] par Geim et Novoselov, lauréats du prix Nobel en 2010 pour cette découverte. Le graphène est considéré comme l'une des formes allotropiques du carbone, constitué d'atomes de carbone hybridés sp^2. Le caractère aromatique des feuillets de graphène avec les atomes de carbone disposés dans une structure plate en nid d'abeilles confère à ce matériau des propriétés physiques et chimiques uniques.[2] Le graphène peut être constitué d'un nombre croissant de couches (graphène mono-feuillet ou multifeuillet). Il a été rapidement suivi de la découverte de dizaines d'autres matériaux bidimensionnels (2D)[3] tels que le nitrure de bore (BN), le disulfure de molybdène (MoS_2), le germanène, etc., caractérisés par des propriétés différentes du graphène, mais partageant tous la morphologie typique en deux dimensions. La découverte du graphène est considérée comme un pas de géant dans le développement d'un domaine de recherche émergeant. Une des caractéristiques les plus prometteuses du graphène est liée à sa haute conductivité électrique qui peut être exploitée en électronique, optoélectronique, pour le stockage d'énergie, le développement de capteurs, de membranes d'eau et de gaz,[4] etc. De plus, les applications de ce matériau ne sont pas limitées à l'exploitation de ses propriétés physiques. Grâce à la caractéristique unique de pénétrer la membrane cellulaire, ses effets biologiques ont été également étudiés, afin d'étendre l'utilisation de ce matériau en nanomédicine et bio-imagerie, notamment pour la vectorisation de médicaments. Sa haute surface spécifique, ainsi que sa capacité à adsorber à sa surface des médicaments et du matériel génétique *via* des interactions π-π ou hydrophobes, font du graphène une plateforme appropriée pour l'élaboration de nouveaux vecteurs thérapeutiques.[5] Les efforts dans cette direction sont corroborés par des études sur la biocompatibilité du graphène qui ont montré sa biodégradation par des enzymes naturelles.[6] L'un des premiers problèmes rencontrés par les scientifiques était lié à l'optimisation de la méthode de production du graphène et d'autres matériaux 2D. L'exfoliation mécanique[7] ou le dépôt chimique en phase vapeur (CVD) peuvent fournir des monocouches extrêmement pures de graphène, mais la quantité de matériaux produits par ces techniques est loin d'être une production à grande échelle. L'exfoliation en phase liquide à l'aide d'un bain de sonication[8] ou par broyage par jet humide à haute pression (high-pressure wet-jet-milling)[9] permettent d'augmenter la quantité de graphène obtenue, généralement sous forme de quelques couches. Mais ses caractéristiques sont légèrement différentes d'une monocouche, notamment en ce qui concerne la conductivité du matériau, sa transparence à la lumière et sa réactivité.[10] Un autre problème est lié aux solvants organiques utilisés pour produire le graphène exfolié. La toxicité de ces solvants n'est pas compatible avec une production à grande échelle et pour des applications biologiques. Le dernier aspect à considérer concernant la chimie du graphène est lié à la fonctionnalisation chimique de sa surface. De nombreuses réactions ont été développées pour le graphène constitué d'une couche ou de plusieurs couches, impliquant différentes familles de molécules organiques.[11] Le contrôle du degré de fonctionnalisation et la caractérisation du graphène sont essentiels afin de contrôler la modification des caractéristiques de ce matériau pour les applications souhaitées. Ces défis sont encore ouverts, et une caractérisation complète du graphène modifié chimiquement nécessite encore de grands efforts en termes de temps et d'utilisation de techniques analytiques appropriées.

Le but de ma thèse est centré sur les applications biomédicales du graphène et des matériaux 2D. J'ai particulièrement concentré mon attention sur le graphène et le nitrure de bore. Je me suis focalisé sur la préparation de ces matériaux dans l'eau et sur les applications possibles comme systèmes de vectorisation de médicaments. La première partie de mon travail était centrée sur la production de graphène et de BN dans l'eau. L'exfoliation de ces matériaux a été étudiée en utilisant des techniques différentes, en présence d'agents tensioactifs organiques pour améliorer la dispersabilité et la stabilisation colloïdale dans différents

solvants. La deuxième partie du travail était orientée à la multifonctionnalisation du graphène pour obtenir un nouveau vecteur de médicaments, liant à la surface des fonctionnalités différentes pour améliorer les effets thérapeutiques de médicaments anti-cancéreux.

Chapitre 2 : Préparation et exfoliation de matériaux 2D

Préparation et exfoliation du nitrure de bore

Le nitrure de bore hexagonal (hBN) est un matériau 2D à structure cristalline hexagonale constituée d'atomes de bore et d'azote, de structure semblable au graphène. Contrairement au graphène, le hBN est un matériau isolant, incapable de conduire l'électricité. Sa surface est hydrophobe, exactement comme le graphène. L'exfoliation de hBN dans l'eau nécessite l'utilisation de surfactants, capables de s'intercaler entre les feuillets, de les séparer et les stabiliser en solution. Le cholate de sodium (SC) a été rapporté comme un bon surfactant pour une grande variété de matériaux 2D,[12] y compris pour le hBN. Le but de mon travail a été d'étudier l'impact de hBN sur les cellules, afin de comprendre si ce matériau peut avoir de potentielles applications biomédicales. La morphologie des particules, en termes d'épaisseur, de taille latérale et de forme, ainsi que la quantité et le type d'agent exfoliant, pourraient avoir des effets cruciaux sur les cellules, conduisant à des réponses biologiques différentes. À cette fin, j'ai concentré mon attention sur la production de hBN présentant des caractéristiques différentes. La préparation de hBN a été réalisée à partir de deux matériaux de départ différents, le premier commercialisé par Alfa Aesar (~20 µm) et le second de taille inférieure, ~1 µm, commercialisé par Sigma Aldrich. Les matériaux exfoliés obtenus à partir de ces deux sources présentent des différences de taille latérale et de forme des feuillets, et ont été nommés "cornered" hBN (c-hBN, obtenu à partir de la poudre Alfa Aesar) et "round" hBN (r-hBN, à partir de la poudre de Sigma Adrich). Pour obtenir le c-hBN, le matériau de départ a été broyé avec une machine planétaire afin de diminuer la taille des particules. Ensuite, la même poudre a été broyée à nouveau en présence de SC pour favoriser l'intercalation du surfactant entre les feuillets. Le mélange a finalement été soniqué dans de l'eau pour obtenir une suspension blanche stable.

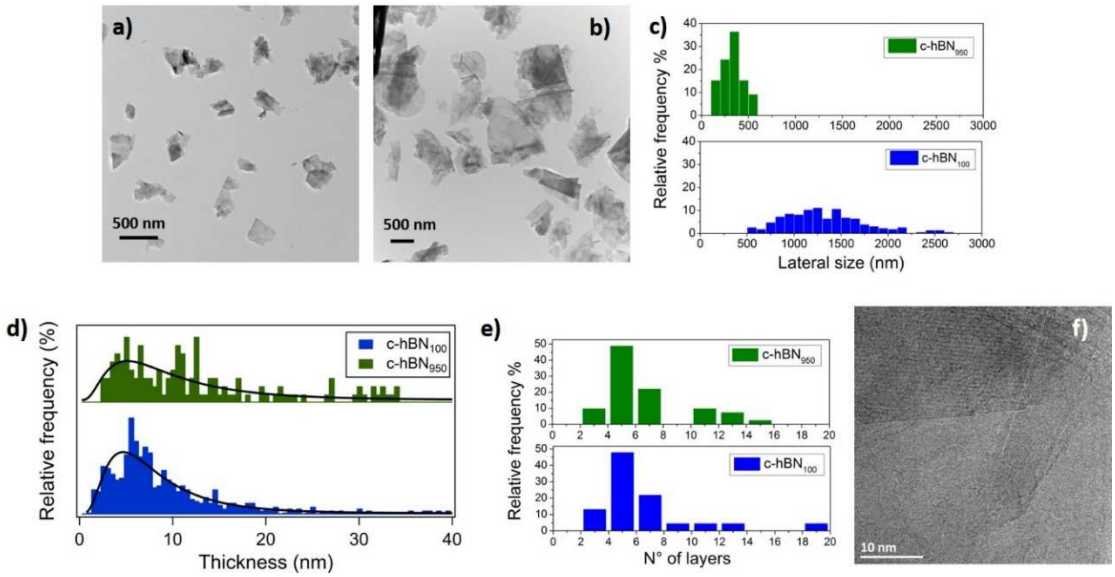

Figure 1: a, b) Images TEM respectivement de c-hBN950 et c-hBN100. c) Distribution de la taille latérale de c-hBN950 et c-hBN100 ; d) Distribution de l'épaisseur des feuillets obtenus par AFM; e) Distribution du nombre de couches de c-hBN950 et de c-hBN100 à partir des images HR-TEM. f) Image HR-TEM du c-hBN950.

Une méthode de sélection de la taille basée sur la centrifugation allant d'une vitesse élevée (~1700 g/min) à une vitesse plus basse (~100 g/min) a été appliquée à la solution afin d'isoler les dispersions de hBN de

différentes tailles latérales. Le hBN obtenu à la suite de cette procédure (c-hBN) montre des angles vifs. La dimension latérale des particules a été évaluée par une analyse statistique d'images obtenues par microscopie électronique à transmission (TEM). Les dispersions c-hBN$_{950}$ et c-hBN$_{100}$ (c-hBNx, où x correspond à la vitesse de centrifugation en g/min) ont été choisies pour les études biologiques en raison de la différence significative de distribution en taille latérale, respectivement de 342 nm et 1321 nm en moyenne (Figures 1a, b et c). L'épaisseur des feuillets a été étudiée par une analyse statistique d'une série de mesures par microscopie à force atomique (AFM) (Figure 1d). Les deux échantillons présentent une distribution moyenne similaire, de 4,69 ± 0.05 nm et de 4,72 ± 0,18 nm respectivement pour le c-hBN$_{950}$ et le c-hBN$_{100}$. Les images TEM à haute résolution (HR-TEM) ont permis de mesurer le nombre de couches (Figure 1e et f). Les deux dispersions contiennent du c-hBN composé de ~6 feuillets. L'étude de l'internalisation et de la cytotoxicité de ces deux différentes dispersions de hBN pourrait avoir un fort intérêt pour comprendre le rôle de la taille latérale sur la viabilité des cellules.

D'autre part, la production de suspensions stables de r-hBN nécessitent seulement une sonication à l'aide d'un bain à ultrasons dans une solution aqueuse de SC. La sonication suivie d'une centrifugation à différentes vitesses a été appliquée aux suspensions de r-hBN, donnant des dispersions de taille latérale similaire. Des différences significatives en termes de taille latérale, de forme et d'épaisseur des feuillets ont été observées pour le r-hBN (Figure 2). Les feuillets sont plus petits que ceux du c-hBN, avec une taille latérale moyenne de ~156 nm et une épaisseur comprise entre 20 et 35 nm. Les mesures HR-TEM et AFM ont permis de déterminer la morphologie des particules de r-hBN. Les particules ne sont pas constituées de feuillets comme on le supposait au départ, mais leur épaisseur décroît près du bord, avec des angles ronds. Les mesures de diffraction électronique ont confirmé une cristallinité hexagonale parfaite des particules, comme dans le cas du c-hBN. Ces observations nous amènent à conclure que la forme de ce matériau correspond à une structure ovoïdale comprimée au centre, à bords cristallins plats et hexagonaux.

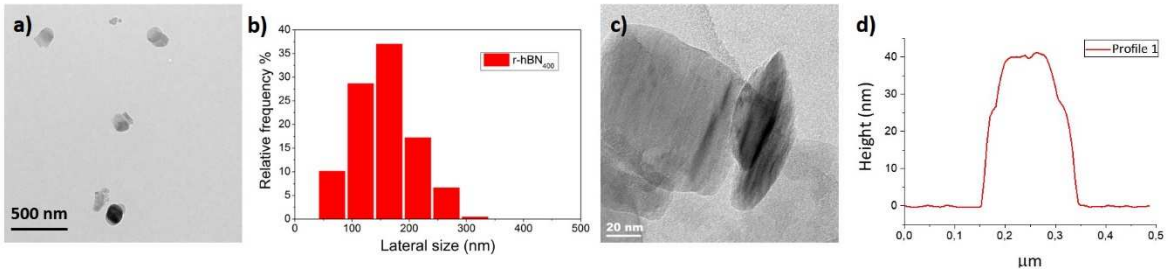

Figure 2: **a)** Image TEM des particules de r-hBN; **b)** Histogramme de la distribution de taille latérale; **c)** Face latérale d'une particule observée par HR-TEM; **d)** Profil de la hauteur AFM de r-hBN.

Des expériences de cytotoxicité sur le c-hBN et le r-hBN ont été menées en collaboration avec le Dr. Annette Von Dem Bussche (Brown University, États-Unis). Les résultats préliminaires sur hBN$_{950}$ ont été réalisés sur des macrophages murins et des cellules H460 (cellules du cancer du poumon), montrant très peu d'effet sur la viabilité cellulaire. À la concentration de 20 ppm après 24 h d'incubation, la viabilité des deux lignées cellulaires est supérieure à 80%.

Préparation du graphène exfolié

Parallèlement à la production de hBN, j'ai étudié la préparation de graphène dans de l'eau pour étudier sa biocompatibilité. Pour les mêmes raisons que hBN, le graphène nécessite la présence de molécules organiques capables de s'intercaler entre les feuillets et de stabiliser les matériaux en solution aqueuse,[13] et j'ai concentré mon attention sur l'utilisation de tensioactifs biocompatibles. La riboflavine 5-phosphate (Rib) s'est révélée être un bon agent exfoliant pour le graphène.[14] La Rib a été utilisée pour produire une dispersion

stable de graphène dans de l'eau (G-Rib), présentant une stabilité élevée (jusqu'à une concentration d'environ 2 mg/ml) et une taille latérale moyenne d'environ 860 nm. Cette dispersion a été exploitée pour étudier la cytotoxicité in vitro sur les cellules HeLa et les macrophages RAW, et la toxicité in vivo du graphène après administration intraveineuse dans un modèle murin. La dispersion de G-Rib a montré une très faible cytotoxicité sur les cellules et aucune toxicité générale chez les animaux. En outre, une technique de sélection de la taille des feuillets basée sur différentes étapes d'ultra-centrifugation a été appliquée sur le matériau G-Rib, afin d'obtenir des dispersions de différentes tailles latérales. Deux dispersions d'une taille latérale moyenne d'environ 351 nm et 1032 nm, ont été testées pour explorer la toxicité du graphène sur des souris après aspiration pharyngée, en collaboration avec les professeurs K. Kostarelos et Cyrill Bussy, à Manchester. Les expériences sont toujours en cours.

La structure chimique de la riboflavine présente des cycles aromatiques capables d'interagir avec le graphène par interaction π-π, et une chaîne hydrophile capable de stabiliser les feuillets dans l'eau. Compte tenu de ces caractéristiques, j'ai étudié l'utilisation de molécules organiques ayant une structure chimique similaire à la riboflavine en tant qu'agents tensioactifs du graphène. J'ai concentré mon attention en particulier sur la famille des rhodamines, en utilisant la rhodamine 6G, la rhodamine b et rhodamine b base, et sur des dérivés de BODIPY (synthétisés par Dr. B. Richichi à l'université de Florence), dans le but d'exploiter leur forte fluorescence pour la traçabilité du graphène dans les cellules. La poudre de graphite a été dispersée dans des solutions des molécules susmentionnées, soumise à un traitement par ultrasons et centrifugée pour isoler les feuillets les plus petits et les plus stables. La rhodamine b base et GIG100 ont donné une dispersion de graphène stable à une concentration allant jusqu'à 1 mg/mL (G-Rbb et G-GIG100 respectivement) (Figure 3).

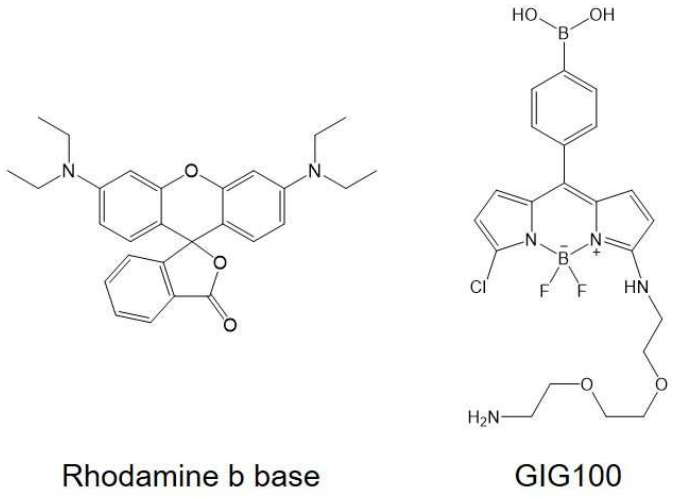

Figure 3: Structure de la rhodamine b base et du dérivé de BODIPY GIG100

Les deux dispersions obtenues sont restées stables pendant plus d'une semaine, sans formation d'agrégat visible, à une concentration de 1 mg/mL. Une analyse TEM a été réalisée pour évaluer la taille latérale moyenne (environ 460 nm pour le G-Rbb et environ 840 nm pour le G-GIG100). La quantité de rhodamine adsorbée a été calculée par analyse XPS et élémentaire (environ 10% w/w) et la qualité des feuillets a été analysée par spectroscopie Raman. Au-delà du bon résultat concernant la possibilité d'exfolier le graphène avec la base de rhodamine b et le GIG100, l'observation la plus surprenante concerne la fluorescence des matériaux. L'une des caractéristiques bien connues du graphène est sa participation aux phénomènes de transfert d'électrons (ET).[15–17] Le graphène peut jouer le rôle de donneur ou d'accepteur d'électrons dans des réactions chimiques ou avec des molécules, provoquant une extinction de la fluorescence de molécules organiques en contact avec sa surface. Nous avons découvert que la fluorescence des deux molécules n'était

pas complètement éteinte après adsorption sur la surface du graphène. La fluorescence des complexes G-Rbb et G-GIG100 a été analysée par fluorimétrie et par microscopie confocale (Figure 4).

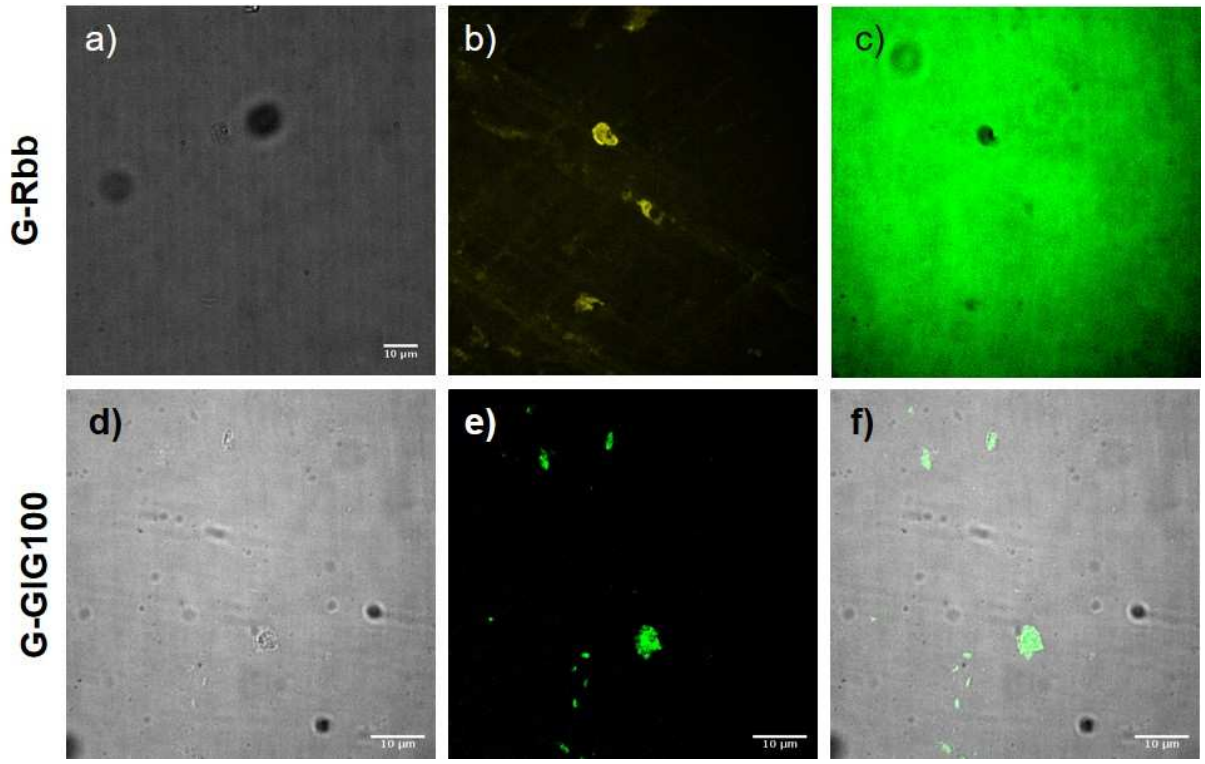

Figure 4: Première ligne : images confocales de G-Rbb dans une solution aqueuse contenant de la fluorescéine (0,01 mg/mL), la fluorescéine a été ajoutée à une dispersion de G-Rbb dans de l'eau, traitée aux ultrasons pendant 5 min et la dispersion a été observée au microscope confocal. Deuxième ligne : images confocales de G-GIG100: a, d) Image en transmission; b) Canal jaune, ext = 561 nm, em = 600-660 nm; les particules jaunes correspondent à des feuillets de graphène fluorescentes ; c) Canal vert, ext = 488 nm, em = 500-550 nm; la fluorescence de la fluorescéine est stoppée par G-Rbb ; e) Canal vert, fluorescence de G-GIG100, ext = 488 nm, em = 500-550 nm ; f) merge de d+ e.

Ces résultats ouvrent la porte à de nouvelles applications du graphène et nécessiteront d'autres recherches pour comprendre les propriétés de fluorescence et l'interaction entre le graphène et les fluorophores.

Chapitre 3 : Fonctionnalisation covalente du graphène

Dans le but d'obtenir du graphène multifonctionnel adapté au développement de supports d'administration de médicaments, j'ai concentré les efforts de synthèse sur la fonctionnalisation du graphène produit dans notre laboratoire par sonication dans des solvants organiques, et sur la fonctionnalisation du graphite intercalé avec du potassium métallique (KC_8).[18] La fonctionnalisation du graphène a été étudiée à travers deux réactions différentes: 1) la cycloaddition 1,3-dipolaire d'ylures d'azométhine,[19] et 2) une réaction d'arylation utilisant des sels de diazonium,[20] conduisant à la formation d'espèces radicalaires très réactives.

La première réaction implique la formation d'une espèce 1,3-dipôlaire capable de réagir avec le graphène en tant que dipolarophile pour former un cycle pyrrolidine. En raison de la basse réactivité du graphène, le degré de fonctionnalisation de cette réaction était faible, ce qui a motivé mes efforts vers l'utilisation de sels de diazonium plus réactifs. À la suite d'études antérieures effectuées dans notre laboratoire,[21] j'ai réalisé la synthèse de trois précurseurs de sels de diazonium, présentant des groupes amines protégés avec trois groupements protecteurs orthogonaux différents (Figure 5).

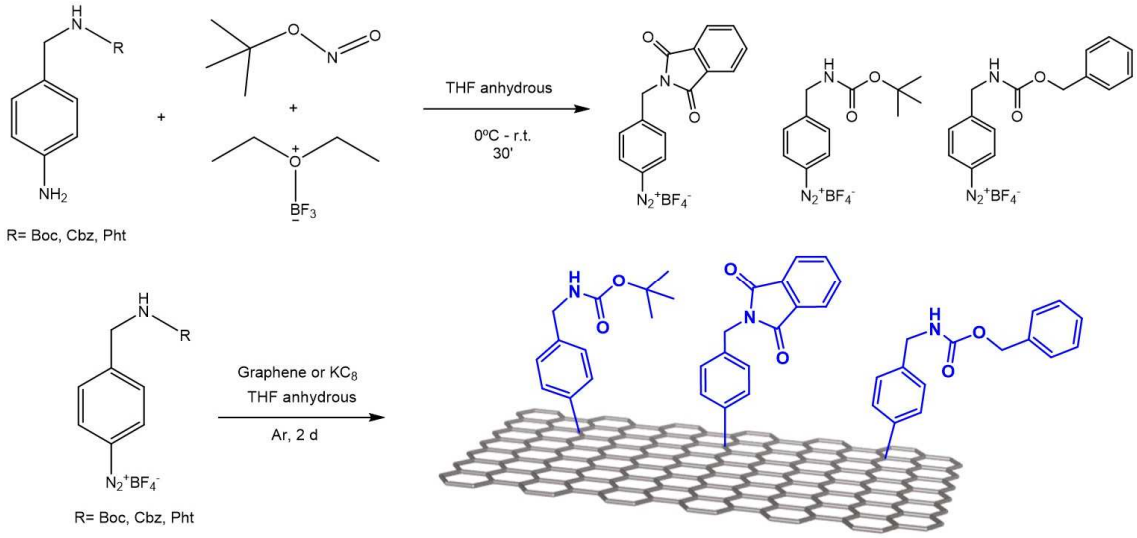

Figure 5: Haut) Synthèse des trois sel de diazonium; Bas) Fonctionnalisation du graphène pour obtenir mf-G.

Au cours d'un stage à l'Université d'Erlangen-Nuremberg, dans un laboratoire ZMP en collaboration avec le Dr. Gonzalo Abellan, j'ai d'abord étudié et comparé la réactivité et le degré de fonctionnalisation de la réaction entre le graphène et les sels de diazonium formés *in situ* (mf-G_{situ}) ou isolés (mf-G_{pre}), et entre le KC_8 et les sels de diazonium isolés, pour obtenir du graphène multifonctionnel (mf-G) (Figure 6, en bas).[22] Comme première preuve de la fonctionnalisation, l'analyse Raman a été réalisée sur le graphène. Le rapport entre l'intensité de la bande D et de la bande G (rapport I_D/I_G) permet d'obtenir des informations sur la quantité de défauts introduits sur la structure du graphène. Comme montré dans les spectres Raman (Figure 6a), la forte augmentation de la bande D du mf-G par rapport au graphène est une première preuve du degré de fonctionnalisation supérieur obtenu à partir de la fonctionnalisation de KC_8. Grâce à l'analyse thermogravimétrique (TGA), nous avons évalué la quantité de groupements organiques liés à la surface du matériau (Figure 6b). De la comparaison de la perte de poids entre les matériaux de départ et le graphène fonctionnalisé (mf-G_{situ} et mf-G_{pre} ~8%, mf-G ~15%), nous pouvons confirmer que la réaction avec le graphène intercalé conduit à un rendement de réaction plus élevé.

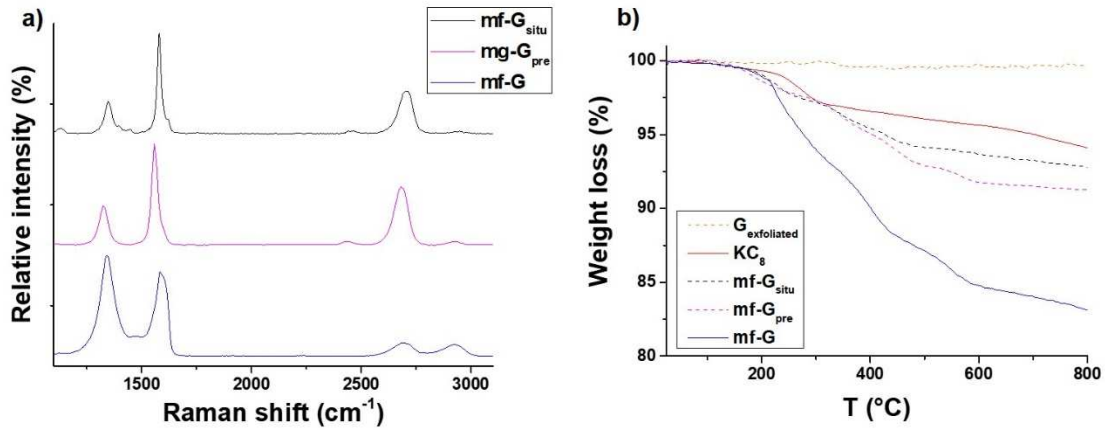

Figure 6: a) Comparaison de spectres Raman de différentes réactions; b) Comparaison de la perte de poids entre les matériaux de départ et le graphène fonctionnalisé.

Compte tenu du bon rendement et de l'homogénéité de la fonctionnalisation obtenus avec le composé de diazonium, de nouvelles réactions ont été étudiées avec différents réactifs dans le but d'obtenir du graphène bifonctionnel avec une amine et un groupement alcyne (Figure 7).

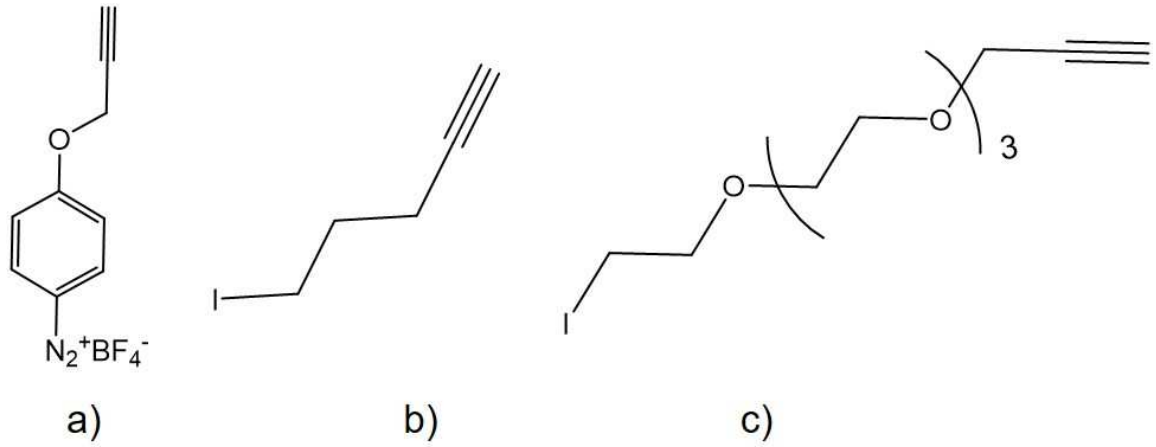

Figure 7: réactifs utilisés pour la fonctionnalisation de KC8: a) tétrafluoroborate de 4-propargyloxybenzène diazonium; b) 4-iodopentyne; c) I-PEG4-alcyne.

Nous avons finalement sélectionné mf-G comme le meilleur candidat pour le développement de notre plateforme d'administration de médicaments. La déprotection sélective des groupes amino et la séquence de réactions pour obtenir un matériau multifonctionnel ont été étudiées, conduisant à la synthèse d'un graphène multifonctionnel (Figure 8). Le vert d'indocyanine (ICG) a été greffé sur du mf-G en tant que fluorophore pour l'imagerie, afin de suivre le matériel dans les cellules. L'acide folique a été sélectionné comme agent de ciblage pour les cellules cancéreuses et lié à la surface de mf-G par un lien PEG. La doxorubicine a été greffée de manière covalente sur du graphène via une liaison imine, pour être clivée sélectivement à pH acide dans les cellules cancéreuses.

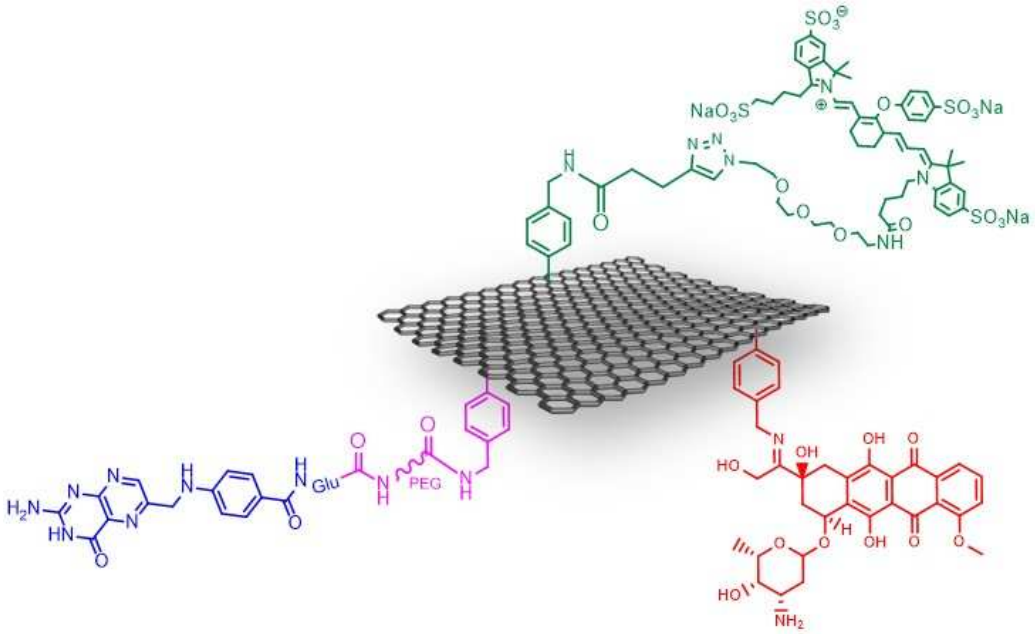

Figure 8: mf-G/PEG-FA/ICG/Dox synthétisé.

J'ai effectué des expériences biologiques au centre de recherche AIST à Tsukuba (Japon) dans le laboratoire du Dr. Eijiro Miyako (où j'ai passé trois mois en tant qu'étudiant invité). Le mf-G a montré des résultats prometteurs en termes de ciblage des cellules et de cytotoxicité pour les cellules cancéreuses (cellules HeLa) (Figure 9).

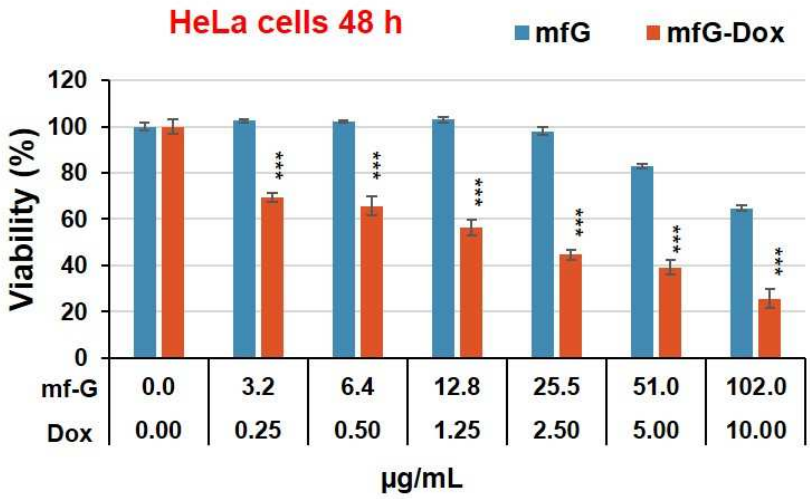

Figure 9: Viabilité des cellules HeLa après 48 h d'incubation avec mf-G/PEG-FA/ICG/Dox (mf-G-Dox) et mf-G (complexe sans Dox. Les données sont présentées sous forme de moyenne ± écart type (n = 3), $p < 0.001$ (test t de Student)

Chapitre 5 : Conclusion

Au cours de mon doctorat, j'ai étudié l'exfoliation de graphène et de nitrure de bore dans l'eau. Le nitrure de bore a été produit par sonication dans un bain d'eau avec l'aide de SC comme surfactant. Les dispersions obtenues par diminution de la vitesse de centrifugation sont caractérisées par une augmentation de la taille latérale de feuillets. Par ailleurs leurs effets biologiques ont été étudiés. La rhodamine b base a été découverte comme étant un surfactant très efficace pour le graphène dans l'eau. Le G_{Rbb} a montré des propriétés intéressantes de fluorescence due à la présence de la rhodamine, permettant le suivi du matériau dans les cellules. L'étude de la multifonctionnalisation du graphène a été réalisée, permettant d'obtenir un matériau présentant différentes fonctionnalités souhaitables pour les applications de vectorisation de médicaments. Les études *in vitro* ont été réalisées afin d'évaluer la capacité de vectorisation de médicaments par le mf-G. Mes résultats peuvent ouvrir de nouvelles perspectives pour les applications biomédicales des matériaux à base de graphène et de matériaux 2D.

Références

1. Novoselov, K. S. *et al.* Electric field in atomically thin carbon films. *Science (80-.).* **306**, 666–669 (2004).
2. Rao, C. N. R., Sood, A. K., Subrahmanyam, K. S. & Govindaraj, A. Graphene: The new two-dimensional nanomaterial. *Angew. Chemie - Int. Ed.* **48**, 7752–7777 (2009).
3. Mas-Ballesté, R., Gómez-Navarro, C., Gómez-Herrero, J. & Zamora, F. 2D materials: To graphene and beyond. *Nanoscale* **3**, 20–30 (2011).
4. Wang, R. *et al.* Graphene based functional devices: A short review. *Front. Phys.* **14**, 13603 (2019).
5. Reina, G. *et al.* Promises, facts and challenges for graphene in biomedical applications. *Chem. Soc. Rev.* **46**, 4400–4416 (2017).
6. Kurapati, R. *et al.* Degradation of Single-Layer and Few-Layer Graphene by Neutrophil Myeloperoxidase. *Angew. Chemie - Int. Ed.* **57**, 11722–11727 (2018).
7. Yi, M. & Shen, Z. A review on mechanical exfoliation for the scalable production of graphene. *J. Mater. Chem. A* **3**, 11700–11715 (2015).

8. Ciesielski, A. & Samorì, P. Graphene via sonication assisted liquid-phase exfoliation. *Chem. Soc. Rev.* **43**, 381–398 (2014).

9. Del Rio Castillo, A. E. *et al.* High-yield production of 2D crystals by wet-jet milling. *Mater. Horizons* **5**, 890–904 (2018).

10. Criado, A., Melchionna, M., Marchesan, S. & Prato, M. The Covalent Functionalization of Graphene on Substrates. *Angew. Chemie - Int. Ed.* **54**, 10734–10750 (2015).

11. Chua, C. K. & Pumera, M. Covalent chemistry on graphene. *Chem. Soc. Rev.* **42**, 3222–3233 (2013).

12. Backes, C. *et al.* Guidelines for exfoliation, characterization and processing of layered materials produced by liquid exfoliation. *Chem. Mater.* **29**, 243–255 (2017).

13. León, V. *et al.* Few-layer graphenes from ball-milling of graphite with melamine. *Chem. Commun.* **47**, 10936–10938 (2011).

14. Ayán-Varela, M. *et al.* Achieving extremely concentrated aqueous dispersions of graphene flakes and catalytically efficient graphene-metal nanoparticle hybrids with flavin mononucleotide as a high-performance stabilizer. *ACS Appl. Mater. Interfaces* **7**, 10293–10307 (2015).

15. Wu, X., Xing, Y., Zeng, K., Huber, K. & Zhao, J. X. Study of Fluorescence Quenching Ability of Graphene Oxide with a Layer of Rigid and Tunable Silica Spacer. *Langmuir* **34**, 603–611 (2018).

16. Kasry, A. *et al.* Highly efficient fluorescence quenching with graphene. *J. Phys. Chem. C* **116**, 2858–2862 (2012).

17. Ramakrishna Matte, H. S. S., Subrahmanyam, K. S., Venkata Rao, K., George, S. J. & Rao, C. N. R. Quenching of fluorescence of aromatic molecules by graphene due to electron transfer. *Chem. Phys. Lett.* **506**, 260–264 (2011).

18. Abellán, G. *et al.* Unifying Principles of the Reductive Covalent Graphene Functionalization. *J. Am. Chem. Soc.* **139**, 5175–5182 (2017).

19. Quintana, M., Vazquez, E. & Prato, M. Organic functionalization of graphene in dispersions. *Acc. Chem. Res.* **46**, 138–148 (2013).

20. Greenwood, J. *et al.* Covalent modification of graphene and graphite using diazonium chemistry: Tunable grafting and nanomanipulation. *ACS Nano* **9**, 5520–5535 (2015).

21. Ménard-Moyon, C., Fabbro, C., Prato, M. & Bianco, A. One-pot triple functionalization of carbon nanotubes. *Chem. - A Eur. J.* **17**, 3222–3227 (2011).

22. Lucherelli, M. A. *et al.* A straightforward approach to multifunctional graphene. *Chem. – A Eur. J.* chem.201903165 (2019). doi:10.1002/chem.201903165

Passion [noun]

[**pash**-*uh*n]

- *Any powerful or compelling emotion or feeling, as love or hate.*

  i.e.: Passion for science and discovery

- *Intense, driving, or overmastering feeling or conviction*

Perseverance [noun]

[pur-s*uh*-**veer**-*uh*ns]

- *The quality that allows someone to continue trying to do something even though it is difficult.*
- *Steady persistence in a course of action, a purpose, a state, etc., especially in spite of difficulties, obstacles, or discouragement.*

This thesis was realized and written with passion and love. Handle it carefully

CHAPTER 1. INTRODUCTION

1.1. Graphene

Graphene has been isolated in 2004 by Geim and Novoselov, leading the two researchers to win the Nobel prize in Physics in 2010 for their discovery.[1] The interest on this material has risen up very fast because of its unique and particular properties, such as the remarkable electrical and thermal conductivity, and the mechanical properties,[2–4] that make graphene one of the most studied materials of the last fifteen years. The applications of graphene are wide, spanning from electronic, optoelectronics, energy storage to sensors, water and gas separation.[4–7] Graphene is one of the allotropic forms of carbon, constituted by sp^2 carbon atoms arranged in a honeycomb structure with a flat shape (Figure 1.1a). The edges of the material are thin and irregulars, characterised by sharp corners (Figure 1.1b). The structure is constituted and classified by its number of layers as mono-, bi- and few-layer graphene.[8] The lateral dimensions of the sheets can vary from few nm to mm, depending on the starting graphite source and from the production techniques.[8]

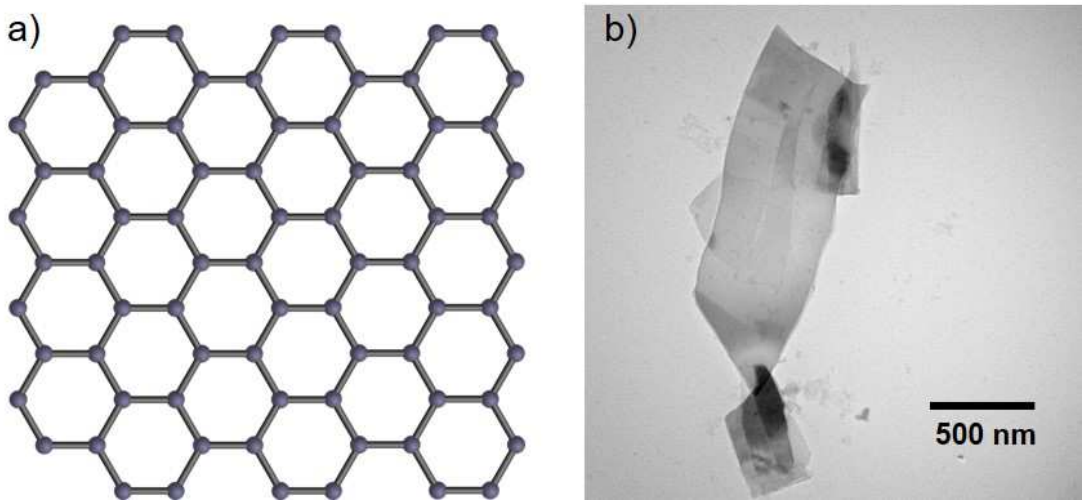

Figure 1.1: a) Graphene molecular structure; b) TEM image of graphene sheets.

The techniques employed for the production are different, from liquid phase exfoliation to chemical vapor deposition (CVD) and will be described below. The sp^2 carbon lattice makes graphene aromatic,[9] differently from fullerenes and carbon nanotubes. The surface of the materials is hydrophobic, able to interact by π-π stacking or hydrophobic interaction with organic molecules. One of the peculiar characteristics of this material is its thickness of ~0.4 nm (for a single layer),[10] that together with its specific large surface area, evaluated theoretically to be of ~2630 m^2/g,[4] make of graphene the thinnest material in the world. Thanks to its flat structure, graphene was the pioneer of a new family of materials, called 2D materials. Boron nitride (BN), molybdenum disulphide (MoS_2), phosphorene and other 2D materials have been discovered quickly after graphene; they present different chemical and physical properties but are characterized by the same flat structure.

Other graphene species have been produced during the years: i) graphene oxide (GO) characterized by a high level of oxidation of the surface, presenting hydroxyl, carboxyl, and epoxide groups.[11] ii) Reduced graphene oxide (r-GO) obtained from the reduction of GO by different chemical agents.[12] iii) Graphene nano-ribbons and nano-sheets (GNs), etc. GO is one of the most studied forms of graphene and present some different properties respect to graphene. The high amount of sp^3 carbon atoms, due to the oxidation of the surface,

makes this material an electric insulator (Figure 1.2). The presence of the oxygenated functional groups increases the water dispersibility of the material and allows a direct chemical functionalization.

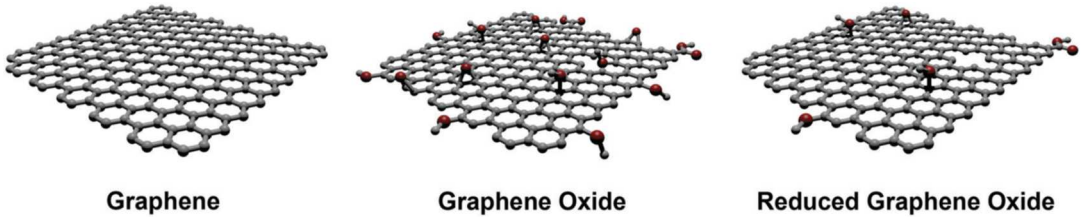

Figure 1.2: Chemical structure of graphene, GO and r-GO.[13]- Published by The Royal Society of Chemistry.

The large quantity of graphene derivatives produced during the last years has created confusion in the nomenclature and in the literature, requiring an important effort to distinguish the properties and characteristic of each material. For this reason, Bianco and co-workers, in two distinguished articles, have proposed a precise nomenclature for the graphene family description.[8,14] In their work, the researcher suggested a classification of graphene derivates based on lateral size, number of layers and C/O ratio. The classification based on the lateral size is important to distinguish between nano-graphene, graphene quantum dots, graphene nanoribbons and other forms of graphene produced during the years. The number of layers is a very important parameter to distinguish between mono-, bi- and few-layer graphene. The number of layers affects the conductivity, the mechanical properties, the reactivity and the biocompatibility of the material. Indeed, it is of crucial importance an accurate description of this characteristic for the good reproducibility of the experiments. As last, the C/O ratio defines the member of the graphene family. In base of the C/O ratio we can distinguish between graphene, graphene oxide, reduced graphene oxide. Moreover, we can distinguish between different degree of oxidation of graphene oxide, presenting different chemical surface and different reactivity. With the aim to clarify and standardize the nomenclature of these carbon nanomaterials, the authors proposed a classification grid (Figure 1.3) to help the categorization of graphene derivates, especially in the field of biological application. In this framework, a standardization on the description of the tested materials is needed, for the comparison of the toxicological aspect involving graphene and its derivates. I will discuss in paragraph 1.4 all the aspects of the biocompatibility of graphene family members.

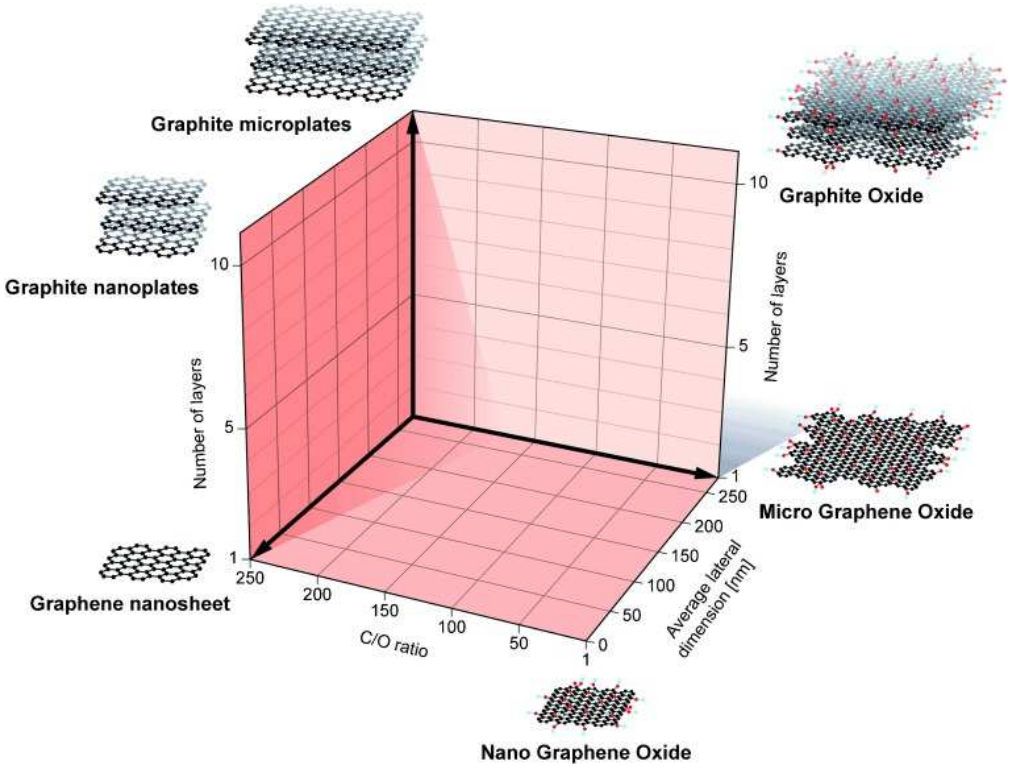

Figure 1.3: Classification grid for the categorization of different graphene types according to three fundamental graphene family properties: number of graphene layers, average lateral dimension, and atomic carbon/oxygen ratio. The different materials drawn at the six corners of the box represent the ideal cases according to the lateral dimensions and the number of layers reported in the literature. The values of the three axes are related to the GBMs at the nanoscale, but it is feasible to expand the values to the microscale.[14] Reproduced with permission of John Wiley and Sons.

1.2. Graphene and 2D materials production

The production of graphene can be divided in two main approaches, the "bottom-up" synthesis or the "top-down" production. The bottom-up approach consists in the organic synthesis of graphene or in the chemical vapour deposition (CVD). The organic synthesis has been developed by different synthetic approaches, leading mainly to the production of graphene nanoribbons (Figure 1.4a).[15] The CVD technique consists in the epitaxial growth of graphene on metallic surface (as Ni, Co, Cu, etc.) by thermal decomposition of various hydrocarbon sources (Figure 1.4b).[16] The characteristics of graphene produced by this technique can be modulated to obtain mono- or bi-layer graphene and it is possible to obtain very large sheets, with a lateral size between mm and few cm.[17] The produced material presents a high quality in terms of crystallinity and quantity of defects on the surface, and it is commonly used to study the optic and electronic properties of the graphene sheets. Despite the high purity of the sheets obtained through "bottom-up" techniques, these approaches do not permit to achieve high quantities of material, required to decrease the production cost and to allow large scale industrial production and applications of graphene. In this work, we will then focus our attention on the "top-down" production methods. The top-down synthesis, called exfoliation, consists on the production of graphene from graphite through the separation of the layers. Different methodologies have been developed during the years, starting from the scotch tape exfoliation applied by Geim and Novoselov, to liquid phase and mechanical exfoliation.[18] The exfoliation requires to overcome the energy of van der Waals interaction between the adjacent layer of graphene and separate them in a solid phase or

liquid phase. Here we will focus our attention on the liquid phase exfoliation, which is the most promising for bulk production of graphene sheets.

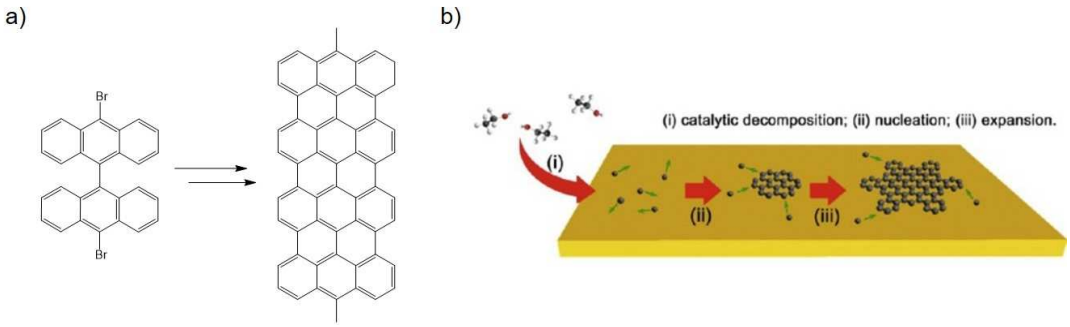

Figure 1.4: a) Bottom-up synthesis of graphene nanoribbons;[15] b) CVD graphene production, reproduced with permission from 17 – Published by Synthetic Metals.

1.2.1. **Liquid phase exfoliation (LPE)**

The liquid phase exfoliation requires the use of organic solvents able to intercalate between the sheets, separate them and stabilize the material in solution. This technique can lead to the production of high quantity of graphene and it is the most promising for industrially scalability. Commonly, graphene produced by LPE is characterised by a wide lateral size dispersion, from few nm to 2-3 µm, a number of layers < 6 and a yield of ~1 wt%. The quality of the sheets obtained from LPE depends on the sonication time applied, the strength of the sonication and the starting graphite source.[19] In general, the sheets obtained through LPE are presenting low quantity of defects (such as the presence of oxygen due to oxidation or structural defects on the surface). Longer sonication times slightly increase the yield of production, but strongly affect the morphology of the materials, increasing the defects on the surface.[20]

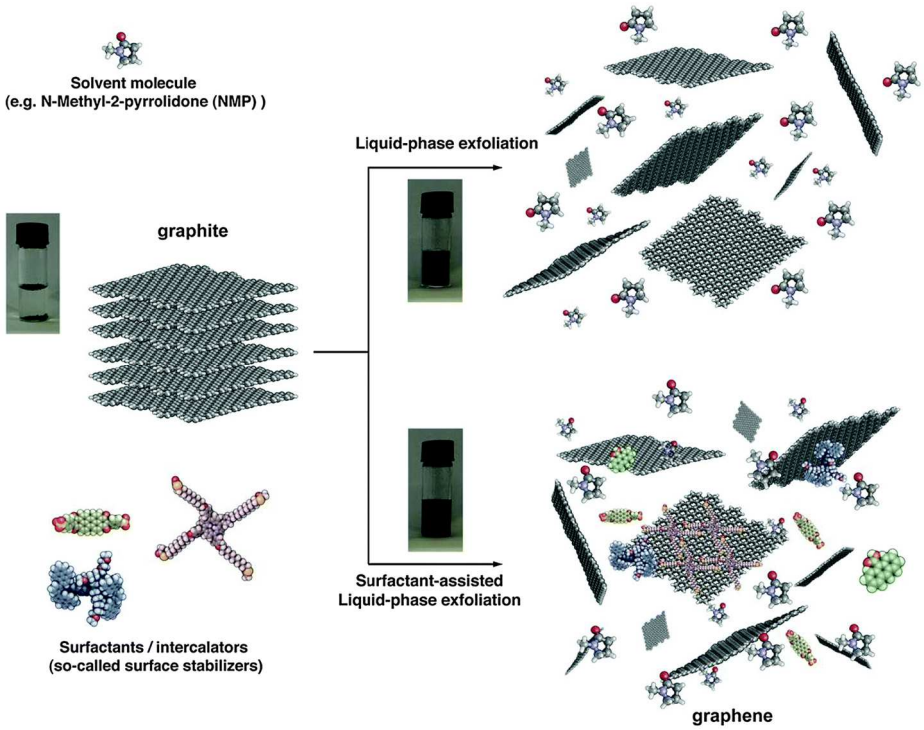

Figure 1.5: LPE production of graphene; top: production in organic solvents; bottom: production by surfactant-assisted exfoliation. Reproduced from [19] with permission from The Royal Society of Chemistry.

Key role for the exfoliation of graphene is played by the nature of the organic solvent. As hypothesized and demonstrated by Coleman and coworkers,[21] solvents with interfacial tension (γ) ~41 mJ·m^{-2} should match the energy surface of the materials (graphene or other 2D material) in order to maximize their interactions, increase the intercalation of the organic molecules between the layers and minimize the energy required for the exfoliation. The most used organic solvents are *N*-methyl 2-pyrrolidone (NMP), *N, N* dimethyl formamide (DMF), tetrahydrofuran (THF) and *ortho*-dichlorobenzene (o-DCB) (Figure 1.5). Moreover, to overcome the van der Waals interlayer interactions and achieve the separation of the sheets, the application of external energy is required. This energy is provided by ultrasonication, microwaves, electric field or shearing.[22]

Unfortunately, in the perspective of future scale-up production, these solvents are presenting different inconvenient. One of the main problems is related to their toxicity, that does not make them attractive for large scale production. Another is related to their high boiling point, making their removing, especially for the molecules adsorbed on the surface, very difficult. Moreover, the graphene produced by LPE is mostly few-layer graphene, where the quantity of mono- and bi-layers is very small. With the purpose of the production of graphene for further functionalization and applications, few-layer graphene is not desirable due to its low reactivity, as will be described in paragraph 1.3. Few-layer graphene is not a suitable material for optic and electronic applications that require monolayer graphene to exploit the desired properties of this material. One great challenge for researchers is still the obtention of high amount of 2D material stables in non-toxic solvents and suitable for different types of applications.

1.2.2. **Water exfoliation**

In view of the problems due to the toxicity of organic solvents, many groups have focused their attention on the water exfoliation of graphene and 2D materials. The use of water is required in the case of biological applications of graphene and desired to obtain a green and environmental-friendly production. The main problem of water exfoliation comes by the hydrophobic surface of these materials, that allow interaction with organic solvents but makes these incredibly hard to be dispersed in water or polar solvents, because of the non-favorable interactions (water energy surface: 72.8 mJ/m^2). The tendency of graphene dispersed in water is to re-aggregate, increasing the re-stacking of the sheets and precipitating in solution. The most common and useful solution to this problem is the use of surfactants.[22,23] Organic molecules soluble in water can interact with graphene surface, intercalating the layers and stabilizing them in solution. Even in this case, external driving forces as ultrasonication are required to win the van der Waals interactions. The first surfactant discovered for the exfoliation has been sodium dodecyl benzene sulfonate (SDBS).[23] After this discovery, many different categories of molecules have been employed for the exfoliation and stabilization of the sheets, such as aromatic and non-aromatic molecules, proteins (i.e. Bovine serum albumin, BSA), ionic liquids and polymers (Figure 1.6).[24–26] However, many of the surfactants employed until now, including SDBS, do not present good biocompatibility for further biological applications.

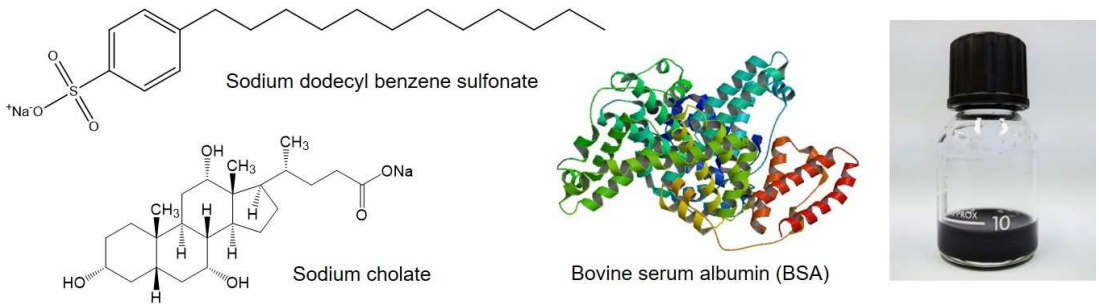

Figure 1.6: Surfactants employed for the exfoliation of graphene in water; 1 mg/mL graphene dispersion in water.

The flexibility of organic chemistry and the variety of organic molecules permit to investigate a wide range of molecules to increase the exfoliating properties. The surfactant permits the obtention of stable graphene dispersions in concentration higher than 2 mg/mL,[27] normally not allowed by simple organic solvent exfoliation (~0.5 mg/mL). The quality of the obtained sheets is not affected by the presence of the surfactant, presenting low amount of defects, average number of layers < 5 and lateral size depending from the following purification techniques applied to the dispersions. Despite these good results, even the use of surfactants present limitations, relative to the removal of the organic molecules adsorbed on the surface for further applications of the material.

On the other side, a few numbers of studies were able to demonstrate the possibility to obtain graphene in aqueous dispersion without the presence of surfactant. Vázquez and co-workers reported the ball milling exfoliation of graphite assisted by melamine, obtaining few-layer graphene in water dispersion without the presence of surfactants after washing the exfoliated material with hot water.[28] The ball milling is a technique employed for the exfoliation and the reduction of the size of particles, consisting on the grinding of the powder in a rotating jar in the presence of spheres. The energy applied to the materials can be variated by controlling the speed rotation of the machine and it is possible to work in dry or wet conditions.

Pénicaud and co-workers demonstrated the surfactant-free stabilization of single-layer graphene in water. They exploited the stabilization through a transfer of a graphenide species (KC_8) from THF to water, showing that single-layer graphene could be stabilized in degassed water without the presence of surfactants.[29] Even in this case, some limitations are affecting these techniques. The higher concentration reachable by graphene dispersion in water without surfactant is very low (maximum 0.1 mg/mL), limiting the biomedical applications due to the need of high concentrations of the dispersions and good stability in PBS or in cell culture medium.

In conclusion, on the light of the above-discussed methodologies, a general simple method to produce graphene materials suitable for all kinds of applications has not been developed yet. Graphene with different qualities and characteristics can be produced in base of the desired applications following the most appropriate technique; but it is still challenging to develop a versatile methodology to produce graphene and 2D materials.

1.3. Covalent functionalization of graphene

After its discovery, one of the most attractive challenges regarding graphene has been its covalent functionalization. The possibility of modulating the properties of the material, changing the chemical structure, implementing features has fascinated the chemists and the physicists.[30] The sp^2 carbon structure of graphene is similar to other allotropic forms of carbon, fullerenes and carbon nanotubes.[31] These two species have been widely investigated during the years, leading to the development of a large number of chemical reactions.[32–35] Reactivity of fullerenes and nanotubes have been demonstrated to be strictly correlated to the strain due to the curvature of the surface.[36] Graphene, conversely, was first theorized as inert due to its flat structure and the consequent absence of surface strain.[37] Nevertheless, many different reactions have been developed for the functionalization of graphene, demonstrating the presence of localized surface strained areas due to the flexibility of the material. Graphene can react as nucleophile or electrophile and be involved in cycloaddition reactions.[38]

The chemical reactions can occur on both surfaces and at the edges of the material. Moreover, the defects present in the structure, like holes generated during the exfoliation process, are active sites that increases

the reactivity of the materials and the functionalization degree. The reactivity of graphene is strictly related to the number of layers constituting the sheets. The increase of the number of layers is correlated to a decrease of the reactivity of the material, making monolayer and bilayer graphene more desirable materials respect to few-layer graphene for chemical functionalization.[39,40]

The methodologies of functionalization are different, from chemical reactions of stables dispersion of exfoliated graphene, intercalation with metals, functionalization on a solid support and electrochemical functionalization. It is possible to obtain material with different characteristics as lateral size, degree of functionalization and oxidation changing the technique and the reaction conditions. One of the great advantages of the reactions on graphene is related to the purification. In most of the cases, simple filtration and wash with different solvents results sufficient to obtain the material clean from reagents. In some cases, vacuum oven is employed to remove trace of solvents adsorbed onto the surface. At the same time, the heterogeneous phase of the reactions is even a disadvantage because of the difficulty of a correct approach between graphene and organic reagents in solution.

1.3.1. **Functionalization of exfoliated graphene**

The most flexible approach is the functionalization of graphene in suspensions, because of the wide types of reagents and solvents that can be employed for the reactions. Liquid phase allows the control and variation of the temperature, the use of inert atmosphere, non-anhydrous solvents and reagents, and easy steps of purification. On the other side, depending on the nature of the starting graphene dispersions, the functionalization degree could be unsatisfactory, due to the low reactivity of few-layer graphene. The reactions developed on LPE graphene dispersions are various: i) Functionalization with diazonium salt (DS) (Scheme 1.1).[21] These organic molecules are generating high reactive radical species, able to react with graphene surface. DS can be generated *in situ* or isolated and used without the presence of other reagents. DS are employed even in electrochemical reactions.[41] Thanks to the easy, scalable and flexible synthesis of DS, this approach is one of the most exploited for the functionalization of graphene and the addition of different functional group onto its surface, such as alkyne,[42] porphyrins[43] and amines.[44] ii) 1,3-Dipolar cycloaddition of azomethine ylides. This reaction has been extensively exploited for the functionalization of fullerenes and carbon nanotubes, thanks to the versatility and easy synthesis of the organic precursors.[45] The use of different aldehydes or N-functionalized glycine leads to the formation of azomethine ylides differently substituted.[46] All the above-mentioned reactions have been demonstrated taking place on the surface and on the edges of graphene. Other reactions, such as cyclopropanation, Diels-Alder cycloaddition, Friedel-craft acylation have been also developed on graphene,[38] but the low yield of functionalization obtained does not make them suitable for further applications of the material.

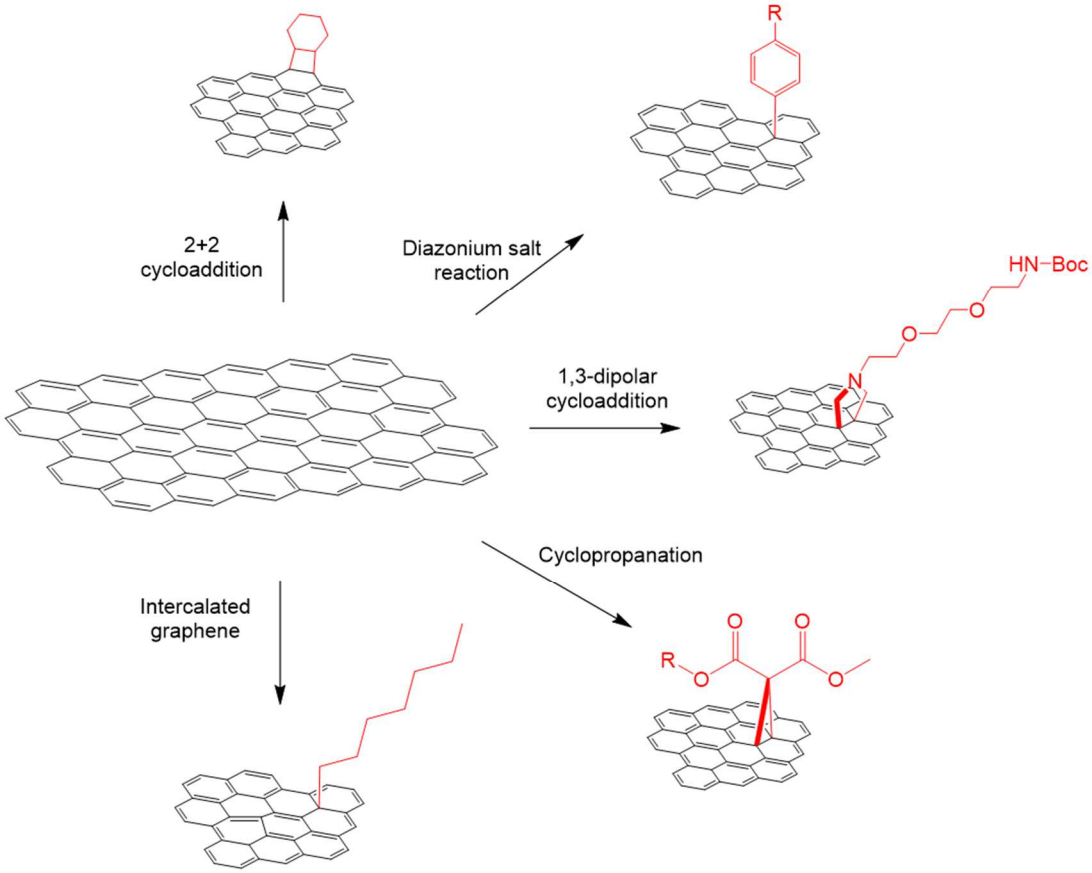

Scheme 1.1: Schematic representation of graphene functionalization.

As the described reactions are taking place on exfoliated graphene, to obtain high degree of functionalization the material employed should be mostly mono- and bi-layer graphene. But one of the main problems arising from LPE, as mentioned, is exactly the low amount of mono- and bi-layers respect to few-layers. If the first two species have good reactivity, the last does not permit to obtain good yield of reactions, requiring the use of great amount of reagents (i.e. ~4-6 eq. of organic molecules respect to carbon atoms).[47] We are therefore facing two problems: 1) The scale-up of the production of functionalized graphene prepared by LPE requires high amount of reagents. This problem could be solved by improving the LPE technique to increase the amount of mono- and bi-layer graphene; 2) The scale-up of graphene functionalization requires more efficient reactions to decrease the amount of reagents employed.

1.3.2. **Functionalization of intercalated graphene**

Differently from the functionalization of LPE graphene, the use of intercalated graphite could solve some of the problems described in the previous paragraph. This approach is based on the intercalation of graphite with alkaline metals, like Na, K, Li, etc. The intercalated graphite is reduced by the metals, giving graphite intercalation compounds (GICs), corresponding to graphene sheets negatively charged, called graphenides.[48] Based on the ratio between carbon and metal atoms, GICs presents different properties, such as high reactivity, different numbers of sheets between every intercalated metal atom, various color, etc. (Figure 1.7).

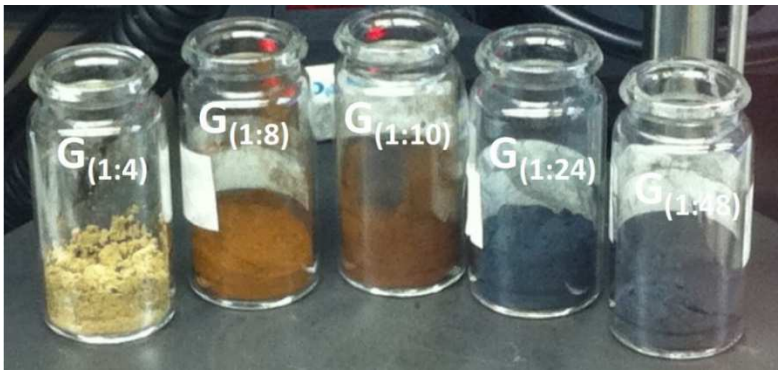

Figure 1.7: GICs with varying carbon/potassium ratio and their respective colour.[49] Reprinted with permission - Copyright 2014 John Wiley and Sons.

KC_8 is the most used graphenide species to perform chemical reactions. GICs present good dispersibility in anhydrous organic solvents as THF or DMF, the sheets can be dispersed by simple stirring or by ultrasonication. The negative charges on the surface of graphenide generate electrical repulsion between the sheets avoiding the re-aggregation in solution, reaching a concentration up to 0.7 mg/mL in NMP. One of the most impressive and visible characteristics of GICs is the color change of the graphite powder after the intercalation, passing from black to brown/yellow/gold based on the K:C ratio. KC_8 is synthesized by mixing graphite and potassium at 250 °C in inert and dry atmosphere for two days (Figure 1.8). The reactivity of graphenides is higher respect to the exfoliated graphene, leading to higher degrees of functionalization employing less amount of reagents (1:1 eq. graphene/reagents).[50]

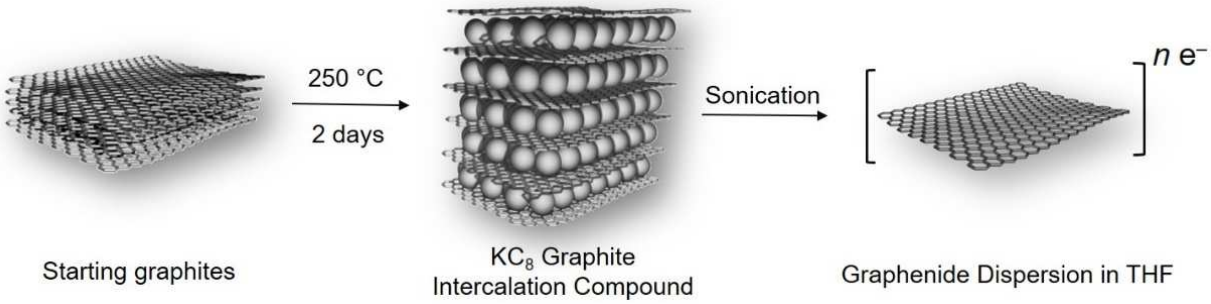

Figure 1.8: Graphite intercalation by metallic potassium and exfoliation of GIC by ultrasonication.

This approach permits the functionalization of bulk graphite in large quantity, allowing the scaling up laboratory production to investigate applications of functional graphene. However, the handling of this species in the laboratory results to be more complicated then exfoliated graphene. GICs are very reactive species, and they must be prepared in completely anhydrous and oxygen-free conditions to avoid the oxidation of the sheets. Therefore, all the solvents and reagents must be anhydrous, that is resulting to be limiting for some liquid reagents that could contain water. Of high importance, after the functionalizations GICs must be discharged from the residual negative charges before the work-up process, to avoid side oxidation reactions with atmospheric O_2.[51] The discharging of graphenides is normally performed with benzonitrile (PhCN).[49] On the other hand, the great and high reactivity of graphenide is not always corresponding to an advantage on the perspective of the chemical functionalization. The drastic conditions of reaction due to the elevated presence of negative charge could affect some functional group on the organic reagents, involving unexpected side reactions. Simple diazonium salts[52] and alkyl iodides[53] have been demonstrated to remain intact to the drastic reaction conditions, as well some diazonium salt made of porphyrins,[43] but no evidence of other functional groups have been shown in the literature until now. It is

then evident that the advantage obtained by the higher reactivity of GICs generates new problems for the development of new flexible synthetic route. Moreover, in an industrial scale-up perspective, the use of GICs could arise some problems of safety and production.

I will show in this Thesis a possible approach to combine the functionalization of KC_8 and further functionalization of the materials for biomedical applications.

1.3.3. Main techniques for graphene characterization

The characterization of graphene, as for other nano-materials, is not easy and it is still one of the open challenges faced by material scientists. The common techniques of characterization can be divided in two main groups: one related to the characterization of the morphology of the sheets, and the others related to the characterization of the chemical structure and the types of functional groups present on the material. The characterization of the morphology consists in the determination of the lateral size, thickness, shape, number of layers and state of aggregation of the sheets. The most common technique employed for this aim are atomic force microscopy (AFM), scanning electron microscopy (SEM), transmission electron microscopy (TEM) and high-resolution transmission electron microscopy (HRTEM). The techniques for second type of characterization are comprise Raman spectroscopy, X-ray photoelectron spectroscopy (XPS), Fourier transform infrared spectroscopy (FT-IR), ultraviolet-visible spectroscopy (UV-vis), thermogravimetric analysis (TGA) and solid-state NMR (MAS NMR).

1.3.4. Morphology characterization

Different microscopy techniques have been applied for the characterization of the morphology of the graphene layers. AFM analysis allows investigating the 3D structure (lateral size and thickness) of graphene sheets (Figure 1.9a). The precision of this technique permit to distinguish between monolayer and bilayer graphene and it is often employed to statistically evaluate the average thickness and number of layers of a dispersion.[54] SEM and TEM are normally employed for the bidimensional observation of the sheets (Figure 1.9b). The lateral size distribution of graphene dispersion and their average is commonly evaluated by statistics on TEM image. TEM is also employed for a direct observation of the morphology of the sheets. The higher magnification reached by HR-TEM allow the observation of the atomic structure of the material (Figure 1.9c). Is it possible to observe through this technique the defects on the structure and the exact conformations of the edges. It is even possible to directly observe the layer stacking, permitting the evaluation of the number of layers constituting a graphene sheet.[55]

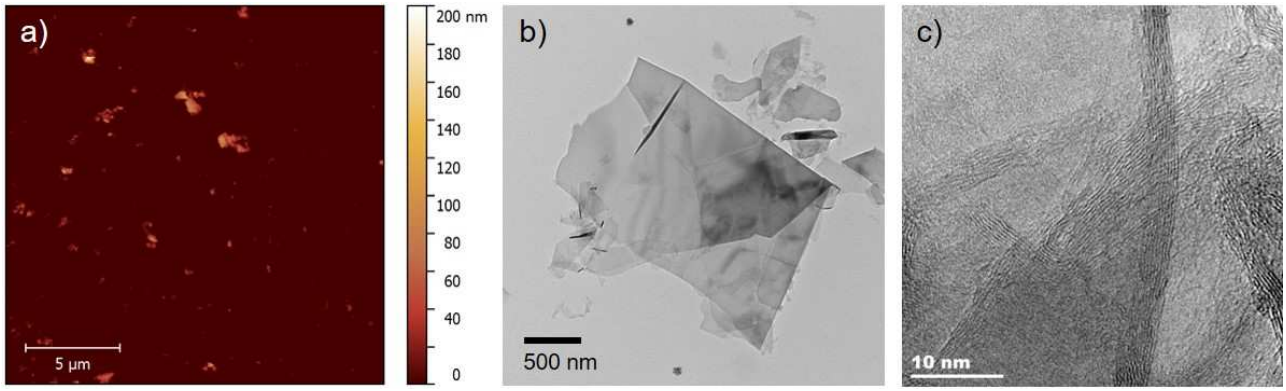

Figure 1.9: Microscopic images of graphene sheets: a) AFM image of graphene deposed on Si support; b) TEM images; c) HR-TEM image of graphene sheets; the stacked layers constituting the sheets are observable.

1.3.5. Chemical characterization

As mentioned, the characterization of the chemical group introduced onto graphene by functionalization is quite difficult and requires the combination of multiple spectroscopic and analytical techniques. One of the most important method applied to graphene is Raman spectroscopy. The Raman spectrum of graphene (Figure 1.10a) is constituted by three main band: The D band (~1335 cm^{-1}), the G band (~1580 cm^{-1}) and the 2D band (~2650 cm^{-1}). The *G* peak corresponds to the E_{2g} phonon at the Brillouin zone center (Γ point). The 2D peak is an overtone peak, associated with the breathing modes of the six-atom rings.[56] Because of the selection rules, the G and 2D bands are always present in the graphene spectra. The forbidden D and D' bands appear in presence of defects. For this reason, they are associated and employed for the evaluation of the quantity of defects in the structure. The Raman spectroscopy is consequently employed for the analysis of the quality of graphene sheets through the evaluation of the intensity (I) of the D and G band (I_G/I_D ratio). The mentioned defects are associated to the presence of sp^3 carbon atoms due to oxidation, formation of holes or functionalization of the structure. On pure graphene, the D band is absent, whereas in GO, where the quantity of oxidized carbon atoms is in some case higher than the sp^2 atoms, the D band is more intense than the G band (Figure 1.10b). Typically, the 2D peak in monolayer graphene present higher intensity respect to the G band, whereas in graphite or few-layer graphene the intensity of 2D peak is lower respect to G peak. By deconvolution of the 2D band it is possible to evaluate the number of layers constituting the sheets from mono- bi- and few layer graphene (<5 layers) (Figure 1.10c).[56,57]

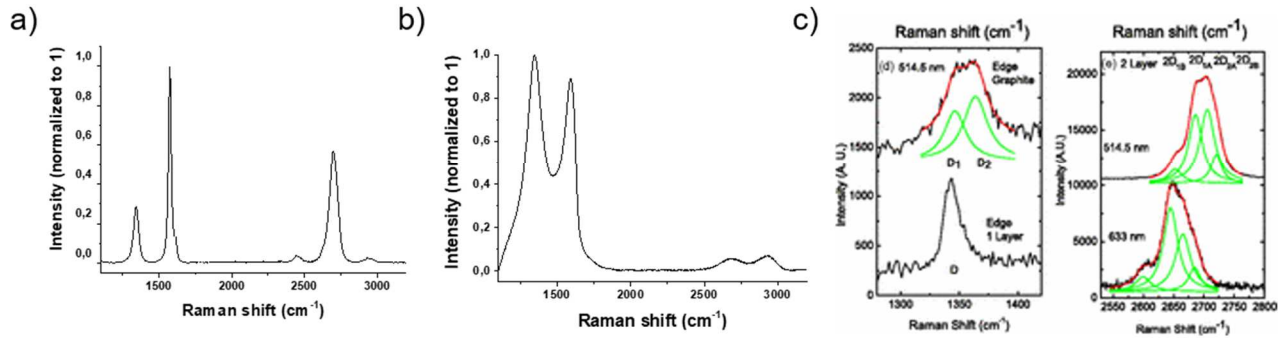

Figure 1.10: Raman spectra of graphene (a) and graphene oxide (b). c) Representation of the deconvolution of 2D band for the evaluation of number of layers of graphene sheets.[57] Reproduced with permission of American Physical Society.

The analysis of the I_G/I_D ratio can give a first idea if a functionalization reaction has really occurred on graphene, measuring the increase of the number of defects of the final material respect to the starting graphene. However, Raman does not give any information about the chemical nature of the defects. For an accurate chemical characterization of the material other techniques must be employed. TGA analysis is often used for the characterization of carbon nanomaterials. This technique is helpful for the evaluation of the quantity of organic compound loaded or grafted onto graphene. By comparison of the mass loss of the starting material and the functionalized graphene, it is possible to evaluate the bulk functionalization of the material. However, TGA does not allow to distinguish the functional groups in case of multifunctionalization or subsequent functionalization of the material (Figure 1.11a). The coupling of this technique with FT-IR or MS spectrometry can provide an analysis of the nature of the organic reagents liberated from the sample, permitting a better understanding of the functionalization of the material. FT-IR spectroscopy is commonly used to analyze the presence of the functional groups on a molecule or a material[42] XPS spectroscopy gives information about the elemental composition, the chemical state and the electronic state of the elements in a sample. From the deconvolution of the C1s spectra it is possible for example to obtain information about the types of carbon bonds (i.e. C-N, C=O, COOH, etc.) (Figure 1.11b).[11]

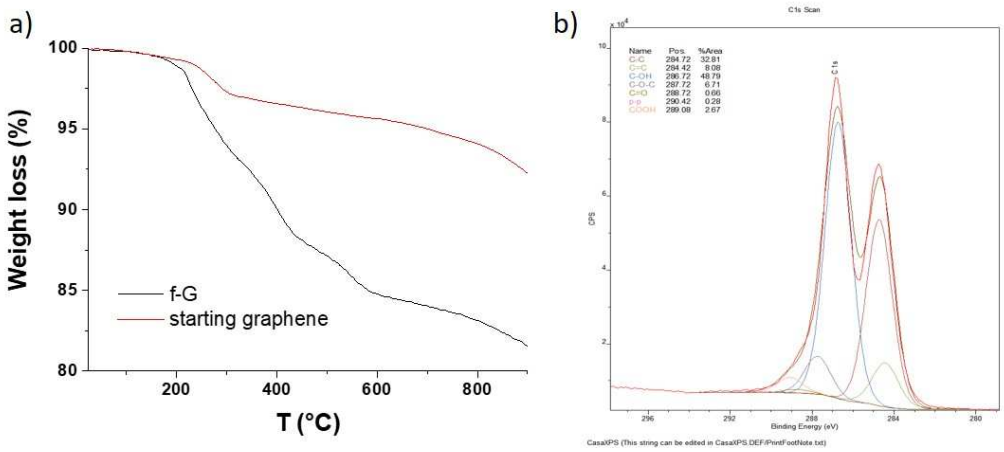

Figure 1.11: a) TGA weight loss profile of starting graphene (red line) and functionalized graphene (black line); b) XPS deconvolution of C1s spectra of GO.

MAS-NMR is generally based on the ^{13}C-NMR analysis of the bulk powder. This can give information about the chemical shift and the nature of the functional groups present on a material. Until now a little number of studies have investigated the use of this technique with graphene, and most of them are focused on GO analysis.[58] The main problem about the application of this technique to graphene is coming from its natural conductivity that generates a current and a new magnetic field, making the stabilization of the sample and the analysis very difficult (see chapter 3). In conclusion, differently from common organic compounds, where the use of NMR, MS or FT-IR are sufficient for their characterization, graphene characterization requires the combination of multiple techniques. Moreover, the direct and clear observation of the functional group is not possible, due to the absence of a specific and reliable technique. As a consequence, the cross-interpretation of the results obtained from the different techniques is required for a reliable characterization of the material.

1.4. Biological applications of graphene

The applications of graphene are not limited to the exploitation of its electronic properties. The investigation of this material has highlighted different characteristics that make of graphene a promising material for biosensor, nanomedicine and bioimaging applications.[13] Its electric properties, as well the possibility of chemical modifying the surface can be exploited for the development of many different products, from biomedical devices to drug delivery platforms. Graphene has been discovered to spontaneously penetrate cell membranes,[59] opening the doors to drug delivery graphene-based carriers. The high ratio between the surface area and its mass and the ability in adsorbing on its surface hydrophobic drugs and genetic materials through π-π staking or hydrophobic interaction could permit a high drug loading compared to the mass of the material.[13] Moreover, the biodegradability of graphene has been demonstrated by natural enzymes as myeloperoxidases, confirming the good opportunities of the research efforts.[60] In this study, I will focus the attention on the drug delivery systems based on graphene, to unroll the state of the art of the research, and to understand the important aspects to take in account when new materials are involved in biomedical applications. A clarification must be done at the beginning of this chapter. Of high relevance is the number of studies published about drug delivery systems based on graphene. The nomenclature of these papers is confusing regarding the use of graphene or graphene oxide and can lead the readers to errors. In fact, most of the studies published are conducted on GO, r-GO, GO carbon dots, but mentioning graphene to identify the material on these publications, generating confusion on the readers and on the classification of the

research. Only a few studies at the moment have investigated the use of pristine graphene for drug delivery applications.

1.4.1. Biocompatibility

One of the most important aspects on the use of nanomaterials for therapeutic applications is their biocompatibility, referred to the effects on the interactions with cells, tissues and organs without causing side-effects.[61] Related to nanomaterials, we cannot find a precise definition of biocompatibility. Citing a work of Langer and Kohane, biocompatibility *"is an expression of the benignity of the relation between a material and its biological environment"*.[62] The presence of nanomaterials in a biological environment could lead, for example, to the uptake of these from macrophages and their elimination from the organism, or to the activation of an inflammatory response or to the accumulation in some specific organs of the body, etc. All these effects are consequences of different properties of the nanomaterials, such as dispersibility in the medium or re-aggregation, lateral size dimension, number of layers, functional groups on the surface, interactions with proteins and tissue, etc.[63] Until now, most of the studies conducted on toxicity and biocompatibility *in vitro* and *in vivo* of graphene family members are involving GO and its derivatives, because of the facility on the production, the easy handling and the good dispersibility in water.

One big issue on the *in vitro* and *in vivo* studies performed on graphene and GO is the comparison of the effects of these materials. A profound and detailed characterization of the materials if fundamental to compare the results obtained by different research groups. Lateral size and number of layers of the sheets are the most evident characteristics to consider for a good comparison, but not the only ones. The toxicity of the particles depends even on the chemical surface of the materials that present big difference between graphene and GO, but even on the different methods of production.[14] The differences in the oxidation degree can affect the interactions between GO and the proteins and other molecules into the organism.[64] The technique employed for the production of the materials can also affect the cytotoxicity, because of eventual residual compounds and impurities absorbed on graphene or GO released into the cells. Furthermore, the functional groups added on the material, like PEG, polyvinyl alcohol, chitosan or surfactants, could modulate the interactions with the environment and affect the biocompatibility.[65] The functional groups can also affect the internalization, the targeting and the biodistribution of the particles, and must be well considered in the moment of a generalization on the effects of these materials.

As already discussed in paragraph 1.2, very important is the dispersibility of the materials. The sheets must be stable for long time in PBS or cell culture media solution to permit the good performing of the *in vitro* experiment. The aggregation of the sheets is affecting the internalization and the interactions with the environment. GO and its derivates present good water solubility and for this, they have been privileged for carrying out these studies. But, despite this property, GO has the tendency to form aggregate and change its chemical surface when dispersed in electrolyte solution (as PBS), risking to make uncertain the biological results.[66] These problems have been faced through the investigation on the use of surfactants, as Pluronic F127 (a triblock amphiphilic copolymer). Pluronic F127 demonstrated to increase the dispersibility of GO in electrolytic solutions and avoid aggregation.[66] Dai and co-workers faced the problem using small GO particles (< 50 nm) functionalized with polyethylene glycol (PEG) derivates increasing the dispersibility of the material and decreasing the aggregation.[67] Some aspect of the biocompatibility of graphene derivates will be treated on the next paragraph, to give an overview of how functionalization, lateral size, intrinsic properties of these materials can affect the interaction with the biological environment, the fate of the particles in the organism and their biocompatibility. Due to its high hydrophobic surface, graphene dispersibility in water or physiological media is very difficult in absence of surfactants. As mentioned above, the use of biocompatible surfactants is of very importance to well-evaluate the biocompatibility of this material.

1.4.2. **Biodegradation**

Very relevant for the biocompatibility of graphene family materials is their fate inside the body after having accomplished their activity. How the materials are eliminated by the organism? One important response came from the discovery of the biodegradability of these materials. Some examples of biodegradation were already showed for carbon nanotubes, reducing the asbestos-like toxic effects due to their shape.[68] Even for graphene and GO the biodegradation was shown by different natural enzymes, depending on the lateral size, number of layers and chemical functionalization of the surface of the materials. Horseradish peroxidase (HRP) is able to degrade GO but not r-GO. The group of Star has suggested as explanation a difference in the interactions with the active site of the enzyme.[69] Using the same enzyme, Li *et al.* investigated the effect of surface coating on cytotoxicity of GO and its derivates. The absorption of BSA and PEG on the surface has been discovered to decrease the cytotoxicity on macrophage U937 cells. But, on the other hand, the presence of these molecules is also producing a resistance to the biodegradability of GO by HRP.[70] In this study, the group has proposed as solution the covalent functionalization of GO with PEG through a disulphide bond, to decrease the cytotoxicity and the biodegradation of the functionalized material. Kurapati *et al*. demonstrated an enhancement of GO degradation by HRP after covalent functionalization of GO with coumarin and catechol. They even discover that human myeloperoxidase (MPO) can degrade GO and FLG (Figure 1.12).[60,71] They investigated the biodegradation properties of MPO on dispersion of GO with different thickness, showing how highly dispersed materials were completely degraded in 24 h, whereas an aggregated sample was showing only slightly change on its structure.

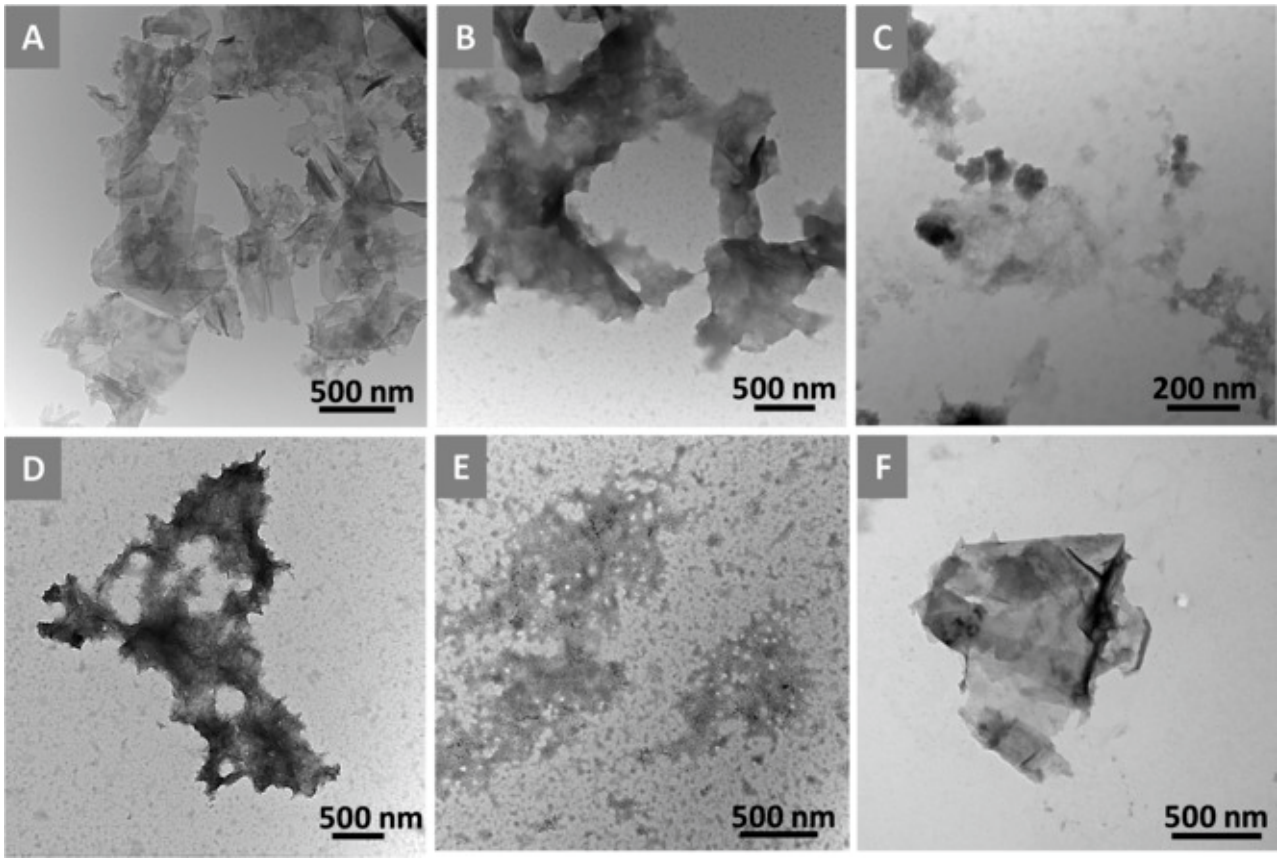

Figure 1.12: TEM images of FLG. A) FLG dispersed in phosphate buffer; after treating with hMPO B),C) for 25 h; D),E) after 40 h; and F) after treating with H_2O_2 in the absence of hMPO for 40 h. Reproduced from [60] with permission of Wiley and Sons.

In vivo studies were performed by Girish *et al*. on the degradation of graphene. Graphene, functionalized with carboxyl group to increase the water dispersibility and with a lateral size of ~200 nm, was shown to be well dispersed into the injected solution, but after 24 h post-injection big aggregates were detected in various organs.[72] By confocal Raman imaging the authors followed the evolution of the sheets during 3 months, showing the increase of structural disorder. The mechanism involved in the degradation is still not clear, but the authors suggested that the degradation was mainly due to macrophage action. Another promising way for the degradation of graphene comes from bacteria. Naphthalene-degrading bacteria were demonstrated to degrade graphitic material.[73] Graphite, GO and r-GO presented different rates of oxidation and degradation after 14 days of incubation with these bacteria, showing promising results for the disposal of these materials. All studies presented here, and others not mentioned in this paragraph, are suggesting the possibility to degrade *in vitro* and *in vivo* graphene family materials by the immune cells. However, more investigations are required to better understand the effects and mechanism on the degradation of these materials and their effects on long term treatment.

1.4.3. Administration and biodistribution of graphene materials

The biodistribution of the particles into a body is fundamental for the efficacy of the therapy and for the cytotoxic effect of the materials. The organ biodistribution is not depending only on the characteristics of the material but it is also affected by the administration route selected. Oral, inhalation, intravenous and intraperitoneal administrations have been employed for the investigation of the *in vivo* toxicity of these graphene materials. Two nanosized distribution of r-GO sheets labelled by ^{125}I were oral administrated to mice and controlled after 1, 15 and 60 days. The materials were found in blood, heart, lungs, liver and in higher amount in kidneys.[74] The quantity decreased during the time, but the material was still present in the organs after 60 days. These results are suggesting that after the administration the materials were adsorbed by the gastrointestinal tract and reached other organs *via* the systemic circulation.

To study the impact of human exposure to nanomaterials, the inhalation route is one of the most relevant. Nanosized GO (10-800 nm) labelled with ^{125}I and few-layer graphene platelets (60-590 nm) labelled with ^{14}C were investigated using this route. For GO, the majority of the material was found in the lungs, decreasing in quantity during the time, from 10 minutes to 12 h after intratracheal instillation, another route to reach the lung alternative to inhalation.[75] Small amounts were also found into the blood, liver and kidneys, suggesting a mechanism of translocation to the blood, either directly from the lungs or *via* intestinal absorption. Macroscopic observation showed a permanence in the lung for more than 90 days, with evidence of decreasing in the quantity. However, the analysis was it was not quantitative. Graphene platelets were administrated by the same route and tracked for 28 days. The material was primarily located into the lungs and in few amounts in the stomach and intestines, suggesting a mucociliary clearance mechanism, followed by swallowing of the inhaled materials.[76]

Intravenous injection (*i.v.*) is the most common route for administration of nanomaterials. Different studies were performed on GO, investigating size (ranging between 300-1000 nm and 300-700 nm), dispersing agent (PBS, 1% Tween 80-PBS) or functionalization of the surface (poly (sodium 4-styrenesulfonate), or PEGylated GO). GO in PBS (300-1000 nm) was found mainly in the lungs, while GO dispersed with Tween was accumulated in the liver, showing that better colloidal stability helps GO in pass through the lung capillaries.[77] GO functionalized with poly(sodium 4-styrenesulfonate), ranging between 300-700 nm lateral size) was followed by fluorescence after functionalization with Cy7 and observed only in the liver after 24 h post-injection.[78] The material was then found also in the spleen and the lungs after 14 days post-injection. PEGylated GO (~1 µm, dispersed in PBS) was found mainly in the liver and the spleen after 3 days post-injection but spread after 7 and 14 days in the brain, decreasing the accumulation after 21 days.[79] Nano-GO

functionalized with PEG (5-50 nm) showed higher accumulation in the spleen compared to the liver during 60 days period.[65] The non-PEGylated GO accumulated 2 times more in the liver respect to the better dispersed PEGylated species.[80]

The groups of Prof. Kostarelos and Bianco have investigated the biodistribution of GO materials with different lateral size and thickness, after functionalization of the sheets with NH_2-PEG_4-DOTA, a chelating agent for radioactive metals (e.g. ^{111}In). Mono- to few-layer GO-DOTA with a lateral size of 100-400 nm and thickness of 2-10 nm were followed in mice during 24 h. After 1 h the material accumulates into the liver and the spleen, with a prevalence into the liver, whereas after 24 h the accumulation was reversed, with a decrease of the radioactivity into the liver and an increase into the spleen.[81] After this study, the groups investigated the distribution of GO-DOTA sheets of different thickness (1-4 nm GO only, 1-10 nm GO-DOTA and 5-30 nm GO-DOTA). The thicker materials resulted in a greater accumulation in liver and spleen respect to the thin sheets after few hours post-injection. Interestingly, for both material a large amount of radioactivity was detected into the bladder, suggesting that the sheets had undergone renal glomerular filtration, hypothesis confirmed by presence of radiolabeled GO into the kidney and the detection of GO material in the urine by TEM and Raman spectroscopy.[82]

Finally, also the fate of few-layer graphene in different form was investigated *in vivo*. Sasidhara *et al.* investigated the biodistribution of graphene (FLG, 100-200 nm), FLG-COOH and FLG-PEG covalently labelled by radioactive marker ^{99}Tc.[83] They studied the biodistribution over 24 h, showing that FLG and FLG-COOH accumulate into the lungs, whereas FLG-PEG accumulated also into the lung, but gradually relocated during the 24 h into the spleen and the liver. By histological analysis the authors showed how FLG and FLG-COOH are accumulated for more than 90 days in the lungs, causing damage, and FLG-PEG left the lungs, without causing damages. Through the mentioned studies it is clear the ability of the graphene family to cross the physiological barrier, reaching different organs inside a body, even far from the point of administration. However, the scarcity of studies conducted on graphene and GO does not allow for the moment a generalization, but they are highlighting the attention on the importance of the dimension and even more on the water dispersibility of the particles. Long-term studies about the effect of the materials in the organism should be conducted, to understand the behavior of graphene into the organism in the perspective of the development of graphene-based therapies.

1.4.4. Drug delivery applications

When speaking about nanomaterials for drug delivery applications, one of the first questions to answer is why we need to develop new drug carriers. Some novel promising developed drugs present poor water solubility, making their therapeutic applications complicated and less effective. Moreover, their distribution into the body and the targeting are non-site specific, leading to a lower and spread effect. Despite these problems, these drugs present promising therapeutic activities that can be exploited using specific nanocarriers.[13] Graphene, as well as nanoparticles, magnetic particles, quantum dots and other nanomaterials, can improve the site-specificity of the drug delivery, increasing the quantity of drug uptake through physical absorption or covalent linkage on their structure, and can enhance the therapeutic effect thanks to their particular properties.[84] Chemical functionalization of nanomaterials can improve the targeting of specific cells, increasing the internalization and the delivery of these materials. The flexibility of the chemical approach could allow the use of the same platform for different applications, simply changing the specific functional groups. Moreover, the exploitation of the properties of these nanomaterials, including for example the photothermal or the photodynamic properties, fluorescence and cells membrane penetration, can improve the therapeutic efficacy of the drugs through a synergistic effect.

Targeting: The targeting of the materials into specific cells is fundamental for the development of new therapies. To begin, we can distinguish between *passive* and *active* targeting, that can affect dramatically the effectiveness of the therapy.[85] The passive strategy takes advantage of the changes and enhancement of vascularization of cancer tissues. The fast-growing of the tumor causes the formation of leaky blood vessel and junction. Taking advantage of the ability to pass through the loose junctions, nanomaterials are preferably accumulated into the tumoral tissue. However, not all the tumors present this extra-vascularization and the uptake from the cells is uncontrolled, causing an off-target drug delivery. The active strategy involves the functionalization of the materials with a targeting moiety (e.g. ligands, antibodies, peptides) that can recognize specific sites at the surface of the cancer cells. The use of targeting molecules on GO has been demonstrated to increase the uptake into specific tissues, increasing the effectiveness of the therapeutic activity and decreasing side-effects respect to passive targeting (Figure 1.13).[86]

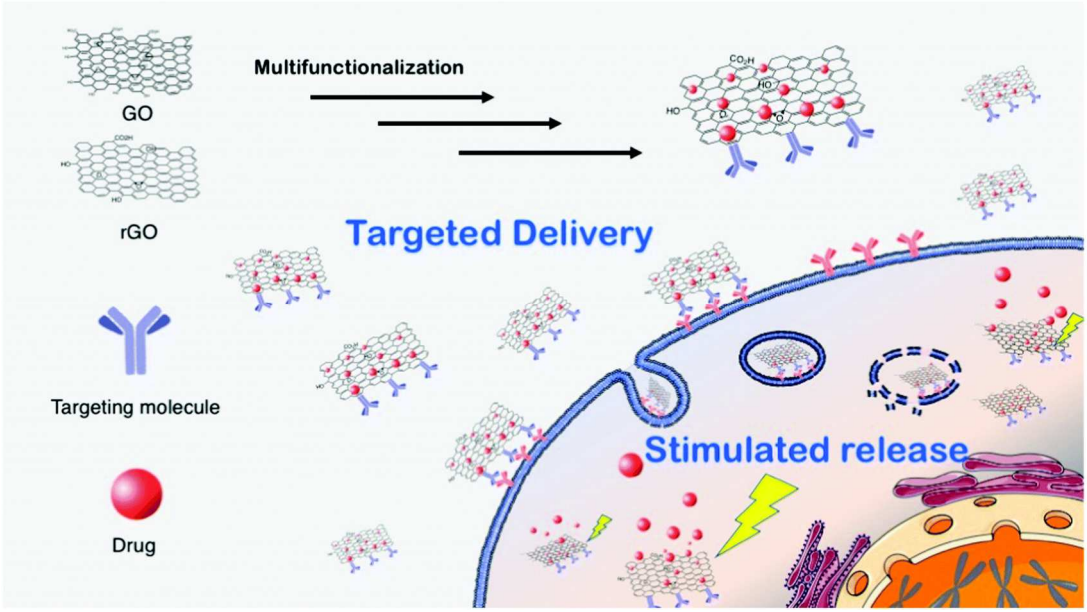

Figure 1.13: Cartoon illustrating the targeting ability of multifunctional GO and r-GO.[13] Published by Reina *et al.* from Royal Society of Chemistry.

Drug release: Very important for the development of the therapeutic strategy is the drug release at the specific site. The release can be triggered by changes in the environment between the extracellular matrix and the cytoplasm, as pH variation. The lowering of the pH and the consequent protonation of the drug, in the case of doxorubicin, lead to a weakening of the interactions with the GO surface and the release of the molecule.[61] However, the drug release due to pH or environmental changing is, on the most of the examples, very slow or not complete, with considerable amount of drug retained on GO thus lowering the specific activity of the therapy. Alternative techniques require an external stimulus, as for example light irradiation, causing the warming of the materials by photothermal effect and the consequent drug release into the cells.[87] A stimulated drug release, in this optic, is more promising for an increase of the therapeutic activity. The near infrared (NIR) irradiation allows a high site-specificity release, decreasing side-effects of the therapy. Moreover, the localized increase of the temperature of the materials into the tumor, thanks to the photothermal activity induced by the irradiation, can act in a synergistic effect with the drug, increasing the therapeutic effect.[88]

Due to its easy functionalization, GO and r-GO are the most commonly employed derivatives of graphene for the development of drug delivery platform. Only in 2017, for the first time, FLG has been shown to have a specific killing action on immune cancer cells (e.g. leukaemic monocytes). Russier *et al.* showed how the

material exhibits a strong anticancer activity against an aggressive form of myelomonocytic leukaemia, whereas no effects on other immunocompetent cells were observed. FLG was demonstrated to specifically cause the necrosis of monocytic cancer cells and also to have more specific activity respect to chemotherapeutic drugs.[89] GO functionalized with biocompatible polymers has been investigated by different group. In one study by Zhang *et al.*, GO/chitosan conjugate was loaded with camptothecin by π-π stacking interactions in high loading amount. The complex exhibits strong cytotoxicity in HeLa and HepG2 cells.[90] A different example comes from Kim and co-workers. Doxorubicin binds to GO functionalized with PEG and branched polyethyleneimine (BPEI), (PEG-BPEI-r-GO). Doxorubicin release was due to the endosomal disruption caused by NIR irradiation.[91] Example of delivery of two drugs comes from Dai and co-worker. In their study, nano GO-PEG was loaded with SN38 and camptothecin, showing great potential of this combined system.[67] Some issues arise from the use of GO or r-GO. One is related, as discussed in the previous paragraph, from possible toxic residues remained adsorbed during the production methods of these materials. These residues can be released in the organism, inducing undesirable side-effects. Another problem comes from the functional group on these materials. The epoxide rings or carboxylic moieties can react or interact uncontrollably with the environment, generating side-reactions. For these reasons, the use of graphene could be desirable thanks to its chemical stability, inertness and the absence of functional group on the surface.

Considering the reported results, and in front of a wide range of studies published about the drug delivery ability of GO and r-GO materials, I would like to underline that graphene family members are showing promising features for therapeutic applications. However, as for the studies about their compatibility, the research in this field is still suffering from a lack of studies on graphene. The obtained results are hard to compare, due to a lack in the information about the tested nanomaterials, such as number of layers, dimension of the particles etc. GO and r-GO can present large differences in their chemical surface based on the preparation method and the covalent functionalization, leading to differences in the drug loading and in the interactions with the environment. Moreover, the presented studies are also employing different drugs or cell lines, making harder the comparison on the delivery effects. It is needed a standardization way to describe, characterized and test the properties of these materials, to allow a better comparison, in order to move forward the research on biomedical applications of these materials and make them considerable for real clinical applications in nanomedicine.

1.5. Boron nitride

Hexagonal boron nitride (hBN) belongs to the 2D materials family and has been discovered after graphene. The structure of hBN is graphene-like, constituted by alternate B and N atoms in a honeycomb arrangement. For these characteristics sometimes it is called “white graphite”. Boron nitride nanotubes and sheets have been isolated during the years, and their properties investigated (Figure 1.14).[92] The morphology of hBN sheets is similar to graphene, with mono- and few layer sheets, characterized by a flat structure with sharp edges.

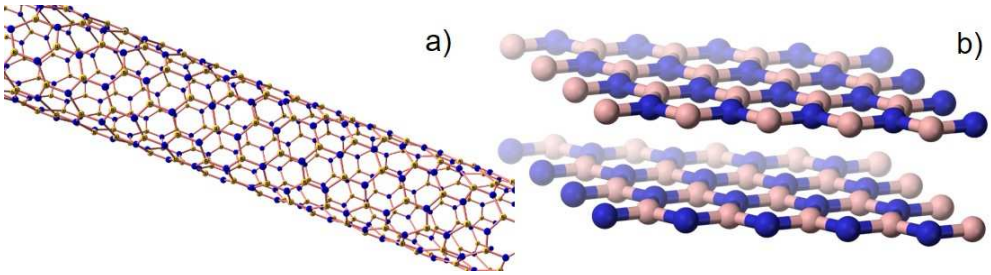

Figure 1.14: a) Boron nitride nanotubes structure; b) boron nitride sheet structure.

Boron nitride, differently from graphene, is an electrical insulator with strong chemical and thermal stabilities.[93] However, like graphene, it presents good thermal conductivity and mechanical strength. The methods for the production of hBN are various. Similar to graphene, the exfoliation is the main production method, including mechanical exfoliation, scotch tape exfoliation and liquid-phase exfoliation.[94,95] Organic solvents, such as NMP, DMF and alcohol, as *tert*-butanol, are good exfoliating agents, able to stabilize the dispersion of hBN. From liquid phase exfoliation, few-layer hBN is normally obtained. Many methods based on ball milling of BN powder have been developed to produce this 2D material, thanks to its chemical stability that allows strong working conditions without affecting the chemical structure.[96–98] The obtaining of hBN sheets in water is requiring the use of surfactants to stabilize the sheets and avoid re-aggregation. Mixture of water and alcohols have been demonstrated to stabilize the sheets in solution, but in the perspective of biological application the use of solvents different from water is undesired. Common surfactants employed for graphene, such as proteins and organic molecules, have been also demonstrated to be suitable surfactants for hBN exfoliation and stabilization.[20,99] The hydrophobicity of the hBN surface permits the absorption of drugs or genetic material by π-π stacking interactions or hydrophobic interactions, opening the doors to drug delivery applications by hBN. On this perspective, almost all studies are performed on BN nanotubes (BNNTs) or nanoparticles, called generically hBN nanomaterials.[100–102] Covalent and non-covalent functionalization of BNNTs have been investigated to study the biomedical applications of these compounds, but respect to graphene and GO the number of publications on this topic is very low (Scheme 1.2).

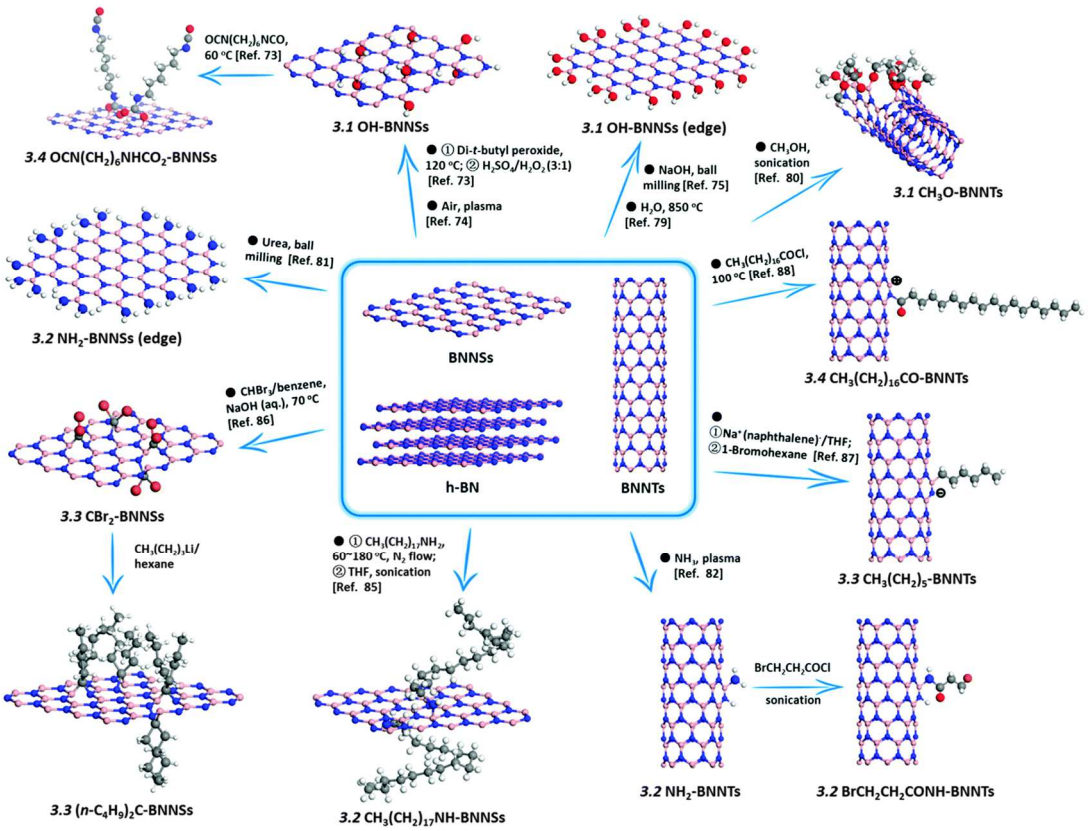

Scheme 1.2: Generic scheme of boron nitride nanotube and sheet functionalization reactions.[102] - Published by The Royal Society of Chemistry.

The biocompatibility of BNNTs have been widely investigated, to corroborate the studies about its medical applications. Chen *et al.* showed that BNNTs are non-cytotoxic and are not inhibiting the proliferation of HEK 293 cells. The tubes could be non-covalently functionalized by DNA and RNA for therapeutic applications.[103] Alternatively, Erdely and co-workers investigated the *in vitro* and *in vivo* toxicity of commercial BNNTs, showing that this materials, exactly as multiwalled carbon nanotubes (MWCNT-7), are inducing an inflammatory response, due in part to NLRP3 inflammasome activation.[104] Different studies are contradictory and of difficult comparison, due to the non-homogeneity of the samples tested, the lack of characterization, the difference on the surfactant employed or the treatment of the materials, making hard a generalization on their effects. Zou and co-workers have faced this problem comparing the same samples of BNNTs with different length and in multiple cell lines.[105] On their study, the researchers showed how the cytotoxicity of BNNTs is affected by the length of the tubes, where short tubes (~240 nm) are less toxic than longer tubes (~450 nm), and how the cytotoxicity is strictly related to the type of cell lines. Despite all the studies regarding the biomedical applications and biocompatibility of BNNTs, only one study has been published about boron nitride biocompatibility. In this work, Mateti *et al.* evaluated the cytotoxicity of BN sheets with a lateral size dimension of < 100 nm and thickness of ~2 nm and of particles with a lateral size of ~1 µm and thickness of ~100 nm.[106] They demonstrated that the nanosheets present low cytotoxicity on SaOS2 cells, whereas the larger particles were less biocompatible. Even if, after the discovery of graphene, the interest in the biomedical applications of 2D materials has increased, no extensive investigations have been performed on hBN. The first evidence of biocompatibility of hBN has been showed by Kurapati *et al.*, demonstrating the biodegradation of hBN nanosheet by MPO. This property, likewise, for graphene, is pushing the researchers on the investigation of the cytotoxicity of hBN sheets *in vitro* and *in vivo* and on drug delivery applications, to develop new platforms for the treatment of different diseases.[107]

1.6. Objectives of the Thesis

The main aim of my Thesis was to explore the possible biomedical applications of graphene and boron nitride. The understanding of their interactions with cells, the *in vitro* and *in vivo* toxicity and biocompatibility are of primary importance to develop a novel therapeutic approach based on 2D materials. We can divide my research work in two main topics: 1) production of graphene and boron nitride in water with biocompatible surfactants for the investigation of their biocompatibility; 2) Multifunctionalization of graphene for the development of a versatile drug delivery platform.

Following the general Introduction (Chapter 1), Chapter 2 is focused on the production of boron nitride and graphene in water, to investigate the biological effects of these materials *in vitro* and *in vivo.* The stability and aggregation state of the particles is strongly affecting the outcome of the cellular experiments. For this reason, I explored the use of different surfactants for graphene and hexagonal boron nitride (hBN), to improve their dispersibility for more than 24 hours in suitable media. To well compare the biological effects of these 2D materials, I also focused my efforts on the tailoring of the lateral size dimension of the particles, applying a technique based on ultracentrifugation.

Stable FLG dispersion using riboflavin-5-phosphate sodium salt were obtained in different media and employed for the investigation on the biodistribution and cytotoxicity of FLG *in vivo* after *i.v.* injection in mice. Moreover, dispersions of hBN and graphene with different lateral size and shape was obtained. In collaboration with Dr. Annette Von Dem Bussche at Brown University, we investigated the *in* vitro cytotoxicity of hBN on H460 lung epithelial cells, comparing the effect of the size of the material and of the edges shape.

Moreover, I also focused my attention on the use of surfactants with strong fluorescence, with the purpose to follow the *in vitro* internalization of graphene by fluorescence microscopy techniques. For this purpose, different molecules were investigated, such as rhodamine derivatives and bodipy-based derivatives. Preliminary results surprisingly showed new fluorescence properties of graphene, suitable for new applications of this material.

In Chapter 3 is studied the reactivity and covalent multifunctionalization of graphene. Different reactions were investigated, such as 1,3-dipolar cycloaddition, diazonium salt reactions and iodonium salt addition, with the purpose to introduce different functional groups with good degree of functionalization. The scale-up of the production from 5-10 mg to 100-200 mg was also explored, to obtain a large production of functional material, required for the *in vitro* and *in vivo* studies. Through the employment of diazonium compounds and alkali metal intercalated graphene, I obtained multifunctionalised graphene (mf-G), constituted by three orthogonally protected amino group. This material is the first generation of multifunctionalised graphen- based materials.

Finally, the synthesis and applications of a multifunctionality drug delivery platform for cancer therapy application was investigated in Chapter 5. I developed a step-by-step strategy of selective deprotection and functionalization of the introduced amines onto mf-G. The final conjugate presents three different functionalities aimed to increase the efficacy of the anticancer treatment: a) Indocyanine green was introduced as fluorophore to track the platform into the cells; b) Folic acid was employed as targeting agent for cancer cells, bonded to graphene through a long PEG chain to increase the biocompatibility of the material; c) Doxorubicin was covalently linked through an imine bond, cleavable at the typical acidic pH of cancer cells. In collaboration with Dr. Eijiro Miyako at the AIST Tsukuba research center (Japan) I investigated the drug delivery properties on HeLa cells of this multifunctionalities platform.

1.7. Literature

1. Novoselov, K. S. *et al.* Electric field in atomically thin carbon films. *Science (80-.).* **306**, 666–669 (2004).

2. Zhang, Y. Y. & Gu, Y. T. Mechanical properties of graphene: Effects of layer number, temperature and isotope. *Comput. Mater. Sci.* **71**, 197–200 (2013).

3. Cao, Y. *et al.* Unconventional superconductivity in magic-angle graphene superlattices. *Nature* **556**, 43–50 (2018).

4. Bonaccorso, F. *et al.* Graphene, related two-dimensional crystals, and hybrid systems for energy conversion and storage. *Science (80-.).* **347**, 1246501 (2015).

5. Wang, R. *et al.* Graphene based functional devices: A short review. *Front. Phys.* **14**, 13603 (2019).

6. Sint, K., Wang, B. & Král, P. Selective ion passage through functionalized graphene nanopores. *J. Am. Chem. Soc.* **130**, 16448–16449 (2008).

7. Nag, A., Mitra, A. & Mukhopadhyay, S. C. Graphene and its sensor-based applications: A review. *Sensors Actuators, A Phys.* **270**, 177–194 (2018).

8. Bianco, A. *et al.* All in the graphene family - A recommended nomenclature for two-dimensional carbon materials. *Carbon N. Y.* **65**, 1–6 (2013).

9. Popov, I. A., Bozhenko, K. V. & Boldyrev, A. I. Is graphene aromatic? *Nano Res.* **5**, 117–123 (2012).

10. Shearer, C. J., Slattery, A. D., Stapleton, A. J., Shapter, J. G. & Gibson, C. T. Accurate thickness measurement of graphene. *Nanotechnology* **27**, 125704 (2016).

11. Vacchi, I. A., Spinato, C., Raya, J., Bianco, A. & Ménard-Moyon, C. Chemical reactivity of graphene oxide towards amines elucidated by solid-state NMR. *Nanoscale* **8**, 13714–13721 (2016).

12. Pei, S. & Cheng, H. M. The reduction of graphene oxide. *Carbon N. Y.* **50**, 3210–3228 (2012).

13. Reina, G. *et al.* Promises, facts and challenges for graphene in biomedical applications. *Chem. Soc. Rev.* **46**, 4400–4416 (2017).

14. Wick, P. *et al.* Classification framework for graphene-based materials. *Angew. Chemie - Int. Ed.* **53**, 7714–7718 (2014).

15. Cai, J. *et al.* Atomically precise bottom-up fabrication of graphene nanoribbons. *Nature* **466**, 470–473 (2010).

16. Zhang, Y., Zhang, L. & Zhou, C. Review of chemical vapor deposition of graphene and related applications. *Acc. Chem. Res.* **46**, 2329–2339 (2013).

17. Chen, X., Zhang, L. & Chen, S. Large area CVD growth of graphene. *Synth. Met.* **210**, 95–108 (2015).

18. Cai, M., Thorpe, D., Adamson, D. H. & Schniepp, H. C. Methods of graphite exfoliation. *J. Mater. Chem.* **22**, 24992–25002 (2012).

19. Ciesielski, A. & Samorì, P. Graphene via sonication assisted liquid-phase exfoliation. *Chem. Soc. Rev.* **43**, 381–398 (2014).

20. Huo, C., Yan, Z., Song, X. & Zeng, H. 2D materials via liquid exfoliation: a review on fabrication and applications. *Sci. Bull.* **60**, 1994–2008 (2015).

21. Hernandez, Y. *et al.* High-yield production of graphene by liquid-phase exfoliation of graphite. *Nat. Nanotechnol.* **3**, 563–568 (2008).

22. Narayan, R. & Kim, S. O. Surfactant mediated liquid phase exfoliation of graphene. *Nano Converg.* **2**, 20 (2015).

23. Lotya, M. *et al.* Liquid phase production of graphene by exfoliation of graphite in surfactant/water solutions. *J. Am. Chem. Soc.* **131**, 3611–3620 (2009).

24. Ciesielski, A. *et al.* Harnessing the liquid-phase exfoliation of graphene using aliphatic compounds: A supramolecular approach. *Angew. Chemie - Int. Ed.* **53**, 10355–10361 (2014).

25. Wang, X. *et al.* Direct exfoliation of natural graphite into micrometre size few layers graphene sheets using ionic liquids. *Chem. Commun.* **46**, 4487–4489 (2010).

26. Guardia, L. *et al.* High-throughput production of pristine graphene in an aqueous dispersion assisted by non-ionic surfactants. *Carbon N. Y.* **49**, 1653–1662 (2011).

27. Sun, Z., Masa, J., Liu, Z., Schuhmann, W. & Muhler, M. Highly concentrated aqueous dispersions of graphene exfoliated by sodium taurodeoxycholate: Dispersion behavior and potential application as a catalyst support for the oxygen-reduction reaction. *Chem. - A Eur. J.* **18**, 6972–6978 (2012).

28. León, V. *et al.* Few-layer graphenes from ball-milling of graphite with melamine. *Chem. Commun.* **47**, 10936–10938 (2011).

29. Bepete, G. *et al.* Surfactant-free single-layer graphene in water. *Nat. Chem.* **9**, 347–352 (2017).

30. Mao, H. Y. *et al.* Manipulating the electronic and chemical properties of graphene via molecular functionalization. *Prog. Surf. Sci.* **88**, 132–159 (2013).

31. Georgakilas, V., Perman, J. A., Tucek, J. & Zboril, R. Broad Family of Carbon Nanoallotropes: Classification, Chemistry, and Applications of Fullerenes, Carbon Dots, Nanotubes, Graphene, Nanodiamonds, and Combined Superstructures. *Chem. Rev.* **115**, 4744–4822 (2015).

32. Criado, A., Melchionna, M., Marchesan, S. & Prato, M. The Covalent Functionalization of Graphene on Substrates. *Angew. Chemie - Int. Ed.* **54**, 10734–10750 (2015).

33. Ciesielski, A. & Samorì, P. Supramolecular Approaches to Graphene: From Self-Assembly to Molecule-Assisted Liquid-Phase Exfoliation. *Adv. Mater.* **28**, 6030–6051 (2016).

34. Englert, J. M. *et al.* Covalent bulk functionalization of graphene. *Nat. Chem.* **3**, 279–286 (2011).

35. Xia, Z. *et al.* Electrochemical Functionalization of Graphene at the Nanoscale with Self-Assembling Diazonium Salts. *ACS Nano* **10**, 7125–7134 (2016).

36. Lin, T., Zhang, W. De, Huang, J. & He, C. A DFT study of the amination of fullerenes and carbon nanotubes: Reactivity and curvature. *J. Phys. Chem. B* **109**, 13755–13760 (2005).

37. Quintana, M., Vazquez, E. & Prato, M. Organic functionalization of graphene in dispersions. *Acc. Chem. Res.* **46**, 138–148 (2013).

38. Aliofkhazraei, M. *et al. Graphene science handbook: Mechanical and chemical properties*. *Graphene Science Handbook: Mechanical and Chemical Properties* (2016).

39. Sharma, R., Baik, J. H., Perera, C. J. & Strano, M. S. Anomalously large reactivity of single graphene layers and edges toward electron transfer chemistries. *Nano Lett.* **10**, 398–405 (2010).

40. Koehler, F. M., Jacobsen, A., Ensslin, K., Stampfer, C. & Stark, W. J. Selective chemical modification of graphene surfaces: Distinction between single- and bilayer graphene. *Small* **6**, 1125–1130 (2010).

41. Xia, Z. *et al.* Electrochemical Functionalization of Graphene at the Nanoscale with Self-Assembling Diazonium Salts. *ACS Nano* **10**, 7125–7134 (2016).

42. Jin, Z. *et al.* Click chemistry on solution-dispersed graphene and monolayer CVD graphene. *Chem. Mater.* **23**, 3362–3370 (2011).

43. Dasler, D. *et al.* Direct Covalent Coupling of Porphyrins to Graphene. *J. Am. Chem. Soc.* **139**, 11760–11765 (2017).

44. Ménard-Moyon, C., Fabbro, C., Prato, M. & Bianco, A. One-pot triple functionalization of carbon nanotubes. *Chem. - A Eur. J.* **17**, 3222–3227 (2011).

45. Prato, M. & Maggini, M. Fulleropyrrolidines: A Family of Full-Fledged Fullerene Derivatives. *Acc. Chem. Res.* **31**, 519–526 (1998).

46. Quintana, M. *et al.* Functionalization of graphene via 1,3-dipolar cycloaddition. *ACS Nano* **4**, 3527–3533 (2010).

47. Hirsch, A., Englert, J. M. & Hauke, F. Wet chemical functionalization of graphene. *Acc. Chem. Res.* **46**, 87–96 (2013).

48. Pénicaud, A. & Drummond, C. Deconstructing graphite: Graphenide solutions. *Acc. Chem. Res.* **46**, 129–137 (2013).

49. Vecera, P., Edelthalhammer, K., Hauke, F. & Hirsch, A. Reductive arylation of graphene: Insights into a reversible carbon allotrope functionalization reaction. *Phys. Status Solidi Basic Res.* **251**, 2536–2540 (2014).

50. Abellán, G. *et al.* Unifying Principles of the Reductive Covalent Graphene Functionalization. *J. Am. Chem. Soc.* **139**, 5175–5182 (2017).

51. Hodge, S. A. *et al.* Chemical routes to discharging graphenides. *Nanoscale* **9**, 3150–3158 (2017).

52. Hadad, C. *et al.* Positive graphene by chemical design: Tuning supramolecular strategies for functional surfaces. *Chem. Commun.* **50**, 885–887 (2014).

53. Knirsch, K. C., Schäfer, R. A., Hauke, F. & Hirsch, A. Mono- and Ditopic Bisfunctionalization of Graphene. *Angew. Chemie - Int. Ed.* **55**, 5861–5864 (2016).

54. Bertolazzi, S. *et al.* Exploring flatland: AFM of mechanical and electrical properties of graphene, MoS2 and other low-dimensional materials. *Microsc. Anal.* **27**, 21–24 (2013).

55. Meyer, J. C. Transmission electron microscopy (TEM) of graphene. in *Graphene: Properties, Preparation, Characterisation and Devices* 101–123 (Elsevier, 2014). doi:10.1533/9780857099334.2.101

56. Eckmann, A., Felten, A., Verzhbitskiy, I., Davey, R. & Casiraghi, C. Raman study on defective graphene: Effect of the excitation energy, type, and amount of defects. *Phys. Rev. B - Condens. Matter Mater. Phys.* **88**, 1–11 (2013).

57. Ferrari, A. C. *et al.* Raman Spectrum of Graphene and Graphene Layers. *Phys. Rev. Lett.* **97**, 187401 (2006).

58. Vacchi, I. A., Spinato, C., Raya, J., Bianco, A. & Ménard-Moyon, C. Chemical reactivity of graphene oxide towards amines elucidated by solid-state NMR. *Nanoscale* **8**, 13714–13721 (2016).

59. Li, Y. *et al.* Graphene microsheets enter cells through spontaneous membrane penetration at edge asperities and corner sites. *Proc. Natl. Acad. Sci. U. S. A.* **110**, 12295–12300 (2013).

60. Kurapati, R. *et al.* Degradation of Single-Layer and Few-Layer Graphene by Neutrophil Myeloperoxidase. *Angew. Chemie - Int. Ed.* **57**, 11722–11727 (2018).

61. Gurunathan, S. & Kim, J. H. Synthesis, toxicity, biocompatibility, and biomedical applications of graphene and graphene-related materials. *Int. J. Nanomedicine* **11**, 1927–1945 (2016).

62. Kohane, D. S. & Langer, R. Biocompatibility and drug delivery systems. *Chemical Science* **1**, 441–446 (2010).

63. Fadeel, B. *et al.* Safety Assessment of Graphene-Based Materials: Focus on Human Health and the Environment. *ACS Nano* **12**, 10582–10620 (2018).

64. Liao, K. H., Lin, Y. S., MacOsko, C. W. & Haynes, C. L. Cytotoxicity of graphene oxide and graphene in human erythrocytes and skin fibroblasts. *ACS Appl. Mater. Interfaces* **3**, 2607–2615 (2011).

65. Yang, K. *et al.* In vivo pharmacokinetics, long-term biodistribution, and toxicology of pegylated graphene in mice. *ACS Nano* **5**, 516–522 (2011).

66. Hong, B. J., Compton, O. C., An, Z., Eryazici, I. & Nguyen, S. T. Successful stabilization of graphene oxide in electrolyte solutions: Enhancement of biofunctionalization and cellular uptake. *ACS Nano* **6**, 63–73 (2012).

67. Liu, Z., Robinson, J. T., Sun, X. & Dai, H. PEGylated nanographene oxide for delivery of water-insoluble cancer drugs. *J. Am. Chem. Soc.* **130**, 10876–10877 (2008).

68. Kagan, V. E. *et al.* Carbon nanotubes degraded by neutrophil myeloperoxidase induce less pulmonary inflammation. *Nat. Nanotechnol.* **5**, 354–359 (2010).

69. Kotchey, G. P. *et al.* The enzymatic oxidation of graphene oxide. *ACS Nano* **5**, 2098–2108 (2011).

70. Li, Y. *et al.* Surface coating-dependent cytotoxicity and degradation of graphene derivatives: Towards the design of non-toxic, degradable nano-graphene. *Small* **10**, 1544–1554 (2014).

71. Kurapati, R. *et al.* Dispersibility-Dependent Biodegradation of Graphene Oxide by Myeloperoxidase. *Small* **11**, 3985–3994 (2015).

72. Girish, C. M., Sasidharan, A., Gowd, G. S., Nair, S. & Koyakutty, M. Confocal raman imaging study showing macrophage mediated biodegradation of graphene in vivo. *Adv. Healthc. Mater.* **2**, 1489–1500 (2013).

73. Liu, L. *et al.* Oxidation and degradation of graphitic materials by naphthalene-degrading bacteria. *Nanoscale* **7**, 13619–13628 (2015).

74. Zhang, D. *et al.* The short- and long-term effects of orally administered high-dose reduced graphene oxide nanosheets on mouse behaviors. *Biomaterials* **68**, 100–113 (2015).

75. Li, B. *et al.* Biodistribution and pulmonary toxicity of intratracheally instilled graphene oxide in mice. *NPG Asia Mater.* **5**, e44–e44 (2013).

76. Mao, L., Hu, M., Pan, B., Xie, Y. & Petersen, E. J. Biodistribution and toxicity of radio-labeled few layer graphene in mice after intratracheal instillation. *Part. Fibre Toxicol.* **13**, 7 (2016).

77. Qu, G. *et al.* The ex vivo and in vivo biological performances of graphene oxide and the impact of surfactant on graphene oxide's biocompatibility. *J. Environ. Sci. (China)* **25**, 873–881 (2013).

78. Wen, K. P. *et al.* Accumulation and toxicity of intravenously-injected functionalized graphene oxide in mice. *J. Appl. Toxicol.* **35**, 1211–1218 (2015).

79. Syama, S., Paul, W., Sabareeswaran, A. & Mohanan, P. V. Raman spectroscopy for the detection of organ distribution and clearance of PEGylated reduced graphene oxide and biological consequences. *Biomaterials* **131**, 121–130 (2017).

80. Li, B. *et al.* Influence of polyethylene glycol coating on biodistribution and toxicity of nanoscale graphene oxide in mice after intravenous injection. *Int. J. Nanomedicine* **9**, 4697–4707 (2014).

81. Jasim, D. A., Ménard-Moyon, C., Bégin, D., Bianco, A. & Kostarelos, K. Tissue distribution and urinary excretion of intravenously administered chemically functionalized graphene oxide sheets. *Chem. Sci.* **6**, 3952–3964 (2015).

82. Jasim, D. A. *et al.* Thickness of functionalized graphene oxide sheets plays critical role in tissue accumulation and urinary excretion: A pilot PET/CT study. *Appl. Mater. Today* **4**, 24–30 (2016).

83. Sasidharan, A. *et al.* Comparative in vivo toxicity, organ biodistribution and immune response of pristine, carboxylated and PEGylated few-layer graphene sheets in Swiss albino mice: A three month study. *Carbon N. Y.* **95**, 511–524 (2015).

84. Sharma, K. Nanomaterials for drug delivery. in *Advances in Personalized Nanotherapeutics* 57–77 (Springer International Publishing, 2017). doi:10.1007/978-3-319-63633-7_5

85. Clemons, T. D. *et al.* Distinction between Active and Passive Targeting of Nanoparticles Dictate Their Overall Therapeutic Efficacy. *Langmuir* **34**, 15343–15349 (2018).

86. Servant, A., Bianco, A., Prato, M. & Kostarelos, K. Graphene for multifunctional synthetic biology: The last 'zeitgeist' in nanomedicine. *Bioorganic Med. Chem. Lett.* **24**, 1638–1649 (2014).

87. Chen, Y. W., Su, Y. L., Hu, S. H. & Chen, S. Y. Functionalized graphene nanocomposites for enhancing photothermal therapy in tumor treatment. *Adv. Drug Deliv. Rev.* **105**, 190–204 (2016).

88. Dhas, N. *et al.* Two dimensional carbon based nanocomposites as multimodal therapeutic and diagnostic platform: A biomedical and toxicological perspective. *J. Control. Release* **308**, 130–161 (2019).

89. Russier, J. *et al.* Few-Layer Graphene Kills Selectively Tumor Cells from Myelomonocytic Leukemia Patients. *Angew. Chemie - Int. Ed.* **56**, 3014–3019 (2017).

90. Zhang, L. *et al.* Enhanced chemotherapy efficacy by sequential delivery of siRNA and anticancer drugs using PEI-grafted graphene oxide. *Small* **7**, 460–464 (2011).

91. Kim, H., Lee, D., Kim, J., Kim, T. Il & Kim, W. J. Photothermally triggered cytosolic drug delivery via endosome disruption using a functionalized reduced graphene oxide. *ACS Nano* **7**, 6735–6746 (2013).

92. Golberg, D. *et al.* Boron nitride nanotubes and nanosheets. *ACS Nano* **4**, 2979–2993 (2010).

93. Paciĺ, D., Meyer, J. C., Girit, Ç. & Zettl, A. The two-dimensional phase of boron nitride: Few-atomic-layer sheets and suspended membranes. *Appl. Phys. Lett.* **92**, 1–4 (2008).

94. Wang, Z. *et al.* Fabrication of Boron Nitride Nanosheets by Exfoliation. *Chem. Rec.* 1204–1215 (2016). doi:10.1002/tcr.201500302

95. Fu, L., Lai, G., Chen, G., Lin, C. Te & Yu, A. Microwave Irradiation-Assisted Exfoliation of Boron Nitride Nanosheets: A Platform for Loading High Density of Nanoparticles. *ChemistrySelect* **1**, 1799–1803 (2016).

96. Li, L. H. *et al.* Large-scale mechanical peeling of boron nitride nanosheets by low-energy ball milling. *J. Mater. Chem.* **21**, 11862–11866 (2011).

97. Rafiei-Sarmazdeh, Z., Jafari, S. H., Ahmadi, S. J. & Zahedi-Dizaji, S. M. Large-scale exfoliation of hexagonal boron nitride with combined fast quenching and liquid exfoliation strategies. *J. Mater. Sci.* **51**, 3162–3169 (2016).

98. Li, L. H., Cervenka, J., Watanabe, K., Taniguchi, T. & Chen, Y. Strong oxidation resistance of atomically thin boron nitride nanosheets. *ACS Nano* **8**, 1457–1462 (2014).

99. Backes, C. *et al.* Guidelines for exfoliation, characterization and processing of layered materials produced by liquid exfoliation. *Chem. Mater.* **29**, 243–255 (2017).

100. Lahiri, D. *et al.* Boron nitride nanotube reinforced hydroxyapatite composite: Mechanical and tribological performance and in-vitro biocompatibility to osteoblasts. *J. Mech. Behav. Biomed. Mater.* **4**, 44–56 (2011).

101. Weng, Q. *et al.* Highly water-soluble, porous, and biocompatible boron nitrides for anticancer drug delivery. *ACS Nano* **8**, 6123–6130 (2014).

102. Weng, Q., Wang, X., Wang, X., Bando, Y. & Golberg, D. Functionalized hexagonal boron nitride nanomaterials: Emerging properties and applications. *Chem. Soc. Rev.* **45**, 3989–4012 (2016).

103. Chen, X. *et al.* Boron nitride nanotubes are noncytotoxic and can be functionalized for interaction with proteins and cells. *J. Am. Chem. Soc.* **131**, 890–891 (2009).

104. Kodali, V. K. *et al.* Acute in vitro and in vivo toxicity of a commercial grade boron nitride nanotube mixture. *Nanotoxicology* **11**, 1040–1058 (2017).

105. Augustine, J. *et al.* Assessing size-dependent cytotoxicity of boron nitride nanotubes using a novel cardiomyocyte AFM assay. *Nanoscale Adv.* **1**, 1914–1923 (2019).

106. Mateti, S. *et al.* Biocompatibility of boron nitride nanosheets. *Nano Res.* **11**, 334–342 (2018).

107. Kurapati, R., Backes, C., Ménard-Moyon, C., Coleman, J. N. & Bianco, A. White Graphene undergoes Peroxidase Degradation. *Angew. Chemie - Int. Ed.* **55**, 5506–5511 (2016).

CHAPTER 2. 2D MATERIAL PRODUCTION

2.1. Introduction

Production of 2D materials in water is of crucial importance for the exploration of their biological effects. The use of surfactants is needed to increase the water dispersibility and to decrease the hydrophobicity of their surface. Moreover, the surfactants employed should be biocompatible, in order to avoid any side-toxicity effects due to the release of these molecules inside a body. Since now, most of the compounds employed for the exfoliation in water are belong to the surfactant family, constituted by long aliphatic chains terminated by a hydrophilic head. Unfortunately, these compounds are not fully biocompatible and cannot be employed for *in vitro* and *in vivo* investigations. On the other side, the use of organic molecules or proteins can increase the biocompatibility (or decrease the toxicity) of 2D materials through the covering of the surface, the lowering of the hydrophobic interactions, the increasing of the stability and the decreasing of re-aggregation in the media. Different techniques can be employed to enhance the layer intercalation by organic molecules, like bath sonication or ball milling (see section 1.2).

2.2. Objectives of this chapter

This chapter covers the production of boron nitride and graphene in water to investigate their cytotoxicity. I investigated the exfoliation of these materials with different families of organic molecules, such as rhodamine dyes, vitamins and bodipy derivatives. As mentioned in paragraph 1.4 one important parameter, that is often missing in the published studies, is a comparison of the dimension of the particles of the same material. For this reason, we focused our attention on the obtaining of dispersions of graphene and boron nitride with different lateral size, to investigate and compare the size effect on cells. To achieve this goal, I employed technique of ultra-centrifugation on raw dispersions of the different materials.

Regarding boron nitride I have investigated the exfoliation of different sources of BN, to obtain particles with different size and shape, to well compare their cytotoxicity based on these parameters.

For graphene, I have investigated the use of different organic molecules and applied techniques of size selection. The main purpose was to obtain a high amount of stable dispersions to test *in vivo* the toxicity of the material. Moreover, with the aim of improving the features of graphene sheets and study the internalization in cells, I have employed strong fluorescent molecules for the exfoliation of the sheets, in order to make graphene fluorescent and trackable by fluorescent microscopy techniques.

A complete understanding of the parameters impacting on cells viability is important for the development of materials for nanomedicine. Knowledge about the size and effects of the functional group are also very important to focus the scientific efforts on the most suitable materials for specific therapeutic applications.

2.3. Results and discussion: Graphene

2.3.1. Exfoliation of graphene with riboflavin-5'-phosphate sodium salt

Many organic molecules are able to exfoliate graphene in water, as sodium dodecyl benzene sulfonate and sodium dodecyl sulfate,[1] melamine,[2] etc. The main problem of these molecules is their cytotoxicity. One of the first studies on the exfoliation of graphene with vitamins has been reported by Tascón and co-workers,

employing riboflavin-5'-phosphate sodium salt (Rib) (Figure 2.1), as exfoliating agent and surfactant for graphene sheets.[3] In this study, the group has obtained highly concentrated graphene dispersions in water through bath sonication of graphite in a solution of Rib. The surfactant was demonstrated to be strongly adsorbed on graphene surface. The authors exploited the negative charge of the phosphate group to functionalize the hydrophilic tail of the molecule with metal nanoparticles for catalysis. Rib is obtained by the natural conversion of vitamin B2by two coenzymes, flavin mononucleotide (FMN) and flavin adenine dinucleotide (FAD), perfectly biocompatible and non-toxic.

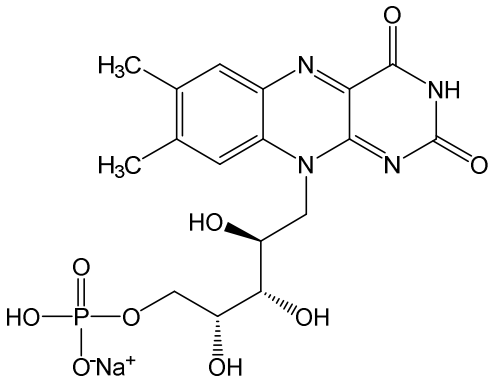

Figure 2.1: Riboflavin-5'-phosphate sodium salt.

Thanks to its biocompatibility and stability on the graphene surface, Rib could be a suitable surfactant to produce graphene and explore its toxicity. I decided first to produce graphene in water using Rib, to study the material obtained. A small modification of the protocol described in the mentioned study has been applied to obtain graphene dispersion (G-Rib) (see methods in paragraph 2.6). After centrifugation and redispersion the concentration obtained was ~2 mg/mL, without the formation of visible aggregate in the dispersion along 1 month. The suspension of the exfoliated graphene was then characterized using different complementary analytical and microscopic techniques. TEM micrographs showed individual sheets with an average size of ~840 nm (Figure 2.2a). The lateral size distribution was calculated from TEM images by measuring at least 300 sheets of graphene. The histogram of this distribution, with ranging values between 200 and 1800 nm, is shown in Figure 2.2b. HR-TEM micrographs allowed the calculation of the number of layers on G-Rib sheets (Figure 2.2c). An average of 5 layers per sheet was observed and ~80% of sheets contain less than 10 layers, confirming the few-layer nature of the material (Figure 2.2d).[4] This result is consistent with other previous studies that reported the successful exfoliation of graphene in water.[5,6] Raman spectroscopy showed sheets with good quality and a low amount of defects, with an average I_D/I_G ratio of ~0.28 (Figure 2.2e). The stability of the dispersion was monitored by ζ potential measurements at different pH, showing high stability of the sheets between pH 4 and 12. In this range of pH the material showed a strongly negative surface charge (-40 to -50 mV), which is indicative of a colloidal suspension suitable for carrying out different tests in a biological environment (Figure 2.2f).

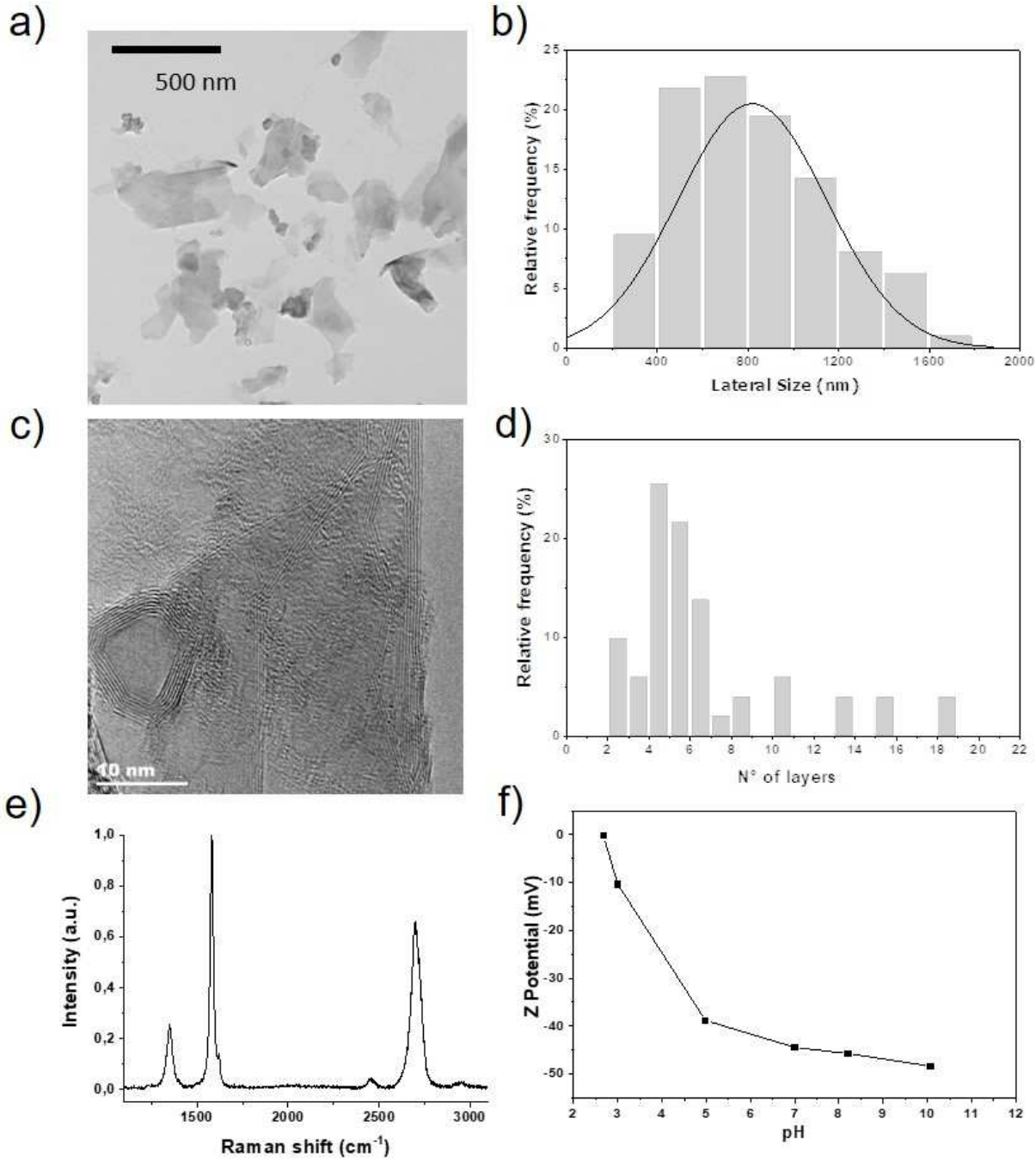

Figure 2.2: a) TEM image of a representative graphene sheet; b) Histogram of lateral size distribution of G-Rib sheets by TEM; c) HR-TEM of graphene sheets; d) Histogram of numbers of layers evaluated by HR-TEM; e) Raman spectra of G-Rib sheet; f) Evolution of ζ potential.

The quantity of riboflavin adsorbed onto the graphene surface was calculated from the percentage of nitrogen measured by elemental analysis. The result showed that the dispersion of G-Rib contains 7% weight of riboflavin, corresponding to roughly 1.9×10^{-4} mol/g, a lower amount respect to what reported since now for the surfactant-assisted exfoliation of graphite.[7]

2.3.1.1. *In vitro* and *in vivo* studies

Very important for to carry out the cytotoxicity studies is the stability of G-Rib in the different media. The sheets resulted not stable in PBS, where after less than one hour re-aggregation is occurring, leading to sedimentation. This behavior is probably due to the high presence of the salts in PBS that can interact with

the anionic part of Rib, decreasing the interaction with graphene surface and leading to the detachment of the surfactant. Opposite, when G-Rib is dispersed in cell culture media the sheets resulted stable for more than 24 hours without the formation of aggregates. This stability is desired to perform *in vitro* cytotoxicity studies. The non-stability of the particles in PBS is a problem in the perspective of *in vivo* studies because PBS is the common medium employed for the injection of drugs and nanomaterials in live organisms. We then focused our attention on other media, finding that the more suitable for our purpose is a 5% solution of dextrose in water. In this solution the particles are stables for more than 24 hours and are not showing aggregation up to a concentration of 2mg/mL.

The *in vitro* and *in vivo* impact of G-Rib was evaluated in collaboration with two biologists of our group, Dr. Diane Murera and Dr. Amalia Ruiz Estrada. The cytotoxicity of the material was evaluated through the degree of cell survival by flow cytometry. We used HeLa cells as both non-phagocytic epithelial and cancer cell model and Raw 264.7 macrophages as immune and phagocytic model. Interestingly, the cell survival after 24-hour incubation with the G-Rib up to 300 µg/mL showed very low toxicity in the cells. Our results showed that G-Rib was slightly less toxic for Raw 264.7 macrophages compared to HeLa cells (Figure 2.3). Nevertheless, overall the values of survival were always above 85% for the graphene. A solution containing the same percentage of riboflavin on FLG determined by elemental analysis was used as a control to assess a possible impact of the surfactant used in the exfoliation of the graphene. As expected, this natural molecule had no statistically significant effect on both cell lines.

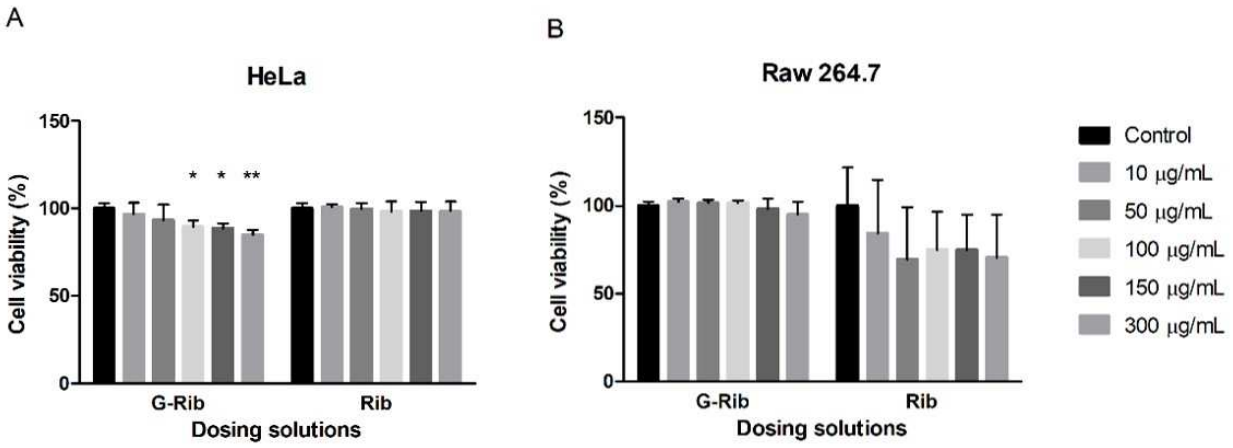

Figure 2.3: Evaluation of cell viability by flow cytometry. (A) HeLa cells; (B) Raw 264.7 cells. The cells were treated with G-Rib and a solution of riboflavin used as control for 24 hours. Data represent means ± SD (n = 3). (Two-way ANOVA followed by Bonferroni's post-test: ns p>0.05, *p<0.05, **p<0.01, ***p<0.001, ****p<0.0001).

We then have evaluated the biological impact of G-Rib after a single intravenous administration in mice. G-Rib was injected intravenously at two dose levels: 5 (~100 µg/mouse) and 15 mg/kg (~300 µg/mouse) body weight. After the injection of the two G-Rib suspensions, clinical observations were performed daily up to 30 days. The experiments finished with a 100% of survival, and no general signs of toxicity (*e.g.* seizures, disheveled hair, irregular respiration, gastrointestinal symptoms, immobility, convulsions, severe decubitus paralysis or death) or dose-related effects were observed in the mice. During macroscopic evaluation of the organs, no pathological changes were observed. To our surprise, the color of liver, kidneys, lungs and spleen retained their dark pink color without changes compared to the untreated control. After 24 h post-injection, brown areas were found into the liver and the kidneys. Regarding the kidney, we could not find large aggregates, suggesting no high accumulation in this tissue (Figure 2.4). Dark brown dots, likely corresponding

to aggregated nanomaterial, were found in the liver 30 days after administration. Furthermore, no organ damage or other structural changes were observed in all examined organs at any time point.

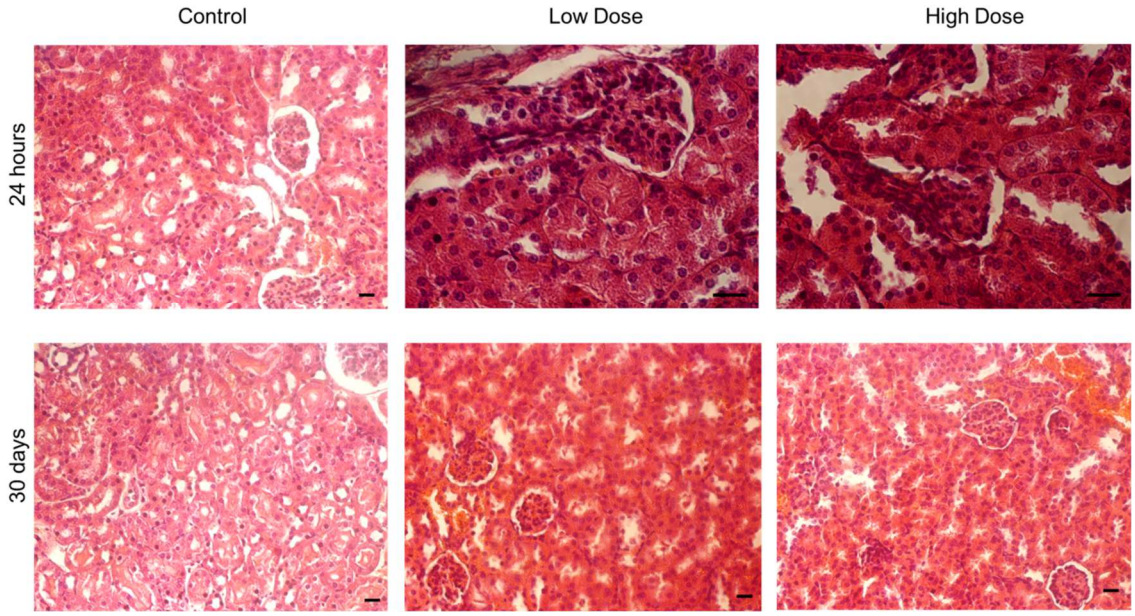

Figure 2.4: Haematoxylin-eosin staining of kidney sections from control or G-Rib-treated mice (Low dose 5 mg/kg body weight and high dose 15 mg/kg body weight) at different times post-administration. Bar: 20 µm.

Overall, G-Rib showed accumulation in the mouse liver and possibly the spleen, which are reticuloendothelial systems (RES) responsible for the clearance of foreign materials by macrophages. Those findings are in good agreement with the reported biodistribution for other graphene-related materials.[8,9] To assess the general toxicity of G-Rib, a complete biochemical analysis and selected haematological parameters of blood samples were measured after the intravenous administration of the material. Blood samples were collected at 24 h, 15 and 30-days post-administration. Normal values across the study were obtained for the serum levels of aspartate transaminase (AST), alanine aminotransferase (ALT), alkaline phosphatase (ALP), and creatinine as an expression of the correct function of the liver. Furthermore, normal levels of urea and creatinine confirmed no toxicological effects on renal function. All the haematological parameters remained within the reference range showing no haematotoxicity compared to the control, which makes this material highly promising for biomedical applications through intravenous administration.

2.3.1.2. Size selection of G-Rib dispersion

The comparison of the effects of graphene dispersion with different lateral size is very important for the understanding of the desired properties of this material in biomedicine. In this perspective, I focused my attention on the size selection of the obtained dispersion of G-Rib. Various are the methodologies to select particles with different size. Techniques are including decantation of the particles during the time, exclusion chromatography[10] or ultra-centrifugation.[11] Due to a common instrumentation required and the easily scalable production, I decided to apply the ultra-centrifugation method to my dispersions. After obtaining the first dispersion described before, with lateral size distribution between 200 nm and 1600 nm (Figure 2.2b), the increase of the centrifugation speed was needed to obtain better separation of the sheets. The raw G-Rib dispersion was therefore centrifuged at different step from high speed (8000g) to low speed (500 g) (Figure 2.5). After every centrifugation, the supernatant was recovered, and a fresh solution of Rib was added to the precipitate for the redispersion of the particles (see methods at paragraph 2.6). As expected, the lateral size of the obtained dispersions was increasing at the decreasing of the centrifugation speed (summarized in Table 2.1). The distribution of the particles is partially superposed between the dispersion,

probably due to the aggregation of the bigger sheets during the centrifugation process and the high concentration of the dispersions. The increasing of the centrifugation time or of the number of centrifugation steps could help to obtain more separated distributions.

Centrifugation speed (g)	Mean (nm)	Median (nm)	Minimum (nm)	Maximum (nm)
500	1032	979	440	2525
2000	608	561	204	1846
5000	351	331	90	841
8000	173	164	60	317

Table 2.1: Summary of the centrifugation condition and average lateral size of the obtained dispersions.

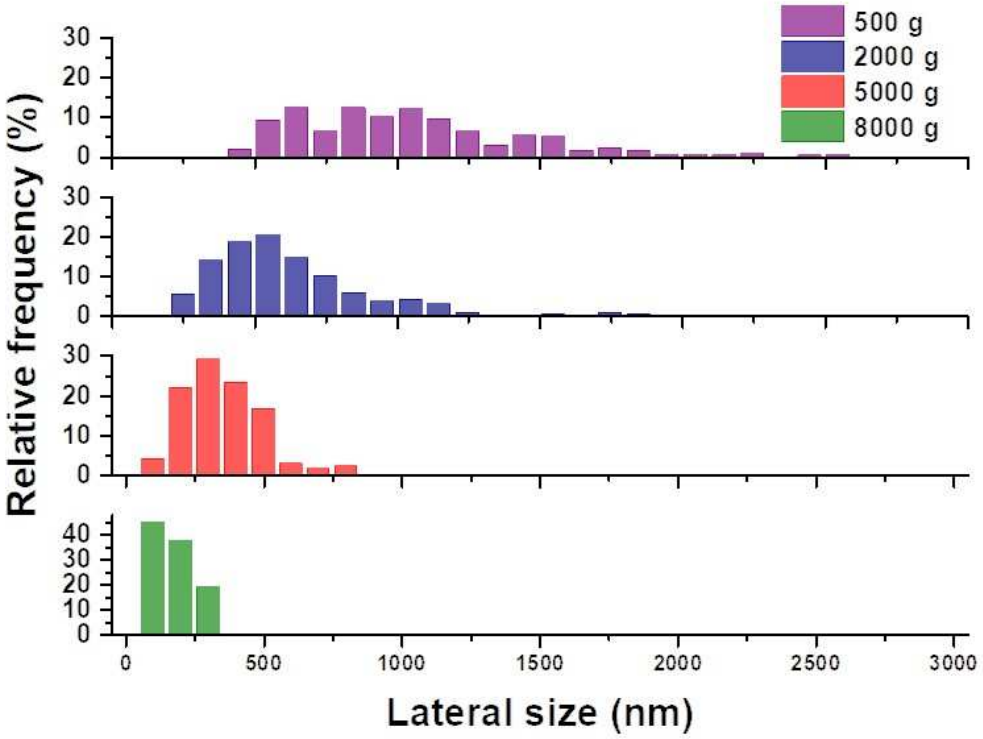

Figure 2.5: Histogram of the lateral size distribution of G-Rib dispersion obtained after centrifugation.

With the aim of investigating the effect of the lateral size of graphene, in collaboration with the group of Prof. K. Kostarelos and Dr. Cyrill Bussy in Manchester, we selected the dispersion 500g (L-FLG) and 5000g (S-FLG) to perform *in vivo* studies. Different groups of mice were exposed to a pharyngeal aspiration of the graphene dispersions. The animals were sacrificed after 1, 7 and 28 days. Histopathological analysis and Raman mapping were carried out to understand the localization of the sheets on the lungs and the spleen. The lungs have been analyzed also to evaluate the DNA damages, the inflammatory response, the oxidative stress and the tissue damages. The histopathology of the lung analysis (Figure 2.6) shows that after 1 day from the exposure is evident the influx of inflammatory cells, while the lung recovery is still ongoing after 7 days from the exposure. After one month a clear recovery, after a typical acute inflammatory response to foreign materials, was demonstrated. This suggests that few-layer graphene is not inducing persistent inflammation and will unlikely cause adverse effects to the lungs (such as fibrosis) at later time point. This statement is supported by the limited but existing persistence of materials in the lungs after 1 month.

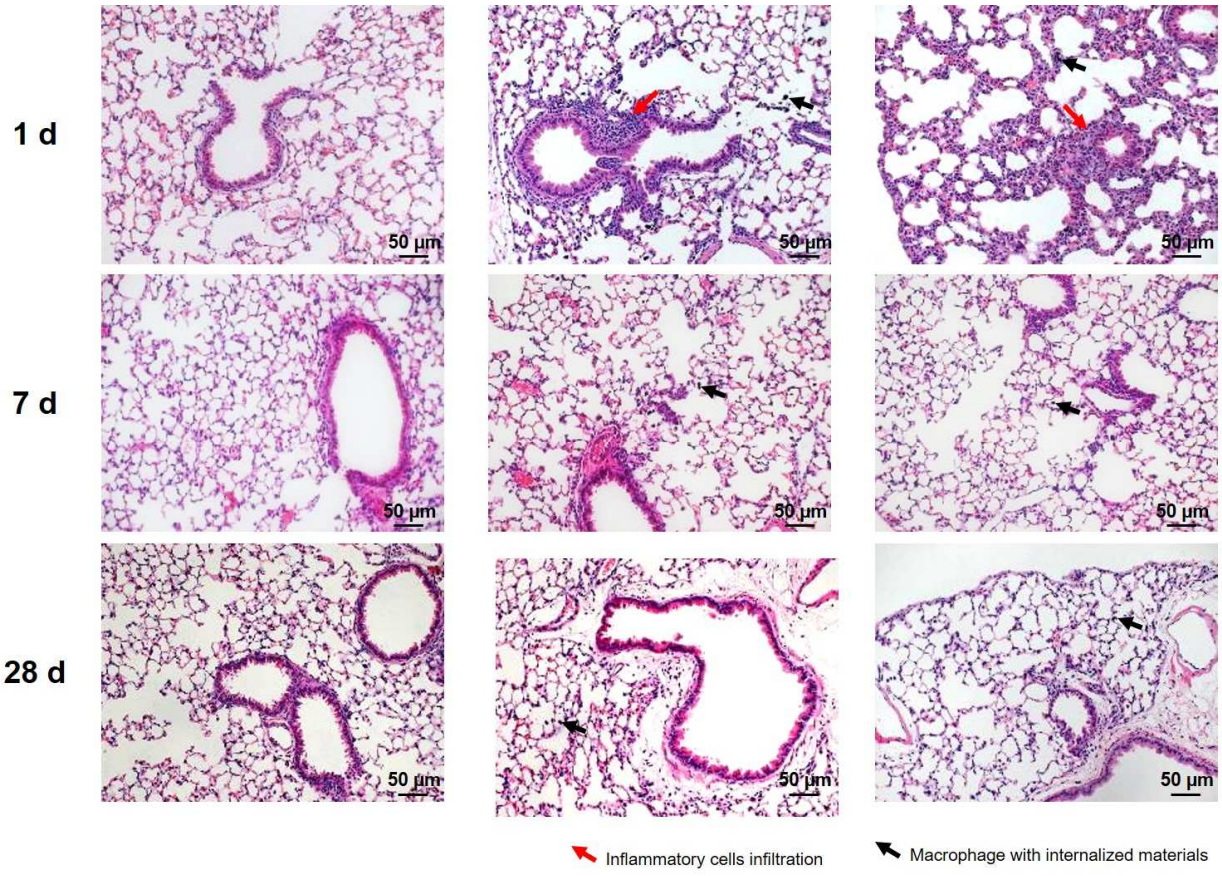

Figure 2.6: Histopathology of the lungs. Red arrows are indicating inflammatory cells infiltration, black arrows are indicating macrophage with internalized material.

The inflammatory response has been investigated also by bronchoalveolar lavage (BAL) cytology. This technique explores large areas of the alveolar compartment providing cells as well as non-cellular constituents from the lower respiratory tract. Alterations in BAL fluid and cells reflect pathological changes in the lung parenchyma and is exploited in diagnostic workup of infectious and non-infectious interstitial lung diseases. From the BAL fluid analysis of the materials we confirmed the behavior observed from the histopathology. A significant pro-inflammatory response is evident after 1 day, whereas after 7 days the recovery is still ongoing and after 28 days only few inflammatory cells remained in the alveolar space. Macrophages with internalized materials are still observed after 28 days from the exposure (Figure 2.7).

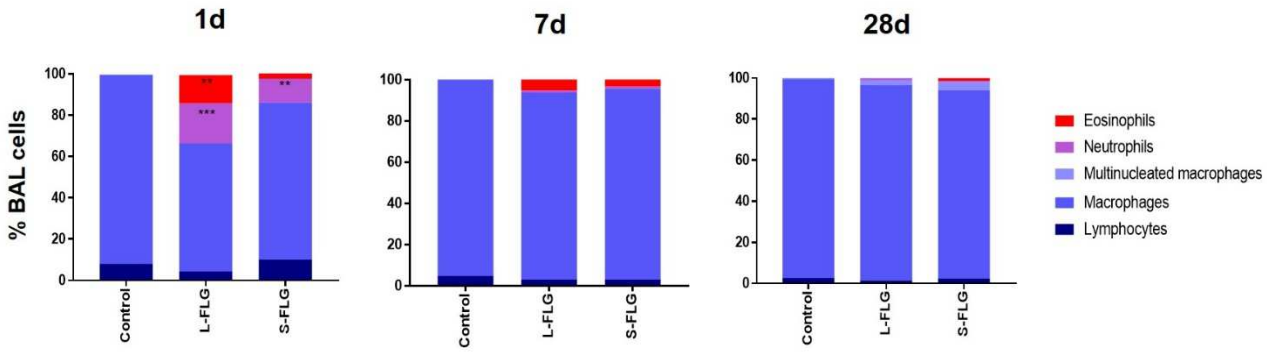

Figure 2.7: Histograms of bronchoalveolar lavage results after 1, 7 and 28 days from the graphene exposure.

The BAL analysis provided important results about the impact of the lateral size dimension of the particles. A size-dependent inflammatory response was observed. The higher impact was observed for the largest

materials compared to the smallest graphene dispersion. These observations are in agreement with similar studies carried out by the same group on GO with different lateral size and could be helpful for a generalization on the impact of the lateral size of these materials in the organisms.

2.3.2. Exfoliation of graphene with other vitamins

The purpose of this work was to find new organic molecules able to intercalate graphene layers and stabilize the sheets in water solution. An important role is played by the properties of these molecules that could allow other functionalization, stability at extreme pH, endowing of new features on graphene, such as fluorescence or catalytic activities. The screening of all possible biocompatible or natural molecules able to exfoliate graphene could require years because of the enormous variety of existing compounds. Many considerations could be extrapolated from the analysis of the Rib structure, reducing the quantity of interesting molecules. Looking at the properties of G-Rib, we observed a strong absorption of the molecule on the graphene surface, at pH > 3, and great stability of the sheets in different media. Rib structure can be divided into two main parts, one aromatic/hydrophobic and one hydrophilic (Figure 2.8).

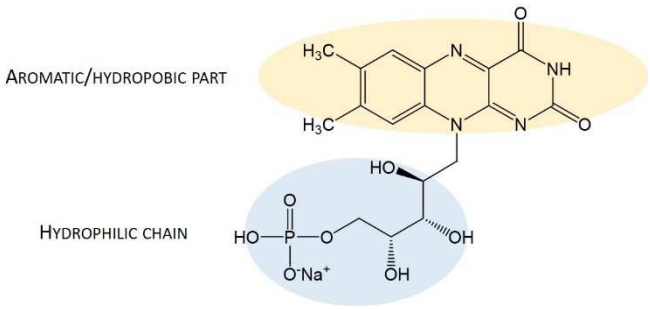

Figure 2.8: Schematic representation of Rib structure.

The aromatic moiety is the one responsible for the strong absorption onto the graphene surface. Through hydrophobic and π-π stacking interaction and thanks to the planar chemical structure, the interactions with the graphene surface are favorable and maximized. Moreover, the water stabilization is given by the hydrophilic chain and the negative charge of the phosphate group is generating electric repulsion between the sheets, avoiding the reaggregation. On the light of these considerations, I looked at water-soluble organic molecules, with a structure similar to riboflavin and especially to vitamins and other biocompatible molecules. As first I selected thiamine mononitrate, methylene blue and vitamin C (Figure 2.9).

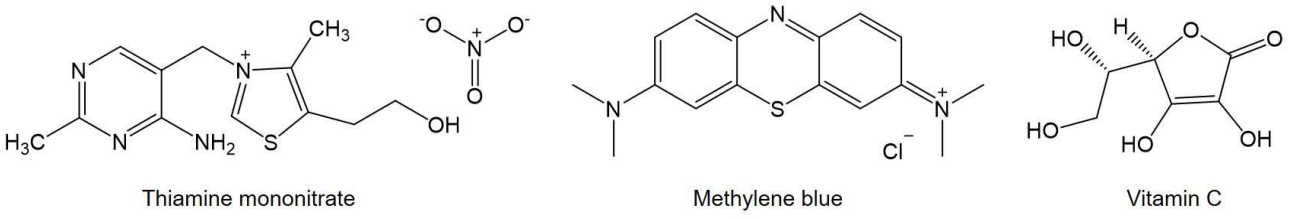

Figure 2.9: Molecules employed for graphene exfoliation.

The aromatic structure of the first two molecules, their high water solubility and the charge present on the structure are favorable features for the intercalation and stabilization of graphene sheets. The exfoliation of graphene has been carried out in similar condition of G-Rib, by bath sonication in a water solution of the selected molecules (1 mg/mL). The results obtained in the three cases were different. Thiamine and vitamin C were not able to stabilize graphene suspension, and few hours after the sonication all the particles were

deposited at the bottom of the vials. The selection of the most stable sheets by centrifugation was not applied in this case because of the clear instability of the suspensions. The suspension obtained with methylene blue remained stable for many hours after sonication. The particles were separated by centrifugation at 1500 g, filtered and washed with water to remove the excess of surfactant. Unfortunately, after redispersion in water, the sheets result to be not stable and precipitate after few hours. Despite the similar structure of riboflavin and the presence of a hydrophilic chain, the selected molecules were not able to stabilize graphene in water.

2.3.3. Exfoliation with rhodamine molecules

On the light of previous results, I decide to move to a different kind of molecules. I selected the rhodamine family, whose chemical structure is more similar to riboflavin and present interesting properties. In low quantity, rhodamine does not have cytotoxic effects and could be suitable as surfactants. Moreover, rhodamine molecules are well-known as strong fluorescent molecules, employed as typical dyes for fluorescence imaging.[12] The purpose of using rhodamine was not only to discover new exfoliating agents for graphene to improve the production of this material in water, but also to exploit the strong fluorescence of this molecule, to explore the opportunity of the obtaining of graphene with new fluorescent properties. The critical point of this approach is the quenching effect of the fluorescence by graphene. Indeed, graphene is participating in phenomena of electron transfer (ET). The material can act as donor or acceptor of electrons in chemical reactions or with molecules in contact with its surface. The ET has been investigated as new synthetic route for the functionalization of graphene and is as well-known as the cause of the fluorescence quenching of the organic molecules in closed contact.[13,14] This properties could quench the fluorescence of the molecules adsorbed on the surface despite their strong fluorescence. To start my investigation, I selected rhodamine b (R_b), rhodamine b base (R_{bb}) and rhodamine 6G (R_{6G}) (Figure 2.10).

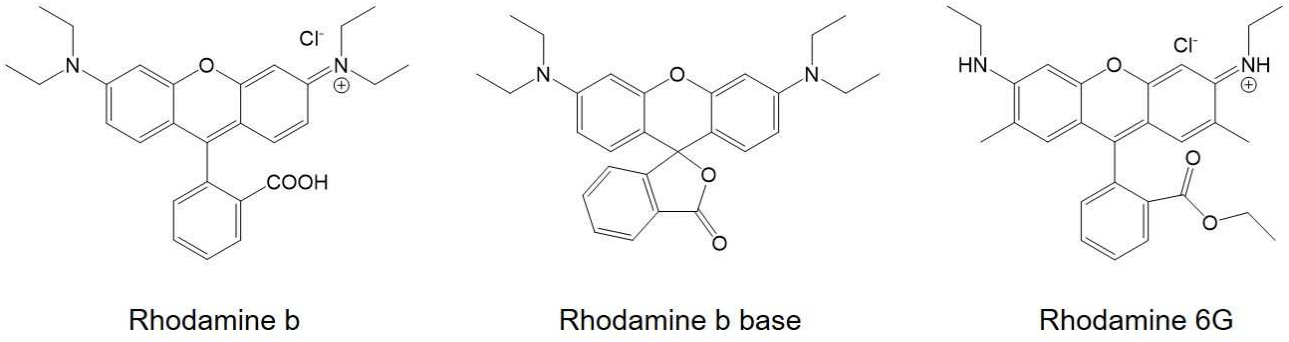

Figure 2.10: Rhodamine molecules tested for graphene exfoliation.

The structures of rhodamine b and b base are very similar. Actually, they are chemical isomers in tautomeric equilibrium between the two forms. The direction of the equilibrium depends on the pH, the solvent, the temperature and the presence of anions.[15,16] The lactone form of rhodamine b base is colourless and the equilibrium is completely moved to this form in non-protic solvents. The zwitterionic form (rhodamine b) is the only present in protic solvents, its absorption is very high and the maximum of the absorption is shifted based on the concentration.[17] I started the investigation focusing on the exfoliation of graphene using R_b. As first I tested the exfoliation varying the concentration of R_b (50, 20, 10, 1 mg/mL) to understand if different doses could lead to different yield of exfoliation. Surprisingly with every concentration employed the dispersions resulted stable until the removal of the excess of rhodamine. Exactly as for methylene blue, after the step of centrifugation and washing of the supernatant, the sheets were precipitating in less than one

hour. After one day it was possible to observe that the solution was colored by the release of R_b from graphene. The instability of the particles could be due to different factors. One could be the tendency of the molecule to migrate in water and detaching from the graphene surface. This behavior could be due to the presence of the counter-anion in solution. The aggregation of the particles could be even related to the presence of the carboxylic group and its tendency to form dimers. This tendency was also observed by Tascón and co-workers using Riboflavin in place of its phosphonate form.[3] To prevent this problem, I tested rhodamine 6G. The carboxylic group is converted in an ethyl ester, avoiding the dimerization. In this case the dispersion was stable after the removing of the excess of surfactants, but after 24 hours the particles were completely deposited (Figure 2.11, vial 87A). Different behavior was instead observed with the use of rhodamine b base. The carboxylic ring, that in the solid form of the molecule is on the form of a spirane, once is solubilized in water should open the ring and moving the equilibrium to the zwitterionic form, but in the absence of the counter-anion. After centrifugation and washing of the supernatant, the particles were stable for more than 24 hours (G-R_{bb}) (Figure 2.11, vial 87B).

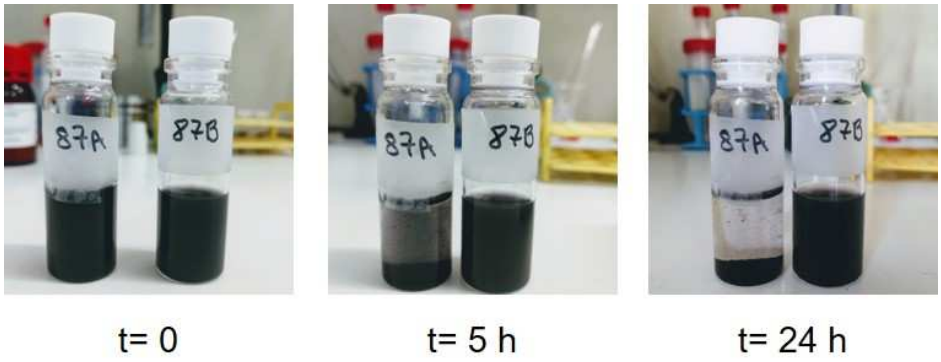

Figure 2.11: G-Rhodamine dispersions at 0, 5 and 24 hours after the centrifugation. 87A) G-R6G; 87B) G-R_{bb}.

The G-R_{bb} dispersion was stable at least for one week at the concentration of 1 mg/mL. After this time visible reaggregation was observed and the solution was colored due to a slight release of rhodamine in water. It is possible that the presence of the carboxylic group in the case of R_{bb} is not causing dimerization. As mentioned before, when rhodamine b is employed, the presence of chlorine anion is promoting the reaggregation. To confirm this hypothesis, when G-R_{bb} is dispersed in PBS solution, after less than one hour the particles are aggregating and the solution becomes pink, due to the fast release of rhodamine. Different is the behavior when the complex is dispersed in cell culture medium; in this case the particles are stable for 24 hours, and the reaggregation starts only after this time. Another remarkable aspect is the instability of R_{bb} to ethanol washing. When the supernatant was filtered and washed with ethanol all the rhodamine was released. The sheets obtained after ethanol washing were not any more stable in water. In contrast, after three days of dialysis, only the excess of rhodamine was eliminated, and the sheets remained stable in water. On this view, the purification of G-R_{bb} by dialysis result to be milder and is suggested for the obtaining of stable dispersions. TEM analysis was performed to evaluate the average lateral size of the dispersion of G-R_{bb} (~460 nm) (Figure 2.12a and b). The G-R_{bb} distribution, compared to G-Rib (Figure 2.2b) present a smaller average lateral size, constituted by sheets between 200 and 1400 nm. The quantity of sheets larger than 800 nm is inferior respect to G-Rib. As the dispersions were prepared following the same protocol, it is possible to make a comparison on the stabilization given by the two surfactants onto graphene. Rhodamine exfoliation produces fewer stable sheets, and during the centrifugation step, only the smaller are maintained stable in dispersion. The quantity of rhodamine absorbed was calculated through XPS and elemental analysis and correspond to ~10% *w/w*. The quality of the sheets was analyzed by Raman spectroscopy, showing a low amount of defects, with

an I_D/I_G ratio of ~0.23, similar to what measured for G-Rib, indicating that the bath sonication process in water is not strongly affecting the structure of graphene (Figure 2.12c).

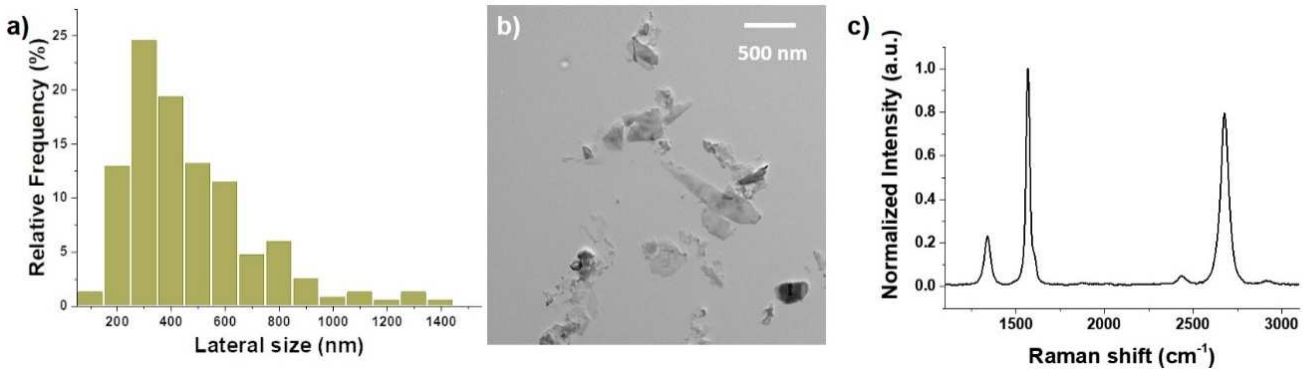

Figure 2.12: a) Distribution of the lateral size of G-Rbb dispersion; b) TEM image of graphene sheets exfoliated with Rbb; c) Raman spectra of graphene sheets exfoliated with Rbb

2.3.3.1. G-R_{bb} fluorescence study

Finally, after obtaining stable dispersions with rhodamine b base, I have investigated in collaboration with Dr. Giacomo Reina, a researcher in our group, the fluorescent properties of G-R_{bb} in water. Surprisingly, despite the different studies about the quenching power of graphene, we were able to observe a fluorescent signal from a 0.1 mg/mL G-R_{bb} dispersion in water. The analysis, performed exciting the sample at 560 nm and collecting the emission spectra between 570 and 800 nm, show a peak with a maximum of emission at 576 nm, the same observed for R_{bb} in water (Figure 2.13).

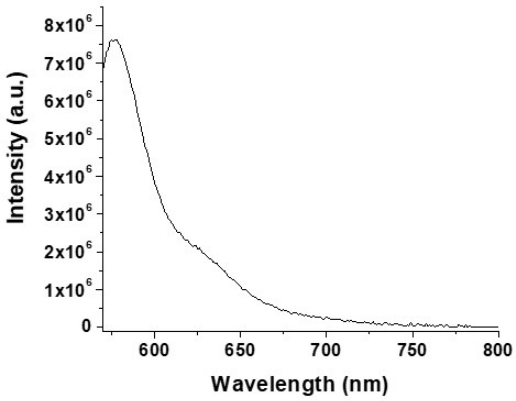

Figure 2.13: Emission spectra of G-Rbb, Ex: 560 nm, Em: 570-800 nm.

The promising observation on G-R_{bb} fluorescence encouraged further studies on this new dispersed graphene. The discovery of the non-complete quenching of the fluorescence of R_{bb} after absorption onto graphene could open the doors to a large variety of applications of this material, such as *in vitro* and *in vivo* tracking of graphene without further functionalization, biosensor, fluorescent nanocomposites, etc. To well understand the behavior of R_{bb} fluorescence and characterized the interactions between graphene and rhodamine, I tried to evaluate the quenching of the rhodamine emission. The quantum yield measured has a value inferior to 5%. Through dynamic fluorescence, we estimated the lifetime of R_{bb} and of the complex G-R_{bb} in water. We calculated a monoexponential curve leading to a lifetime of 1.58 ns for R_{bb}, and a biexponential curve with lifetimes of 1.64 ns and 72.7 ps for G-R_{bb} (Table 2.2). The G-R_{bb} complex presents two lifetimes, one related to free R_{bb} in solution and one of R_{bb} adsorbed onto graphene. What clearly arose from this measurement is that the lifetime of rhodamine is becoming shorter once the molecule is absorbed

onto graphene. For the G-R_{bb} dispersion, it was evaluated the populations (B) leading to the two different lifetimes, of 92% and 8%, respectively corresponding to G-R_{bb} and free R_{bb}. From these values we can assume that only ~8% of the adsorbed rhodamine is released in solution. Thanks to these data it has been possible to calculate the fluorescence quenching of rhodamine due to graphene absorption. The quenching (Q) was evaluated by the following equation: $Q = \frac{\tau_1}{\tau_2}$, were τ_1 is constituted by the relative contribution of the two species ($\tau_{G\text{-}Rbb}$* $B_{G\text{-}Rbb}$ + τ_{Rbb}* B_{Rbb}) and τ_2 is the lifetime of free R_{bb}. The quenching of the dispersion constituted by G-R_{bb} + R_{bb} is of ~87%. We also calculated the quenching for the G-R_{bb} (from the same equation, τ_1 = lifetime of G-R_{bb} only) corresponding to ~95%.

Specie	Lifetime (τ)	Populations (B) in solution	Std dev of B
R_{bb}	1.58 ns	8 %	0.00068
G-R_{bb}	72.7 ps	92 %	0.000013

Table 2.2: Table of lifetime and population evaluated for G-R_{bb} in water solution.

To exploit this new fluorescence property of graphene, we observed G-R_{bb} through confocal microscope in water. A drop of solution was deposited between a glass slide and coverslip. The sheets were observed exciting the sample with a laser at 561 nm and collecting the emission between 600 and 660 nm. The transmission image (Figure 2.14a) shows graphene sheets in dispersion, while the image from the yellow channel shows the emission from the graphene sheets (Figure 2.14b). The absence of background fluorescence is a confirmation of the emission from G-R_{bb} complex and not from free R_{bb} in solution. As additional confirmation of the normal quenching activity of graphene, fluorescein was added to the dispersion. Figure 2.14c shows the fluorescence emission of fluorescein from the solution (green colour), while the black spots, corresponding to graphene quenching the fluorescein fluorescence, are evident in the dispersion. This experiment is confirming a special property given by R_{bb} to graphene and the possibility to apply G-R_{bb} complex in different research fields.

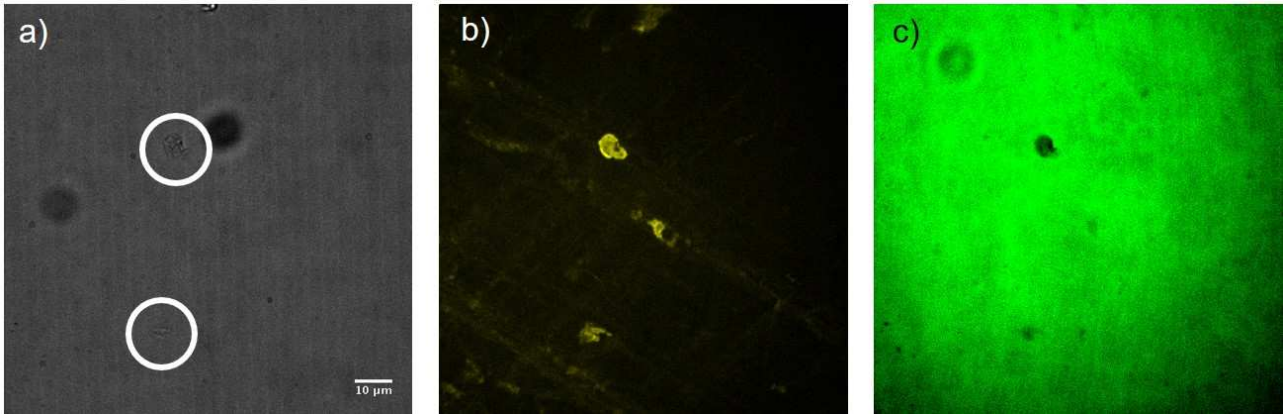

Figure 2.14: Confocal images of G-Rbb in water. a) Transmission confocal images of G-Rbb in water; b) Yellow channel, ext = 561 nm, em = 600-660 nm; the yellow particles correspond to fluorescent graphene sheets. c) Green channel, ext = 488 nm, em = 500-550 nm.

2.3.1. Exfoliation with bodipy molecules

The experiment described above were performed employing commercially available products, with the purpose to discover new surfactants allowing a scalable, economical, non-toxic and easy production of exfoliated graphene. In this paragraph I will describe the preliminary results of a synthetic approach for the development of new surfactants for graphene. In collaboration with Dr B. Richichi of the University of Florence, who designed new bodipy molecules, I explored the possibility to use them for the exfoliation of

graphene. Bodipy derivatives are biocompatible and in some studies have been employed for cellular staining.[19] Their strong fluorescence could help to deeply study the properties of graphene when exfoliated with fluorescent molecules. Moreover, their structure can be functionalized with a large variety of organic compounds, opening the doors to a specific functionalization. The structures of the three molecules tested are shown in Figure 2.15. The bodipy moiety is planar and could be strongly adsorbed onto graphene surface. The functional groups are playing a key role in the solubilization of the molecules and on the fluorescence emissions.

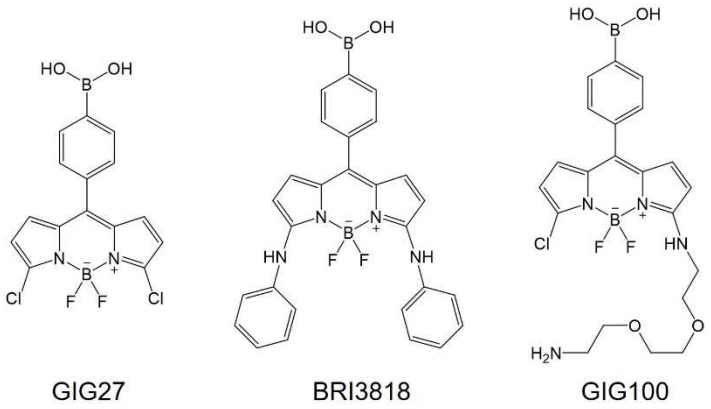

Figure 2.15: Structure of bodipy derivatives tested for graphene exfoliation.

GIG27 and BRI3818 are the first two molecules provided to our group from our collaborator and tested. These two molecules are characterized by low water solubility and require the addition of MeOH, DCM or EtOH for their dissolution. I tested the exfoliation in a mixture of MeOH/H_2O 4:1 (see the procedure in paragraph 2.6). After bath sonication, the resulting dispersions were left to rest for 24 hours. After this time the dispersion of GIG27 was completely precipitated, whereas the dispersion of BRI3818 (G-BRI3818) was stable without the formation of aggregates. To test the stability of the sheets in a higher percentage of water, G-BRI3818 was diluted in water in a ratio of 1:10. The particles start to aggregate after less than one hour, and after two hours all the sheets were deposited. This behavior is probably due to the low water solubility of the molecule, unable to stabilize the particles in this solution. Of important interest was, in any case, the investigation of the fluorescence properties of the graphene-bodipy complex. BRI3818 present a strong fluorescence emission peak in MeOH at ~610 nm when excited at 560 nm. I then explored the fluorescence emission of a 0.1 mg/mL dispersion of G-BRI3818 in MeOH. In this case, our expectations were not met, and the complex, excited at different wavelength, was not presenting any fluorescence emission. This behavior is more similar to the normal observation made on the quenching effect of graphene and may be ascribed to a stronger interaction of the molecule with the graphene surface, leading to an increase of the ET effects.

Comparing the structure of BRI3818 and GIG27 to Rib, we may hypothesize that the absence of a hydrophilic chain is playing a key role in the stabilization of the sheets in water. To confirm this hypothesis, in Florence they designed a new bodipy derivate, GIG100, functionalized by an amino-terminal TEG chain. TEG is known for its ability to improve the water solubility of organic molecule and the water dispersibility of nanomaterials such as graphene and nanoparticles. As expected, the molecule resulted soluble in water, differently from the other two derivates. This new characteristic is encouraging for the use of GIG100 as graphene exfoliating agent. I tested the exfoliation of graphene with GIG100 following the same protocol of G-Rib preparation (see procedure in paragraph 2.6). After the process of centrifugation and elimination of surfactant excess the G-GIG100 dispersion in water (1 mg/mL) was stable for more than 48 hours without the formation of aggregates. With the aim of a biological application of this new surfactant, I tested subsequently the stability in PBS and cell culture medium. After 48 hours in PBS (Figure 2.16a, b) and in cell culture medium (Figure

2.16 c, d) the particles were completely precipitated whereas in water the particles result to be stable at the concentration of 1 mg/mL (Figure 2.16e) and 0.1 mg/mL (Figure 2.16f) for 24 hours.

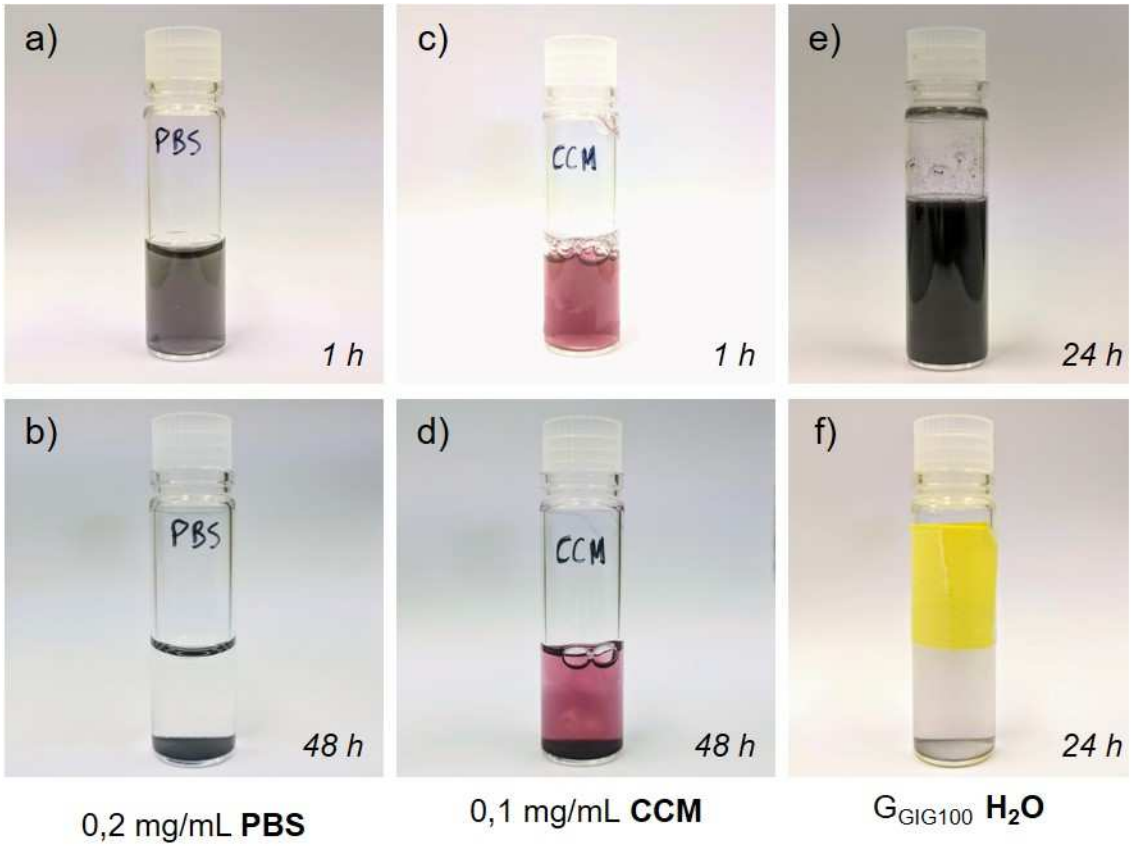

Figure 2.16: G-GIG100 dispersions in different media. a, b) G-GIG100 in PBS, 0.2 mg/mL after 1 h and 48 h; b, c) G-GIG100 in cell culture medium (CCM), 0.1 mg/mL after 1 h and 48 h; e) G-GIG100 in water, 1 mg/mL after 24 h; f) G-GIG100 in water, 0.1 mg/mL after 24 h.

The lateral size distribution of the sheets was evaluated by a statistic analysis using the TEM images (Figure 2.17). The distribution results to have an average lateral size of ~756 nm, with sheets between 143 and 1870 nm. More than the 60 % have lateral size between 400 and 1000 nm, and only 5 % is bigger than 1400 nm. The G-GIG100 distribution is comparable with the G-Rib distribution in terms of average lateral size (Figure 2.2b, ~840 nm, sheets between 200-1800 nm). Both dispersions were treated following the same protocol of sonication and centrifugation speed (5 h bath sonication, centrifugation: 1500g), permitting a comparison on the obtained results. The similarity on the distributions in terms of lateral size is confirming that the treatment applied to the starting material is directly affecting the lateral size distribution of the dispersion. Furthermore, the similarity in the chemical structure of the surfactant, especially the presence of the hydrophilic chain, is suggesting the importance of these molecules on the stabilization and on the production of sheets with different characters and properties.

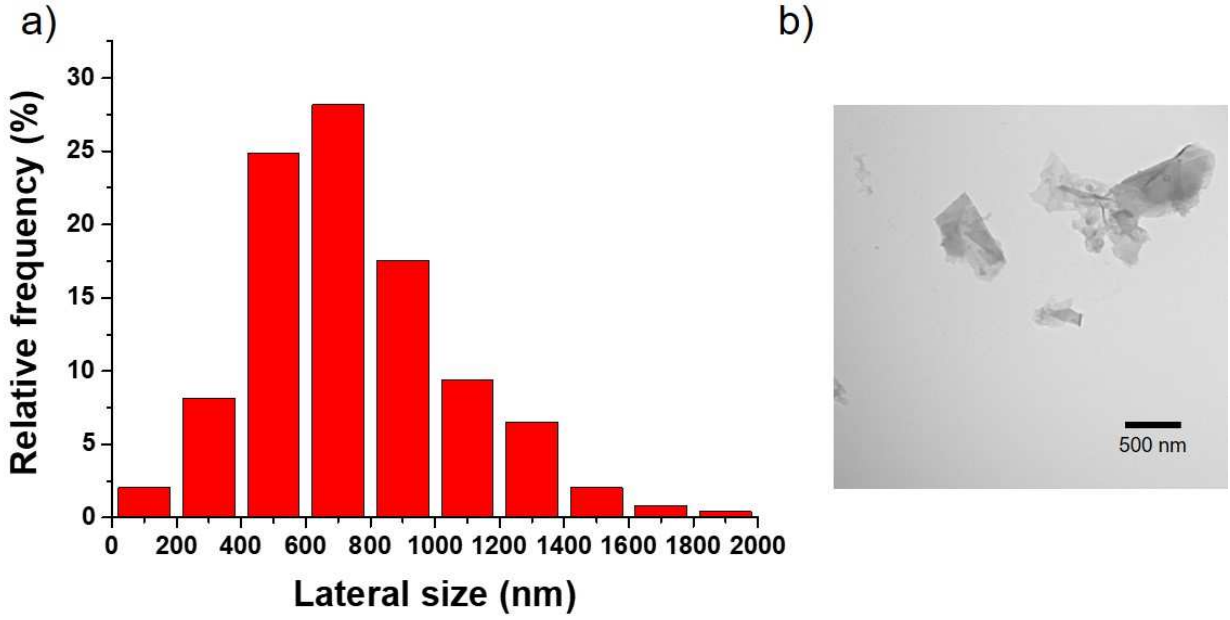

Figure 2.17: a) Histogram of the distribution of the lateral size of G-GIG100; b) TEM image of G-GIG100 graphene sheet.

Finally, I have investigated the fluorescence properties of the complex. The absorbance spectra of GIG100 and G-GIG100 were measured, finding a maximum of absorbance for GIG100 at ~460 nm (Figure 2.18a). The complex G-GIG100 does not show any kind of absorbance related to the bodipy derivate adsorbed on the surface. The fluorescence emission of the two samples was then analyzed, exciting the solution at 460 nm and collecting the emission between 480 nm and 800 nm. Figure 2.18b shows the emission spectra of GIG100 (black line) and of G-GIG100 (Blue line). The shape of the main peak, at ~540 nm is slightly different from the peak of GIG100, suggesting that the interactions with graphene can influence the emission of the molecule. The strong band at ~690 is due to Raman vibration of the water. As expected, the emission intensity of G-GIG100 is much lower respect to GIG100, confirming the fluorescence quenching of graphene. However, the fluorescence is not completely quenched, confirming the discovery made for R_{bb} and new property of graphene.

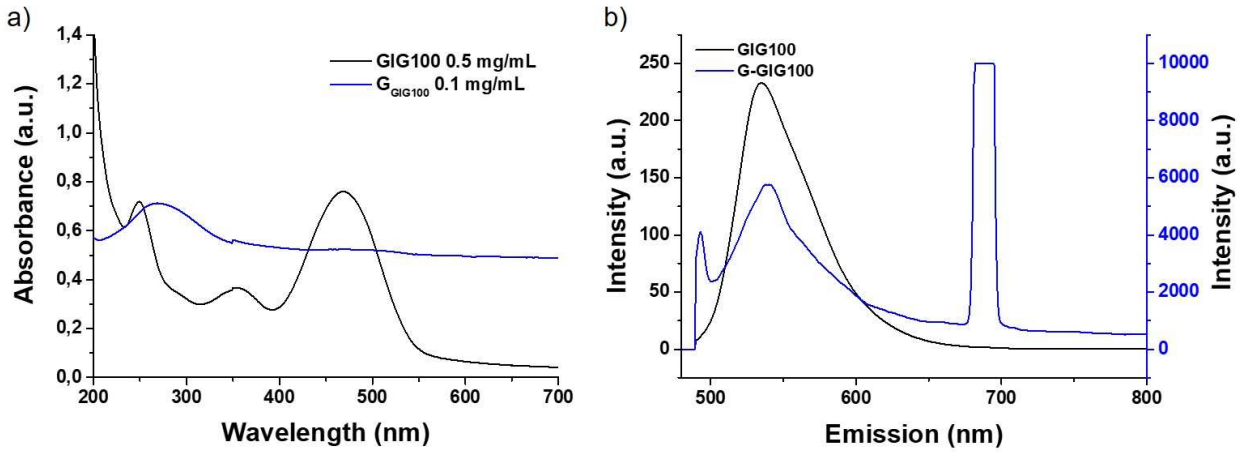

Figure 2.18: Absorbance and emission spectra of GIG100 and G-GIG100. a) Absorbance spectra of GIG100 (black line, 0.5 mg/mL) and G-GIG100 (blue line, 0.1 mg/mL); b) Fluorescence emission spectra of GIG100 (Black line, 0.1 mg/mL) and G-GIG100 (blue line, 0.1 mg/mL).

In view of these data, new studies must be performed, to deeply understand the reasons for the behavior of this complex. Computational studies should be carried out, to simulate the interaction between graphene surface and the molecules.

As for the study conducted on G-R_{bb}, G-GIG100 was observed by confocal microscopy in water dispersion. Figure 2.19 shows the images from the microscope. On the merged images c and f, it is possible to observe the fluorescence coming from the graphene sheets present in the dispersion.

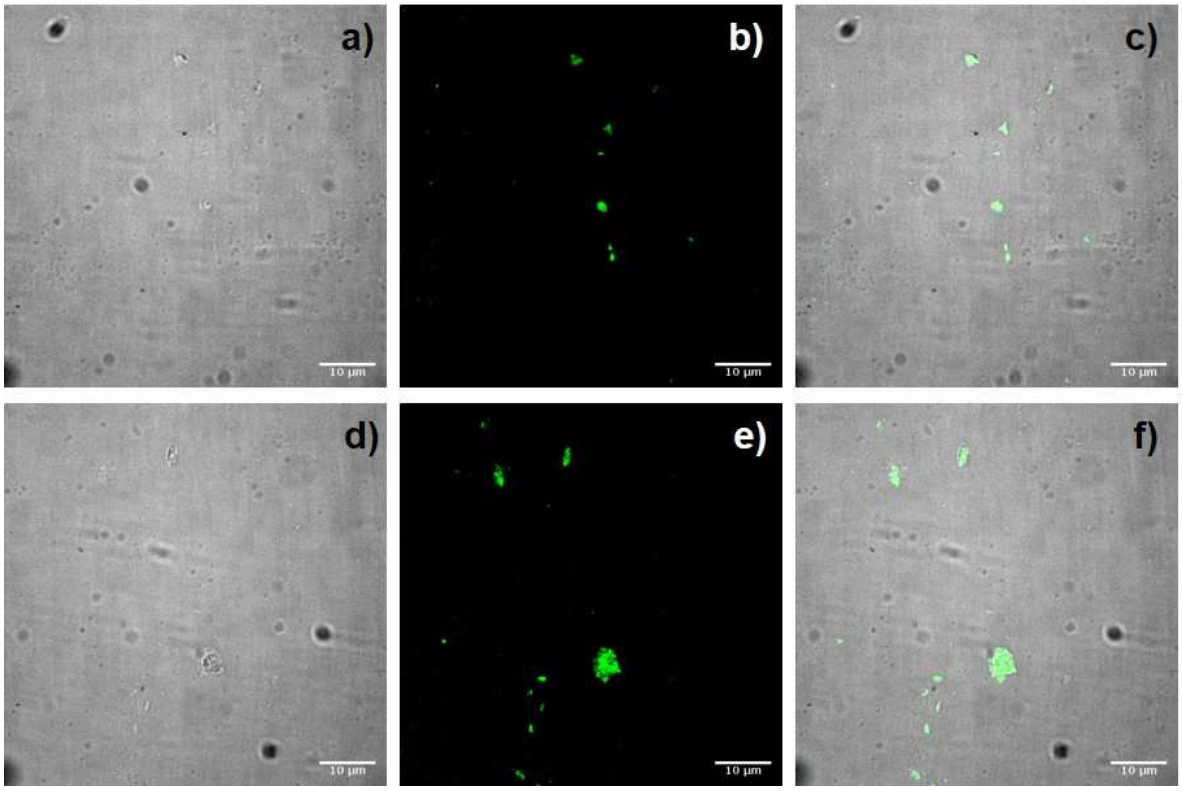

Figure 2.19: Confocal images of G-GIG100, 0.1 mg/mL in water. a, d) transmission images; b, e) fluorescence emission of G-GIG100 sheets, ext = 488 nm, em = 500-550 nm; c, f) merged images of a+b and d+e.

These images are preliminary results on the investigation of bodipy derivate as exfoliating agent and fluorophore for the production and tracking of graphene in cells. In the next months, we will investigate the lifetime of the G-GIG100 respect to GIG100 molecule, the release of the bodipy in water and the internalization in cells.

2.4. Results and discussion: Boron nitride

As discussed in the Introduction of this chapter, hexagonal boron nitride, a 2D materials with morphology similar to graphene but opposite properties, could have interesting biological applications for drug delivery, for imaging, in composites, etc. The aim of my research was to prepare hBN sheets in water and the investigation of their biocompatibility. The morphology of the particles, in terms of thickness, lateral size, shape, quantity and type of exfoliating agent, might have crucial effects on the cells, leading to different biological responses. For this purpose, I focused my attention on the production of hBN with different characteristics.

Exfoliation of hydrophobic hBN in water needs the assistance of surfactants, able to intercalate, separate and stabilize the sheets in solution. Sodium cholate (SC) was reported as a good surfactant for a wide variety of

2D materials, including hBN.[20–22]. The preparation of hBN was made using two different sources of BN, one starting from bulk material of ~20 µm (Alfa Aesar) and the other with dimension < 1 µm (Sigma) in lateral size. From these sources I obtained materials with different shape, one with sharp edges and a graphene-like morphology, called cornered boron nitride (c-hBN) and the other with round corners, called round boron nitride (r-hBN).

2.4.1. Cornered boron nitride – c-HBN

Cornered-hBN was obtained from Alfa Aesar powder. As first method of exfoliation, I have applied a protocol commonly employed by our collaborator Dr. A. von Dem Bussche from Brown University for the dispersion of nanomaterials, such as carbon black and carbon nanotubes. The method consists in different steps of bath sonication, starting from the dispersion and sonication in a solution of DPPC (dipalmitoyl phosphatidylcholine) in EtOH, followed by the addition of a BSA solution to the mixture and a successive sonication. Unfortunately, the application of this easy method has not allowed the exfoliation and stabilization of the hBN sheets in water. I decided to apply the tested method for G-Rib and G-R_{bb} exfoliation to the BN powder. BN was mixed in water solutions of Rib, BSA or sodium cholate and sonicated by bath sonication for 5 hours. The obtained white dispersion was left to rest, and all the particles were precipitated in less than 2 hours. I hypothesized that the instability of the particles and the difficulty in the exfoliation was due to the large lateral dimension of the starting material. To solve this problem, I decided to combine different exfoliation techniques to the powder. Bulk BN was first milled on a planetary machine in order to decrease the size of the particles (see procedure in paragraph 2.6). The same powder was then milled again in solid mixture with SC, to promote the intercalation of the surfactant within the sheets. The mixture was finally sonicated in water to obtain a white stable suspension. To this suspension I applied directly a size selection method based on centrifugation[11] from high (~1700 g/min) to low speed (~100 g/min), obtaining hBN dispersions with different lateral size, evaluated by statistical analysis using TEM images. The characteristics of the distributions are shown in Table 2.3 and the histograms of the distributions are shown in Figure 2.20.

Sample	Speed (g/min)	Mean (nm)	Min (nm)	Max (nm)
c-hBN$_{1700}$	1700	398	133	996
c-hBN$_{950}$	950	342	107	792
c-hBN$_{420}$	420	591	203	1.251
c-hBN$_{100}$	100	1.321	544	2.610

Table 2.3: Centrifugation speeds and lateral size dimensions of the obtained c-hBN dispersions.

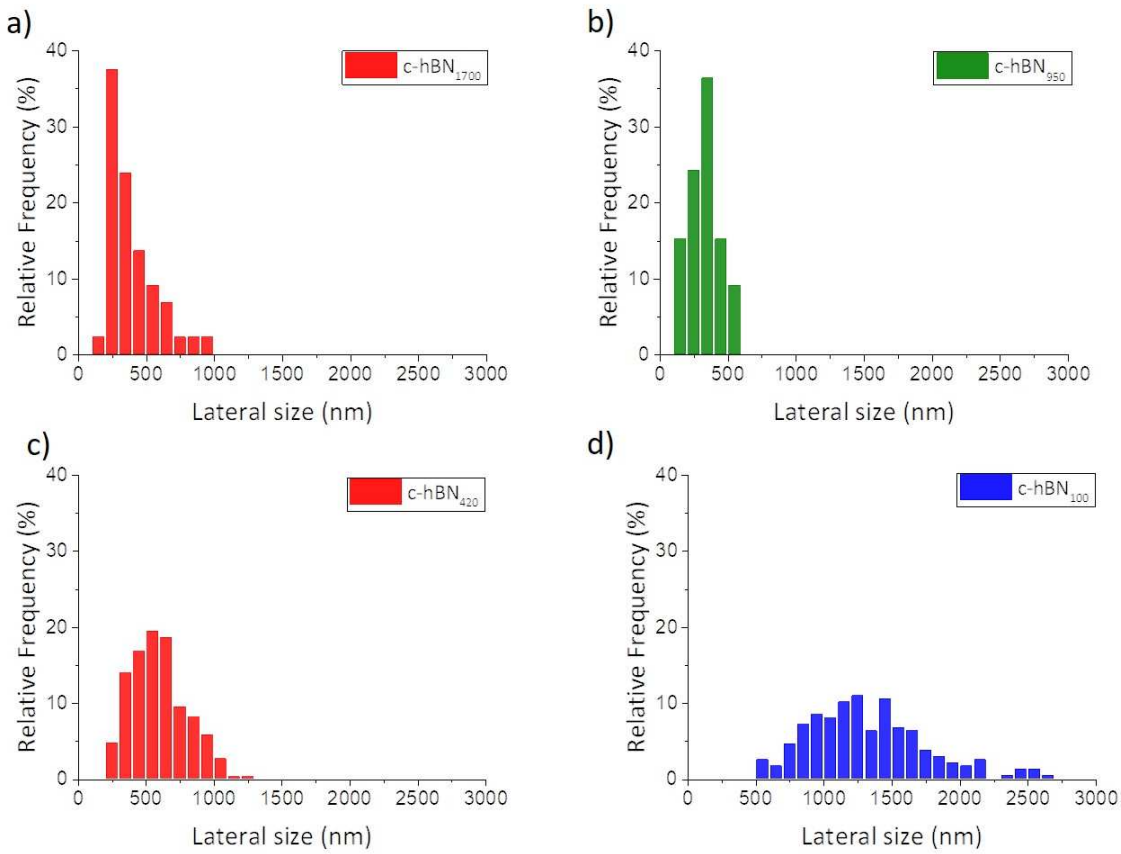

Figure 2.20: Histogram of the lateral size distribution of r-hBN obtained by centrifugation.

The hBN obtained following this procedure showed sharp corners and was named cornered-hBN (c-hBN$_x$, where x corresponds to the centrifugation speed in g/min). We thoroughly characterized the different dispersions using complementary spectroscopic techniques. The dispersion c-hBN$_{950}$ and c-hBN$_{100}$ were selected for the biological studies because of their significant difference in lateral size distribution, of 342 nm and 1321 nm, respectively (Figure 2.20b and d). The thickness of the sheets was investigated by a statistical analysis of a series of AFM measurements (Figure 2.21c). The two samples showed similar mean distribution, of 4.69 ± 0.05 nm and 4.72 ± 0.18 nm for c-hBN$_{950}$ and c-hBN$_{100}$, respectively. HR-TEM images allowed to measure the numbers of layers of the materials (Figure 2.21d and e). Both dispersions contain cornered-hBN composed of ~6 sheets. Electron diffraction analysis on the particles evidenced the typical hexagonal crystallinity of graphene-like materials, as expected for hBN sheets (Figure 2.21f).[23] These data are in agreement with previous studies on 2D materials and confirm the few-layer nature of hBN dispersions.[24,25]

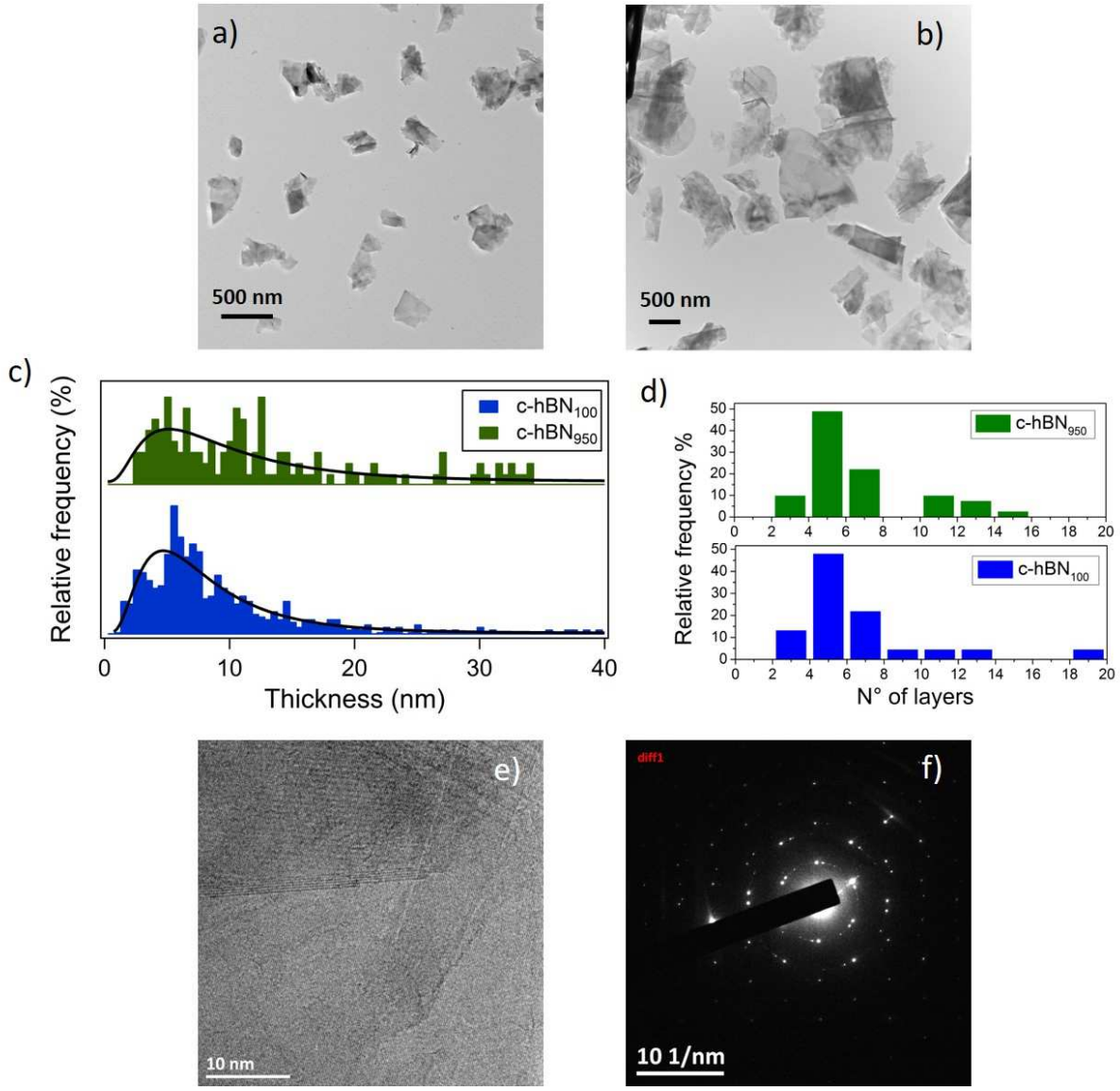

Figure 2.21: a, b) TEM images of c-hBN$_{950}$ and c-hBN$_{100}$, respectively. c) Distribution of the sheets thickness from AFM Electron; d) Distribution of the number of layers of c-hBN$_{950}$ and c-hBN$_{100}$ from HR-TEM images.; e) HR-TEM image of c-hBN$_{950}$; f) **Electron** diffraction analysis of c-hBN$_{950}$.

2.4.2. **Round boron nitride**

The round-hBN was obtained from the exfoliation of the Sigma powder (lateral size < 1 µm) and presented completely different shape and characteristics. First, the production does not require the assistance of the ball milling treatment, giving stable dispersions with the only sonication in the presence of SC. Surprisingly, the sheets obtained from this source of BN showed round shape and were named round-hBN (r-hBN$_x$ where x corresponds again to the centrifugation speed in g/min). To understand if the shape of the sheets depended by the ball milling treatment or by the BN source, the Sigma powder was milled following the same protocol of c-hBN giving, even in this case, round sheets. The distribution of the lateral size was evaluated by a statistical analysis of TEM images (Figure 2.22a), giving results significantly different respect to c-hBN. The dispersions were centrifuged at different speeds following the same procedure of c-hBN, the lateral size distribution resulted very small and quite narrow (see Table 2.4).

Sample	Speed (g/min)	Mean (nm)	Min (nm)	Max (nm)
r-hBN$_{420}$	420	156	62	324
r-hBN$_{100}$	100	210	41	573
r-hBN$_{30}$	30	234	100	473

Table 2.4: Centrifugation speeds and lateral size dimensions of the obtained r-hBN dispersions.

The dispersion r-hBN$_{420}$, selected for the further studies, present a mean lateral size distribution of 156 nm and a narrow distribution (Figure 2.22b).

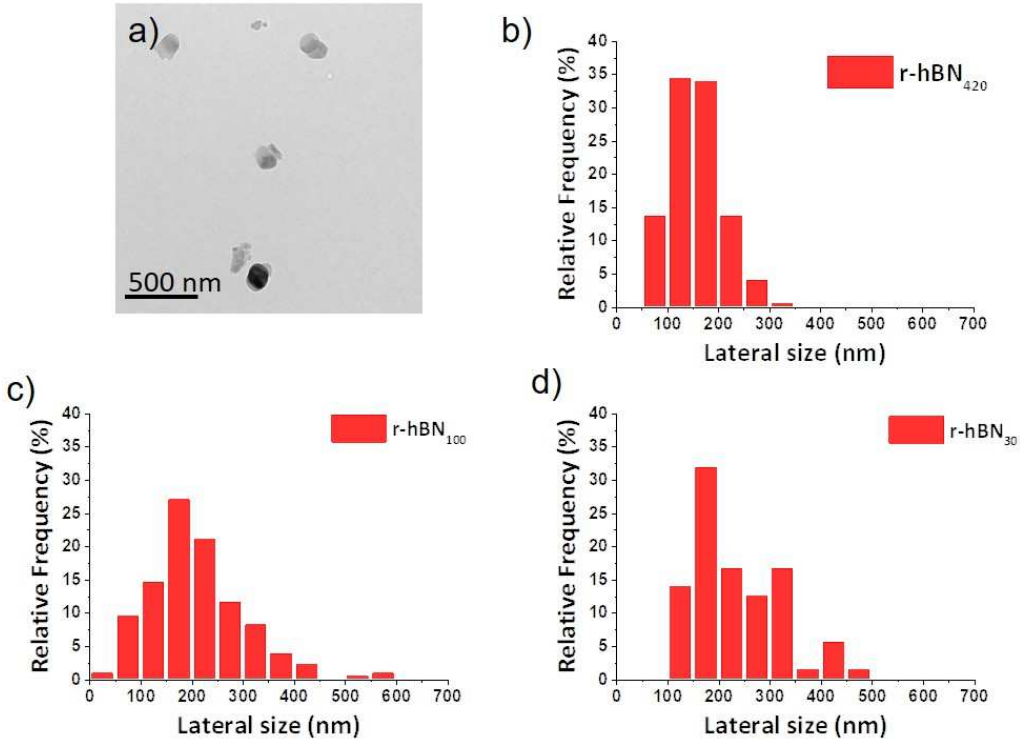

Figure 2.22: a) TEM image of r-hBN; b, c, d) Histograms of lateral size distribution of the different dispersions.

From the HR-TEM images it was possible to understand the particular morphology of this material (Figure 2.23a). If the main shape is round, as observed by TEM, the lateral sides, observed with higher magnification, initially hypothesized as flat, are decreasing in thickness in correspondence of the border, with sharp round edges and no evidence of clear layers. The electron diffraction measurements confirmed a perfect hexagonal crystallinity of the particles, as in the case of c-hBN (Figure 2.23b). These observations lead us to conclude that the shape of this material corresponds to an ovoidal structure compressed in the center, with flat and hexagonal crystalline edges. From the HR-TEM image of the tilted particles it was possible to measure the thickness of the material. This value is between 20 and 35 nm, resulting higher respect to what observed for c-hBN. The observation made by HR-TEM is corroborate by the height profiles measurement from AFM images (Figure 2.23c, d, e and f). The profiles 1 and 2 show clearly thickness of 26 and 15 nm for the first, and 21, 35 and 19 nm, respectively for the second, confirming a 3D structure of the material rather than a 2D.

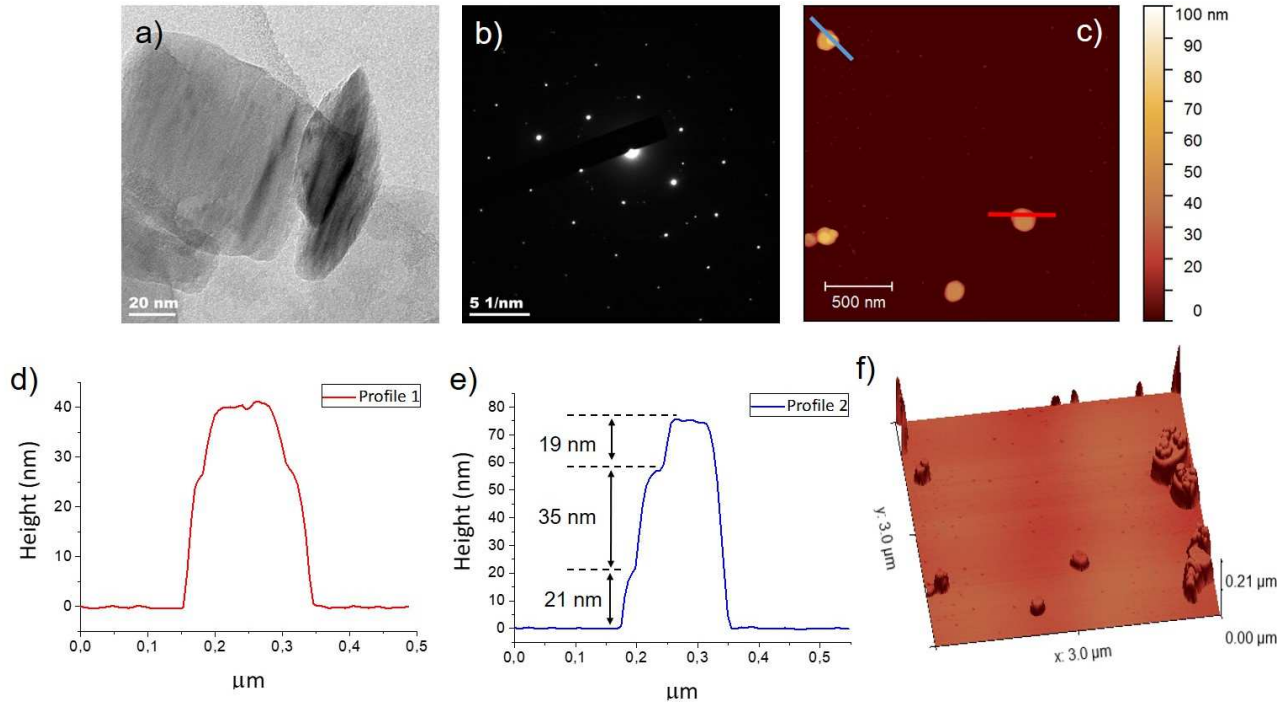

Figure 2.23: a) Lateral side of an r-hBN particle observed by HR-TEM; b) Electron diffraction of r-hBN particles; c) AFM image of r-hBN420; d, e) AFM height profile of r-hBN420; f) 3D representation of r-hBN particles from AFM measurement.

This difference in the shape between the two types of hBN is certainly deriving from the source of BN used to produce the materials.

The investigation on the cell uptake of these two different types of hBN could have strong interest in understanding the role of the edge's morphology interaction with cell membrane. The quantity of SC adsorbed on the surface of the materials was also evaluated, to understand if there was any difference in the loading of the surfactant based on the different structure of the two hBN materials. XPS analysis and elemental analysis (Table 2.5) confirmed similar results for all the three materials used in this study, showing loading of 4.5 % *w/w* and 4.2 % *w/w* for c-hBN$_{950}$ and c-hBN$_{100}$, respectively, and a 2.7 % for r-hBN$_{420}$ (Figure 2.24).

Sample	Weight % C (XPS)	Weight % C (E.A.)	*w/w* % SC/hBN (XPS)	*w/w* % SC/hBN (E.A.)	N_{SC} molecules (XPS)	N_{SC} molecules (E.A.)
c-hBN$_{950}$	2,98	2,42	4,5	3,6	1,12	1,02
c-hBN$_{100}$	2,78	2,82	4,2	4,2	0,86	1,18
r-hBN$_{420}$	1,87	1,75	2,8	2,6	0.78	0,73

Table 2.5: Evaluation of adsorbed sodium cholate par hBN unit from XPS and elemental analysis

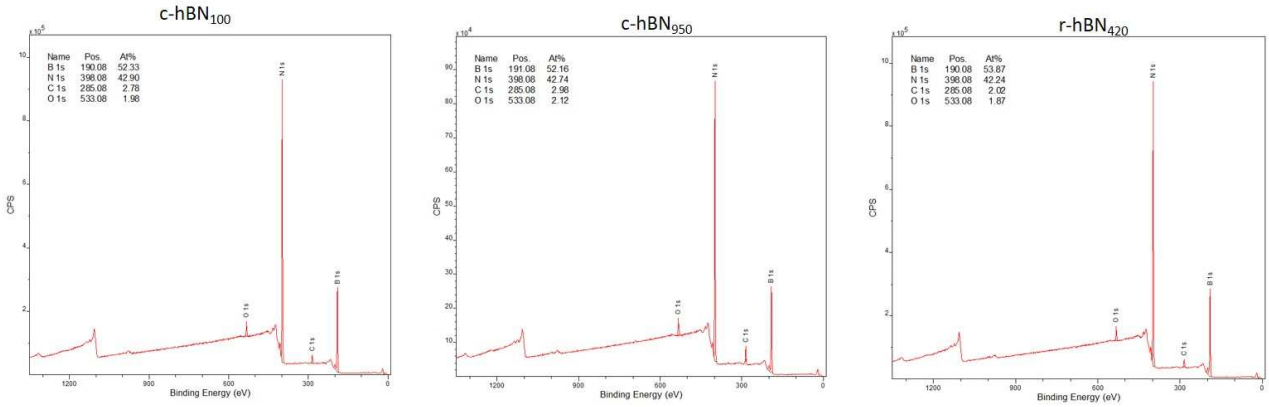

Figure 2.24: XPS survey spectra of hBN powder

Finally, we investigated if the ball milling treatment of sodium cholate was leading to a degradation of the molecule. SC was milled on the same condition of the exfoliation process, for 3 h at 100 RPM. After that the powder was recover and analysed by ^{1}H-NMR (Figure 2.25). The two spectra are not presenting differences between pure SC and SC after 3 h of milling, leading us to assume that no degradation of the organic molecule is occurring during the exfoliation treatment of hBN.

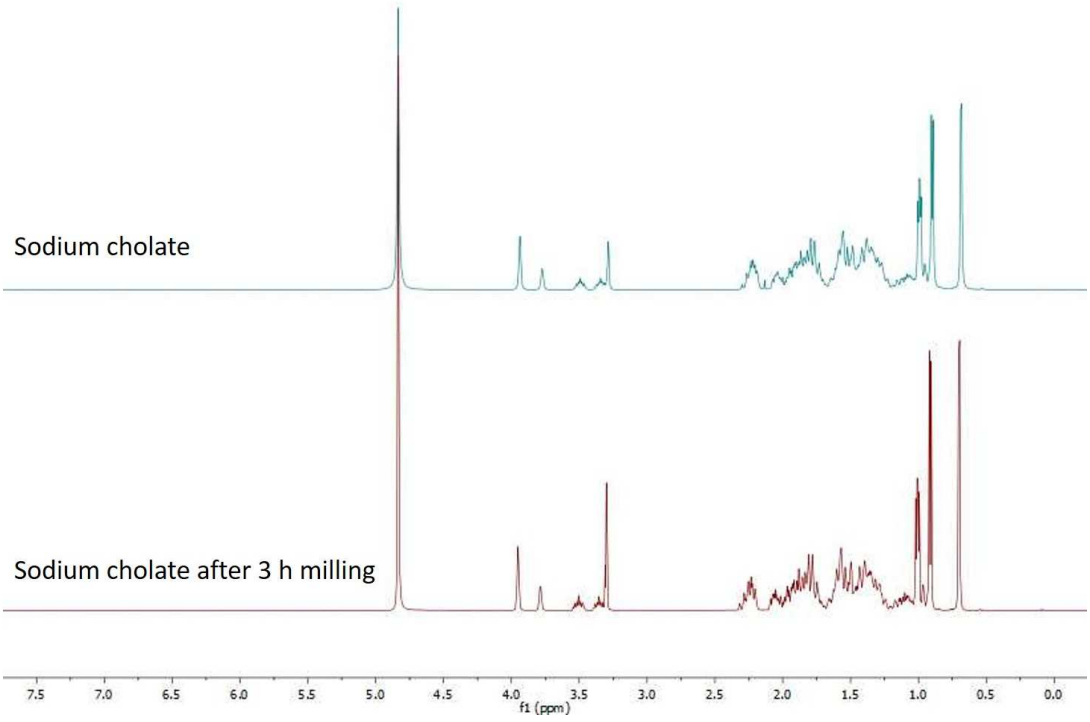

Figure 2.25: 1H-NMR of pure sodium cholate (top) and sodium cholate after 3 h milling (bottom).

2.4.3. **Cytotoxicity of c-hBN and r-hBN**

The study of hBN cytotoxicity was performed on H460 cells (epithelial cells) using the two described dispersion of c-hBN in collaboration with Dr. A. Von Dem Bussche. A dose-dependent cytotoxic effect was observed for the small dispersion c-hBN$_{950}$ in comparison to the larger c-hBN$_{100}$. As consequence, we decided to focus our further cellular investigations on the comparison between the c-hBN$_{950}$ and r-hBN$_{420}$, presenting similar lateral size distribution but important difference in terms of edges shape. We exposed lung epithelial

cells to c-hBN and r-hBN and observed that c-hBN but not r-hBN resulted in a decrease of viability in a dose-dependent manner (Figure 2.26).

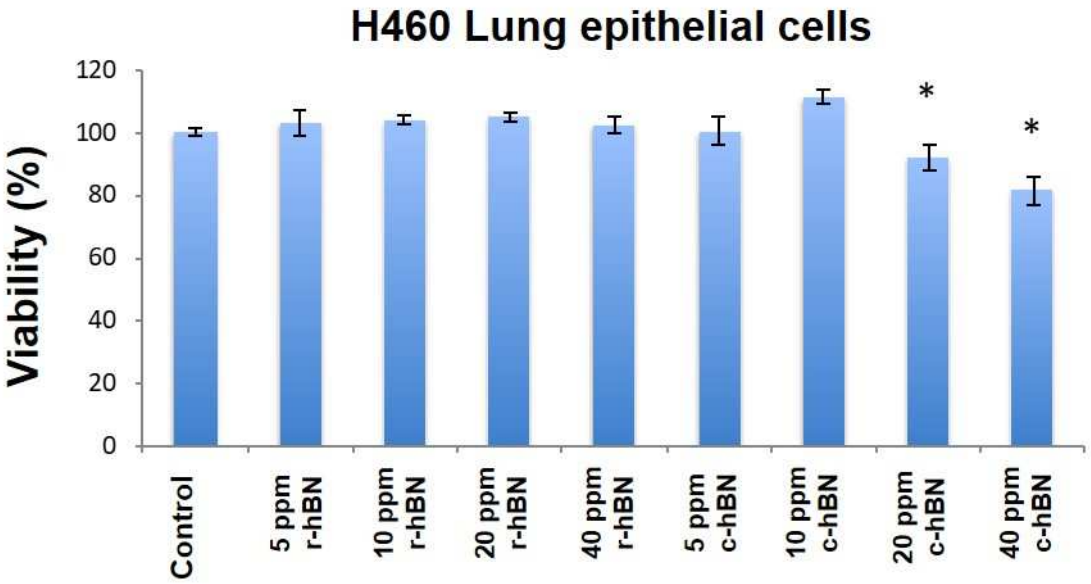

Figure 2.26: Cells viability of H460 cells after 24 h incubation with different concentrations of r-hBN and c-hBN. Cell viability was confirmed using Quant-iT™ PicoGreen® dsDNA Assay Kit that quantitates DNA content.

To understand how c-hBN causes a decrease in viability in H460 cells, not observed by r-hBN exposed cells, the localization of the two types of hBN, r-hBN and c-hBN, in lung epithelial cells was determined using TEM. We detected that r-hBN was mainly localized within the lysosomes, whereas c-hBN was also found within the cytoplasm (Figure 2.27).

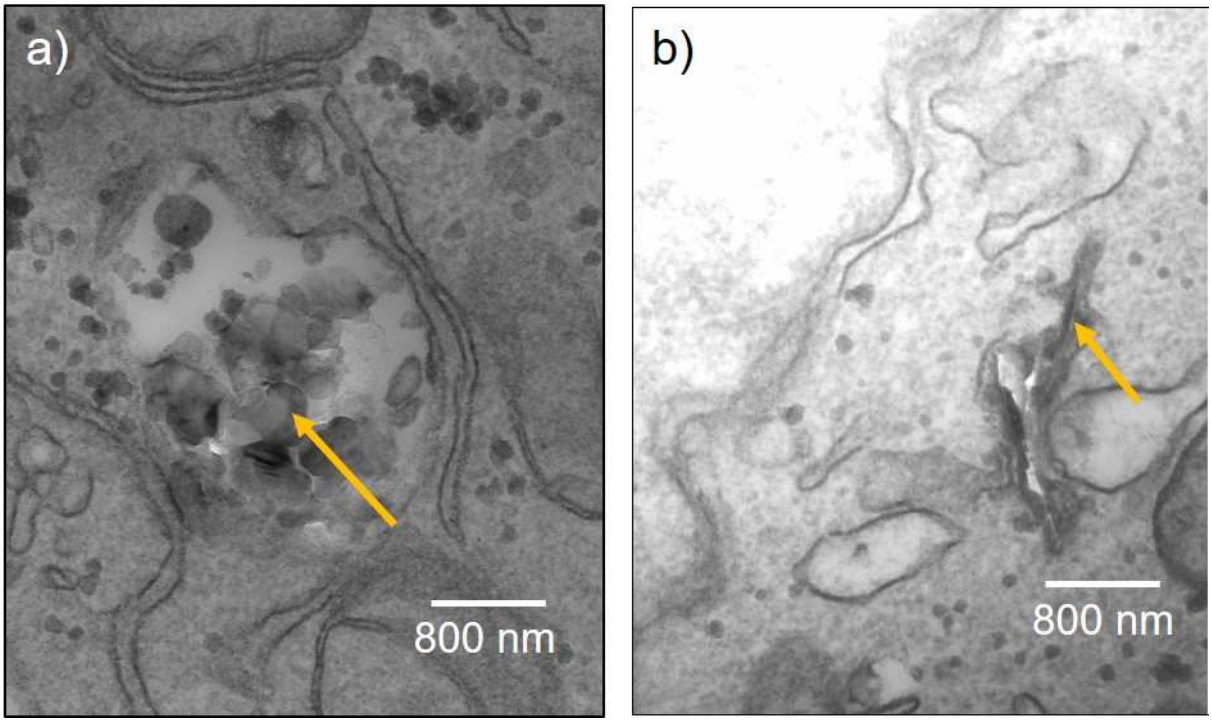

Figure 2.27: TEM of lung epithelial cells exposed to r-hBN and c-hBN. Intracellular localization of hBN after 24 h as visualized by TEM. R-hBN is mainly localized within the lysosomes (a), where c-hBN (B) is also localized within the cytoplasm.

The localization on the cytoplasm of c-hBN could cause damage to the lysosomal membrane leading to cathepsin B release. Cathepsin B release could trigger apoptotic mechanism through superoxide anion generation. For these reasons, cathepsin B assay and superoxide anion generation (using Mitosox as a mitochondrial superoxide indicator) were determined, to verify a possible connection between the damage of the lysosomes and the downstream effect leading to apoptosis of cells. r-hBN data showed that this material lead to damages of lysosomes, resulting in the release of cathepsin B. To further investigate if cell death occurred due to apoptosis, the cells were exposed to different concentrations of r-hBN or c-HBN. H460 lung epithelial cells exposed to c-HBN showed an increase of TUNEL positive cells whereas cells exposed to r-hBN did not show significant cell death. TUNEL assay is a method for detecting apoptotic DNA fragmentation or excessive DNA breakage in individual cells. All these results taken together are suggesting the importance of the particle shape on the cytotoxicity of 2D materials on cells, and the high importance of further studies to understand the interaction between the biological systems and these materials.

2.5. Conclusion

Graphene and boron nitride production in water was explored to achieve stable dispersion at concentration > 1 mg/mL. Riboflavin-5-phosphate, rhodamine b base and bodipy derivatives have been demonstrated to be good surfactants for the graphene sheets. G-Rib presents a great stability in different media, permitting the investigations *in vitro* and *in vivo*, showing low cytotoxicity and good biocompatibility at high doses with Hela cells, macrophages and also in mice. G-R_{bb} and G-GIG100 showed new fluorescence properties, in contrast to what has been reported until now about graphene quenching capability. The sheets, exfoliated with high fluorescent molecules, showed fluorescence detectable by confocal microscope, opening the doors to complete new applications of graphene-based materials.

Boron nitride was exfoliated in water using ball milling and bath sonication in the presence of sodium cholate as surfactant. Starting from two different sources of BN, particles with different shape and morphology have been produced, and these different characteristics exploited for understanding the cytotoxicity of the material on H460 epithelial cells. The obtained results are showing a dependence of the cytotoxicity on the shape of the material and its localization inside the cells.

2.6. Material and methods

Two sources of boron nitride (BN) were purchased, from Sigma Aldrich (powder ~1 µm, 98%, Lot # STBG8107) and from Alfa Aesar (powder ~325 mesh, 99.5 %, Lot B21Z024), respectively. Graphite (LOT #BCBS5850V) powder (powder < 20 µm) was purchased from Sigma-Aldrich. All the reagents and organic molecules employed for exfoliation of graphene were purchased from Sigma-Aldrich. BN powder was milled for 20 h at 100 RPM with a Rescht Planetary Ball Mill PM 100. MilliQ water, purified using a Millipore filter system MilliQ® and free endotoxin Polisseur Biopak®, was used for the preparation of the solutions. Sonication bath Elma model Elmasonic P was used for the exfoliation of graphite. Ominpore membrane filters 0.1 µm JH was used for the filtration of all dispersions of graphene. The centrifugation of the dispersions was performed with Beckman Avant J-25 centrifuge. The lateral size dimension was measured with a Hitachi 7500 transmission electron microscope (Hitachi High Technologies Corporation, Tokyo, Japan) equipped with an AMT Hamamatsu digital camera (Hamamatsu Photonics, Hamamatsu City, Japan). HR-TEM and SAED analyses were performed on a JEOL 2100F TEM/STEM electron microscope operating at 200 kV. ζ-potential was evaluated using a HPPS from Malvern. Atomic force microscopy (AFM) images were recorded in tapping

mode using a Veeco/Bruker Dimension 3100 AFM, equipped with Nanoscope 4 controller, and with a Bruker Multimode V AFM, equipped with Nanoscope 5 controller. Samples for AFM imaging were prepared depositing the dispersions by spin-coating on native silicon. X-ray photoelectron spectroscopy (XPS) analyses were carried out using a Thermo Scientific KAlpha X-ray photoelectron spectrometer equipped with an aluminium X-ray source (energy 1.4866 keV) and working at pressure of 10^{-8}–10^{-9} mbar in the main chamber. All the images are treated with Fiji (ImageJ) software.

Lifetime measurement

Lifetime measurements were recorded using light-emitting diodes (NanoLED) excited at 460 nm at a fixed emission of 710 nm

Exfoliation of graphene with riboflavin-5'-phosphate sodium salt

Exfoliation of graphene was carried out directly in water using 1.5 g of graphite dispersed in 200 mL of a solution of riboflavin-5'-phosphate sodium salt (Rib) at 1 mg/mL. The solution was sonicated at 37 MHz for 5 hours at temperature < 30 °C. After sonication, the dispersion was centrifugated at 1500 g for 1 hour to recover the most stable sheets. The supernatant containing the exfoliated layers of graphene was collected, filtered and washed with 300 mL of water to remove the excess of Rib. The powder was then sonicated for 5 min in 20 mL of MilliQ water obtaining the final graphene aqueous dispersion (G-Rib) in a concentration of ~2 mg/mL.

Size selection of G-Rib

One g of graphite was dispersed in 100 mL of milli-Q water with Rib (1mg/mL). The mixture was sonicated by horn tip sonication for 1h, 35% amplitude, with step of 6 s sonication + 2 s stop. The black dispersion was centrifuged at 8000 g for 1 hour at 15 °C. The supernatant collected (G-Rib-8000) and the residue dispersed in 100 mL of Rib solution (1mg/mL). The new dispersion was sonicated for 5 minutes and then centrifuged at lower speed. Centrifugation speed applied: 8000g, 5000g, 2000g, 500g.

The collected supernatants were filtered on Millipore filters (0.1 µm pore size) and washed twice with 100 mL of milli-Q water to remove the excess of Rib. The filtrate was then re-dispersed in 20 mL of milli-Q water by bath sonication for 5 minutes.

Exfoliation of graphene with rhodamine

Similarly, as described for the exfoliation of graphene wit Rib, the material was directly obtained in water using 1.5 g of graphite dispersed in 200 mL of a solution of rhodamine (Rb, Rbb, R6G), at 1 mg/mL. The solution was sonicated at 37 MHz for 5 hours at temperature < 30 °C. After sonication, the dispersion was centrifugated at 1500 g for 1 hour to recover the most stable sheets. The supernatant containing the exfoliated layers of graphene was collected, filtered and washed with 300 mL of water to remove the excess of rhodamine. The powder was then sonicated for 5 min in 20 mL of MilliQ water obtaining the final graphene aqueous dispersion (G-R_{bb}) in a concentration of ~2 mg/mL.

Graphene exfoliation with bodipy

Exfoliation of graphene was carried out in MeOH/H_2O 4:1 solution (3 mL). One hundred mg of graphite was dispersed into a 1 mg/mL solution of bodipy-derivate. The solution was sonicated at 37 MHz for 5 hours at temperature < 30 °C. After sonication, the stable dispersion was centrifugated at 1500 g for 45 minutes to recover the most stable sheets. The supernatant containing the exfoliated layers of graphene was collected,

filtered and washed with 30 mL of water to remove the excess of surfactant. The powder was then sonicated for 5 min in 10 mL of MilliQ water obtaining the final graphene aqueous dispersion.

Boron nitride production

Two sources of boron nitride (BN) were purchased, from Sigma Aldrich (powder ~1 µm, 98%, Lot # STBG8107) and from Alfa Aesar (powder ~325 mesh, 99.5 %, Lot B21Z024), respectively. Sodium cholate was purchased from Sigma Aldrich. Milli-Q water was used for the preparation of the solutions. BN powder was milled for 20 h at 100 RPM with a Rescht Planetary Ball Mill PM 100. The exfoliation of BN was performed on a solution of 60 mg of BN containing 30 mg of sodium cholate in 20 mL of water, using a bath Sonicator Elmasonic P at 37 MHz, 100% power for 1 h. Omnipore membrane filters 0.1 µm JH was used for the filtration of all the solutions of BN. The centrifugation of the dispersion was performed with a Beckman Avant J-25 centrifuge.

c-hBN production

Three g of BN powder from Alfa Aesar was milled with steel balls at 100 RPM for 20 h (b-BN_{20h}). Thirty mg of b-BN_{20h} was milled with 60 mg of sodium cholate (SC) with steel balls at 100 RPM for 3 h (m-BN_{3h}). The powder was recovered with 20 mL of Milli-Q water, transferred in a round flask and sonicated at 37 MHz and 100% of power bath at a T < 35°C for 1 h, giving a white dispersion. The dispersion was centrifuged at decreasing speeds. After each centrifugation step the supernatant was recovered (c-hBN_x where x is the centrifugation speed), filtered and washed with 100 mL of water and 100 mL of ethanol, then dispersed by sonication in 10 mL of water. The residue was dispersed in 20 mL of water by sonication on the same condition described for 5 minutes to be further centrifuged.

Round hBN (r-hBN)

Thirty mg of Sigma Aldrich powder was added to a solution of SC in Milli-Q water (1 mg/mL, 20 mL) and sonicated at 37 MHz, 100 % power bath for 1 h to a T < 35°C. After this time the white dispersion was centrifuged at different speed, following the same procedure of c-hBN.

Evaluation of quantity of sodium cholate adsorbed on hBN materials

The quantity of SC was evaluated through XPS analysis and elemental analysis (E.A.) of the r-hBN and c-hBN after lyophilization process. The XPS analysis was carried out on the hBN powder deposited on double face Cu scotch tape (Farnell, 19mm, mod. 1182). The percentual composition of the samples was evaluated through the deconvolution of survey spectra (Figure S6). By elemental analysis was measured the percentual amount of C, N and O constituting the powder. From the quantity of C measured from the mentioned techniques was calculated the amount of SC adsorbed on the materials. The numbers of SC molecules were calculated for the theoretical SC unit (1344 B and N atoms total, 6x6 nm). The results obtained are in according to both techniques and for each sample.

Cellular studies

Cell culture. HeLa (epithelial, human cervical adenocarcinoma) and Raw 264.7 (macrophages, Abelson murine leukaemia virus-induced tumour) cells were cultured as monolayers in Dulbecco's modified Eagle medium supplemented with 10 µg/mL gentamycin (Lonza BioWhittaker), 10 mM HEPES (Lonza BioWhittaker), 0.05 mM β-mercaptoethanol (Lonza BioWhittaker) and 10 % FCS, in a humidified incubator (37 °C, 5% CO_2). For the toxicity experiments, cells were seeded in 24-well plates (approximately 1×10^5 cells/well, 1 mL/well). The cells were left to grow until 70-80 % confluency and exposed up to 24 hours to graphene. Graphene was diluted in the cell culture medium at different concentrations and subsequently the cells were exposed for 24 hours with the treatments.

Cytotoxicity assay. Cell viability was determined by flow cytometry using the standard assay with FVD (Fixable Viability Dyes) 24 h after exposure to the materials. The supernatant was aspirated and discarded, and the cells were washed twice with PBS. Cells were detached from the plates using a scraper in the case of Raw 264.7, and for HeLa cells a solution of 0.25% Trypsin/0.53 mM EDTA was used. The cells were washed with PBS, 2 % foetal bovine serum and then were incubated (20 min, 4 °C) with the dye (dilution 1:2000). Thereafter, cells were washed with PBS, 2 % FCS and resuspended in 300 µL and immediately acquired on the cytometer. At least 10 000 cells were counted for each sample, and experiments were performed in triplicate.

Data analysis and statistical methods. Flow cytometry data were saved as LMD files and subsequently analyzed using FlowJo software (FlowJo LLC, software version 7.6.5. Ashland, OR, USA) and. Cell viability (%) was calculated as [(A − B)/A × 100], where A and B are the number of dead cells of control and treated cells, respectively. Values represent mean ± SD (n = 3). Two-way analysis of variance (ANOVA) and Bonferroni's multiple comparisons test was adopted for statistical significance ($p<0.05$).

Animal studies

Toxicological characterization of exfoliated graphene after a single intravenous administration was performed in a murine model (BALB/c mice (11–13 weeks, 18-20 g, n=5/group). Mice were housed in the IBMC animal facility (agreement number G67-482-2). They were maintained under controlled conditions before and during the experiments (*i.e.*, room temperature at 25 °C; relative humidity of 65%; 12 h light/dark cycle). Access to food and water was provided *ad libitum*. All experiments were carried out in conformity with the 2010/63/UE European animal bioethics legislation (French decree #2013-118 – 1st February 2013) and were approved by the Regional Ethics Committee of Strasbourg (CREMEAS) and by the French Ministry of Higher Education and Research (APAFIS#3280-2015121815099907 v2). An acute toxicity assay was performed using exfoliated graphene at two dose levels: 5 and 15 mg/kg body weight (injections of 100 and 300 µg/mouse, respectively). After a single intravenous injection of graphene suspensions, clinical observations were performed daily up to 30 days. Animals were sacrificed at 24 hours, 14 and 30 days after injection and liver, kidneys and spleen were collected for analysis. After extraction, the organs were fixed in 10% paraformaldehyde and embedded in paraffin blocks. Sections of 8 µm were deparaffinised and rehydrated before staining. Haematoxylin and eosin staining was used for the determination of histopathological changes in the tissue. Blood was collected in EDTA (10%) and analyzed using a Cell Counter. The biochemical and haematological analyses were performed at the Mouse Clinical Institute (MCI, Illkirch, France).

2.7. References

1. Lotya, M. *et al.* Liquid phase production of graphene by exfoliation of graphite in surfactant/water solutions. *J. Am. Chem. Soc.* **131**, 3611–3620 (2009).

2. León, V. *et al.* Few-layer graphenes from ball-milling of graphite with melamine. *Chem. Commun.* **47**, 10936–10938 (2011).

3. Ayán-Varela, M. *et al.* Achieving extremely concentrated aqueous dispersions of graphene flakes and catalytically efficient graphene-metal nanoparticle hybrids with flavin mononucleotide as a high-performance stabilizer. *ACS Appl. Mater. Interfaces* **7**, 10293–10307 (2015).

4. Bianco, A. *et al.* All in the graphene family - A recommended nomenclature for two-dimensional carbon materials. *Carbon N. Y.* **65**, 1–6 (2013).

5. Lotya, M. *et al.* Liquid phase production of graphene by exfoliation of graphite in surfactant/water solutions. *J. Am. Chem. Soc.* **131**, 3611–3620 (2009).

6. Ciesielski, A. & Samorì, P. Graphene via sonication assisted liquid-phase exfoliation. *Chem. Soc. Rev.* **43**, 381–398 (2014).

7. Sun, Z., Masa, J., Liu, Z., Schuhmann, W. & Muhler, M. Highly concentrated aqueous dispersions of graphene exfoliated by sodium taurodeoxycholate: Dispersion behavior and potential application as a catalyst support for the oxygen-reduction reaction. *Chem. - A Eur. J.* **18**, 6972–6978 (2012).

8. Zhang, X. *et al.* Distribution and biocompatibility studies of graphene oxide in mice after intravenous administration. *Carbon N. Y.* **49**, 986–995 (2011).

9. Amrollahi-Sharifabadi, M. *et al.* In vivo toxicological evaluation of graphene oxide nanoplatelets for clinical application. *Int. J. Nanomedicine* **13**, 4757–4769 (2018).

10. Smith, R. J., King, P. J., Wirtz, C., Duesberg, G. S. & Coleman, J. N. Lateral size selection of surfactant-stabilised graphene flakes using size exclusion chromatography. *Chem. Phys. Lett.* **531**, 169–172 (2012).

11. Khan, U. *et al.* Size selection of dispersed, exfoliated graphene flakes by controlled centrifugation. *Carbon N. Y.* **50**, 470–475 (2012).

12. Sakai, M., Ohmori, T. & Fujii, M. Chapter 12 Two-color picosecond time-resolved infrared super-resolution microscopy. in *Handai Nanophotonics* **3**, 189–195 (2007).

13. Kasry, A. *et al.* Highly efficient fluorescence quenching with graphene. *J. Phys. Chem. C* **116**, 2858–2862 (2012).

14. Ramakrishna Matte, H. S. S., Subrahmanyam, K. S., Venkata Rao, K., George, S. J. & Rao, C. N. R. Quenching of fluorescence of aromatic molecules by graphene due to electron transfer. *Chem. Phys. Lett.* **506**, 260–264 (2011).

15. Ramette, R. W. & Sandell, E. B. Rhodamine b equilibria. *J. Am. Chem. Soc.* **78**, 4872–4878 (1956).

16. Seybold, P. G. Thermodynamics of the rhodamine B lactone zwitterion equilibrium : An undergraduate laboratory experiment Thermodynamics of the Rhodamine B Lactone- Zwitterion Equilibrium. *J. Chem. Educ.* **64**, 2–5 (2015).

17. Rosenthal, I., Peretz, P. & Muszkat, K. A. Thermochromic and hyperchromic effects in rhodamine B solutions. *J. Phys. Chem.* **83**, 350–353 (1979).

18. Lv, Z. *et al.* Assembly of α-synuclein aggregates on phospholipid bilayers. *Biochim. Biophys. Acta - Proteins Proteomics* **1867**, 802–812 (2019).

19. Franke, J. M. *et al.* BODIPY Fluorophores for Membrane Potential Imaging. *J. Am. Chem. Soc.* **141**, jacs.9b05912 (2019).

20. Khan, A. F., Down, M. P., Smith, G. C., Foster, C. W. & Banks, C. E. Surfactant-exfoliated 2D hexagonal boron nitride (2D-hBN): role of surfactant upon the electrochemical reduction of oxygen and capacitance applications. *J. Mater. Chem. A* **5**, 4103–4113 (2017).

21. Lotya, M., King, P. J., Khan, U., De, S. & Coleman, J. N. High-concentration, surfactant-stabilized graphene dispersions. *ACS Nano* **4**, 3155–3162 (2010).

22. Smith, R. J. *et al.* Large-scale exfoliation of inorganic layered compounds in aqueous surfactant solutions. *Adv. Mater.* **23**, 3944–3948 (2011).

23. Song, L. *et al.* Large scale growth and characterization of atomic hexagonal boron nitride layers. *Nano Lett.* **10**, 3209–3215 (2010).

24. Kim, K. K. *et al.* Synthesis of monolayer hexagonal boron nitride on Cu foil using chemical vapor deposition. *Nano Lett.* **12**, 161–166 (2012).

25. Coleman, J. N. *et al.* Two-dimensional nanosheets produced by liquid exfoliation of layered materials. *Science (80-.).* **331**, 568–571 (2011).

CHAPTER 3. COVALENT FUNCTIONALIZATION OF GRAPHENE

3.1. Introduction

The functionalization of graphene has been a challenge for the chemist since the discovery of this material. The controlled modification of the surface of graphene can allow the tuning of its electric properties, changing the bandgap for the development of new type of devices.[1,2] Moreover, the introduction of functional groups on the surface can permit the sequent functionalization and introduction of new chemical compounds, improving the features and applications of graphene in different fields, from optoelectronics to biological applications.[3–5] As discussed in the Introduction, the biocompatibility of graphene is strongly affected by the chemical groups on the surface, and the controlled functionalization could then help the development of new smart materials.[6] Despite similar chemical structure and carbon atom hybridization of graphene to fullerene and carbon nanotubes, the reactivity of these carbon materials is not the same. Graphene resulted to be less reactive respect to the other carbon allotropes. The reactivity of graphene depends on its form (graphene, GO, r-GO), from the number of layers, from the dispersion of the layers and from the reaction conditions. Speaking about graphene, different types of reactions have been developed, with a high reaction yield on monolayer graphene. Most of the reactions and methodology described in the literature presents issues for scale-up productions and are normally involving only one functional group.[7–9] Very few are the studies showing bis-functionalization of graphene,[10] and no studies are showing, until now, the addition of two or more functional groups to obtain a multifunctional material.

3.2. Objective of this chapter

The aim of this chapter is the development of methods for the multifunctionalization of graphene, to obtain a functional material suitable for further modifications for the development of a drug delivery graphene-based carrier. In this chapter, I will describe the reactions investigated for obtaining the multifunctional graphene. The reactivity of different graphene species has been explored, to discover the most convenient functionalization route. With this purpose, we investigated different type of reactions and reagents, varying the reaction conditions to improve the final degree of functionalization. Important attention has been given to the scale-up of the reactions, from few mg to hundreds of mg of graphene functionalized in one step. I mainly focused on one-step reaction to functionalize graphene with different functional groups, for further production of a multifunctional platform suitable for drug delivery applications.

3.3. FLG functionalization

The functionalization of graphene has been investigated at the beginning on FLG, produced by exfoliation of graphite in NMP (see paragraph 3.6 for details).[11] The sheets obtained through this protocol present a low amount of defects (I_D/I_G ratio ~0.21-0.30) confirmed by TGA analysis, with a weight loss of the different batches produced between 1 and 5 %. The average lateral size of the distribution resulted ~900 nm, with sheets between 200 and 2400 nm. 1,3-Dipolar cycloaddition and functionalization with diazonium salt derivatives have been exploited for the functionalization of graphene surface.

3.3.1. **1,3-Dipolar cycloaddition**

The 1,3-dipolar cycloaddition involves the reaction between a N-functionalized amino acid and an aldehyde, leading to the *in situ* formation of an azomethine ylide and the subsequent cycloaddition onto graphene surface. The reaction was first developed for the functionalization of fullerene,[12–14] becoming famous with the name of Prato reaction. Prato and co-workers successfully applied this reaction to the functionalization of carbon nanotubes and graphene.[15] The reaction has been demonstrated to take place not only at the edges of graphene but even on the surface of the material, with the possibility to obtain homogeneous functionalized sheets. To explore the use of this reaction for our multifunctionalization route investigation, the precursor of the reaction, the (2-{2-[2-(tert-butyl-oxy-carbonyl amino)-ethoxy]-ethoxy}-ethylamino)-acetic acid (**ML11**) was synthesized (see paragraph 3.6 for the procedure).

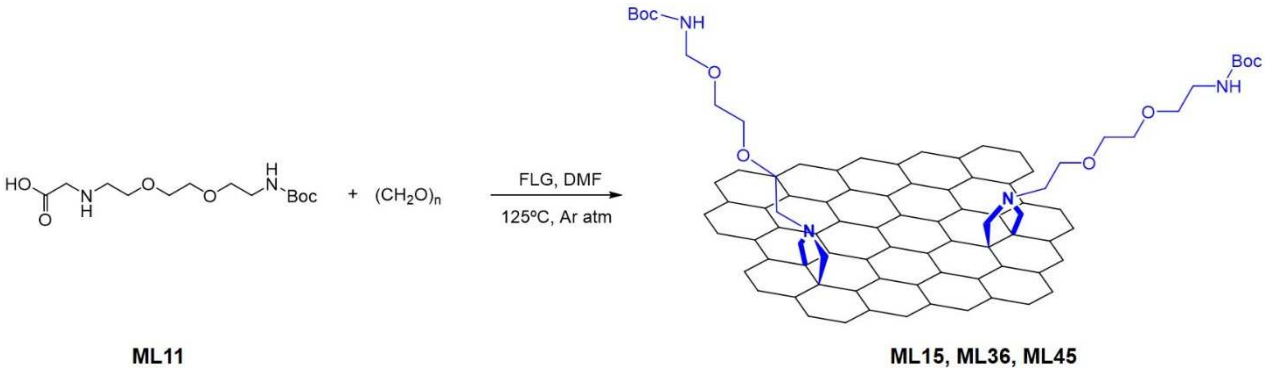

Scheme 3.1: Scheme of 1,3-dipolar cycloaddition to FLG.

The protocol described in the literature requires the use of 4 eq. of reagent respect to the carbon atoms constituting graphene, and 4 days of reaction at 125 °C, with the addition of an extra eq. of reagent every day. Due to the low yield of the reaction obtained from the synthesis of the organic precursor and the long-time required for its preparation, I tested at first the reaction using a lower amount of reagent ML11 respect to the described protocol, and decreasing the reaction time, from 4 to 1 day. Five mg of FLG was reacted with 1.5 eq. of ML11, adding every 2 h 1 eq. more of **reagents-** (yielding **ML15**) (Scheme 3.1). The formation of the final conjugate was investigated by Raman spectroscopy and Kaiser test. Raman spectroscopy showed no significant increase in the I_D/I_G ratio (from 0.22 of the starting graphene to 0.26 of the final product). After Boc deprotection of the amine, I obtained from Kaiser test an average value of ~13 µmol/g, very far from what described in the literature for this reaction (~640 µmol/g).[15] After this poor level of functionalization, the reaction was tested again reacting graphene for one day with 1.5 eq. of **ML11**, adding 0.5 eq. more of reagent every day (yielding **ML36**). The final product was characterized again by Kaiser test, giving a value of ~20 µmol/g. Finally, the reaction was tested again employing 3 eq. of **ML11** and adding 1 eq. more of compound every day (yielding **ML45**). Even in this case, the result obtained was unsatisfactory, with a Kaiser test value of ~18 µmol/g. This poor reactivity and level of functionalization could be due to different factors. One could be due to the nature of the graphene employed, its number of layers and the quantity of defects present on the surface (the defects on the surface are corresponding to reactive sites for the functionalization). The second reason could be the low amount of reagents employed for performing the reaction. In this context, I would like to draw the attention on the amount of reagents required: for the functionalization of 5 mg of graphene, between 500 and 800 mg of compound **ML11** are needed. We believe that the synthetic effort required for the synthesis of **ML11** and the large amount needed to functionalize a small quantity of graphene are not suitable for the development of a synthetic strategy, which will demand

high quantity of functional material (at least 20/30 mg for *in vitro* studies and more than 150 mg for *in vivo* studies) and we decided to move on different functionalization reaction.

3.3.2. Functionalization of FLG by in situ formations of diazonium salts

In view of the low degree of functionalization obtained through the 1,3-dipolar cycloaddition reaction and the elevate demand of reagents to perform the reaction, we decided to move on a different type of reaction. Aryl diazonium compounds (or diazonium salt, DS) are extremely reactive compounds, forming radical species through the elimination of N_2 from their structure. The radical aryl species formed is a suitable reagent for the functionalization of carbon nanomaterials.[16,17] The production of the diazonium compounds require a small synthetic effort, with a high yield of reaction and easy scale-up production. In the past, our group published the synthesis and post-modification of multifunctional carbon nanotubes using three derivatives of 4-aminobenzylamine.[16] With the purpose to obtain multifunctional graphene, we decided to apply a similar functionalization strategy to graphene, using the above-described FLG as starting material. Three derivatives of 4-aminobenzylamine were synthesized following the procedure reported in the previous work.[16] The amino group of benzylamine was protected by three orthogonal protecting groups, Boc (*tert*-butyloxycarbonyl), Cbz (benzyloxycarbonyl) and Pht (phtalimide) (Figure 3.1, see paragraph 3.6 for the synthesis). The different protection is the key to the multifunctionalization strategy, permitting the selective deprotection and modification of each group on graphene after the first functionalization of the surface.

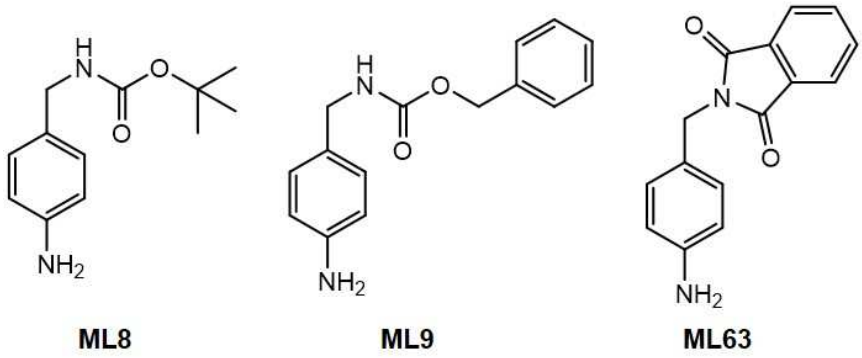

Figure 3.1: 4-Aminobenzylamine derivatives protected with Boc (*tert*-butyloxycarbonyl), Cbz (benzyloxycarbonyl) and Pht (phtalimide).

The DS functionalization of graphene is well described in the literature, and many experimental and theoretical studies are supporting the evolution of the reaction.[17–19] In our case, we decided to start the study using only the Boc protected DS due to its easy laboratory production in gram scale. Following the procedure already employed in our laboratory, the DS was synthesized *in situ* in presence of graphene. Graphene (1 eq.) was dispersed in NMP/H_2O (5:1), the Boc-benzylamine derivate (0.2 eq., 1:5 *w/w* ratio G:DS) was added to the mixture together with 3-methylbutyl nitrite to form the correspondent DS. The reaction was stirred at 80 °C for 24 h (Scheme 3.2) (see paragraph 3.6 for the procedure).

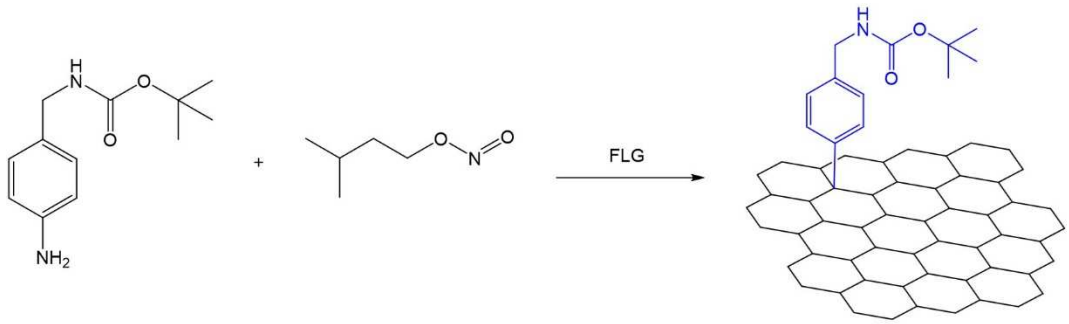

ML8 ***In situ:*** **ML20, 31, 52, 81, 82**

Scheme 3.2: Functionalization of graphene by *in situ* formations of Boc-DS. Reaction **ML20, 31, 52, 81, 82**.

I decided to test as first the use of a low amount of DS respect to graphene, to understand if it would have been possible to use of small amount of reagent for the functionalization of the material. The DS was used in a mass/mass ratio of 5:1 respect to graphene, mixing 10 mg of graphene with 50 mg of Boc-derivate (reaction **ML20**). The occurrence of the reaction was measured by Kaiser test, after the deprotection of the amino group. Boc protecting group was removed as described for 1,3-dipolar cycloaddition graphene-derivate and the Kaiser test was performed on the obtained material, giving a result of almost zero free amines present on graphene. Because of the non-functionalization of graphene using this low amount of material, no other characterization techniques were applied to this product. The negligible value obtained from the Kaiser test was a confirmation of the need of a large amount of reagents for the functionalization of FLG. Even in the case of this functionalization way, the problem of the low reactivity of FLG is evident. Hirsch *et al.* suggested that to successfully obtain high degree of functionalization of FLG, it is necessary to employ from 4 to 6 eq. of reagents respect to graphene. Ratios of 1:1 or 1:2 eq. of G:DS are leading to poor functionalization degree of the material. The purpose of our investigation was the production of graphene with a large amount of functional group (>100 µmol/g), to covalently functionalize the material with a sufficient amount of functionalities for the desired biomedical applications. With this purpose, I decided to follow on the investigation on the functionalization of graphene with Boc-DS increasing the quantity of reagents employed. Reaction **ML37** was performed in the same conditions using 1.5 eq. of DS. In this case the Kaiser test gave a value of ~30 µmol/g, a promising result for the improvement of the reaction yield. To increase more the yield of this reaction I decided to change solvent, from NMP to DMF (DMF/H_2O 5:1). In DMF the DS precursor resulted to have a better solubility that could lead to increase the favorable interactions between the reagent and the surface of graphene. I also increased the amount of Boc-DS to 4 eq. (yielding **ML52**). Unfortunately, the Kaiser test resulted in lower value respect to the previous experiment, with a value of ~18 µmol/g. Kaiser test was performed since the beginning of my investigation because to the low amount of material (~0.5 mg total) and short time required to perform the analysis. In front of these conflicting results I decided to use TGA for the analysis of the functionalized graphene (f-G), following the weight loss as parameter for the functionalization degree. TGA is giving an idea of the behavior of the material at the increasing temperature. The comparison between the starting and functionalized material is useful to measure the weight loss due to the release of the functional groups introduced after the reaction, and to evaluate the amount of organic moieties loaded onto the surface. Contrarily, the amount of material required for the TGA is of ~2 mg, corresponding to a huge consumption of f-G. Due to the difficult production of graphene, the described reactions were always performed on few amounts of material (5-8 mg), as a consequence, TGA was not our first choice because of the destruction of the final f-G.

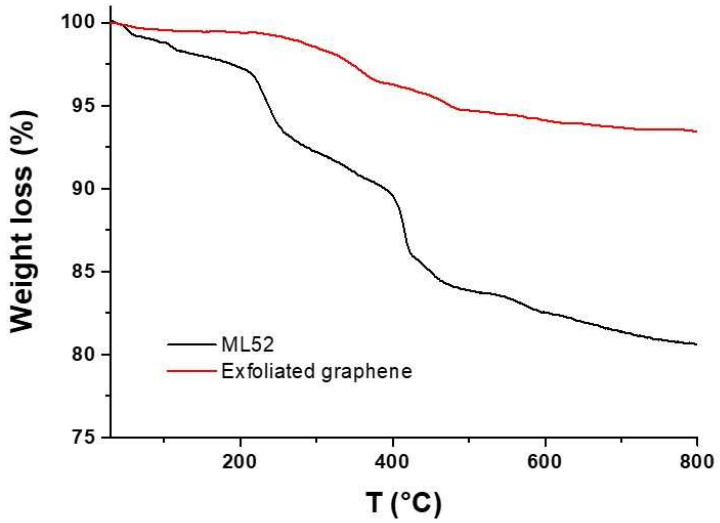

Figure 3.2: TGA weight lost profile of ML52 reaction. Red line: Starting material; black line: functionalized graphene

ML52 presented a weight lost respect to the starting graphene of ~8%. This weight loss, if completely related to the covalent functional groups grafted onto graphene, would correspond to ~360 µmol/g of functionalization (Figure 3.2), higher respect to what observed by Kaiser test. This difference could be due to a non-complete deprotection of the amine, to a wrong response of the Kaiser test, strongly dependent on the aggregation state of the material in solution, or to a misinterpretation of the TGA analysis.

The black line weight loss profile is corresponding to **ML52** functionalized material. The material presents two change of slope at ~220 °C and at ~410 °C. The total weight loss was calculated at 600 °C between the exfoliated graphene and the functionalized graphene.

The interpretation of the TGA data is of not easy without further characterizations. The first weight loss, at ~220 °C is to attribute to the degrafting of functional groups covalently linked to graphene. The second curve, due to the high temperature of ~400 °C, could correspond to salts remained adsorbed on the surface and not removed during the work-up procedure.

However, it is not possible to evaluate the real weight loss corresponding to the functional group bound onto the surface due to the double contribution of unknown species on the analysis. Due to the few amounts of f-G I repeated the reaction (yielding **ML82**) looking for confirmation to the obtained results and to perform new characterization on the material.

For an easy comprehension, the different conditions tested, and the results obtained from the first reaction of functionalization are summarized in Table 3.1.

Entry	G:DS ratio eq.	Solvent	T (°C)	Kaiser test (µmol/g)	TGA	Raman G (I_D/I_G)	Raman f-G (I_D/I_G)
ML20	1:5 *w/w*	NMP/H_2O 1:5	80	0	-	-	-
ML31	1.5	NMP/H_2O 1:5	80	31	-	-	-
ML52	4	DMF/H_2O 1:5	80	13	8 %	-	-
ML81	4	ACN/H_2O 1:5	80	-	8 %	0.28	0.31
ML82	4	DMF/H_2O 1:5	80	-	6 %	0.28	0.29

Table 3.1: Table of the reaction conditions tested for the functionalization of FLG with *in situ* formed DS.

Two new reactions were performed, investigating ACN as new solvent (yielding **ML81**) and DMF (yielding **ML82**), using 4 eq. of Boc-DS. The TGA measurement presents a weight loss of ~8 % and 6 %, respectively, but the weight loss profiles are of difficult comparison and interpretation (Figure 3.3)

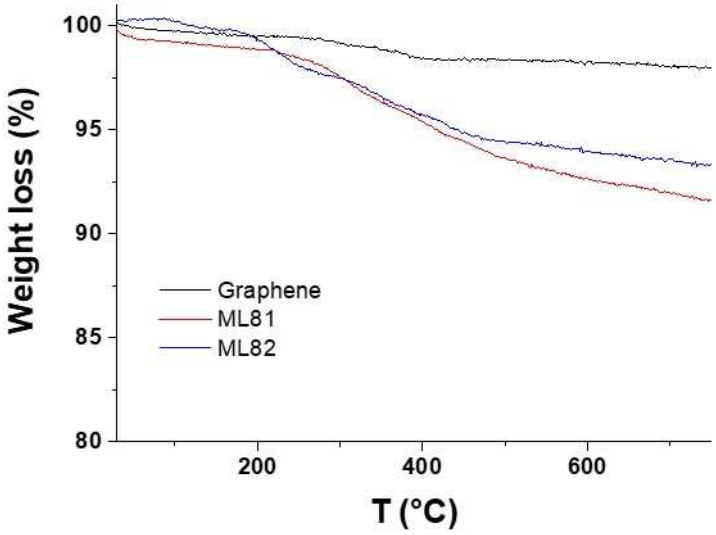

Figure 3.3: TGA analysis of f-G corresponding to ML81 (red line) and ML82 (blue line), respectively, in comparison to starting graphene (black line).

The samples were also analyzed by statistic Raman analysis. With this technique we can investigate the occurrence of the reaction by the evolution of the D band (~1350 cm^{-1}) and G band (~1582 cm^{-1}). The increasing of the D band signal respect to the starting material is corresponding to an increase in the quantity of sp^3 carbon atoms on the structure of graphene, due to an increase of the functional groups or defects introduced in the structure, after functionalization or oxidation process. The I_D/I_G ratio of the starting graphene was of ~0.28, corresponding to graphene with a low amount of defects on the surface. From the Raman analysis performed on **ML81** and **ML82**, I found a ratio of 0.31 and 0.28, respectively (analysis performed on graphene sheets deposited on a substrate of SiO_2). These values are not corresponding to a successful functionalization of the material and may fall into the statistic error of the analysis. The data obtained from the two analysis techniques are not in agreement. If in the case of TGA it is possible to observe a weight loss, leading to think that functionalization occurred on graphene, from Raman analysis we were not observing an increase on the I_D/I_G, corresponding to a non-functionalization of the material. TGA is analyzing the entire bulk material, eventual inhomogeneity on the functionalization are not affecting the final result, whereas Raman strongly depends on the sheets analyzed. Inhomogeneity on the sample, such as wrong deposition or aggregation during the deposition, depending on how the analysis is performed, could lead to a false negative or positive result. Even in this case, due to a low amount of material obtained, it was not possible to continue the characterization using Kaiser test that could have provided interesting information about the nature of the weight loss observed on TGA.

3.3.3. **Functionalization of FLG with pre-formed diazonium salts**

To increase the functionalization degree of graphene, I decided to change the strategy of functionalization with the DS. Until now the reactive species were produced *in situ*, which could lead to uncertainty about the real formation of the salt, due to interaction of the reagent with graphene (i.e. the reactive species could be adsorbed on graphene before the formation of the salts). To avoid this problem, I decided to pre-synthesize and isolate the DS salts, adding directly the reactive species to the reaction mixture (see paragraph 3.6 for

the synthesis and characterization). The reaction was first tested in ACN/DMF (5:1) due to the good solubility of the DS in ACN (yielding **ML84**) (Scheme 3.3).

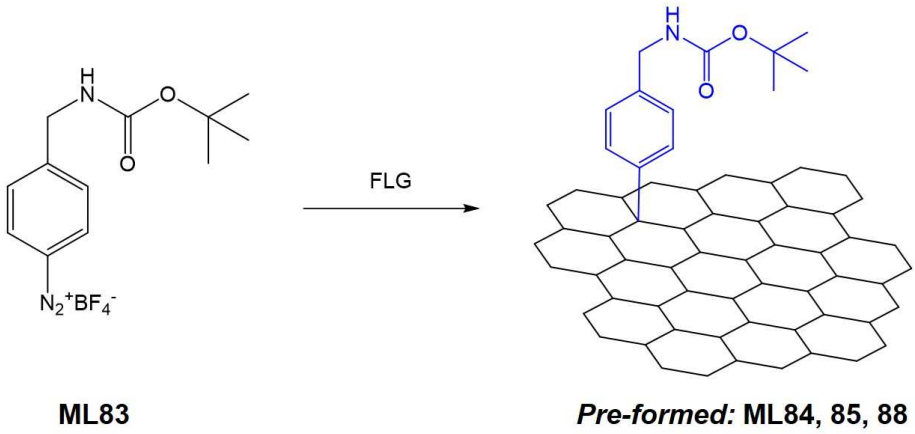

ML83 **Pre-formed: ML84, 85, 88**

Scheme 3.3: Scheme of reaction for the functionalization of FLG with pre-formed diazonium compound.

Three eq. of Boc-DS was mixed with graphene and the reaction stirred at 45 °C overnight. The TGA showed a weight loss of ~6% (Figure 3.4, blue line). From Raman analysis I observed an increase of the I_D/I_G from 0.28 of graphene to 0.39 of f-G. The increase on the D band intensity, together with the weight loss, is a first proof of the possible successful functionalization of graphene. Direct observation of the reaction mixture showed the formation of aggregates of graphene after few hours after the beginning of the reaction. The aggregation of graphene lead to a reduction of the material surface exposed to the reaction environment, decreasing the possible interactions between graphene and the reagents. To avoid this behavior, I decided to change the solvent from ACN/DMF to DMF/H_2O (5:1) (yielding **ML85**). DMF has better action in graphene dispersion respect to ACN. Unfortunately, the solubility of the DS is lower in DMF than in ACN. TGA showed a weight loss of ~6% (Figure 3.4, purple line), while through Raman I measured an increase of I_D/I_G from 0.21 to 0.38. The increase on the Raman band of **ML85** is slightly higher with respect to **ML84**, probably due to the less aggregation during the reaction. **ML88** was obtained using 6 eq. of Boc-DS in DMF/H_2O, leading to a conjugate with a higher weight loss respect to **ML85**, of ~12%, but not to a proportional increase of the D band intensity, which evolved from 0.21 to 0.35. In Table 3.2 are summarized the conditions tested for the above-mentioned reactions.

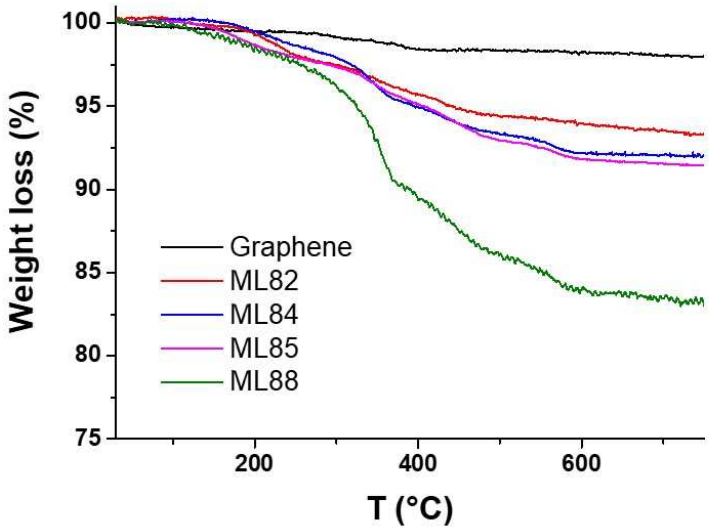

Figure 3.4: TGA analysis of f-G functionalized by *in situ* formations of DS (ML82, red line) and by pre-formation of Boc-DS (ML84, 85 and 88). (Graphene source for ML 85 and 88 are the same, while for ML84 I employed a different batch of FLG, but with similar TGA profile)

Entry	G:DS ratio eq.	Solvent	T (°C)	Kaiser test (µmol/g)	TGA	Raman G (I_D/I_G)	Raman f-G (I_D/I_G)
ML84	3	ACN/DMF 5:1	45	-	6 %	0.28	0.39
ML85	3	DMF/H_2O 5:1	45	38	7 %	0.21	0.38
ML88	6	DMF/H_2O 5:1	45	40	12 %	0.21	0.35

Table 3.2: Table of the reaction conditions tested for the functionalization of FLG with *pre-formed* DS. (Graphene source for ML 85 and 88 are the same, while for ML84 I employed a different batch of FLG, but with similar TGA profile)

The comparison between **ML85** and **ML88** is controversial. The second reaction was performed employing a double amount of DS, and only looking at the TGA curves we can see an increase of the weight loss from 7 to 12 %. On the other hand, the increase on the I_D/I_G ratio corresponds to 0.17 for the first reaction and only to 0.14 for the second, showing an inverse behavior and not confirming the increasing of the graphene functionalization. Neither from Kaiser test it was possible to observe an increase of free amines on graphene. A high amount of reagent could lead to side-reactions between the DS already grafted onto the graphene surface and the reactive species in solution. This behavior, that leads to the formation of polymeric functions on graphene, can cause an increase of the weight loss without a consequent increase of the I_D/I_G ratio.[20] However, we would have expected an increase in the Kaiser test result, that was not the case. Moreover, as demonstrated by Greenwood *et al.*, the presence of functional groups on the aryl moiety can avoid the occurrence of side reactions. The increase of weight loss together with the Raman behavior could be explained even by an increase of non-reacted molecules on graphene surface. But in this case, I would have expected the starting of the weight loss to temperature lower than 200 °C. Unfortunately, the characterization of graphene materials is not obvious, and in some cases, the combination of the most common analysis technique is enough for a precise determination of the surface modifications. Despite the uncertain characterization of the material, the presence of amino groups on the surface encouraged the investigation of new functionalization of graphene, in order to study the preparation of a platform for drug delivery.

3.3.3.1. Functionalization of f-G-NH_2

Boc protecting group on **ML88** was removed (yielding f-G-NH_2) to further modify the amine groups. Compound **ML11** was selected for the functionalization due to the presence of TEG chain, known to increase the water dispersibility and the biocompatibility of graphene materials. The carboxylic group was activated with EDC and NHS and reacted with the free amines present onto graphene, to obtain f-G-TEG-Boc (**ML90**) (Scheme 3.4) (see paragraph 3.6 for the protocol).

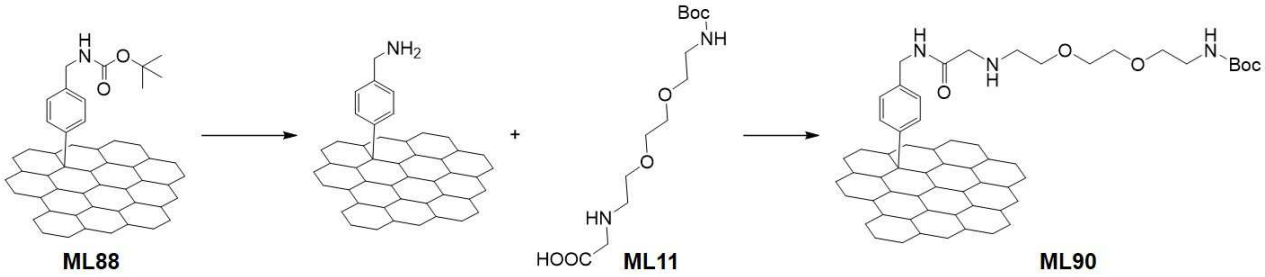

Scheme 3.4: Scheme of the functionalization reaction of f-G-NH_2 with a TEG derivative.

After purification, the final material was analyzed first by TGA, with the aim to observe the increase of the weight loss of the material due to the functionalization with the TEG derivate. Unfortunately, the TGA profiles was not very clear. The weight loss of the reaction is lower respect to the unprotected graphene (Figure 3.5). This strange behavior pushes in the direction of a non-occurred reaction, followed by a release of possible adsorbed molecules from the surface or trapped between the graphene layer, and a consequent decrease of the mass of the organic compound on the material. On the other hand, as the quantity of free amines (evaluated by Kaiser test in ~40 µmol/g) is very low, it is possible that the reaction occurred, but the amount of functional group was not enough to significantly change the weight loss of the material. In comparison the amount of adsorbed organic compound was very high (exactly as hypothesized on the precedent paragraph for **ML88** reaction). I decided to do not go further with the characterization of the material and switch to a completely different route for the functionalization of the material (paragraph 3.4).

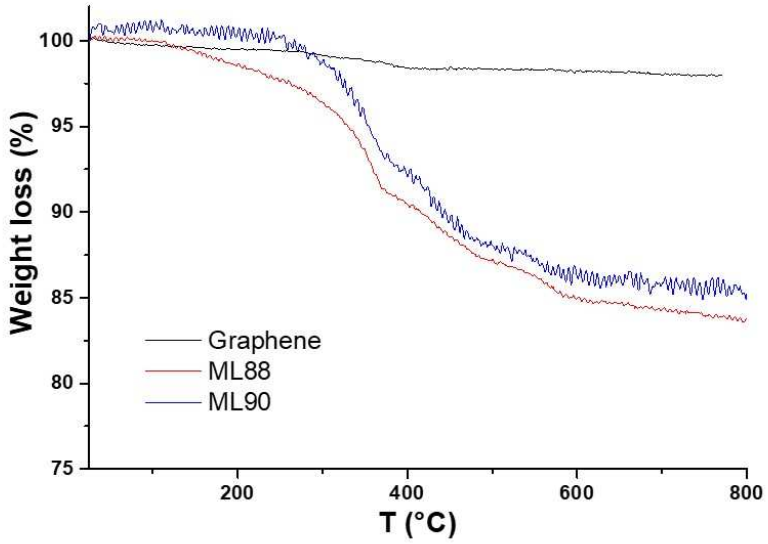

Figure 3.5: TGA analysis of starting graphene (black line), ML88 (red line) and ML90 (blue line).

3.3.3.2. Functionalization of graphene with 4-propargyloxybenzene diazonium tetrafluoroborate

The study on the multifunctionalization of FLG was not only focused on the use of 4-aminobenzylamine derivatives. My primary intent was to include on graphene functional groups with orthogonal reactivity, to allow multifunctionalization through few and easy reaction steps. In this context, Strano and co-workers developed the synthesis and functionalization of graphene using 4-propargyloxybenzene diazonium tetrafluoroborate, an aryl diazonium salt derivate with an alkyne as functional group.[21] The alkyne moiety has different reactivity respect to the amino group of the DS already tested for the functionalization of graphene and could be suitable for an orthogonal synthetic strategy. An approach based on double functionalization of graphene with an alkyne and an amino group would permit easily the functionalization of the material with new organic compounds. The synthesis of the 4-propargyloxybenzene diazonium tetrafluoroborate (alkyne-DS) started from available commercial compounds and it is shown in Scheme 3.5 (see paragraph 3.6 for the protocol).

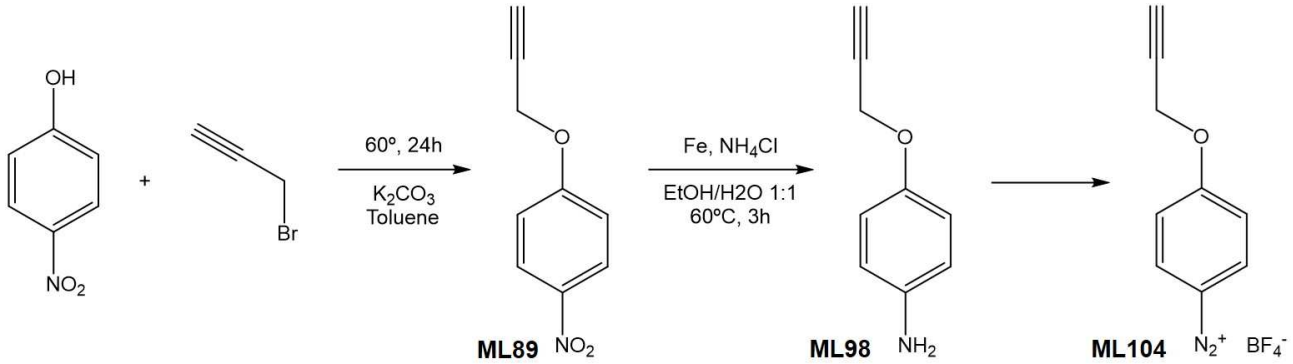

Scheme 3.5: Scheme of the synthesis of 4-propargyloxybenzene diazonium tetrafluoroborate.

The alkyne-DS was then tested for the functionalization of FLG (**ML104**). Graphene was dispersed in DMF by bath sonication, the mixture was warmed up at 45 °C and alkyne-DS was added to the reaction (5 eq.) and stirred for 24 h. The characterization was conducted by TGA (Figure 3.6a), showing a weight loss of ~5% and by Raman spectroscopy, with an increase of I_D/I_G ratio of ~0.03 (from 0.26 to 0.29, Figure 3.6b).

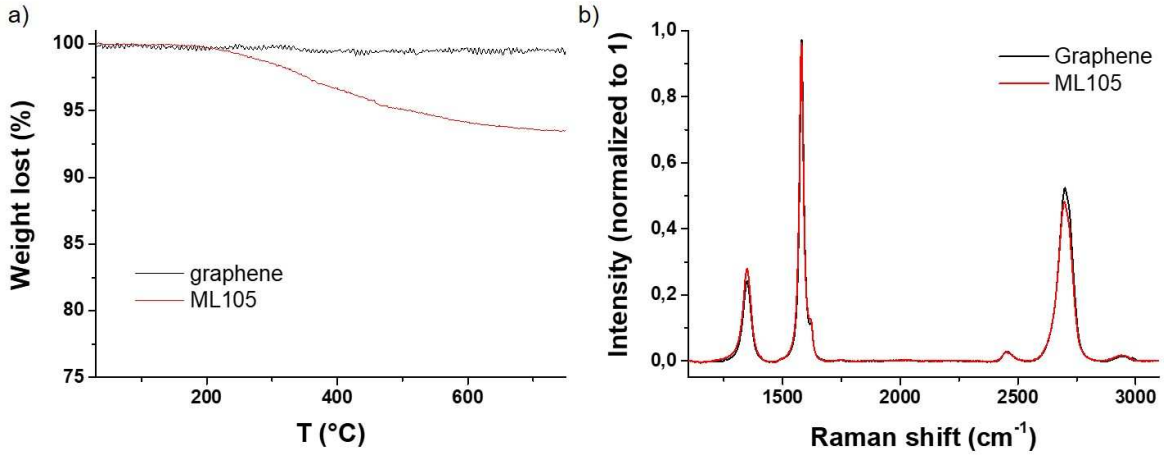

Figure 3.6: Characterization of reaction ML105. a) TGA weight loss profile of graphene (black line) and f-G (red line); b) Superposed Raman spectra of graphene (black line) and ML105 (red line).

Even for this reaction the Raman analysis and TGA disagree. The increase of the Raman D band is very poor to confirm a successful functionalization of graphene, while TGA is showing a loss of mass of ~5 % from 210 °C to ~600 °C that could correspond to the defunctionalization of graphene surface. In this case I am hypothesizing that the weight loss is corresponding to organic molecules (reagents and solvents) hardly eliminated from the material. On the light of these results, as mentioned before for the Boc-DS functionalization, I decided to move to another technique of graphene functionalization, starting from intercalated graphite to obtain functionalized graphene with a higher degree of functionalization.

3.4. Functionalization of intercalated graphite (KC_8)[22]

As described in the introduction, many advantages arise from the graphite intercalation with alkaline metals for the functionalization of graphene.[23,24] Through this approach it is possible to obtain the functionalization of graphene starting directly from bulk graphite. The material obtained presents a homogeneous functionalization of the surface and a high degree of functionalization.[25,26] The scale-up of these reactions is easy, passing from the common 5-10 mg to 100-200 mg of material functionalization. Moreover, thanks to the high reactivity of the reduced graphene, the performance of the reactions requires lower amount of reagents in respect to the reactions with FLG, with the consequence of a reduced synthetic effort. We decided to move on the direction of this synthetic approach to increase the functionalization degree of graphene, to achieve the synthesis of multifunctional graphene using the above-mentioned diazonium salts and follow up our investigation on drug delivery applications of graphene. Hirsch's group has intensely investigated and developed the synthesis, reactivity and characterization of graphene intercalated compounds (GICs).[10,18,26] To investigate the functionalization strategy of GICs with our reagents, I have been hosted in Hirsch's group, at the University of Erlangen-Nuremberg. During a period of three months I worked with graphite intercalated with metallic potassium, called KC_8, and on the multifunctionalization of this graphene species.

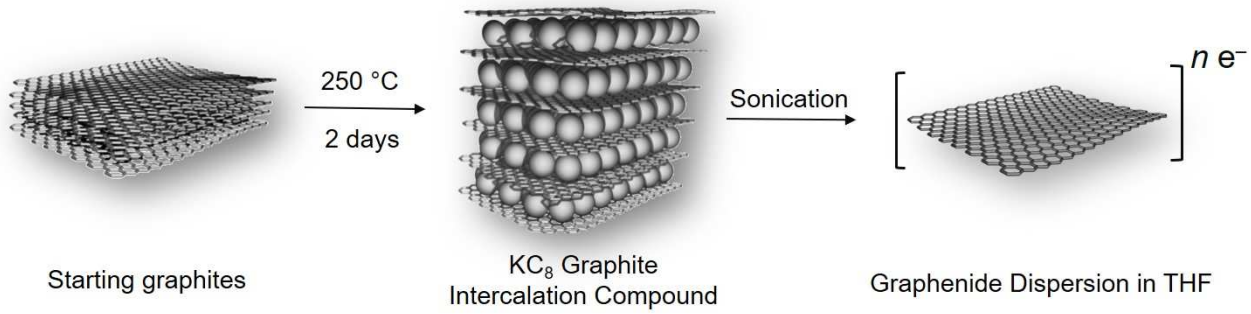

Figure 3.7: Graphite intercalation with metallic potassium and exfoliation of the graphenide species in anhydrous and degassed THF.

The obtaining of KC_8 requires very careful handling of all compounds and the laboratory equipment, the work in a glovebox under inert atmosphere and the use of completely dried glassware and reagents. The reactivity of KC_8 is so high that the contact with a not properly dried glassware leads to the immediate oxidation of the powder to GO. Graphite must be dried, and the presence of oxygen removed from the powder before the use. Inside the glovebox the graphite powder is mixed with metallic potassium in a ratio of 1:8 between K and C, the mixture is warmed up at 250 °C to melt the potassium and manually mixed for two days to enhance the intercalation of the potassium atoms between the graphene layers. To obtain the graphenide dispersion, the KC_8 powder is dispersed in anhydrous and de-oxygenated THF and sonicated by tip sonication to separate

the sheets (see paragraph 3.6 for the detailed production). The characteristics of KC_8 graphenide species is the typical brown/gold color of the powder, giving a brown coloration to the THF dispersion. After the addition of the reagents to this dispersion it is possible to observe the change of the color to black, indicating the occurrence of the reaction and the formation of functionalized graphene. Using KC_8, I investigated the synthesis of multifunctional graphene using different reagents, to obtain a material with multiple functional groups.

3.4.1. Functionalization of KC_8 with pre-formed 4-aminobenzylamine DS derivatives

The three orthogonal protected DS derivatives of 4-aminobenzylamine have been reacted with KC_8 dispersion for 2 days at room temperature in a ratio G/DS of 1:1 eq. (0.33 eq. of each DS) (yielding **ML125**). After few minutes from the addition of the reagents, the color of the suspension change from brown to black and bubble evolution was observed (formation of N_2), confirming the proceeding of the reaction (Scheme 3.6).

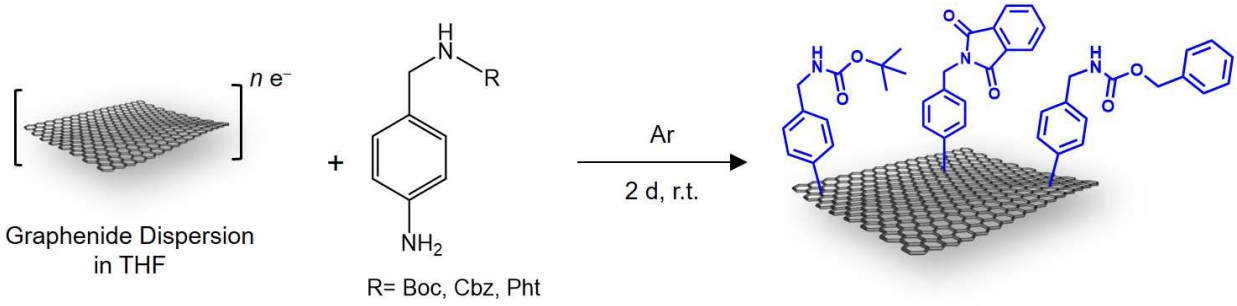

Scheme 3.6: Reaction scheme of reduced graphene with DS-derivatives (yielding **ML125**)

Very important to obtain sheets with good quality is the quenching of the unreacted charges on graphene.[23,27] This was achieved adding benzonitrile (PhCN) to the final mixture before the exposition to the air.

The evaluation of the functionalization of graphene (mf-G) started with statistical Raman spectroscopy (SRS). The analysis of the average Raman spectra revealed an increase of the intensity of the D band respect to the G band of the bulk graphite (I_D/I_G ratio 0.1), and the appearance of the D' band. Moreover, the typical 2D band at ~2690 cm^{-1} is combined by the appearance of a D+D' band at ~2900 cm^{-1}. This phenomenon is in agreement with the data reported in the literature and is a consequence of the A_{1g} mode-breathing vibrations of six-membered sp^2 carbon rings, which becomes Raman active after the symmetry of the nearby lattice is reduced (sp^2 carbons are converted to sp^3 hybridization) by the covalent functionalization with the diazonium salts.[25,28–30] The calculation of the intensity I_D/I_G distribution functions between the D band (~1350 cm^{-1}) and the G band (~1582 cm^{-1}) resulted in a value of 1.3, analyzing three different areas of the sample (Figure 3.8a). The narrow statistical distribution of the I_D/I_G shows a residual contribution of pristine unreacted graphite and high homogeneity of the entire bulk functionalization (H_{bulk}, Figure 3.8b).[31]

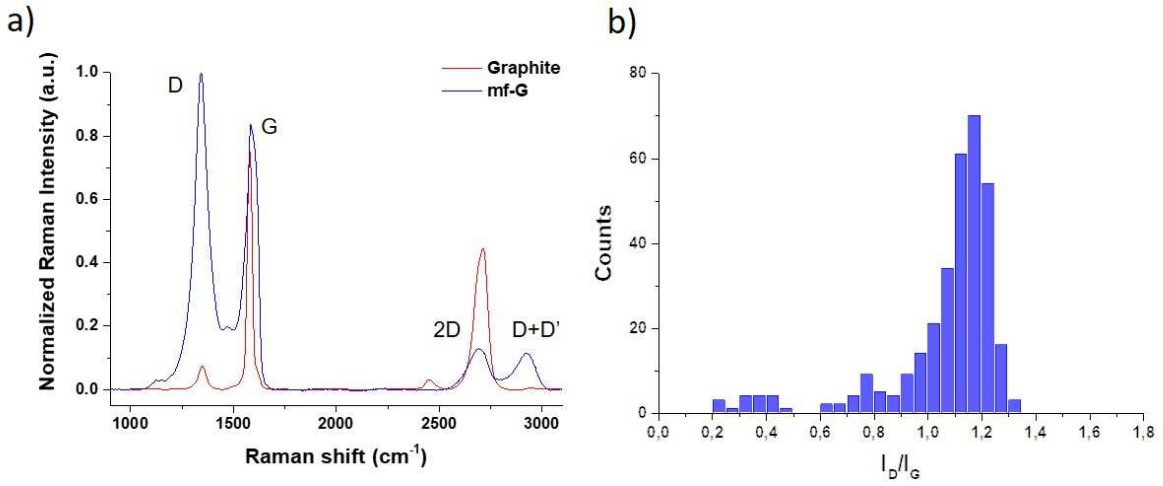

Figure 3.8: a) Comparison between mean Raman spectra (~500 single-point spectra) of graphite and mf-G; b) Distribution of I_D/I_G ratio from the Raman statistical analysis.

This first analysis is confirming the high reactivity of intercalated graphite respect to FLG. The use of only 1 eq. of reagents respect to 4 eq. employed for FLG permit the achieving of high functionalization degree, as indicated by the high increase of the D band of Raman spectra. The comparison of the Raman spectra highlights the great difference between the FLG functionalized material and the intercalated graphite (Figure 3.9).

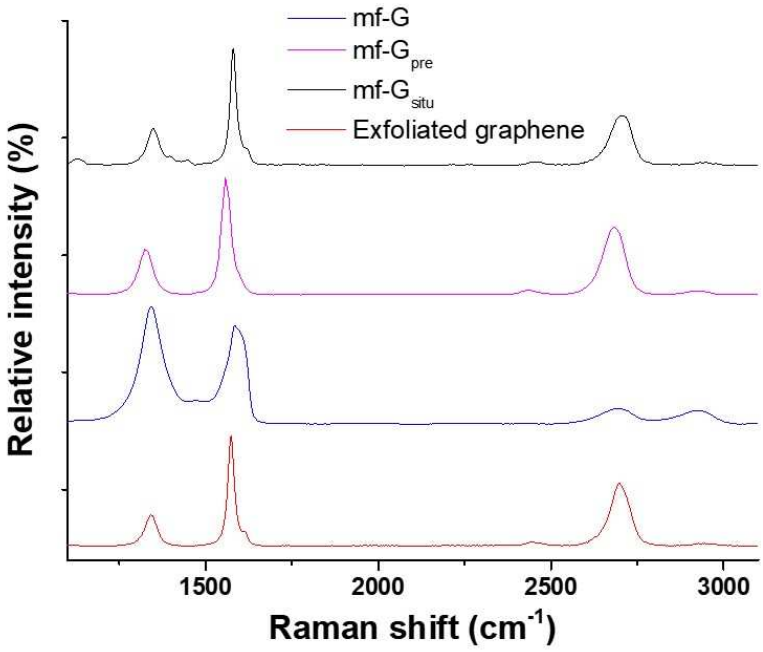

Figure 3.9: Comparison between Raman spectra of FLG functionalized graphene (**ML81**: black line, **ML88**: purple lines), mf-G (**ML125**: blue line) and starting FLG (red line).

To assure that the drastic conditions of the reactions on graphene and that the functionalization do not affect the morphology of the layers, mf-G was dispersed in DMF by bath sonication and observed by transmission electron microscopy (TEM), confirming the typical shape of 2D materials (Figure 3.10a).

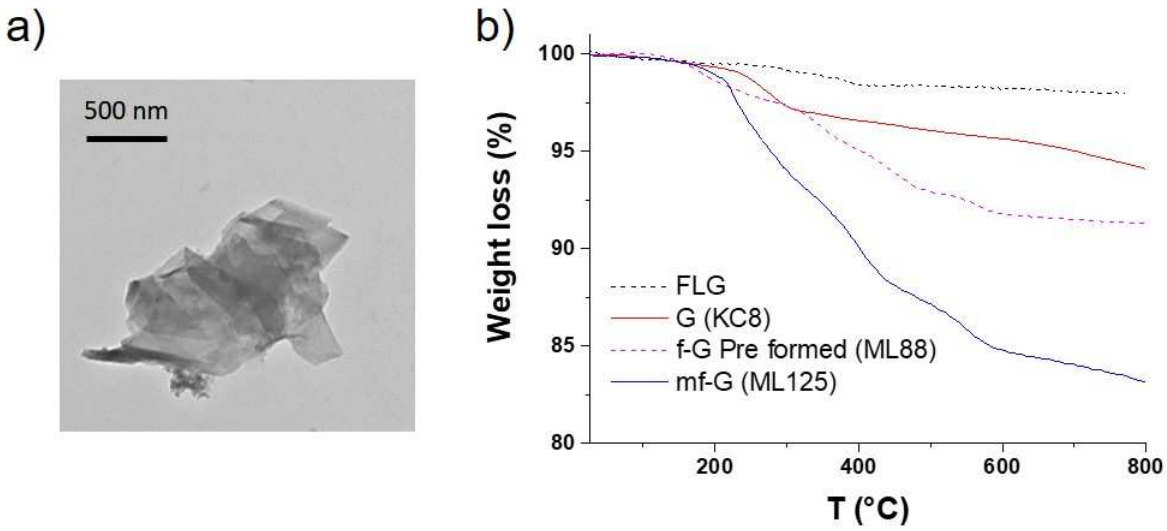

Figure 3.10: a) Low-magnification TEM image of mf-G; b) TGA comparison of KC_8 after charge quenching (red line), mf-G from ML125 (blue line), FLG (dashed black line), f-G from pre-formed DS (ML85, dashed magenta line).

Interesting is the comparison between the TGA weight loss of **ML88** (functionalized FLG with pre-formed DS, 4 eq. of reagents) and **ML125** just described (Figure 3.10b). The first compound presents a weight loss of ~7%, but an I_D/I_G ratio of only 0.17, whereas the second present a weight loss of ~12% and an I_D/I_G ratio increase of 1.2 with the use of only 1 eq. of reagents. From this comparison, we can clearly understand the difference in reactivity of the two species, with the intercalate graphene that allows the use of low amount of organic compounds to obtain a large and homogeneous functionalization of the surface. Besides, the use of high amount of reactive species is leading to side reactions, such as modification of the introduced functional groups or quenching of the reactive species by radical recombination, leading to the preferable choice of GICs for large scale production of functional material. However, before making quick conclusions, it is crucial to understand the fate of the organic compounds employed in the reaction, to recognize if their chemical structure has been modified by the strong reaction environment due to the presence of metallic potassium and highly reactive graphene. With this purpose, we investigate, through temperature-dependent statistical Raman spectroscopy (T-SRS), the thermal evolution of the material between 25 and 450 °C. The I_D/I_G ratio slowly diminishes until 200 °C and then starts to decrease dramatically reaching mean I_D/I_G values of 0.45 at 425 °C (Figure 3.11a, black dotted line). This phenomenon is due to the detachment of the functional groups from the surface of graphene and corresponds to the rehybridization from sp^3 to sp^2 of the carbon atoms, thus restoring of graphitic configuration. In addition, it is also remarkable the increase of the 2D band and the decrease of the D+D' band, confirming that the defunctionalization process of the diazonium salt derivatives was occurring (Figure 3.11b). The observation of the detachment of covalently bound moieties was corroborated by the TGA. The weight loss profile (Figure 3.11a, blue line) is stable until 220 °C, temperature above which the drastic weight loss began. To well understand the slight difference in the defunctionalization temperature observed between the two above-mentioned techniques, we must consider that the warming-up ramp programs present small differences. TGA program warm-up the samples at 10°C/min uniformly, while during Raman analysis the sample is warmed-up in successive steps, keeping stable the settled temperature during the scanning time. We can then affirm that the overall defunctionalization starts between 200° and 220° C. Moreover, the observed weight loss of ~12% is in good agreement with the I_D/I_G ratio value of 1.3, corresponding to a high degree of functionalization of graphene.[25] In addition, these results suggest the absence of secondary products, again in good agreement with combined thermogravimetry gas chromatography and mass spectrometry analysis (see below).

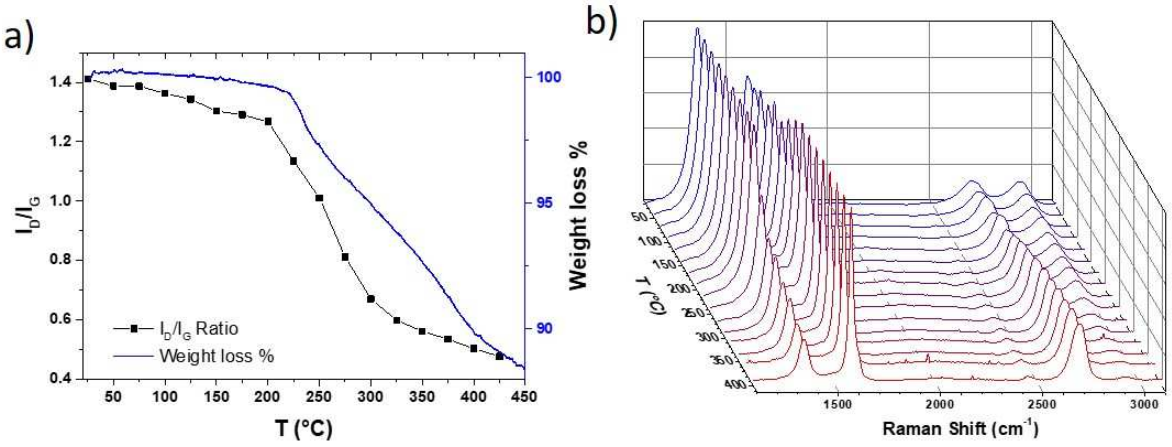

Figure 3.11: Temperature-dependent statistical Raman spectroscopy (TSRS) of mf-G in the temperature region between 25 and 450 °C. a) I_D/I_G ratio plotted respect to temperature and TGA analysis of mf-G. b) Means of the Raman temperature depending spectra.

The data obtained from the Raman analysis and the TGA are relative to the quantity of defects introduced on graphene surface during the functionalization reactions, but do not provide information about the chemical nature of these defects. To verify the effective functionalization with the different diazonium salt derivatives, several techniques were applied. First, the presence of nitrogen was investigated by X-ray photoelectron spectroscopy (XPS). The atomic percentage composition of mf-G was measured, revealing a ratio between C, O and N of 86.2%, 10.8% and 3.00% for the mf-G, respectively, and of 94.5%, 5.2% and 0.35%for graphene, respectively, after the initial potassium intercalation. The increment of N is the first sign that the increase of the defects observed by Raman spectroscopy is related to the grafting of the new functional groups and not due to a simple oxidation of graphene. In order to obtain a direct and unique confirmation of the presence of the functional groups on graphene, the Kaiser test was performed on mf-G.[32,33] The obtained results of 76, 42 and 46 µmol/g for Boc, Cbz and Pht protected amines, respectively, are the proof of the presence of the expected functional groups grafted on graphene. The abundance of Boc protected amine respect to Cbz and Pht is due to the reactivity of the species, similarly to the data that we previously reported (Boc>Pht>Cbz).[16]

To further explore the presence of the functional groups on the graphene structure, we analyzed mf-G using MAS-NMR. ^{13}C solid state NMR on graphitic samples,[34,35] and particularly in the case of single graphene sheets, is known to be rather challenging as it faces specific issues lying on high electric conductivity. Electric conductivity causes probe tuning problems,[34,36] and very often gives rise to extremely wide lines[37] that may become undetectable or indistinguishable from probe background signal when using DP/MAS (Direct Polarization/Magic Angle Spinning). As in pure graphene sheets, no protons are available to perform CP/MAS experiments (Cross Polarization/Magic Angle Spinning) we recorded here a series of DP/MAS on a 750MHz spectrometer (17.8 Tesla) with a spin-echo sequence[38] that cures the background signal problem and gives flat baselines and undistorted line shapes. We performed and compared the spectra of graphene after the intercalation of potassium (KC_8), of KC_8 mixed with the starting reagent (G_{mixed}) and of the final mf-G. In the case of the KC_8 sample, as expected for graphene, we had to finely mix it with an insulating powder (SiO_2 in a ratio of 1:4 graphene to SiO_2) to avoid the sample behaves as a bulk conductor[34] and to achieve correct probe tuning and fast sample spinning. In addition, no clear signal of functional carbon atoms was detected (Figure 3.12a, bottom), which may be an indication of KC_8 ^{13}C nuclei strongly affected by their interactions with conductive electrons.[35,39] It appears that when compared with the residual probe background signal (Figure 3.12a, bottom) very small contribution could be ascribed to KC_8 while the major part of the spectral

bands are resulting from the probe/spinner system. Clearly both signals, probe background and KC_8, are much wider than the filter size used in the spin-echo sequence and they were mostly removed together by the filter. As first evidence of the occurred modification of graphene surface, the electrical conductivity in mf-G results to be much lower if not negligible respective to KC_8. The probe was perfectly tuned, and the spectrum was collected without mixing with any insulating powder. Three peaks, at 7.0, 49.0 and 103 ppm (Figure 3.17a top) with rather wide (5 kHz) but detectable lines, are visible. This clearly implies a structural modification that cannot be due to simple stacking of reagents on graphene surface: the case is given in G_{mixed} spectrum (Figure 3.17b, top) where the pure reagents (Figure 3.12b, bottom) mostly keep their chemical shifts (30.0 ppm, 81.3 ppm and 146.2 ppm) together with a small line widening (50 Hz), probably due to magnetic susceptibility effects arising from KC_8. It is important to note that mf-G presents the same peak series than G_{mixed}, but with big differences in chemical shift. Such difference in mf-G and G_{mixed} spectral features strongly pleads in favor of the covalent functional groups grafting. Indeed, these kind of unexpected variations in chemical shifts are not uncommon in graphene systems and have been ascribed to magnetic susceptibility effect,[36] knight shift effects (due to electronic conductivity) or to the nucleus independent chemical shift (NICS), due to graphene sheet curvature.[40] It has also been recently shown that the presence of local structural distortions in graphene can affect the values of the ^{13}C isotropic shielding constant leading to additional shifts in the same orders than those found for mf-G.[41] However, due to this shifts variance, it is resulting arduous a confident assignment of a peak to a functional group. Nevertheless, based upon our experience, we hypothesized that the peak at 7.0 ppm can be assigned to the aliphatic carbon atoms, likely corresponding to the CH_3 of Boc protecting group. The second peak at 49.0 ppm can correspond to the carbon atoms bound to oxygen (CH_2-O and CH_2-N) and the last at 103 ppm could be related to carbon atoms arranged in aromatic rings. As a confirmation of the covalent grafting of the functional groups, this last assignment is corroborated by the hypothesis that with the increasing of defects on graphene surface, the aromatics rings could result as more localized on the structure.

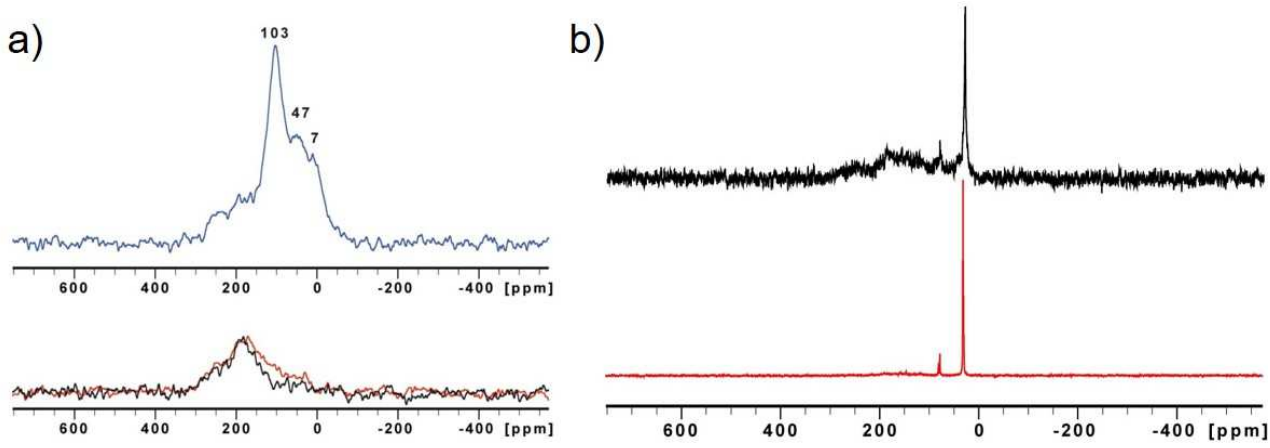

Figure 3.12: ^{13}C SS NMR spectra of mf-G and KC_8. a) Top: DP spin-echo on mf-G. Peaks at 7, 47 and 103 ppm superimpose with probe background signal (bottom, black). Bottom: KC_8 (red) and probe background signal (black) in the same conditions; b) ^{13}C SS NMR spectra of G_{mixed} (fine mixture of KC_8 with reagents) and pure reagents. Top: DP spin-echo on G_{mixed} (KC_8 + reagents). Broad lines between 100 and 300ppm are mainly probe background residuals. Comparison with pure reagents (bottom, red) shows quite no differences except small effects on linewidths (50Hz increase) together with a big change in the ratio peaks/background signal as there is much less reagents in the G_{mixed}.

Last but not least, to face the problem of the direct identification of the functional groups grafted onto graphene, we analyzed the mf-G with a technique based on the coupling between TGA, gas chromatography and mass spectroscopy (TG-GC-MS).[25,26] We collected and eluted by GC the molecules and fragments in gas phase generated by the TGA at different temperature of the analysis, to evaluate the composition of the samples. In conventional TG-MS experiments, the interpretation of the MS spectra collected is not easy

because of the difficulty to predict the evolution of the organic moieties during the TGA process. Not all the *m/z* fragments collected could be assigned with certainty to a correspondent functional group. In this sense, GC allowed the separation and the mass analysis of each molecule developed during the TGA process, enhancing the interpretation of the MS spectra, a process that is crucial in the case of multifunctionalized materials. From the chromatogram of the gas injected at the temperature of 320 °C (Figure 3.13a), evidence of the presence of Boc protecting group was derived from the characteristic mass signal at *m/z* 57 eluted with the peak at 3.57 min. Moreover, two different peaks at 8.60 and 9.72 min were detected. From the chromatogram of the gas injected at 200 °C is it possible to predominantly observe the peak at 4.37 min, corresponding to THF adsorbed on mf-G (Figure 3.13b).

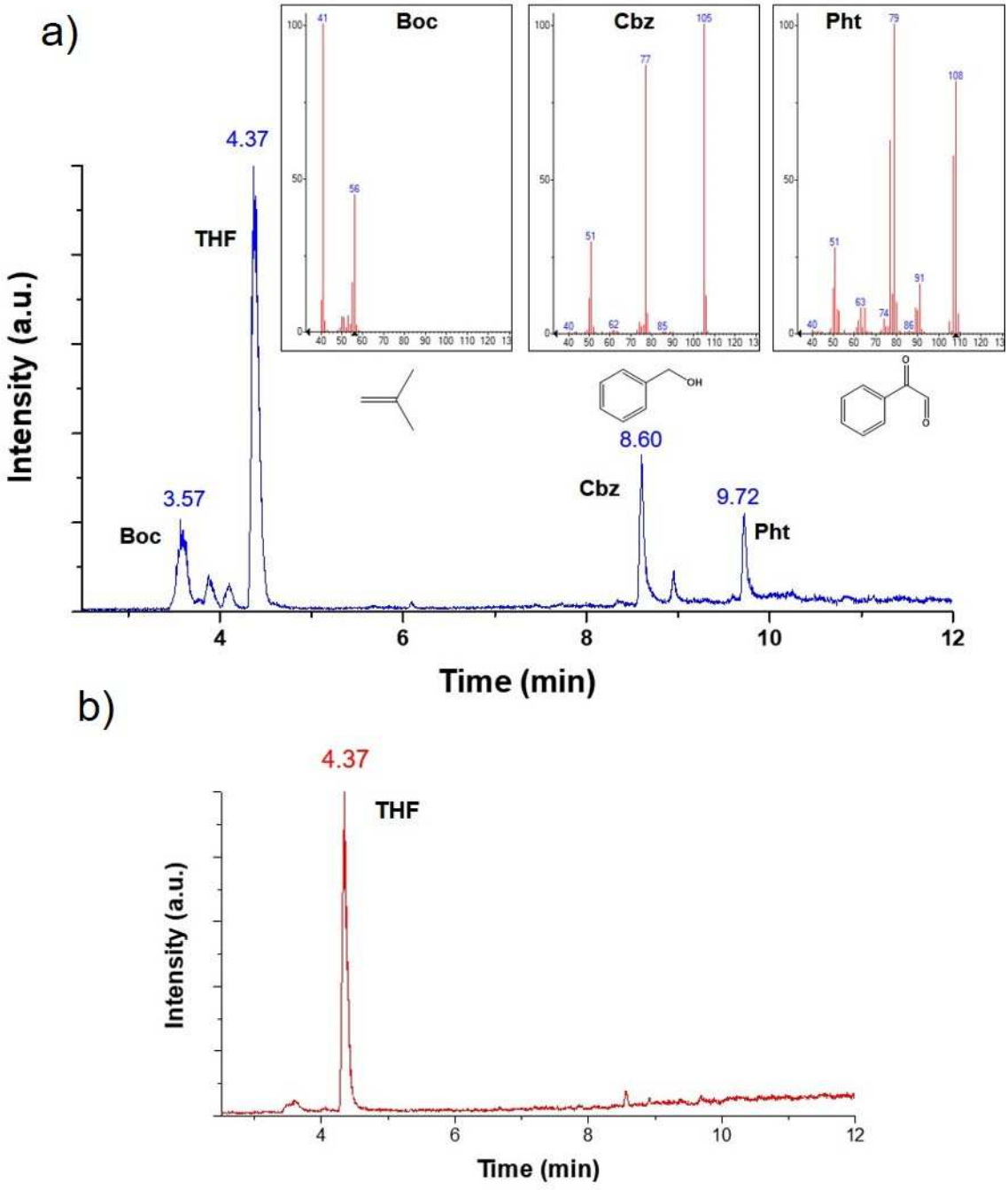

Figure 3.13: GC-Ms spectrum from the TG-GC-MS measurement. a) Injection at 320 °C: the peaks at 3.57, 8.6 and 9.72 s were associated to Boc, Cbz and Pht, respectively; b) Chromatogram of GC-MS coupled TGA after injection at 220 °C, the peak at 4.37 min corresponds to THF adsorbed on mf-G.

The peak at 8.60 min contains mass fragments with *m/z* ratio of 51, 77 and 105 (Figure 3.14b). Comparing our MS spectra with a library of spectra, we could observe that these fragments match with the spectra of phenylglyoxal. This molecule is a structural isomer of the fragment of Cbz protecting group. To verify if the observed peak was really related to Cbz fragmentation, we prepared a control experiment consisting of functionalized graphene with only the Cbz diazonium salt derivate, observing the appearance of the same peak at 8.60 min, thus confirming the presence of this functional group. Finally, the peak at 9.72 min showed fragments with *m/z* of 77 and 108 (Figure 3.14c), matching with the MS spectra of benzyl alcohol. We hypothesized that this fragment could be generated from a rearrangement of the structure of the phenyl protecting group during the TGA process, after losing a NHCO group. Thanks to the coupling between TGA, GC and MS it was possible to observe fragments with similar *m/z* at different retention times and assign each one of these to the correspondent functional group on graphene, that would be impossible without the elution of GC.

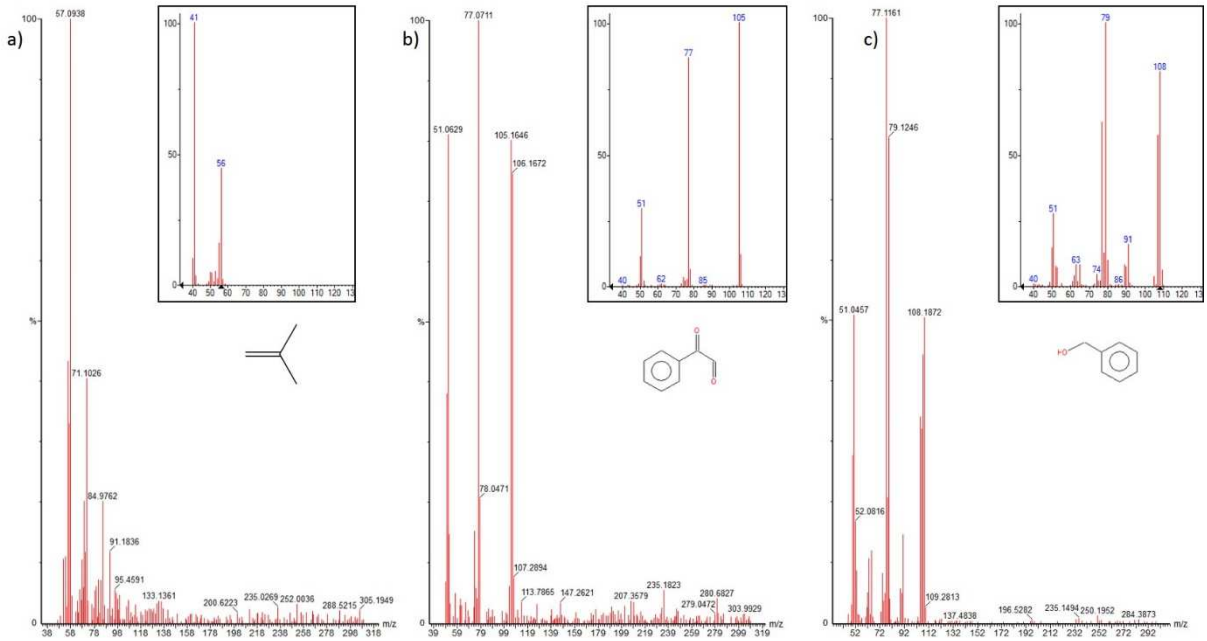

Figure 3.14: Mass spectra of a) Boc fragment at 3.57 min; b) Cbz MS fragment at 8.60 min, small spectra: MS spectra corresponding to phenylglyoxal; c) Pht MS fragment at 9.72 min, small spectra: MS spectra of benzyl alcohol.

Finally, after the complete characterization showed, we can confirm the presence of the occurred functionalization by the three diazonium salts and the obtaining of the multifunctional graphene desired to further investigate the drug delivery properties of graphene. In Chapter 4 I will present the functionalization strategy for the production of a drug delivery carrier based on mf-G and its first *in vitro* applications for cancer therapy.

3.4.2. Multifunctionalization of KC_8 with iodonium salt derivatives and diazonium salt.

In view of the high degree of functionalization and the good quality of the materials obtained via the approach described above, I decided to proceed further with the investigation of the multifunctionalization of graphene, to introduce on the material different functional groups in one-pot reaction. Knirsch *et al.* demonstrated the possibility to multifunctionalize graphene using 4-methoxyphenyl diazonium tetrafluoroborate and n-hexyl iodide.[10] In this study, the authors showed the possibility of functionalizing graphene adding to a dispersion one reagent after the other (Scheme 3.7). They investigated the reaction

using intercalated and exfoliated graphite and CVD graphene, discovering for the latter a process of retro-functionalization when the diazonium salt was employed as first reagent, thus acting as good leaving group during the alkylation reaction.

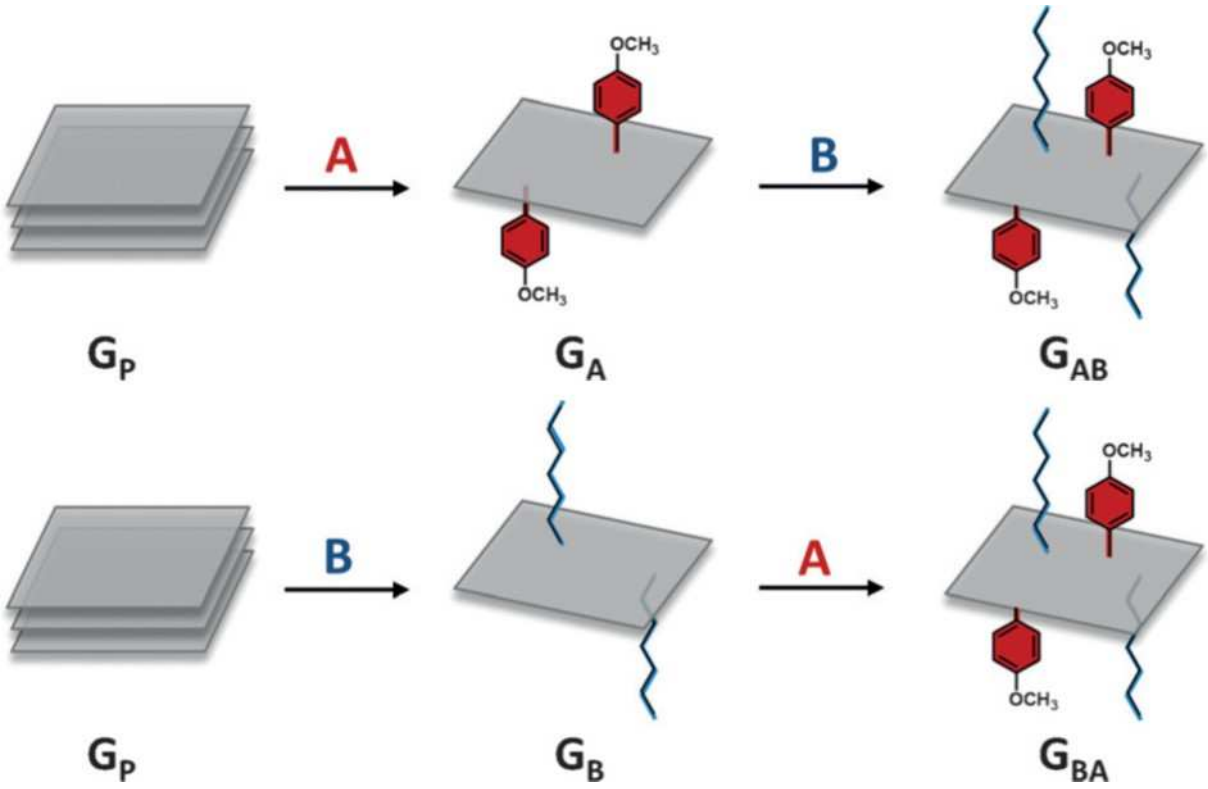

Scheme 3.7: Scheme of the bis-functionalization of intercalated graphite with DS and alkyne iodide. Reagent A: 4-methoxyphenyl diazonium tetrafluoroborate; reagent B: n-hexyl iodide.[10] Adapted with permission from John Wiley and Sons.

The flexibility in the synthesis of aryl diazonium salts and alkyne-iodide derivatives together with the already commercial availability of different of those products, could allow an extended investigation on the multiple possibilities offered by this type of functionalization.

As described in paragraph 3.3.3.2, one of the purposes of graphene multifunctionalization was the introduction of an alkyne moiety through a one-step reaction. This would allow a direct coupling by click chemistry reaction of a wide range of new functionalities. With this purpose, two iodonium salts were investigated for the functionalization of graphene. The first, 5-iodo-pentyne (Figure 3.15a) is a commercially available product, while the second is propargyl-PEG_4-I (Figure 3.15b), selected for the presence of PEG chain that can increase the water dispersibility of the material and add the alkyne moiety through an easy functionalization reaction.

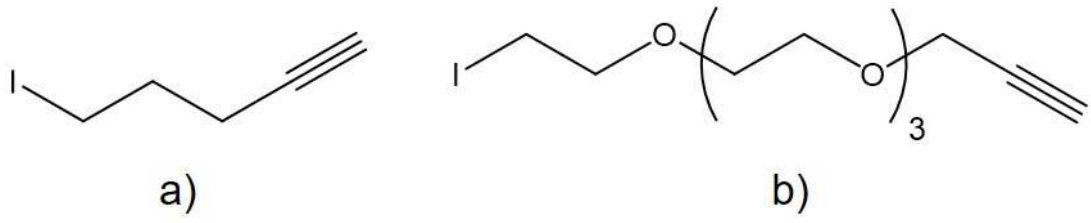

Figure 3.15: Alkyne-iodide derivatives for graphene bis-functionalization: a) 5-iodo-pentyne; b) propargyl-PEG_4-I.

The synthesis of propargyl-PEG$_4$-I was performed following the work of Lalit *et al.*, starting from HO-PEG$_4$-OH to obtain in 3 steps the final product (Scheme 3.8) (see paragraph 3.6 for the complete synthesis).

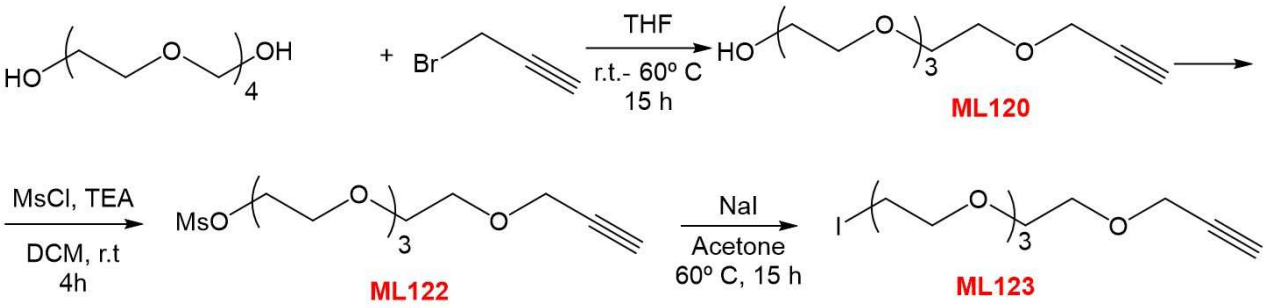

Scheme 3.8: Scheme of the synthesis of the I-PEG$_4$-propargyl derivative.

3.4.2.1. Functionalization of KC_8 with 5-iodo-pentyne and Boc-DS

5-Iodo-pentyne was already investigated by the group of Hirsch. Following an approach similar to that described previously, KC_8 was dispersed in THF and reacted with 5-iodo-pentyne (yielding **ML119a**). After one day of reaction, Boc-DS was added to the dispersion and the mixture stirred for one more day (yielding **ML119b**) (Scheme 3.9).

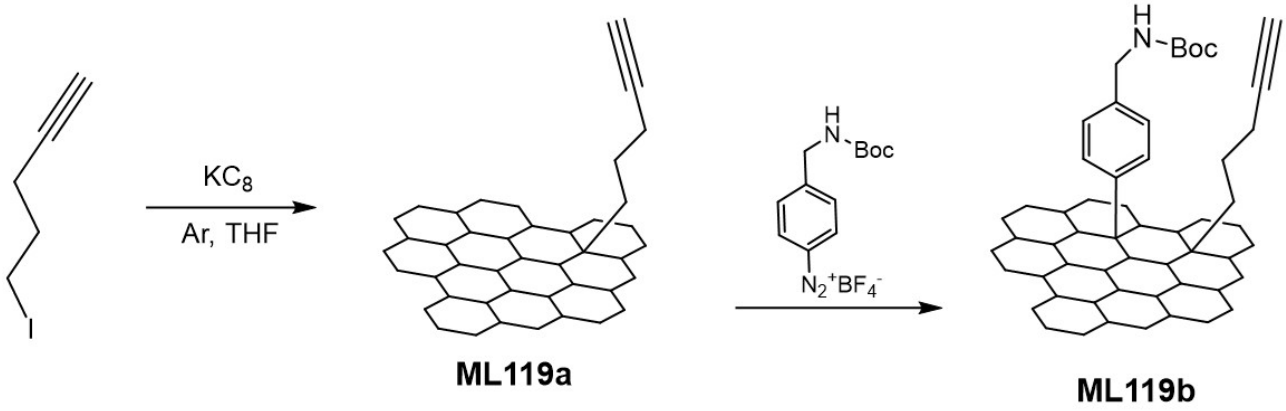

Scheme 3.9: Scheme of the sequence of reaction for the functionalization of KC_8 with 5-iodo-alkyne and Boc-DS.

The evolution of the reaction was analyzed first by Raman spectroscopy on a sample of **ML119a** isolated before the addition of Boc-DS and on **ML119b**. After the addition of the Boc-DS, the I_D/I_G ratio presents a slight change, from 0.9 to 1.1 that could be due to inhomogeneity of the surface rather than a real increase in the functionalization of the material. Moreover, there is no evident change of the 2D and D+D' bands, as observed for the functionalization of **ML125** (Figure 3.16).

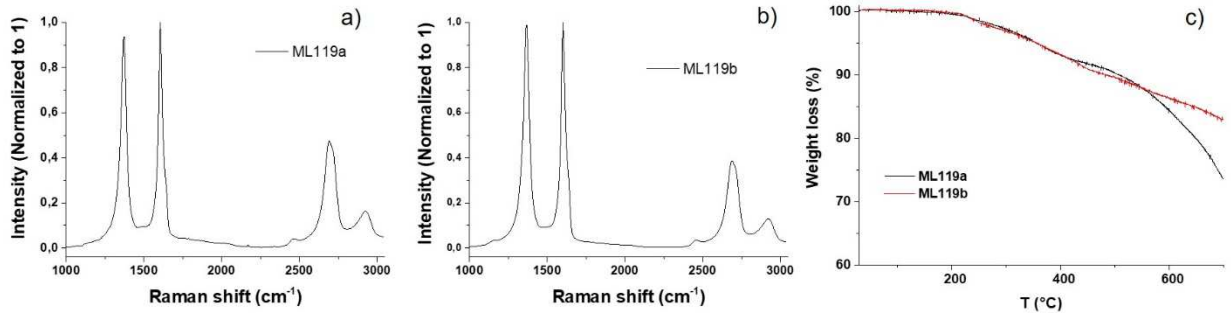

Figure 3.16: Raman spectra of functionalized graphene: a) ML119a; b) ML119b.

The TGA comparison between the two products did not show any difference in weight loss, bringing to the conclusion that the second reaction did not occur properly. It is possible that the second reaction does not work due to the discharging of graphene after the alkylation and as consequence, a minor reactivity of the material. It is also possible that an excess of iodo-alkyne present in solution has reacted with the DS, quenching the radical species formed before the grafting onto graphene. A possible solution to this problem could be a second intercalation/activation of graphene with metallic potassium. Unfortunately, it is also strongly possible that this route will affect the alkyne structure, transforming or making react the functional group, with the inevitable loss of this functionality. Another challenge faced during my internship concerned the detection of the alkyne moiety and the understanding of its presence on graphene. As described before, due to the nature of graphene, the detection of specific functional group is not of easy comprehension. In the study of Strano and co-workers,[21] the authors observed the presence of the alkyne using ATR-IR spectroscopy (attenuated total reflection infrared spectroscopy). As shown in Figure 3.17a, they were able to observe a faint peak at ~3300 cm^{-1} associated to the C-H stretching of the alkyne. After a click reaction, they were able to functionalize the alkyne with N_3-PEG-COOH, and to observe the presence of the carboxylic group by ATR-IR spectroscopy, thus confirming by an indirect analysis the presence of the alkyne.

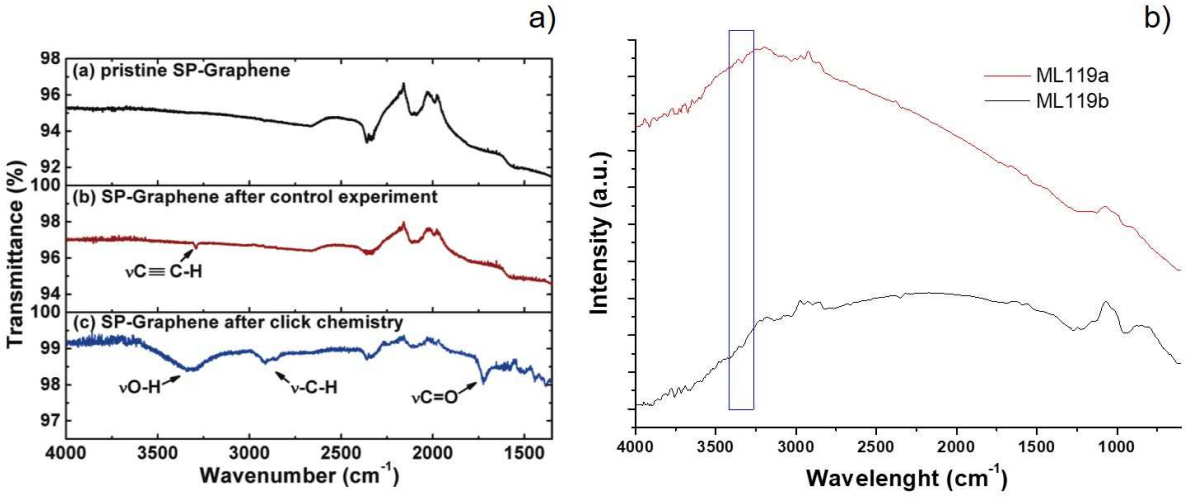

Figure 3.17: ATR-IR spectra of graphene and functionalized graphene. a) Spectra from Strano and co-workers, reproduced with permission of Ref. 21, copyright of American Chemical Society; b) ATR-IR performed on **ML119a** (red line) and **ML119b** (black line).

With the aim of confirming the presence of the alkyne moiety inserted onto graphene, I performed ATR-IR analysis on the two products **ML119a** and **ML119b** (Figure 3.17b). The presence of a very weak peak is observed to a wavelength of ~3350 cm^{-1}. Due to the difficulty on the treatment of the obtained data, especially the application of baseline correction and a correct subtraction of the atmospheric signal, the interpretation of the data is not simple. For reasons of time I could not deeply investigate further these conjugates.

3.4.2.2. Functionalization of KC_8 with iodo-hexane and DS-alkyne

After this non-satisfactory test, performed for the obtention of a bifunctional graphene, I tried the functionalization following a two-step strategy. It is known that the presence of defects on graphene is increasing its reactivity. The defects, corresponding to sp^3 carbon atoms, cause an increase of the surface strain and, as a consequence, a higher reactivity. This new strategy is based on the first functionalization of KC_8 with iodo-hexane (yielding **ML120a,** Scheme 3.10**)**, followed by the charge quenching and the functionalization of the obtained functional graphene. The first step of functionalization serves to

homogeneously introduce the defects increasing the strain of the material, for an easier following functionalization step. After the first functionalization, I purified the material and performed a new reaction of functionalization, using 4-propargyloxybenzene diazonium tetrafluoroborate (described in paragraph 663.3.3.2) (yielding **ML120b**). The aim was to obtain the introduction of the alkyne-DS derivative onto graphene through the functionalization of the obtained FLG, without the presence of potassium in the reaction environment, to avoid possible side-reactions and keep intact the alkyne moiety. Moreover, the functionalization with 4-propargyloxybenzene diazonium tetrafluoroborate was not successfully obtained on exfoliated FLG, but the use of a "defect-activated" FLG could allow the second functionalization (Scheme 3.10).

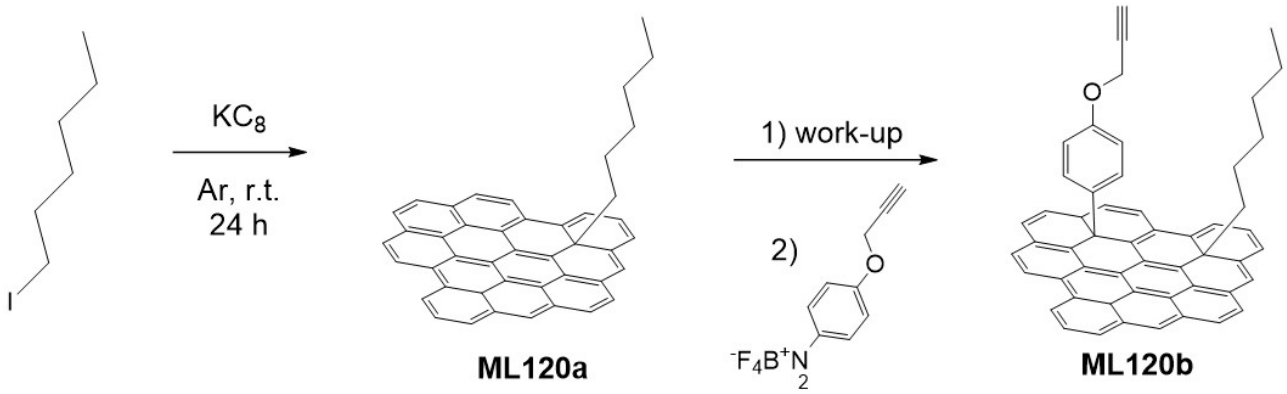

Scheme 3.10: Scheme of the functionalization of KC_8 by sequence of reactions: a) functionalization with iodo-hexane; b) functionalization with alkyne-DS.

Following the same characterization procedure, Raman spectroscopy was performed first, showing an I_D/I_G ratio of ~1.2 for the **ML120a** (Figure 3.18a). However, the Raman spectra obtained for the compound **ML120b** presented a complex and unexpected change on the Raman band of the material (Figure 3.18b). A complete change on the band ratio and shape occurred to the spectra, with a great increase of the intensity of D+D' band and the broadening of the D band. This result is very hard to explain, and completely unexpected respect to what observed until now for the functionalization of FLG. The observed behavior It may be due by fluorescence interference in Raman spectra, caused by fluorescent species absorbed onto graphene. Raman scattering and fluorescence emission may compete with each other when the excitation laser energy is close to the electronic transition energy of the material. At the same time, I cannot exclude that other reactions occurred on the material, even involving the alkyne moiety of the DS, forming different species respect to what expected. An over functionalization of graphene could lead to the formation of sp^3 zone of the material characterized by photoluminescence,[42] generating interference in Raman spectra. A complete characterization of the material to understand the modification occurred on graphene was not performed for reasons of time.

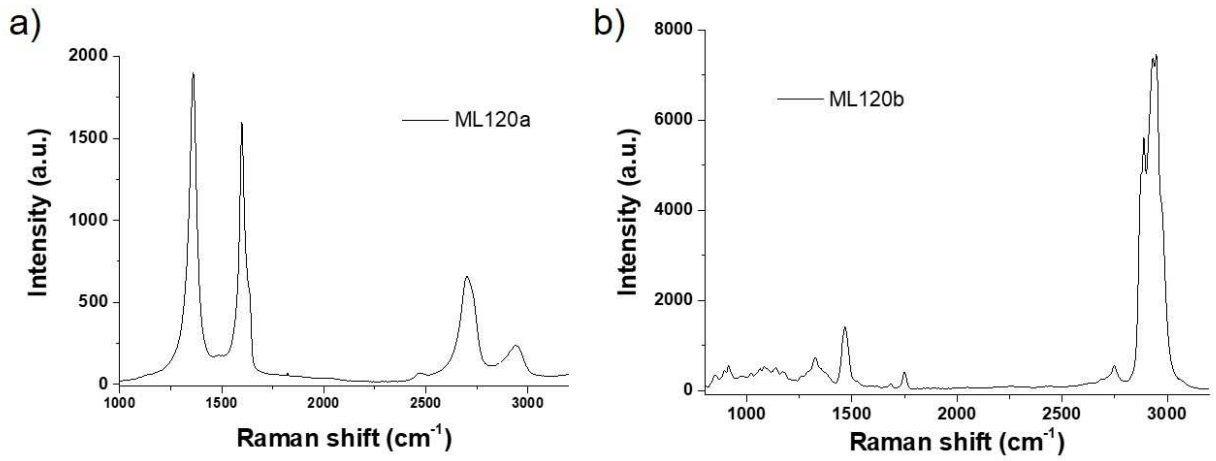

Figure 3.18: Raman spectra of ML120a and ML120b

3.4.2.3. Functionalization of KC_8 with iodo-PEG_4-alkyne

Finally, the functionalization of KC_8 with the synthetized I-PEG_4-alkyne was investigated. Following the same protocol applied above, 1 eq. of reagent was added to the graphenide dispersion and stirred at room temperature for 2 days (Scheme 3.11) (yielding **ML124**).

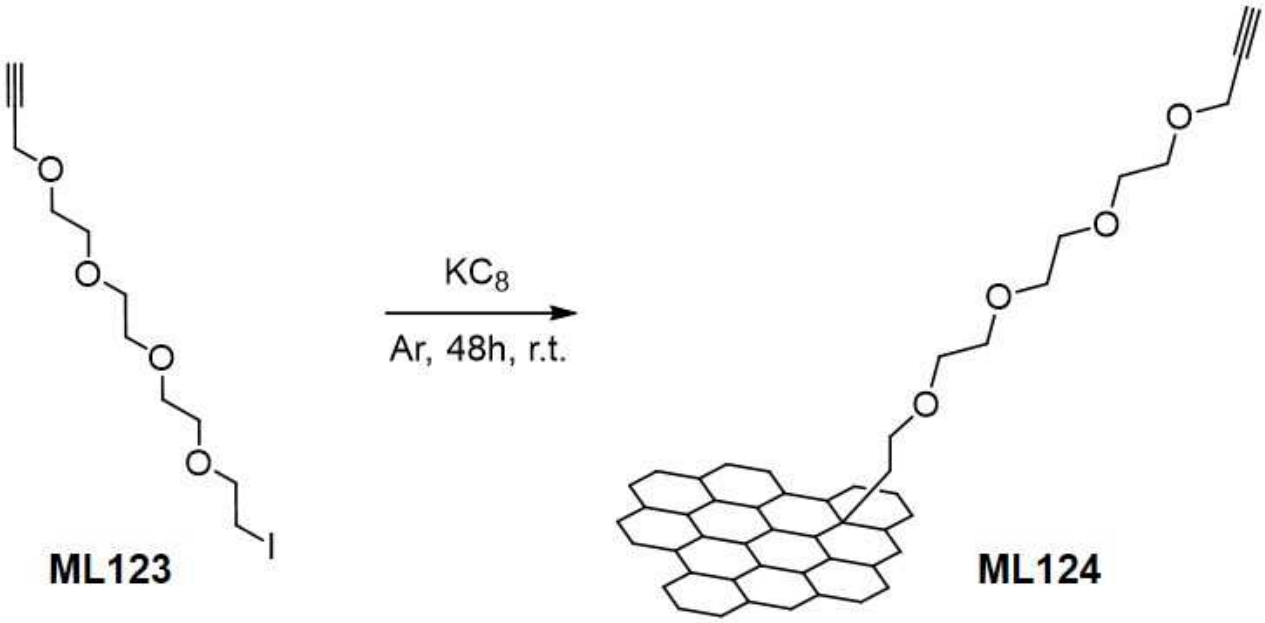

Scheme 3.11: Scheme of reaction of KC_8 with I-PEG_4-alkyne.

By Raman spectroscopy, I observed an increase of the I_D/I_G ratio to ~0.6 (Figure 3.19a). The surface of the material did not present a good homogeneity as shown by the statistical Raman analysis (Figure 3.19b). The ATR-IR spectroscopy is not exploitable (Figure 3.19c). The noise between 4000 and 3000 nm did not permit the identification of the peak at ~3300 nm corresponding to the presence of the alkyne, and other characterizations are required to confirm the presence of the desired functional group.

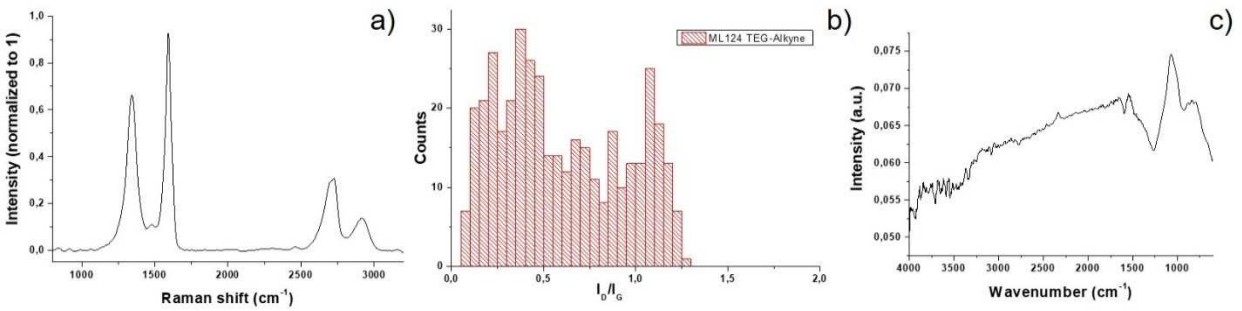

Figure 3.19: Characterization of ML124: a) Raman average spectra; b) histogram of I_D/I_G ratio from Raman statistical analysis; c) ATR-It spectroscopy of **ML124**.

TG-GC-MS technique was applied to the products from **ML124** and **ML119b**. Despite the interesting results about the characterization of the mf-G described above, with these two compounds it was not possible to isolate by GC-MS the fragments relative to the molecules grafted onto graphene, making not possible the understanding of the evolution of the reaction.

3.4.2.4. Click chemistry on functionalized graphene

As previously described, the spectroscopic and analytical techniques applied for the characterization of the last synthesized materials allowed to recognize the presence of the alkyne moiety. However, the understanding of the fate of the alkyne functional group is of high interest in the application of multifunctionalization strategies. Following the strategy of Strano and co-workers,[21] I tried to functionalize the alkyne through a click reaction employing N_3-PEG-COOH. The functionalization was tested on the compounds **ML119a** and **ML124** to first investigate if, after the simple functionalization of the interacted graphene, the alkyne group was kept intact. The two compounds were dispersed in a mixture of DMF/H_2O (1:1) and the reagent together with the catalyst ($CuSO_4$/sodium ascorbate) were added to the reaction. The mixture was stirred at r.t. for 24 h (yielding **ML127** and **ML128**, Scheme 3.12) (see paragraph 3.6 for the complete procedure).

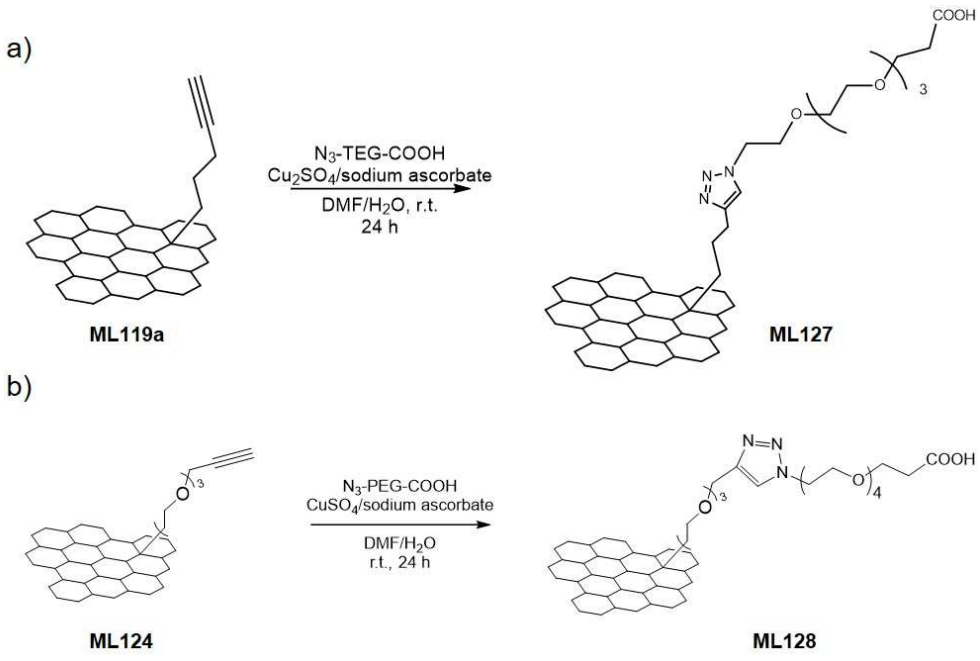

Scheme 3.12: Scheme of click chemistry reaction of graphene derivatives: a) click chemistry on ML119a; b) Click chemistry reaction on ML124.

After purification, both compounds were analyzed by ATR-IR spectroscopy and TG-GC-MS, trying to evidence the presence of the TGE-COOH introduced through the reaction. In Figure 3.20a it is shown the weight loss for the reaction on **ML119a**. In the final compound **ML127** it is possible to observe a double curve of mass loss: one at 250 °C, already present in the starting compound, and another at 150 °C, not present on the precursor of the reaction. In our experience, this low temperature weight loss is normally corresponding to solvents or organic molecules just adsorbed on the surface. The total weight loss of ~8% could correspond to a first breaking of the long TEG chain added onto the surface of graphene, or to the burning of the same chain remained adsorbed on the surface and not reacted. Unfortunately, from the GC-MS it was not possible to detect fragments associated to the entire functional group. Many small fragments were detected by this technique but cannot confirm the occurred functionalization. ATR-IR spectroscopy was performed to investigate the presence of the COOH moiety and compare the change on the spectra (Figure 3.20b). From the spectra of **ML127** the is evident the presence of a broad peak between 3100 and 2500 cm^{-1} , as well the increase of multiple peaks between 4000 and 3200 cm^{-1}. The increase of the peak at ~950 cm^{-1} could be related to the symmetric C-O stretching of ethers, acetals or ketals, and then correspond to the addition of the PEG chain on the structure. At the same time, this functional group could be just adsorbed on the surface and not covalently bonded, leading in any case to an increase of the IR band. In contrast, there is no presence of peak at ~1730 cm^{-1} relative to COOH. Unfortunately, the typical band at ~1630 and 1457 cm^{-1} corresponding to the triazole ring is not present in our spectra,[43] accounting for a simple absorption of the PEG chain instead of a covalent functionalization. Similar results were obtained for the reaction **ML128**.

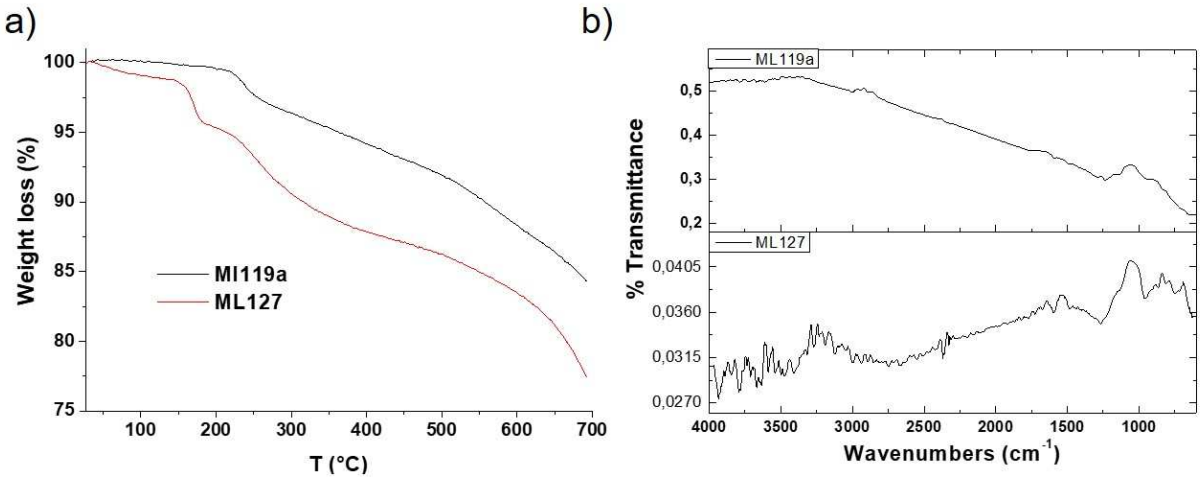

Figure 3.20: Characterization performed of **ML127** compound: a) TGA analysis of the precursor (**ML119a**, black line) and of the final compound **ML127** (red line); ATR-IR spectroscopy of the precursor (**ML119a**, top) and of the final compound **ML127** (bottom).

Based on these results, it is very difficult to confirm the presence of the alkyne moiety after functionalization of graphene. The common spectroscopic techniques normally employed for material characterization are not allowing an accurate observation of the samples, and neither through an indirect analysis of the different derivatives is possible to confidently follow the fate of the reaction. To conclude for the characterization of this reaction other techniques instrument with higher accuracy must be employed. An alternative approach to the introduction of the alkyne moiety will be described in the next chapter.

3.5. Conclusion

In conclusion, different reactions were investigated on FLG and intercalated graphene. Through the results obtained, we confirmed the high reactivity of graphenide species with respect to FLG. The comparison on the use of diazonium compounds with these two species of graphene clearly shows the possibility to obtain a high degree of functionalization with good surface homogeneity of the functional groups, using low amount of reagent when GICs compound are employed. For the first time, the triple functionalization of graphene using a one-pot reaction was demonstrated, to obtain a multifunctional material suitable for the development of drug delivery platforms. The use of different characterization techniques allowed a full characterization of the mf-G obtained. The functionalization of graphene was also investigated with a combined strategy based on the use of iodo-alkyne derivatives and diazonium salts, with the aim of the introduction of alkyne functional groups and protected amine, but unsatisfactory results were obtained from the combined approach.

3.6. Materials and methods

3.6.1. Materials

Synthetic spherical graphite (SGN18, 99.99 % C, TGA residue 0.01 % wt—Future Carbon, Germany) mean grain size of 18 µm, specific surface area of 6.2 $m^2 \cdot g^{-1}$ was used after annealing under vacuum (300 °C) for 24 h. Graphite powder (powder < 20 µm, Sigma Aldrich, code: 282863) was used after exfoliation in N-methyl-2-pyrrolidone (NMP) (see description below) from Sigma Aldrich Chemical and solvents were used purchased by Sigma Aldrich Co. and were used as received.

Tetrahydrofuran (THF) was stored under Ar over molecular sieve (4 Å) for 3 days. Afterwards the dry solvent (H_2O <10 ppm, determined by using the "Karl Fischer" method) was pump-freeze 8 times to eliminate oxygen residue and then was introduced in the glovebox. Omnipore membrane filters 0.1 µm JH was used for the filtration of all the solutions of graphene. Bath sonicator Elmasonic P at 37 MHz, 100% power was used for preparing graphene dispersions.

3.6.2. Instruments

^{1}H-NMR

^{1}H-NMR spectra were recorded on Bruker DPX 300 instrument. The peak values were obtained as ppm (δ) and referenced to the solvent. The resonance multiplicity is indicated as s (singlet), d (doublet), t (triplet), m (multiplet).

Glovebox

Graphene functionalization was carried out in an argon-filled LABmasterpro sp glovebox (MBraun), equipped with a gas purifier and solvent vapour removal unit (oxygen and water content lower than 0.1 ppm).

Raman spectroscopy

Raman spectroscopic characterization was carried out on on a Horiba LabRAM Aramis confocal Raman microscope (λ_{exc}=532 nm) with a laser spot size of *ca*. 1 µm and equipped with an automated XYZ table using 0.80 NA objectives. The incident laser power was kept as low as possible to avoid structural sample damage. Spectra were obtained with a CCD array at −70 °C and using a grating of 600 grooves per mm. Temperature-depending Raman measurements were performed in a Linkam stage THMS 600, equipped with a liquid

nitrogen pump TMS94 for temperature stabilization under a constant flow of nitrogen. The measurements were carried out on Si/SiO_2 substrates (300 nm oxide layer) with a heating rate of 10 $K \cdot min^{-1}$.

Thermogravimetric analysis combined with gas-chromatographic separation (GC) and coupled with a mass spectrometer

Thermogravimetric analysis was carried out on a PerkinElmer Pyris 1 TGA instrument. Time-dependent temperature profiles in the range of 20 and 700 °C (20 $K \cdot min^{-1}$ gradient) were recorded under a constant flow of N2 (70 mL min^{-1}). About 2.0 mg initial sample mass was used. The evolved gases detached from the respective sample in combination with the N_2 carrier gas is transferred into the GC system through a TL9000 TG-IR-GC interface at a constant temperature of 280 °C. The gas-chromatographic separation was achieved by a GCClarus 680 with a polysiloxane-coated Elite-5MS capillary column: 30 m length, 0.25 mm diameter, 0.25 µm film thickness. A GC injection fraction of 150 µL was collected at the selected TG temperature (in the range of 200–300 °C), parameters: injector zone = 280 °C, detection zone = 250 °C, flow rate helium = 10 $mL \cdot min^{-1}$, temperature profile = 34 min total run time, dynamic ramp = 24 min, 40–280 °C with a 10 $K \cdot min^{-1}$ gradient followed by an isothermal step of 10 min at 280 °C. The obtained data were processed with the TurboMass Software and Bibliographic searches were performed with NIST MS Search 2.0.

Transmission electron microscopy

TEM images were collected with a Hitachi 7500 transmission electron microscope (TEM) (Hitachi High Technologies Corporation, Tokyo, Japan) equipped with an AMT Hamamatsu digital camera (Hamamatsu Photonics, Hamamatsu City, Japan)

Solid-State NMR

^{13}C Solid-State NMR experiments were performed at room temperature on an AVANCE 750 MHz wide-bore spectrometer (Bruker™) operating at a frequency of 188.5 MHz for ^{13}C. All the samples were spun at 30 kHz in a double resonance MAS probe designed for 2.5 mm o.d. zirconia rotors (closed with Kel-F caps). In order to filter out probe background signal and also to get undistorted lineshapes and baselines we used a spin-echo experiment,[38] synchronized with the rotation (echo time = 6 rotation periods = 200µs). Durations were 2.22 µs and 4.44 µs for π/2 and π pulses respectively, ensuring proper spectral coverage for such wide lines (113 kHz ^{13}C B_1 field). Proton decoupling during acquisition was done using the SPINAL-64[44] decoupling scheme at a 105 kHz RF field and the recycle time was set to 4 s. The spectral width was set to 250 kHz and 16384 transients per FID were acquired on 8192-time domain points. A 1 kHz Lorentzian filter was applied prior to Fourier transform without zero fillings. Chemical shifts are given respective to tetramethylsilane (TMS) using adamantane as a secondary reference.

3.6.3. Protocols

Quantitative Kaiser test protocol[16]

Three solutions were prepared separately:

- (I): 10 g of phenol in 20 mL of absolute ethanol.

- (II): 2 mL of potassium cyanide 1 mM (aqueous solution) dissolved in 98 mL of pyridine.

- (III): 1 g of ninhydrin in 20 mL of absolute ethanol.

A mass of approximately 300 µg of functionalized graphene was carefully weighted in a haemolysis test tube and dispersed in 300 µL of DMF. Then, 75 µL of solution (I), 100 µL of solution (II), and 75 µL of solution (III)

were successively added to the dispersion and sonicated for 2 minutes to well disperse the material. After heating at 120 °C for 5 min in a heating block (Bioblock Scientific), the suspension was immediately diluted with 4450 µL of 60% ethanol. After centrifugation at 15000 rpm, the supernatant was analyzed by UV-Vis spectroscopy. The absorbance at 570 nm was correlated to the amount of free amine functions on the graphene surface using the equation:

$$NH \text{ loading (µmol/g)} = \frac{\left[Abs_{sample} - Abs_{blank}\right] \times \text{diluition (mL)} \times 10^6}{\text{Extinction coefficient} \times \text{sample weight (mg)}}$$

Dilution is 5 mL and extinction coefficient is 15000 $m^{-1}cm^{-1}$.

The blank was prepared exactly the same way but without graphene.

The result is expressed as micromole of amino groups per gram of material.

The Kaiser test is repeated at least three times for each sample to ensure reproducibility.

Graphene exfoliation

1.5 g of graphite (Sigma Aldrich, particle size < 20 µm, different LOT) was dispersed in 400 mL of NMP. The mixture was sonicated for 2 h in bath sonicator (37 MHZ, 100 % power). After sonication the black dispersion was centrifuged at 1500 g for 1 h. The supernatant was recovered and filtered on Millipore filter (0.1 µm porous size). Graphene on filter was re-dispersed in NMP (40 mL) by bath sonication for 5 minutes, to give stable dispersion of FLG in a concentration of ~0.08 mg/mL.

Synthesis of (2-{2-[2-(1,3-Dioxo-1,3-dihydro-isoindol-2-yl)-ethoxy]-ethoxy}-ethylamino)-acetic acid (ML11)

i) Synthesis of Boc-2,2'-(ethylene-dioxy) bis(ethylamine) (ML4)

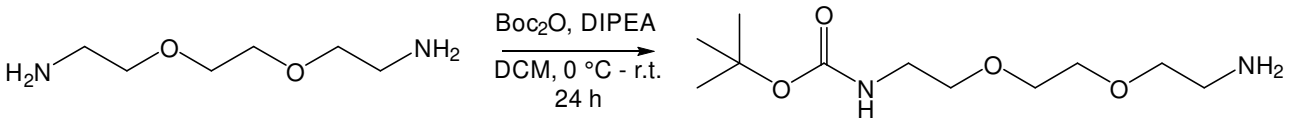

ML4

A solution of 2,2'-(ethylene-dioxy) bis(ethylamine) (20 g) in dichloromethane (130 mL) was cooled to ice-cold temperature and N,N-diisopropylethylamine (10.6 mL) (DIPEA) was added. After 10 min, di-tert-butyl dicarbonate (Boc_2O) (12.4 g) in dichloromethane (100 ml) was added under stirring during 3 h. After completion of the addition, the reaction mixture was stirred overnight at room temperature. The solvent was removed under reduced pressure. The residue was dissolved in water and filtered on a celite pad (to remove the diprotected derivative). The filtrate was extracted with dichloromethane and washed with brine and dried over sodium sulphate and evaporated to yield a Boc-2,2'-(ethylene-dioxy) bis(ethylamine) **(ML4)**. The unreacted diamine (after TLC) is to be removed by flash chromatography an in suitable solvent system (DCM/MeOH/Et3N 87:10:03 would be ideal).

^{1}H NMR: (400 MHz, $CDCl_3$) δ= 3.56 (s, 4H), 3.48 (dt, *J*= 10.3, 5.2 Hz, 4H), 3.25 (q, *J*= 5.4 Hz, 2H), 2.83 (t, *J*= 5.2 Hz, 2H), 1.38 (s, 9H).

ii) Synthesis of (2-{2-[2-(tert-butyl-oxy-carbonyl amino)-ethoxy]-ethoxy}-ethylamino)-acetic acid benzyl ester (ML6)

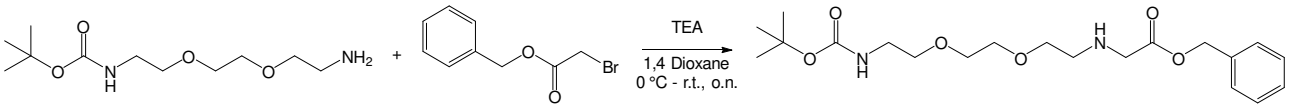

ML4 **ML6**

To a solution of Boc-2,2'-(ethylene-dioxy)bis(ethylamine) **(ML4)** in 1,4-dioxane (3 eq) and Triethylamine (TEA) (2.5 eq) cooled to 0 °C, was added benzyl bromoacetate (1 eq) in 1,4-dioxane (5 ml), dropwise over a period of 1.5 hours. The reaction mixture was allowed to warm to room temperature and stirred for 6 hours (overnight). The solvent was removed under reduced pressure. The final product was purified by flash chromatography in AcOEt/Pet. Ether (8:2) to obtain the desired product **(ML6)** as white gummy solid.

^{1}H NMR (400 MHz, $CDCl_3$) δ= 7.30 – 7.18 (m, 5H), 5.08 (s, 2H), 3.50 (m, 6H), 3.43 (t, *J*= 5.2 Hz, 2H), 3.41 (s, 2H), 3.21 (q, *J*= 5.4 Hz, 2H), 2.77 – 2.69 (m, 2H), 1.35 (s, 9H).

iii) Synthesis of (2-{2-[2-(1,3-Dioxo-1,3-dihydro-isoindol-2-yl)-ethoxy]-ethoxy}-ethylamino)-acetic acid (ML11)

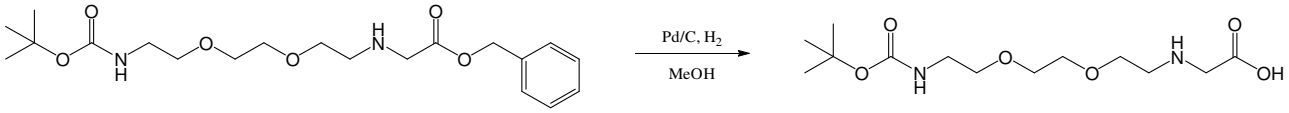

ML6 **ML11**

To a solution of (2-{2-[2-(tert-butyl-oxy-carbonyl amino)-ethoxy]-ethoxy}-ethylamino)-acetic acid benzyl ester **(ML4)** (0.5 g, 1.3 mmol) in methanol (20 ml), were added 50 mg of Pd/C (10%), in the presence of H_2. The reaction mixture was stirred for 5 hours at room temperature. The solution was filtered through a celite pad and the solvent was evaporated under reduced pressure to obtain **ML11** as a white powder.

^{1}H NMR (400 MHz, [D4]-Methanol) δ= 4.91 (s, 3H), 3.86 – 3.79 (m, 2H), 3.77 – 3.67 (m, 3H), 3.62 – 3.53 (m, 4H), 3.34 – 3.26 (m, 4H), 1.50 (s, 9H).

General procedure for 1,3-dipolar cycloaddition on FLG (ML15)[15]

FLG (1eq.) was dispersed in NMP (conc. 0.5 mg/mL) in a round bottom flask equipped with a cooling system. Compound **ML11** (1-3 eq.) and para-formaldehyde (1-3 eq.) were added and the mixture stirred under Ar atmosphere for 1 day (or 4 days) at 125 °C. After this time the mixture reaction was filtered on Millipore filters (0.1 µm pore size) and washed with NMP, DCM, EtOH and water (2x30 mL). The filter was then dried *in vacuo* and the solid recover from the filter.

Synthesis of the 4-aminobenzylamine derivatives[16]

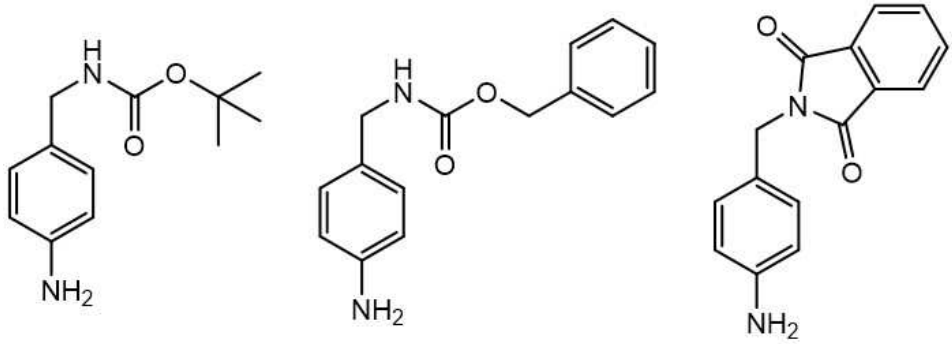

(4-amino-benzyl)-carbamic acid tert-butyl ester (ML8).

To a solution of 4-aminobenzylamine (2 g, 16.4 mmol, 1 eq.) in tetrahydrofuran (15 mL) was added dropwise a solution of di-tert-butyl dicarbonate (3.93 g, 1.1 eq.) in tetrahydrofuran (18 mL). The reaction was monitored by TLC. After stirring for 5 h, the reaction mixture was evaporated in vacuo. The residue was purified by chromatography on silica gel using ethyl acetate/cyclohexane 3:7 as eluant. 3.26 g of (4-amino-benzyl)-carbamic acid tert-butyl ester **2** was obtained as a yellow solid (yield: 90%).

^{1}H NMR (300 MHz, $CDCl_3$) δ= 1.45 (s, 9 H), 3.647 (broad s, 2 H), 4.18 (d, J= 5.4 Hz, 2 H), 4.73 (broad s, 1 H), 6.64 (d, J= 8.4 Hz, 2 H), 7.07 ppm (d, J= 8.1 Hz, 2 H).

(4-amino-benzyl)-carbamic acid benzyl ester (ML9).

To a solution of 4-aminobenzylamine (2 g, 16.4 mmol, 1 eq.) in 1,4-dioxane (15 mL) was added triethylamine (2.51 mL, 1.1 eq.). A solution of *N*-(benzyloxy carbonyloxy) succinimide (4.29 g, 1.05 eq.) in 1,4-dioxane (18 mL) was added dropwise. The reaction was monitored by TLC. After stirring for 5.5 h, the reaction mixture was evaporated *in vacuo*. The residue was dissolved in dichloromethane and deionized water was added. The two phases were separated, and the aqueous phase extracted with dichloromethane. The combined organic phases were washed with deionized water and with brine, dried over sodium sulphate, filtered and evaporated *in vacuo*. The residue was purified by chromatography on silica gel using ethyl acetate/cyclohexane 3:7 to 4:6 as eluant. 3.72 g of (4-amino-benzyl)-carbamic acid benzyl ester **2** was obtained as a brown solid (yield: 93%).

^{1}H NMR (400 MHz, [D6]-DMSO]) *δ*= 3.33 (s, 1 H), 4.03 (d, *J*= 6.12 Hz, 2 H), 4.93 (s, 2 H), 5.03 (s, 2 H), 6.50 (d, *J*= 8.3, 2 H), 6.91 (d, *J*= 8.2 Hz, 2 H), 7.31-7.37 ppm (m, 5 H).

2-(4-amino-benzyl)-isoindole-1,3-dione (ML63).

To a solution of 4-aminobenzylamine (2.5 g, 20.5 mmol, 1 eq.) in acetonitrile (40 mL) were added mono-methyl phthalate (3.69 g, 1 eq.), BOP reagent (benzotriazol-1-yloxytris(dimethylamino)-phosphonium hexafluorophosphate) (9 g, 1 eq.), and *N*,*N* diisopropylethylamine (11.4 mL, 3 eq.). The reaction was monitored by TLC (100% dichloromethane). After stirring for 3h, a solution of sodium carbonate (4.1 g) in deionized water (60 mL) was added. The mixture was vigorously stirred over the night, a yellow solid was formed and recovered by filtration. The solid was used without further purification. 3.5 g of 2-(4-amino-benzyl)-isoindole-1,3-dione **1** was obtained as a yellow solid (yield: 75%).

^{1}H NMR (400 MHz, [D6]-DMSO) *δ*= 4,56 (s, 2 H), 5.03 (s, 2 H), 6.49 (d, *J*= 8.36 Hz, 2 H), 6.98 (d, *J*= 8.32, 2 H), 7.81-7.87 (m, 4 H).

***General synthesis of diazonium salts*[45]**

A solution of **1**, **2** or **3** (2 mmol, 1 eq.) in anhydrous THF (20 mL) under Ar atmosphere was cooled at 0 °C and boron trifluoride diethyl etherate (8 mmol, 4 eq.) was added dropwise through a syringe. Tert-butyl nitrite (6 mmol, 3 eq.) in 5 mL of THF was added dropwise to the solution and stirred vigorously in the dark at room temperature. The reaction was monitored by TLC. After 30 min an orange solid was formed. The mixture was poured in 100 mL of ethyl ether, filter and washed with ethyl ether (100 mL). The yellowish solid was dried in vacuum and correspond to the pure diazonium salt derivate with 99 % yield reaction.

Boc-protected derivate: ^{1}H NMR (400 MHz, [D4]-Methanol) *δ*= 1.35 (s, 9H), 4.36 (s, 2H), 7.75 (d, *J*=8.52, 2H), 8.46 (d, *J*= 8.56, 2H).

Pht-protected derivate: ^{1}H NMR (400 MHz, [D6]-DMSO) δ= 5.03 (s, 2 H), 7.88-7.38 (m, 6 H), 8.60 (d, *J*= 8.80, 2 H)

Cbz protected derivate: ^{1}H NMR (400 MHz, [D6]-DMSO) δ= 4.46 (d, *J*= 6.00, 2 H), 5.07 (s, 2 H), 7.33-7.45 (m, 5 H), 7.82 (d, *J*= 8.7, 2 H), 8.61 (d, *J*= 8.7, 2 H).

***Deprotection of protected amines*[33]**

***Pht deprotection*[46]**

mf-G was suspended (concentration 1 mg/mL) in a solution of hydrazine hydrate in ethanol (1:25 *v/v)*. the mixture was sonicated for 5 min in a bath sonicator to disperse the graphene and stirred for 17 h at r.t. in the dark. After this time, the dispersion was filtered and washed with 20 mL of dichloromethane (DCM), EtOH and water. The resulting solid was dried under vacuum. Kaiser test was performed on dispersion of the obtained powder to evaluate the amount of free amines, compared to mf-G protected (46 µmol/g of primary amines).

Boc deprotection

mf-G was suspended (concentration 1 mg/mL) in a solution of HCl 4 M in 1,4-dioxane (purchased Sigma Aldrich). The suspension was sonicated for 5 min in a bath sonicator and stirred for 17 h at r.t. in the dark. After this time, the dispersion was filtered and washed with 20 mL of dichloromethane (DCM), EtOH and water. The resulting solid was dried under vacuum. Kaiser test was performed on dispersion of the obtained powder to evaluate the amount of free amines, compared to mf-G protected (76 µmol/g of primary amines)

Cbz deprotection

A solution of trifluoroacetic acid (TFA), TMSOTf and *p*-cresol (ratio 3.8:1 *v/v* and 10 mg *p*-cresol) was prepared. mf-G was dispersed in the solution and sonicated for 5 min in bath sonicator and stirred for 15 h at r.t. in the dark. After this time the dispersion was filtered and washed with 20 mL of dichloromethane (DCM), EtOH and water. The resulting solid was dried under vacuum. To evaluate the amount of amines deprotected from Cbz protecting group, the deprotection was performed on the mf-G Boc deprotected. The amount of Cbz deprotected amines was evaluated subtracting the amount of Boc deprotected amines from

the values obtained through the Kaiser test on the contemporary Boc and Cbz deprotected graphene (118 µmol/g of primary amines total, 46 µmol/g of Cbz protected amines).

General procedure for the functionalization of FLG by in situ formation of diazonium salts. (ML20, ML31, ML52, ML81, ML82

FLG was dispersed in DMF/H_2O (5:1, 0.5 mg/mL of graphene), 4-aminobenzylamine derivates (1-4 eq.) and 3-methyl butyl nitrite (2.5 eq. respect to 4-aminobenzylamine derivates) were added and the solution immediately warmed up at 80 °C. The mixture solution was stirred for 24 h and then cooled down at room temperature and filtered. Graphene on the filter was washed with ACN, DMF, DCM and water (2x30 mL) and the filter dried *in vacuo*. The solid was then recover for further characterization.

General procedure for the functionalization of FLG by pre-formed diazonium salts. (ML84, ML85, ML88)

FLG was dispersed in DMF/H_2O (5:1, 0.5 mg/mL of graphene), the DS-derivate was added (1-6 eq and the solution immediately warmed up at 45 °C. The mixture solution was stirred for 24 h and then cooled down at room temperature and filtered. Graphene on the filter was washed with ACN, DMF, DCM and water (2x30 mL) and the filter dried *in vacuo*. The solid was then recover for further characterization.

Amidation of ML88 to ML90 with ML11

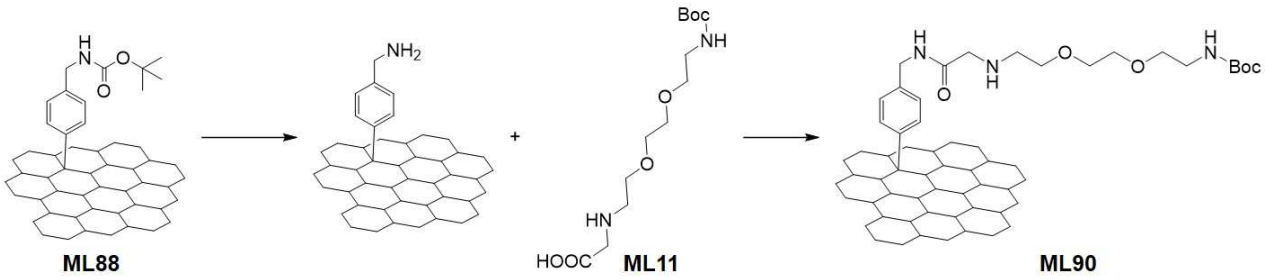

ML88 (8 mg) was deprotected from Boc protecting group and re-dispersed in DMF (15 mL). compound **ML11** (2 eq.) was dissolved in DMF (5mL), cooled at 0°C and stirred for 1 h with EDC·HCl (4 eq.) in Ar atmosphere. After NHS (4 eq.) dissolved in 2 mL of DMF was added and the mixture stirred for 1 h more. After this time, the activated **ML11**-NHS salt was added to ML88 deprotected dispersion and stirred at room temperature for 24 h under Ar atmosphere. After this time the reaction mixture was filtered and graphene washed with water, DMC, DCM and EtOH (2x20 mL). The filter with graphene was dried *in vacuo* and the final product, ML90, recovered for further characterization.

Synthesis of 4-propargyloxybenzene diazonium tetrafluoroborate (ML104)

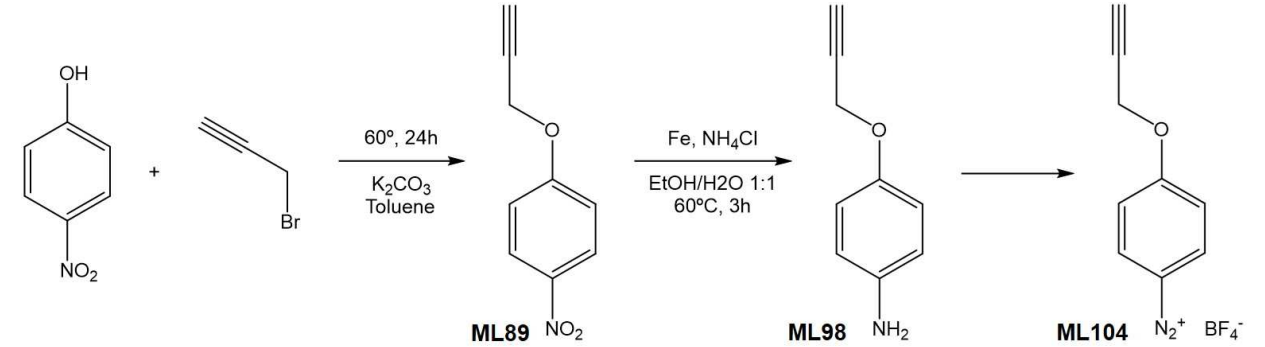

Synthesis of p-nitrophenyl propargyl ether (ML89)

Para-nitrophenol (1 eq, 36 mmol, 5g) was dissolved in DMF (70 mL) and stirred with K_2CO_3 (2 eq, 72 mmol, 9,95 g) for 1h. The solution appears as a white/yellow suspension. Propargyl bromide (1,67 eq, 60 mmol, 7,14 g, 7 mL) was then added (dropwise through a syringe) and the mixture stirred at room temperature. after less than one hour the mixture solution begins yellow and transparent. TLC control (cyclohexane/EtOAc 7:3) was performed to check if the reaction were completed. After 3 h the reagent was completely consumed, and the reaction was poured in a beaker containing water and ice (300 mL) and stirred for 10 minutes. A white/yellow precipitate was immediately formatted. The mixture was filtered and the solid, corresponding to the pure expected compound, recovered and dried *in vacuo*.

^{1}H NMR (200 MHz, $CDCl_3$): δ= 2.58 (t, 1 H, *J*= 2.4 Hz), 4.79 (d, 2 H, *J*= 2.4 Hz), 7.05 (d, 2 H, *J*= 9.3 Hz), 8.22 (d, 2 H, *J*= 9.3 Hz).

Synthesis of p-aminophenyl propargyl ether (ML98)

4-(allyloxy)nitrophenol (1eq, 5,64 mmol, 1 g) and NH_4Cl (2,5 eq, 14,1 mmol, 0,790 g) was dispersed in a mixture of water/EtOH 1:1 (60 mL) and stirred at 60˚C for 40 minutes in a round bottom flask equipped with cooling system (the first compound is slightly soluble). After that time Fe (iron powder, 5 eq, 28,25 mmol, 1,56 g) was added at the mixture under strong agitation and the mixture was stirred at 60˚C until completed. The evolution of the reaction was followed by TLC (cyclohexane/EtOAc 7:3). After 2 h the reaction was completed, and the mixture was filtered hot through a celite pad. The solvent was evaporated to give a yellow solid mixture. The solid was then dissolved in a mixture of CH_2Cl_2/MeOH 9:1 (50 mL) and washed before with NH_3 2M (2x25 mL) and after with water (2x25 mL). The organic phase (yellow/brown) was dried with $MgSO_4$ anhydrous, filtered and the solvent evaporated, to give a brown liquid that is the pure expected compound.

^{1}H NMR (200 MHz, $CDCl_3$) δ = 2.49 (t, 1 H, *J*= 2.3 Hz), 3.42 (d, 2 H), 4.60 (d, 2 H, *J*= 2.3 Hz), 6.63 (d, 2 H, *J*= 8.9 Hz), 6.82 (d, 2 H, *J*= 8.7).

Synthesis of 4-propargyloxybenzene diazonium tetrafluoroborate (ML104)

The general synthesis of the diazonium salt is described in the general synthesis of diazonium salts above.

Graphite intercalation

Synthetic spherical graphite (SGN18, 99.99 % C, TGA residue 0.01 % wt—Future Carbon, Germany) after annealing under vacuum (300 °C) for 24 h was introduced inside the glovebox. The powder was mixed with metallic potassium in a glass vial in mol ratio 1:8 K/C (mixtures were prepared from 20 to 300 mg of graphite). The mixture K/C was warmed up at 250 °C and mixed manually with a ceramic spatula after the melting of K. The powder mixture was kept at 250 °C for 2 days and mixed manually at least 6 times per day. The color of the powder change from black to brown/gold in less than 3 hours of intercalation.

Exfoliation of KC_8 powder was performed dispersing the powder in dried THF (conc. 0.5 mg/mL) and sonicated by tip sonicator (inside the glove box) for 15 minutes (40 % amplitude, cycle of 3 s sonication + 1 s pause). The brown dispersion was then immediately used for the functionalization.

General procedure for functionalization of graphenide dispersion

Graphenide dispersion was stirred in a round bottom flask at room temperature and the reagent was carefully added to the solution (pre-formed diazonium salts or iodo-alkyne derivatives). The mixture reaction was then stirred at room temperature for 1-2 days.

The quenching of the reaction is performed by addition of 3 mL of PhCN to the reaction. The mixture was stirred for 10 minutes more and then removed from the glovebox.

The THF solution was then mixed with DCM and extracted with water (3x100 mL). The organic layer was finally filtered and washed with DMF, ACN, DCM and water, and dried overnight in vacuum hoven at 80 °C.

Synthesis of I-PEG$_4$-alkyne.[47]

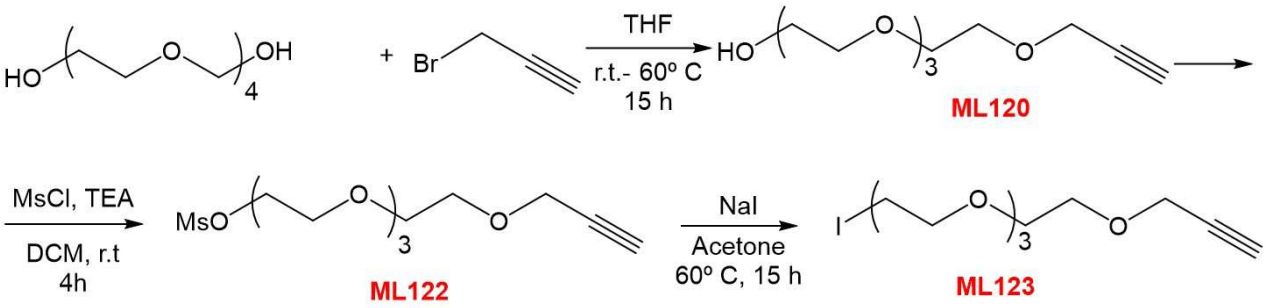

a) Synthesis of HO-PEG$_4$-alkyne (ML120)

Tetra ethylene glycol (1 eq., 10 g) was added dropwise at room temperature during 30 min to a solution of NaH in THF (30 mL). During the addition the solution becomes yellow. After 1 h propargyl bromide in THF (30 mL) was added dropwise. The mixture reaction was equipped with a cooling system, warmed up at 60 °C and stirred over the night. After this time the reaction was quenched by addition of a solution of HCl 3% (100 mL) and the organic part removed by rotary evaporation. 100 mL of DCM was added to the aqueous layer and the solution extracted with brine (50 mL) and water (2x50 mL). The organic phase was ried with $MgSO_4$, filtered and the organic solvent evaporated *in vacuum*, to give the crude product as a yellow oil. The product was purified by flash column chromatography starting with DCM/cyclohexane 8:2 to DCM/MeOH 95:5. The final product obtained (3.7 g) is a yellow viscous oil.

^{1}H NMR (400 MHz, $CDCl_3$) δ 4.14 (d, *J* = 2.4 Hz, 2H), 3.71 – 3.57 (m, 13H), 3.56 – 3.50 (m, 2H), 2.40 (t, *J* = 2.4 Hz, 1H).

b) Synthesis of MsO-PEG$_4$-alkyne (ML122)

Compound ML120 (1 eq.) was dissolved in DCM (50 mL) and Et_3N added (2 eq.). The solution was cooled at 0 °C and MsCl in DCM (40 mL) added dropwise over a period of 30 min. The mixture was stirred for 90 min at 0 °C and then warmed up at room temperature and keep under stirring for 2 h more. After this, the solvent was evaporated *in vacuo* to obtain a yellow solid. The crude product was dissolved in DCM (100 mL), washed with HCl 3% (50 mL), brine (50 mL) and water (50 mL) and finally dried over $MgSO_4$, filtered and the organic solvent evaporated *in vacuum* to obtain the final product as a yellow oil (3.2 g), directly used for the sequent reaction without further purifications.

c) Synthesis of I-PEG$_4$-alkyne (ML123)

Compound ML122 as dissolved in acetone (60 mL) and NaI was added. The reaction mixture was warmed up at 60 °C and stirred overnight. After the reaction time, the mixture was cooled at room temperature and the solvent evaporated *in vacuo* to give a yellow solid. The solid was dissolved in DCM and filtered over celite to remove the residues of NaI. The organic solvent was evaporated to give a yellow oil (3.8 g, crude of reaction). The mixture was purified by flash chromatography in DCM/cyclohexane 8:2 to DCM/MeOH 9.1. The final desired compound was obtained as a yellow oil (2.2 g).

^{1}H NMR (400 MHz, Chloroform-*d*) δ 4.14 (d, *J* = 2.4 Hz, 2H), 3.69 (dd, *J* = 7.3, 6.5 Hz, 2H), 3.66 – 3.56 (m, 14H), 3.20 (dd, *J* = 7.4, 6.5 Hz, 2H), 2.36 (t, *J* = 2.4 Hz, 1H).

3.7. Literature

1. Hu, Y. & Su, X. Chemically Functionalized Graphene and Their Applications in Electrochemical Energy Conversion and Storage. *Adv. Graphene Sci.* 161–189 (2013). doi:10.5772/55666

2. Englert, J. M. *et al.* Covalent bulk functionalization of graphene. *Nat. Chem.* **3**, 279–286 (2011).

3. Bonaccorso, F. *et al.* Graphene, related two-dimensional crystals, and hybrid systems for energy conversion and storage. *Science (80-.).* **347**, 1246501 (2015).

4. Nag, A., Mitra, A. & Mukhopadhyay, S. C. Graphene and its sensor-based applications: A review. *Sensors Actuators, A Phys.* **270**, 177–194 (2018).

5. Reina, G. *et al.* Promises, facts and challenges for graphene in biomedical applications. *Chem. Soc. Rev.* **46**, 4400–4416 (2017).

6. Martín, C., Kostarelos, K., Prato, M. & Bianco, A. Biocompatibility and biodegradability of 2D materials: Graphene and beyond. *Chem. Commun.* **55**, 5540–5546 (2019).

7. Sharma, R., Baik, J. H., Perera, C. J. & Strano, M. S. Anomalously large reactivity of single graphene layers and edges toward electron transfer chemistries. *Nano Lett.* **10**, 398–405 (2010).

8. Dasler, D. *et al.* Direct Covalent Coupling of Porphyrins to Graphene. *J. Am. Chem. Soc.* **139**, 11760–11765 (2017).

9. Lomeda, J. R., Doyle, C. D., Kosynkin, D. V., Hwang, W. F. & Tour, J. M. Diazonium functionalization of surfactant-wrapped chemically converted graphene sheets. *J. Am. Chem. Soc.* **130**, 16201–16206 (2008).

10. Knirsch, K. C., Schäfer, R. A., Hauke, F. & Hirsch, A. Mono- and Ditopic Bisfunctionalization of Graphene. *Angew. Chemie - Int. Ed.* **55**, 5861–5864 (2016).

11. Hernandez, Y. *et al.* High-yield production of graphene by liquid-phase exfoliation of graphite. *Nat. Nanotechnol.* **3**, 563–568 (2008).

12. Prato, M. & Maggini, M. Fulleropyrrolidines: A Family of Full-Fledged Fullerene Derivatives. *Acc. Chem. Res.* **31**, 519–526 (1998).

13. Delgado, J. L. *et al.* Buckyballs. in *Topics in Current Chemistry* **350**, 1–64 (2014).

14. Maroto, E. E. *et al.* Chiral fullerenes from asymmetric catalysis. *Acc. Chem. Res.* **47**, 2660–2670 (2014).

15. Quintana, M. *et al.* Functionalization of graphene via 1,3-dipolar cycloaddition. *ACS Nano* **4**, 3527–3533 (2010).

16. Ménard-Moyon, C., Fabbro, C., Prato, M. & Bianco, A. One-pot triple functionalization of carbon nanotubes. *Chem. - A Eur. J.* **17**, 3222–3227 (2011).

17. Paulus, G. L. C., Wang, Q. H. & Strano, M. S. Covalent electron transfer chemistry of graphene with diazonium salts. *Acc. Chem. Res.* **46**, 160–170 (2013).

18. Hirsch, A., Englert, J. M. & Hauke, F. Wet chemical functionalization of graphene. *Acc. Chem. Res.* **46**, 87–96 (2013).

19. Sharma, R., Baik, J. H., Perera, C. J. & Strano, M. S. Anomalously large reactivity of single graphene

layers and edges toward electron transfer chemistries. *Nano Lett.* **10**, 398–405 (2010).

20. Greenwood, J. *et al.* Covalent modification of graphene and graphite using diazonium chemistry: Tunable grafting and nanomanipulation. *ACS Nano* **9**, 5520–5535 (2015).

21. Jin, Z. *et al.* Click Chemistry on Solution-Dispersed Graphene and Monolayer CVD Graphene. *Chem. Mater.* **23**, 3362–3370 (2011).

22. Lucherelli, M. A. *et al.* A straightforward approach to multifunctional graphene. *Chem. – A Eur. J.* chem.201903165 (2019). doi:10.1002/chem.201903165

23. Pénicaud, A. & Drummond, C. Deconstructing graphite: Graphenide solutions. *Acc. Chem. Res.* **46**, 129–137 (2013).

24. Vecera, P., Edelthalhammer, K., Hauke, F. & Hirsch, A. Reductive arylation of graphene: Insights into a reversible carbon allotrope functionalization reaction. *Phys. Status Solidi Basic Res.* **251**, 2536–2540 (2014).

25. Abellán, G. *et al.* Unifying Principles of the Reductive Covalent Graphene Functionalization. *J. Am. Chem. Soc.* **139**, 5175–5182 (2017).

26. Schirowski, M. *et al.* Fundamental Insights into the Reductive Covalent Cross-Linking of Single-Walled Carbon Nanotubes. *J. Am. Chem. Soc.* **140**, 3352–3360 (2018).

27. Vecera, P. *et al.* Solvent-driven electron trapping and mass transport in reduced graphites to access perfect graphene. *Nat. Commun.* **7**, 12411 (2016).

28. Eckmann, A., Felten, A., Verzhbitskiy, I., Davey, R. & Casiraghi, C. Raman study on defective graphene: Effect of the excitation energy, type, and amount of defects. *Phys. Rev. B - Condens. Matter Mater. Phys.* **88**, 1–11 (2013).

29. Cançado, L. G. *et al.* Quantifying defects in graphene via Raman spectroscopy at different excitation energies. *Nano Lett.* **11**, 3190–3196 (2011).

30. Niyogi, S. *et al.* Spectroscopy of covalently functionalized graphene. *Nano Lett.* **10**, 4061–4066 (2010).

31. Englert, J. M. *et al.* Scanning-Raman-microscopy for the statistical analysis of covalently functionalized graphene. *ACS Nano* **7**, 5472–5482 (2013).

32. Sarin, V. K., Kent, S. B. H., Tam, J. P. & Merrifield, R. B. Quantitative monitoring of solid-phase peptide synthesis by the ninhydrin reaction. *Anal. Biochem.* **117**, 147–157 (1981).

33. Kaiser, E., Colescott, R. L., Bossinger, C. D. & Cook, P. I. Color test for detection of free terminal amino groups in the solid-phase synthesis of peptides. *Anal. Biochem.* **34**, 595–598 (1970).

34. Toyoda, M. *et al.* Carbon materials in photocatalysis. *Chem. Phys. Carbon Vol. 31* 171–368 (2012). doi:10.1201/b12960

35. Vieira, M. A. *et al.* Synthesis of graphite oxide from milled graphite studied by solid-state 13C nuclear magnetic resonance. *Carbon N. Y.* **98**, 496–503 (2016).

36. Freitas, J. C. C., Emmerich, F. G., Cernicchiaro, G. R. C., Sampaio, L. C. & Bonagamba, T. J. Magnetic susceptibility effects on 13C MAS NMR spectra of carbon materials and graphite. *Solid State Nucl. Magn. Reson.* **20**, 61–73 (2001).

37. Vieira, M. A. *et al.* Estudo através de rmn de 13c no estado sólido sobre a síntese de oxido de grafite utilizando diferentes precursores grafíticos. *Quim. Nova* **40**, 1164–1171 (2017).

38. Hahn, E. L. Spin echoes. *Phys. Rev.* **80**, 580–594 (1950).

39. Franck, J. M. & Han, S. Overhauser Dynamic Nuclear Polarization for the Study of Hydration Dynamics,

Explained. *Methods Enzymol.* **615**, 131–175 (2019).

40. Casabianca, L. B. Effect of Curvature on Carbon Chemical Shielding in Extended Carbon Systems. *J. Phys. Chem. A* **120**, 7011–7019 (2016).

41. De Souza, F. A. L. *et al.* NMR spectral parameters in graphene, graphite, and related materials: Ab initio calculations and experimental results. *J. Phys. Chem. C* **120**, 27707–27716 (2016).

42. Jeon, K. J. *et al.* Fluorographene: A wide bandgap semiconductor with ultraviolet luminescence. *ACS Nano* **5**, 1042–1046 (2011).

43. Li, H., Zheng, Q. & Han, C. Click synthesis of podand triazole-linked gold nanoparticles as highly selective and sensitive colorimetric probes for lead(ii) ions. *Analyst* **135**, 1360–1364 (2010).

44. Fung, B. M., Khitrin, A. K. & Ermolaev, K. An Improved Broadband Decoupling Sequence for Liquid Crystals and Solids. *J. Magn. Reson.* **142**, 97–101 (2000).

45. Xia, Z. *et al.* Electrochemical Functionalization of Graphene at the Nanoscale with Self-Assembling Diazonium Salts. *ACS Nano* **10**, 7125–7134 (2016).

46. Ménard-Moyon, C. *et al.* Controlled Chemical Derivatisation of Carbon Nanotubes with Imaging, Targeting, and Therapeutic Capabilities. *Chem. - A Eur. J.* **21**, 14886–14892 (2015).

47. Goswami, L. N., Houston, Z. H., Sarma, S. J., Jalisatgi, S. S. & Hawthorne, M. F. Efficient synthesis of diverse heterobifunctionalized clickable oligo(ethylene glycol) linkers: Potential applications in bioconjugation and targeted drug delivery. *Org. Biomol. Chem.* **11**, 1116–1126 (2013).

CHAPTER 4. MULTIFUNCTIONAL GRAPHENE FOR DRUG DELIVERY

4.1. Introduction

In the literature there are various examples reporting the use of functionalized GO for drug delivery.[1–3] The characteristic of this 2D material, like a high drug loading capacity and photothermal and photodynamic properties, has been exploited for therapeutic applications, . Instead, no examples of functional graphene applied to drug delivery has been published yet. As discussed in the introduction, many are the advantages of the use of graphene, such as great chemical stability, biocompatibility, large- surface area and biodegradation. The ability to penetrate the cell membrane is one of the reasons why graphene could be a suitable vector for hydrophobic drugs.[4] The functionalization of the material could improve water stability and biocompatibility,[5] allowing the introduction of new functionalities. An exhaustive investigation of the possible applications of this material is desirable for the development of new therapies based on graphene.

4.2. Aim of the chapter

In this chapter I will show the synthesis of a graphene-based multifunctional platform for cancer therapy. The platform has been developed starting from mf-G described in Chapter 3, and is constituted by three different functionalities, for targeting, imaging and drug release into cancer cells. Indocyanine green has been employed as fluorophore to study the internalization of the materials. Folic acid was selected as targeting agent for HeLa cells. Doxorubicin, covalently bound and adsorbed onto the surface, was used as anti-cancer agent. Finally, the photothermal properties of the platform have been exploited to obtain a synergistic effect in combination with the anti-cancer activity of doxorubicin. In collaboration with Dr. Eijiro Miyako, at AIST research center (Tsukuba, Japan), I investigated the anti-cancer activity of the obtained material on HeLa cells, showing promising results for the application of graphene for biomedical applications.

4.3. Results and discussion

4.3.1. Multifunctionalization approach

One of the great advantages of using nanomaterials for biomedical applications is their ability in targeting cancer cells and the high drug loading that can be obtained thanks to covalent and non-covalent interactions. The multifunctionalization of graphene can impart new features to the material, such as targeting properties, water dispersibility, fluorescence or biocompatibility. With this purpose, the functionalization of graphene is desirable to increase the effectiveness of the therapies in which they will be included. The limits to their functionalization are due only to the nature of the functional group present on the material and their reactivity. In this view, the multifunctional graphene described in Chapter 3 is a suitable material for the development of a new drug delivery system. The three quasi-orthogonally protected amines allow a precise strategy of functionalization, for the obtaining of the final desired multifunctional material.

Here I am proposing a new nomenclature for the distinction of the desired and developed material. Similar to dendrimers, I will distinguish the functional material by generations. On this light, the mf-G after the functionalization with diazonium compound would be the first generation of multifunctional graphene.

After the complete functionalization of the three amines, we could obtain a second generation of multifunctional graphene (mf-G^2). Depending on the functional group introduced, this second-generation

could already correspond to the drug delivery platform or could be the base for a third and final generation of functional materials (mf-G^3). During this work I developed a second generation of mf-G and studied its drug delivery properties. Before the description of the above-mentioned platform, I will describe first the concept for the obtaining of a second generation of mf-G, a material with a quasi-orthogonal reactive groups, allowing multiple combination of functionalization for many different applications.

4.3.1.1. Second generation of mf-G: a desirable and flexible platform for all therapies.

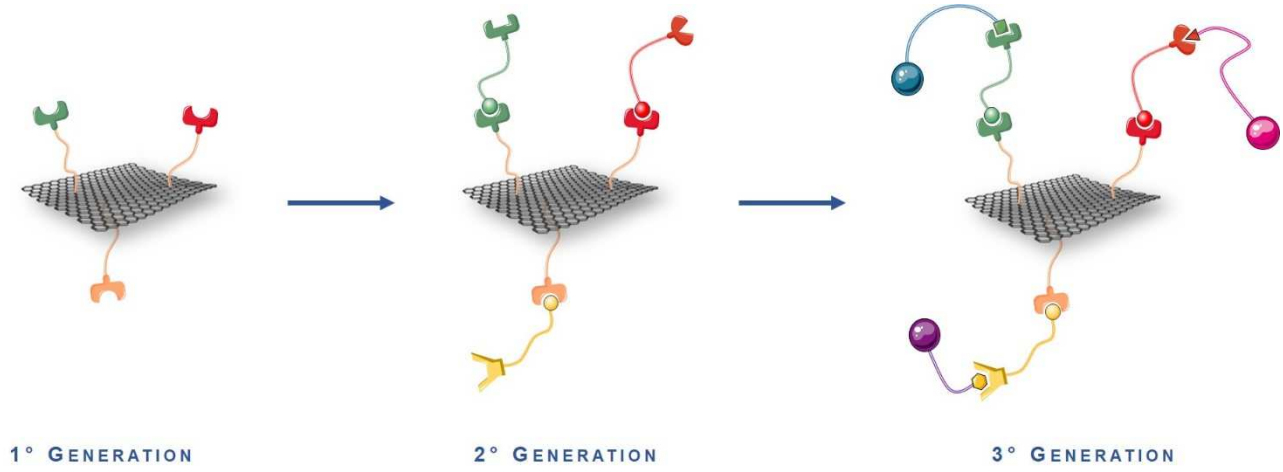

Figure 4.1: Representation of the three designed generation of multifunctional graphene.

The ambition for this project was the development of the second generation of mf-G shown in Figure 4.1. The aim was the obtaining of a multifunctional graphene, bearing three different reactive groups, with orthogonal reactivity, in order to allow the selective functionalization of each of these groups in mild reactions conditions and without the involvement of other side-reactions. This platform would present a wide combination of functionalization, only limited by the organic chemistry modifications allowed on the selected functional groups to be introduced. The further development is the easy preparation of various mf-G^3, to extensively investigate the contribution of the different functionalities to new graphene-based drug carriers. In this view, the suitable functional group are various, from alkyne (or cyclooctyne for click chemistry reaction), thiols, maleimides, amines, carboxylic acids, etc. (Figure 4.2).

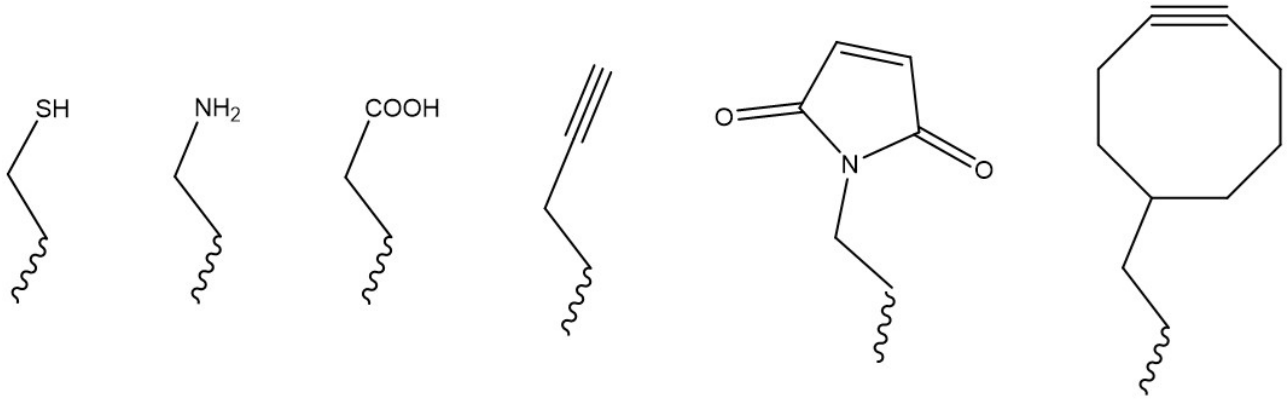

Figure 4.2: Possible functional groups for the synthesis of second-generation mf-G.

One important characteristic required by these moieties is their stability to the deprotection conditions of the amines present onto mf-G. The functionalization strategy for the obtaining of mf-G^2 is based on the step-by-step deprotection and functionalization of the amine introduced onto mf-G. The first functional group will be introduced after the deprotection of one amine and must be chemically stable and inert to the

deprotection conditions of the remaining two amines. The second group instead must be stable to the deprotection condition of the last protecting group (Cbz). A thiol group would probably require a protecting group until its functionalization, to avoid the formation of disulphide bridge between different sheets. Moreover, the functional groups should not be involved in the reaction of functionalization of the amines.

4.3.1.2. Stability of functional groups

To start the investigation on the stability of the functional groups, I selected the alkyne and maleimide moieties. Two model compounds have been synthesized, to study the stability of the functional groups to the deprotection conditions (Figure 4.3).

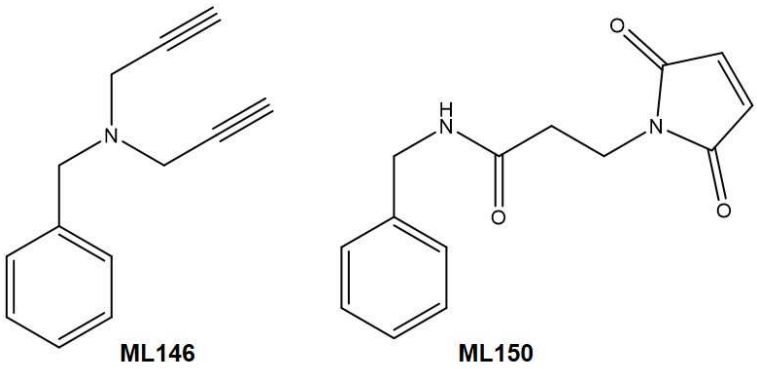

Figure 4.3: Model compound for the investigation on the stability of alkyne and maleimide moieties.

The two compounds were synthesized from benzylamine to simulate the functionalization of the amines present on mf-G (see paragraph 4.5 for the synthesis). Following a similar study performed in our laboratory,[6] our strategy started by the first deprotection of Pht group. The stability of the two compounds was then investigated in the deprotection conditions of Boc and Cbz groups (conditions described in Chapter 3). After the reaction, the reagents were removed by extraction and the obtained organic compounds analyzed by ^{1}H-NMR. The alkyne moiety of compound **ML146** resulted stable in both deprotection conditions. The chemical stability of the alkyne group makes it suitable for the functionalization of the first amine after Pht deprotection. Besides, the compound **ML150** resulted not stable in the deprotection conditions of Boc group, whereas after treatment in Cbz conditions it was possible to recover the initial product. With these results we could already design a first mf-G^2 platform, applying the following strategy: Pht deprotection and functionalization with alkyne-derivatives, Boc deprotection and functionalization with maleimide moiety and as last, Cbz deprotection to obtain the free amine as last reactive center (Scheme 4.1).

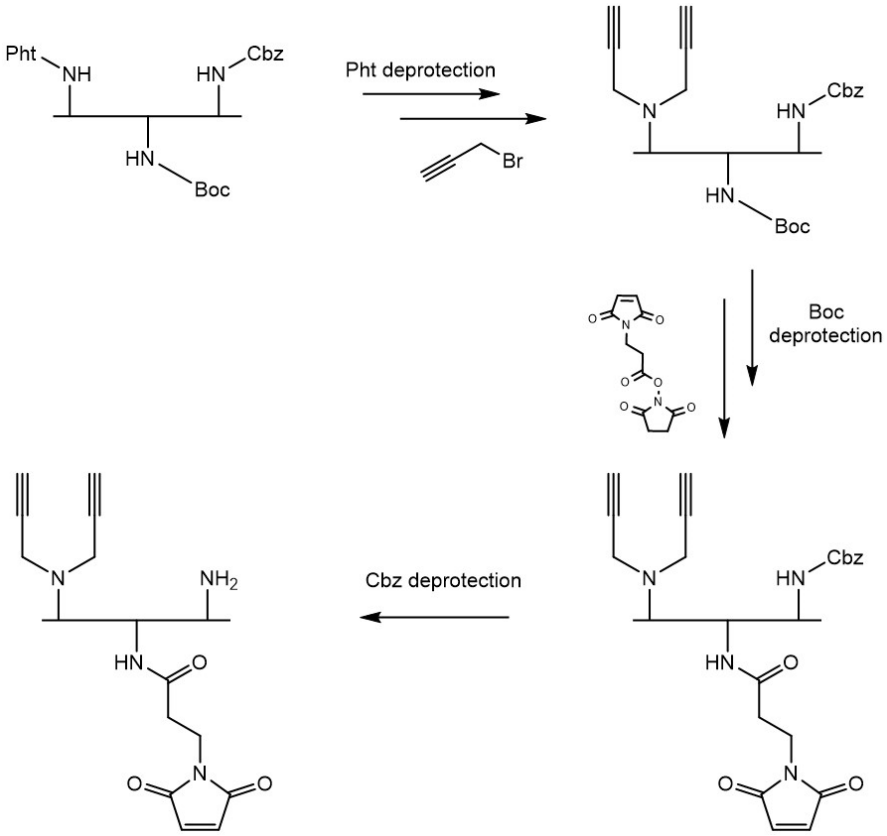

Scheme 4.1: Synthetic approach for the obtaining of mf-G2 with alkyne and maleimide moieties.

Finally, due to a lack of time, the above described second-generation platform, has not been synthetized. As an alternative, I focused my attention on the development of a different second-generation of mf-G, bearing the functionalities to explore the drug delivery properties of graphene. The selected functionalities make this platform directly useful for the investigation of anti-cancer therapy.

4.3.2. **Synthesis of multifunctional graphene for cancer therapy applications**

We designed the multifunctional platform in order to bear three different functionalities grafted onto graphene. The first is folic acid (FA), to exploit its properties as cancer cells targeting.[7] Folic acid was added onto graphene through a PEG linker (MW 3000 Da). The PEG chain as the double role of spacer between FA and graphene and it is useful for the increasing of the biocompatibility and water dispersibility of the material. Indocyanine green (ICG) was used as fluorophore, for the investigation of the internalization of mf-G sheets into cancer cells. Finally, we selected doxorubicin (Dox) as anti-cancer drug. The synthetic strategy for the functionalization of the starting material is shown in Scheme 4.2. As anticipated, the order of introduction of the different functionalities is crucial for the obtaining of the final material. The first problem that I had to face about the functionalization of this material was following the occurring of the reaction with the most common techniques. The organic functionalization of the amines already presents on graphene is not causing change into the Raman spectra of the material. The mass of the molecule introduced and their quantity are not sufficient to produce remarkable and quantifiable weight loss for TGA analysis. XPS spectroscopy could give information about the atomic percentage composition of the surface but it is not possible to understand if these changes are due to covalent functionalization or absorption of the organic molecule on graphene. As consequence of this lack of direct characterization techniques, we decided to follow the evolution of the reaction exploiting the primary amines on graphene surface. As the majority of the reactions applied is

involving the amines functionalization, we evaluated through Kaiser test the quantity of free amines after deprotection and after the functionalization, to quantify the amount of functional groups introduced.

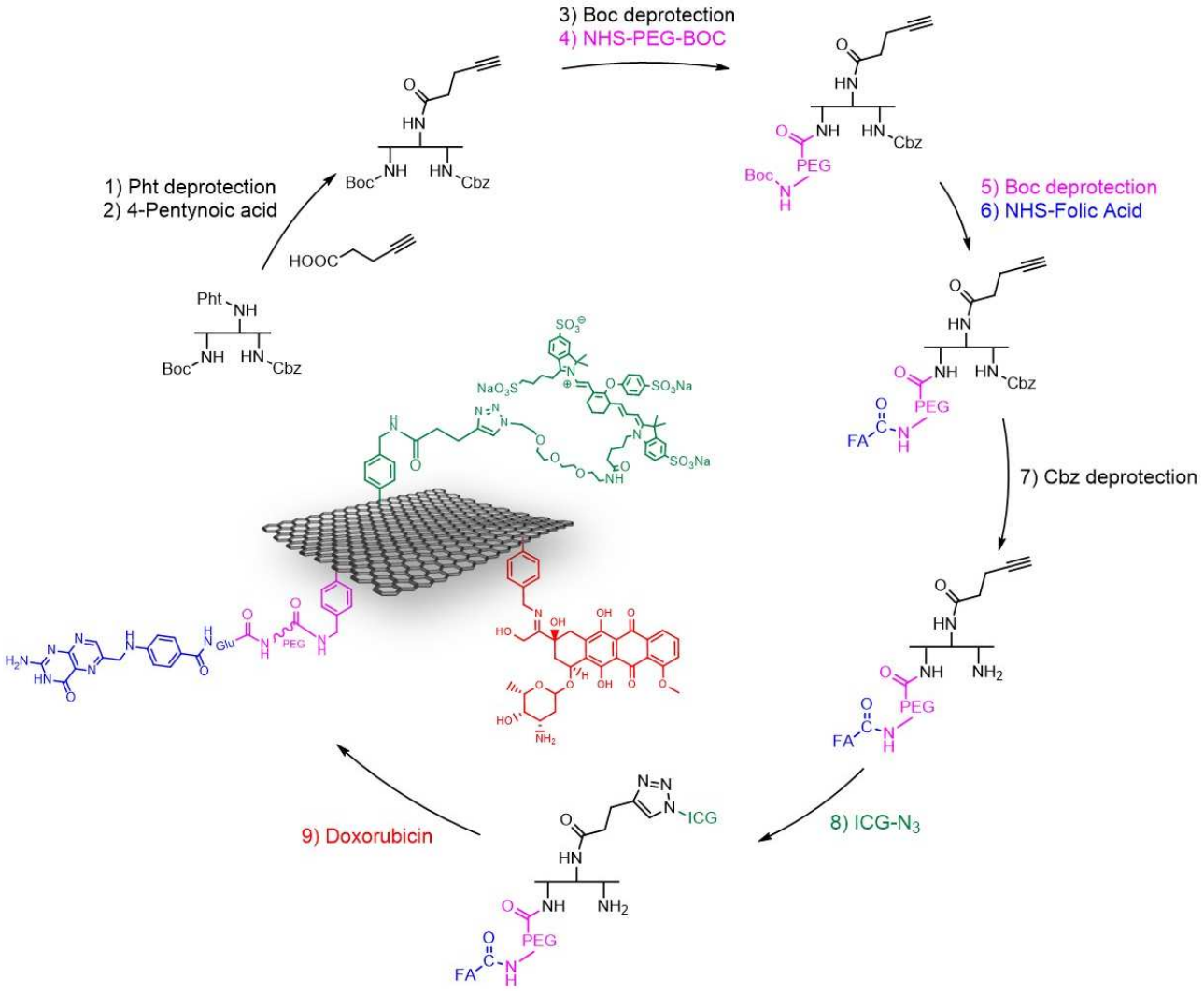

Scheme 4.2: Synthetic strategy for the obtaining of multifunctional graphene for anti-cancer therapy.

The synthesis of mf-G[2] started from the deprotection of Pht group (1) (~55 µmol/g free amines) and was followed by amidation with 4-penthynoic acid (2), introducing the alkyne moiety as first functional group (~40 µmol/g loading). After this, Boc group was deprotected (3) (~33 µmol/g) and the amine functionalized with NHS-PEG-Boc (4) to get mfG/PEG-Boc (Kaiser test after reaction: 0 µmol/g). The long PEG chain introduced present an amine protected with Boc group that has been subsequently deprotected (5) (~30 µmol/g) and functionalized with a pre-synthetized NHS-FA (6) giving mfG/PEG-FA (Kaiser test after reaction: ~0 µmol/g). The stability of folic acid to Cbz deprotection condition was already investigated by our group and exploited here for the success of the synthetic strategy.[6] After the introduction of FA, the last amine was deprotected removing Cbz group (7) (~30 µmol/g). Before carrying out the functionalization of the last amine, the alkyne group was functionalized. Click chemistry reaction with commercially available N_3-ICG, catalyzed by $CuSO_4$ and sodium ascorbate, was performed, to achieve the introduction of the fluorophore (8) (mfG/PEG-FA/ICG). The ICG does not present stability in the hard deprotection conditions of Boc and Cbz and was necessary its introduction after the amines deprotection. In this case, due to the absence of primary amines, it was not possible to evaluate the occurring of the reaction through Kaiser test. To prove the covalent grafting of ICG on graphene, a reaction control was carried out, in the same conditions but in

absence of catalyst. The fluorescence emission of the two products was afterwards investigated, to understand the effect of the covalent and non-covalent reactions. As expected, mf-G functionalized with ICG showed fluorescence after excitation at 750 nm, while the control reaction did not present any fluorescence (Figure 4.4).

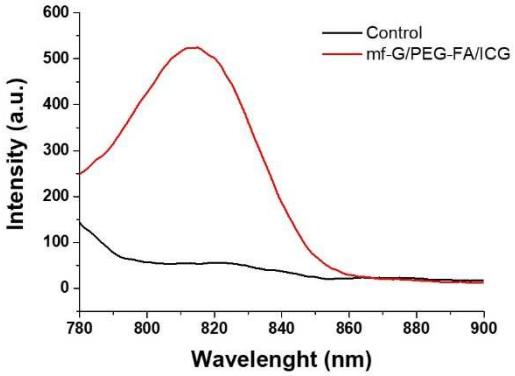

Figure 4.4: Fluorescence of mfG/PEG-FA/ICG and mfG/PEG-FA control reaction. 0.1 mg/mL of graphene in NMP. Ex: 750 nm, Em: 780-900 nm.

Finally, mfG/PEG-FA/ICG was covalently functionalized introducing doxorubicin (9) (mfG/PEG-FA/ICG/Dox). The ketone group of doxorubicin was employed to form an imine bond with the last free amine of graphene. The imine bond has the important characteristic to be cleavable at acid pH < 5.5.[8] Our strategy for the delivery of Dox is based on the selective release of the drug inside cancer cells, whose pH is lower respect to normal cells. Due to the presence of an amine on Dox structure, Kaiser test cannot be applied to evaluate the loading of the drug on graphene. To evaluate the quantity of Dox loaded on mfG we measured through HPLC analysis the concentration of the solution after washing of the functionalized material. Steps of dispersion of the material in PBS, centrifugation and removal of the supernatant containing free Dox were repeated until no presence of drug were found in the recovered solution. The quantity of Dox linked to graphene was then evaluated to ~60 µg/g (~0.10 µmol/g). We hypothesized that the low reaction yield was due to a difficult interaction between the drug and the free amines, caused by the steric hindrance of PEG chain and of the other functionalities on graphene surface. Finally, as last characterization of the material, I evaluated the lateral size dimensions of the sheets.

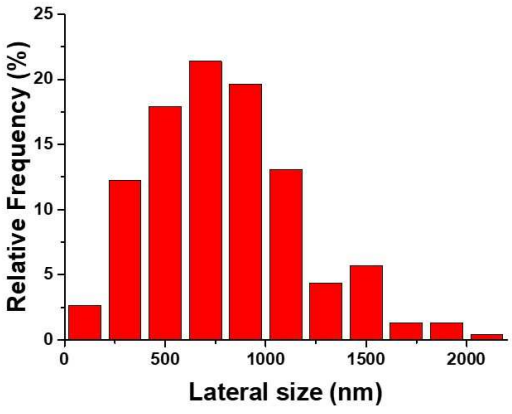

Figure 4.5**:** Histogram of the lateral size distribution of the graphene dispersion.

This, as already discussed in the introduction, could affect the cells uptake and the cytotoxic effect, and in addition it is crucial for a good comparison with other materials. I evaluate the average lateral size of the particles by statistic on TEM images, founding a value of ~794 nm, with the presence of few particles smaller than 200 nm or bigger than 1.5 µm (Figure 4.5).

4.3.3. Cancer therapy applications of mfG/PEG-FA/ICG/Dox

The final material, mfG/PEG-FA/ICG/Dox (simplified as mfG-Dox. mfG is the control sample without drug) was finally tested *in vitro* for anti-cancer therapy. During a period of two months, I have been hosted by Dr Eijiro Miyako, at AIST research center (Tsukuba, Japan), to investigate the drug delivery properties of the developed platform. The applications of our platform were evaluated in HeLa cells (cancer cells) and MRC5 (fibroblast) employed as healthy cell control. The cells were incubated for 24 and 48 h with mfG and mfG-Dox dispersed in cell culture media. In figure 4.8 are shown the viability results after 48 h of treatment. The cells viability of MRC5 (Figure 4.6a) clearly shows dose-dependent toxicity of these cells to mfG. Interesting, the toxicity of mfG and mfG-Dox result to be very similar, suggesting no drug release from mfG-Dox on these cells. The same behavior is shown for HeLa cells (Figure 4.6b). In this case, the viability of the cells is only slightly affected by the presence of graphene, and even at high concentration (150 µg/mL) the viability is decreasing of only 10%, suggesting that the material is not toxic for this type of cells. Even in this case, we are not observing a decreasing of the cell viability in presence of mfG-Dox, suggesting the absence of drug release from the platform.

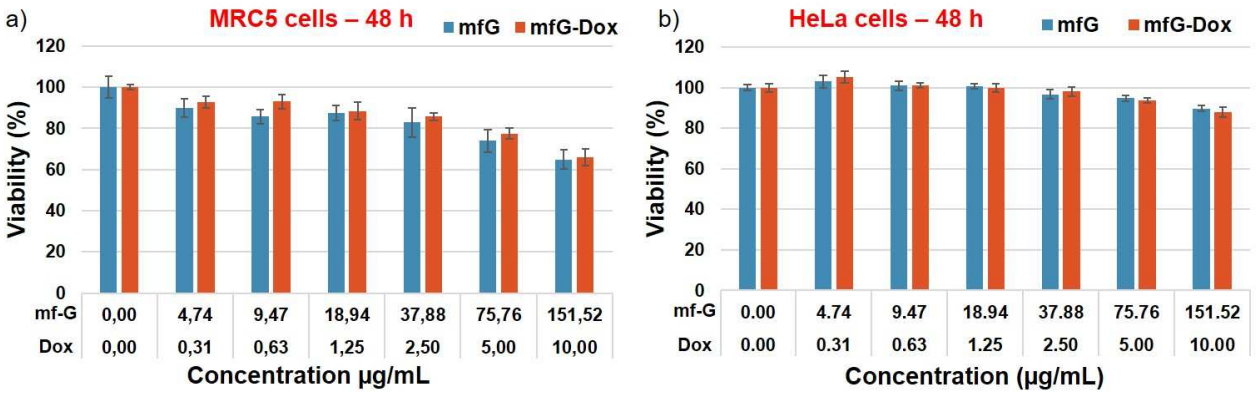

Figure 4.6: Cells viability of MRC5 cells (fibroblast) and HeLa cells (cancer cells) in presence of mfG-Dox and mfG. Data are presented as mean ± s.d. (n = 3).

The unexpected high cell viability obtained with mfG-Dox could be due by two main factors: 1) Aggregations of the sheets in solution. Despite the presence of PEG, graphene was not showing good water dispersibility, leading to fast aggregation in cell culture media. The aggregations would hinder the cells uptake. Moreover, the sedimentation of graphene aggregates on the top of MRC5 cells could cause cells death, decreasing the viability as observed. 2) Low amount of doxorubicin on graphene. It is possible that the total amount of Dox or the total release of the drug is not sufficient to lead to an efficient anti-cancer activity. To solve the problem of water solubility we decide to employ bovine serum albumin (BSA) as surfactant. This protein is well-known to be a biocompatible surfactant, able to maintain graphene suspended in water.[9] To increase the quantity of Dox we decided then to follow a combined strategy, based on the use of doxorubicin covalently linked and also physically adsorbed onto graphene surface. Both approaches were applied in one step, sonicating mfG/PEG-FA/ICG/Dox in BSA solution (1 mg/mL) in the presence of Dox (ratio mfG/Dox 1:0.25 *w/w*). The final material resulted stable in water and in cell culture media for more than 24 h (mfG at conc. 1 mg/mL) and

the total quantity of Dox was evaluated to be 101 µg/mg. Thanks to the increase of the amount of Dox on graphene, it was possible to use a small amount of mfG to deliver the same relative amount of drug, decreasing the toxicity relative to the material observed for MRC5 cells.

We then evaluated the *in vitro* performance of the new complex mfG/PEG-FA/ICG/Dox. After 48 h treatment, Dox-conjugated mfG showed a dose-dependent cytotoxicity to HeLa cells, whereas BSA (vehicle control) and mfG (the free nanocarrier) did not induce any significant difference in viability (Figure 4.7a, b). After 48 h the viability resulted to be lower respect to the cells treated for only 24 h. Remarkable is the difference in the viability of the cells at the concentration of 25 µg/mL of mfG-Dox and mfG after 48 h. The mfG alone is not affecting the cell viability, while mfG-Dox is decreasing the viability to ~42%. Of note, mfG/PEG-FA/ICG/Dox showed greater toxicity to HeLa cells at all doses as compared to MRC5 normal fibroblasts (Figure 4.7c, d and Figure 4.8). Moreover, it is very interesting that the viability of MRC5 in presence of mfG or mfG-Dox have a difference of only 1-2%, confirming the selective drug release only in cancer cells and not in normal cells.

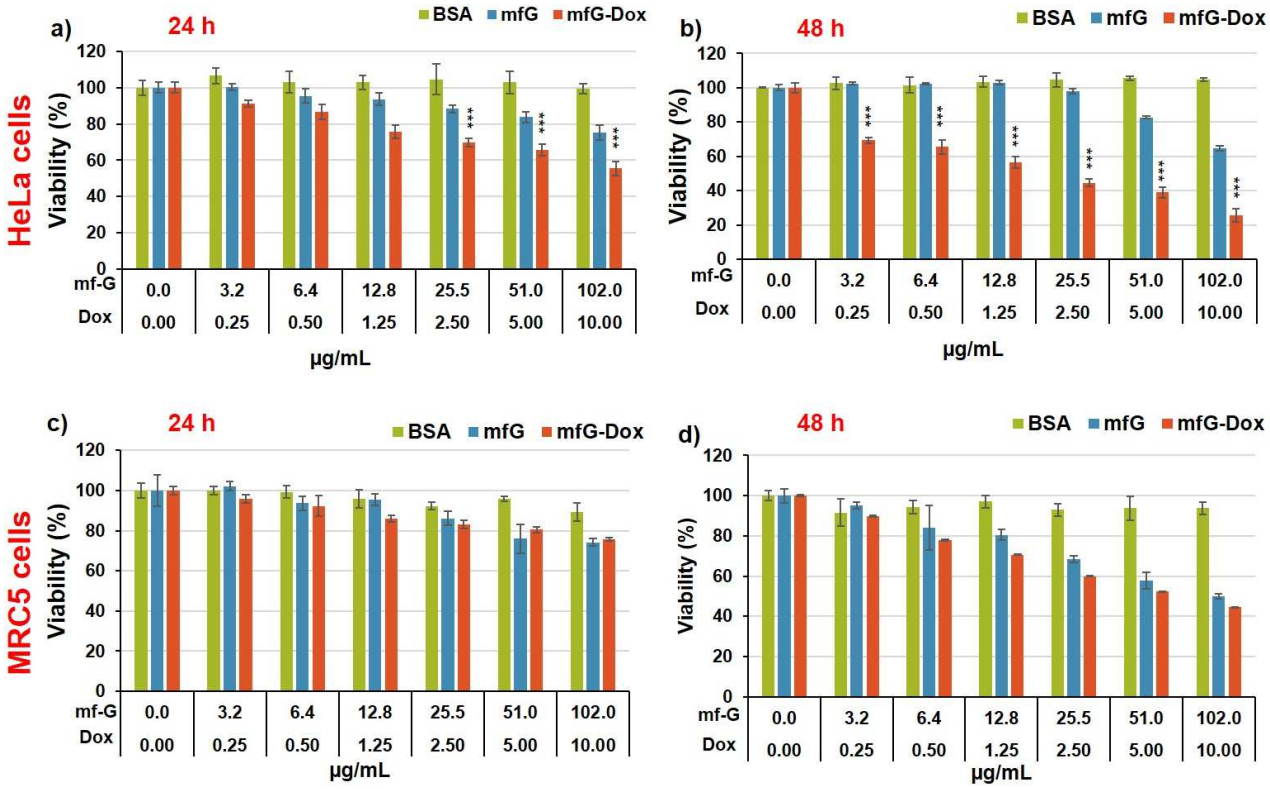

Figure 4.7: Cells viability of HeLa cells and MRC5 cells. First row: HeLa cells; second row: MRC5 cells. Data are presented as mean ± s.d. (n = 3), ***p < 0.001 (Student's t-test).

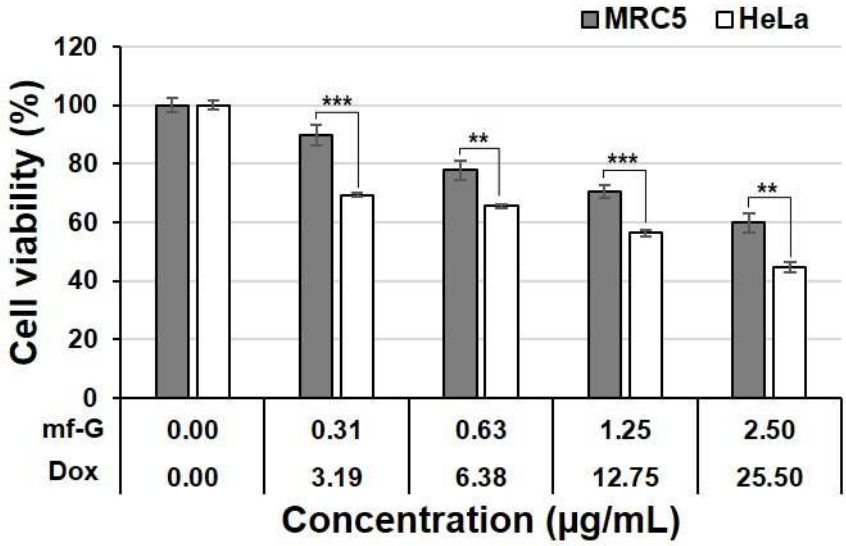

Figure 4.8: Comparison of the cells viability results after 48 h. Cell viability assay shows mfG/PEG-FA/ICG/Dox induced stronger cytotoxicity to cervix adenocarcinoma (HeLa) as compared to normal fibroblasts (MRC5). Cells were treated with nanoconjugates for 48 h. Data are expressed as means ± s.e.m. (n=4), **P* < 0.01 ****P* < 0.001(Student's t-test).

As folate receptor (FR) is overexpressed in cancer cells,[10] we hypothesized that such selective anticancer activity was mediated by folate receptor-directed targeting effect. To test this, we subjected HeLa cells under folate starvation and performed an antagonist experiment by pre-incubating these cells with or without an excess of folic acid (10 µM). As shown in Figure 4.9, the cancer-killing activity of mfG-Dox was retarded by pre-blocking folate receptor. This is likely because the excess folic acid blocked folate receptors and interfered with the internalization of mfG conjugates by cells. Taken together, these results demonstrate that Dox- and folic acid-functionalized mfG nanocomposite could be used as an effective nanocarrier for selective cancer-killing.

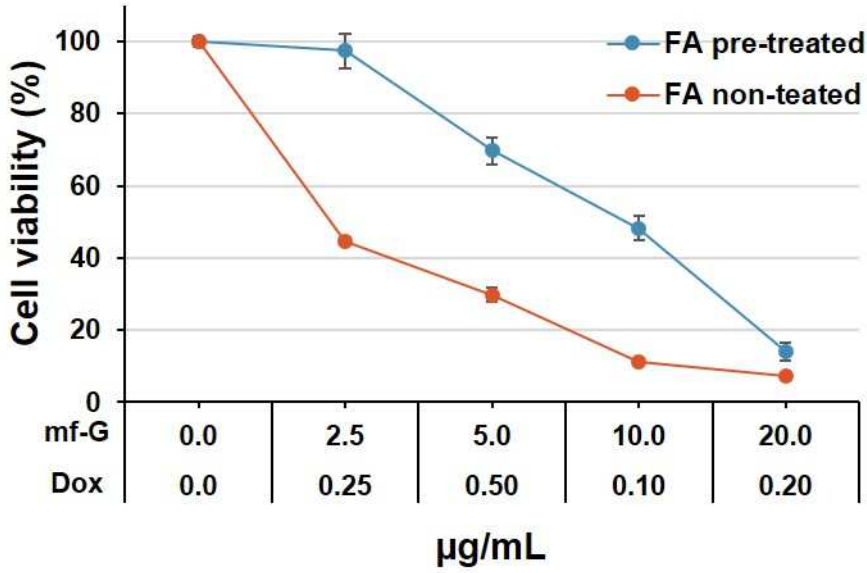

Figure 4.9: Viability of HeLa cells treated with mfG/PEG-FA/ICG/Dox for 48 h with/without pretreatment of free folic acid (FA; 10 µm). Data are expressed as means ± s.e.m. (n=4), ***P < 0.001(Student's t-test comparisons with the equivalent concentration of FA pretreated counterpart.)

To further explore the combination of the photothermal properties of graphene with the activity of doxorubicin, we investigated the anticancer effect of mfG/PEG-FA/ICG/Dox after NIR irradiation. Accordingly, HeLa cells incubated with BSA, ICG or ICG-conjugated mfG were irradiated using a 785 nm fiber-coupled continuous-wave NIR laser at 1 W (ca. 8 W/cm^2). The viability of cells was measured at 0 h or 24 h post irradiation. As shown in Figure 4.10, laser irradiation did not alter the viability of cells treated with BSA and ICG. Interestingly, although photoinduced mfG/PEG-FA/ICG/Dox show no effect on viability immediately after laser irradiation, a significant viability reduction was observed with additional 24 h of incubation (Figure 4.10). This is probably attributed to two possibilities: 1) heat induced by laser irradiation assists Dox release that exerts cell killing effect in the following 24 h; 2) impact on the regulation of cell signaling, including metabolism and inflammation, with cellular consequences after 24 h. This result is indicating that mfG/PEG-FA/ICG/Dox has potentials to be used for multimodal synergistic therapy (photo- and chemo-therapies) for efficient cancer eradication.

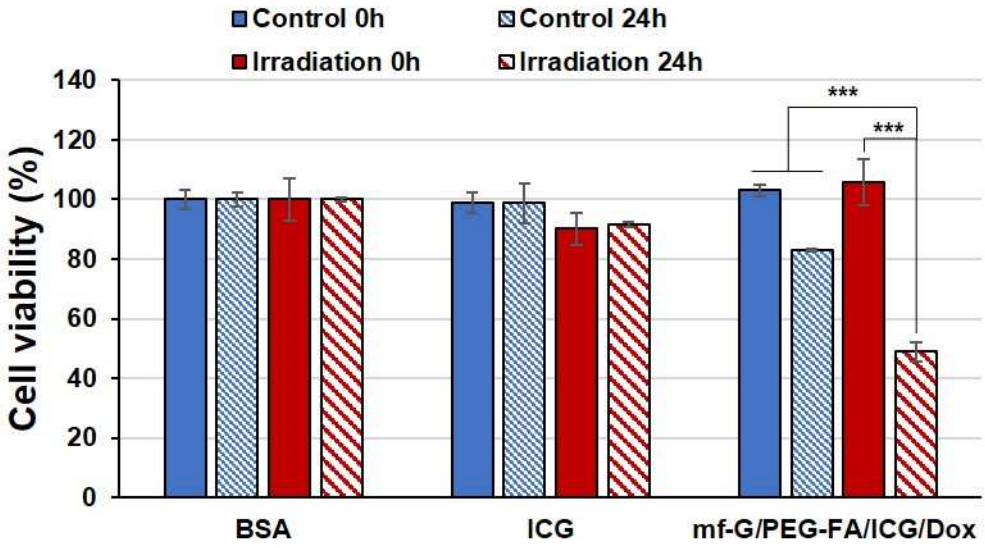

Figure 4.10: Cell viability of HeLa cells treated with BSA (20 µg/mL), ICG (0.9 µg/mL) and mfG/PEG-FA/ICG/Dox (20 µg/mL) with/without 785 nm laser irradiation for 10 min. The cell viability was tested at 0 and 24 h after irradiation. The concentrations of BSA and ICG were carefully adjusted to the equivalent amounts loading on the mfG nanoconjugates. Data are presented as mean ± s.d. (n = 3), ***p < 0.001 (Student's t-test).

In addition, *in vitro* cytotoxicity evaluation was performed to assess the biosafety of mfG nanosheets. The result revealed that mfG without any modifications did not affect cell viability up to the concentration of ca. 150 µg/mL, showing they are intrinsically nontoxic. *In vivo* biocompatibility was also examined by blood tests. The haematological and biochemical parameters did not differ between the mice intravenously injected with mfG nanosheets (2.5 mg/kg) and PBS, demonstrating the lack of acute inflammatory response and underscoring the biosafety of mfG.

Finally, to visualize the cellular uptake of mfG nanoconjugates, HeLa cells were incubated with mfG/PEG-FA/ICG for 4 h and were subjected to live-cell imaging after washing with PBS. In line with fluorescence spectra results, the fluorescence of mfG/PEG-FA/ICG was clearly observed using 800 nm filter setup (Figure 4.11a), confirming the successful incorporation of ICG fluorophore onto mfG. Image merged with DIC revealed that mfG nanoconjugates were mostly accumulated in the perinuclear area in the cytoplasm, although ICG moieties were partly quenched, as shown by the presence of the black aggregates (Figure 4.11b).

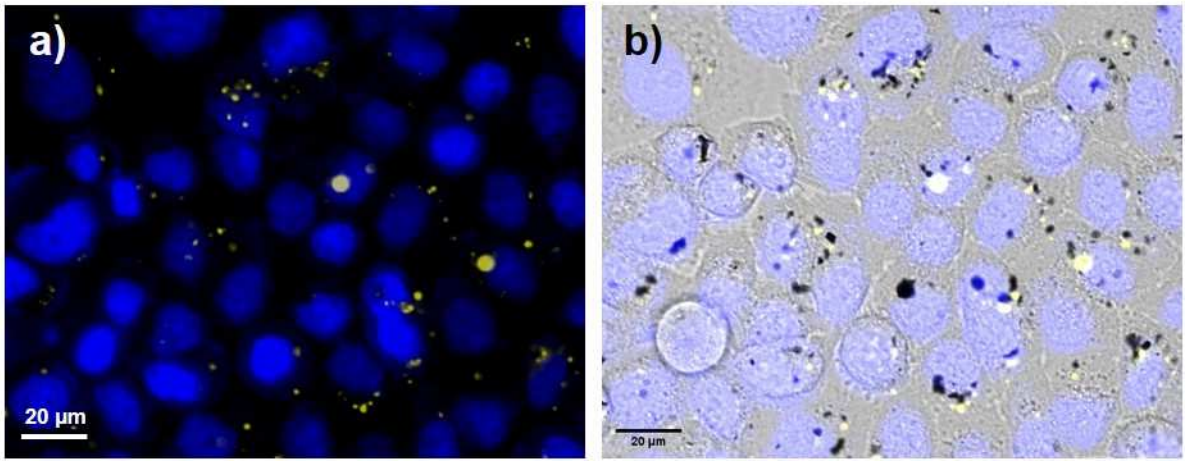

Figure 4.11: a) Fluorescence imaging of HeLa cells incubated with mfG/PEG-FA/ICG (10 µg/mL; yellow) for 4 h. Nucleus was stained with Hoechst (blue); b) Images merged with DIC.

4.4. Conclusion

After a well-designed step-by-step synthetic strategy of amine deprotection and functionalization, I obtained a new multifunctional drug delivery carrier, mfG/PEG-FA/ICG/Dox. This platform presents three functionalities useful to improve the properties of graphene as drug delivery carrier. I performed *in vitro* studies to explore the use of this platform for anti-cancer therapy. mfG/PEG-FA/ICG/Dox showed good specific targeting activity for HeLa cells and great anti-cancer activity, and of high importance, the material itself without the drug showed very low cytotoxicity and not *in vivo* toxicity. The functionalization of graphene with a fluorophore allowed the *in vitro* localization, promising for *in vivo* tracking of the platform. We also demonstrated that the combination of the photothermal properties of graphene and the anti-cancer activity of the drug is increasing the effectiveness of the therapy, leading to a faster and enhanced cell-killing effect.

4.5. Materials and methods

Transmission electron microscopy (TEM)

TEM images were collected with a Hitachi 7500 transmission electron microscope (TEM) (Hitachi High Technologies Corporation, Tokyo, Japan) equipped with an AMT Hamamatsu digital camera (Hamamatsu Photonics, Hamamatsu City, Japan)

Fluorescence measurement of mfG/ICG

Fluorescence measurement of mfG/ICG conjugate was performed on 0.1 mg/mL dispersion in DMF with a Jasco FP8003 fluorimeter using a swig xenon 450 W lamp and were corrected for the baseline and the solvent. Ex: 750 nm, Em: 780-900 nm.

UV-Vis spectroscopy

UV-Vis absorption spectra were recorded on a Cary 5000 UV-Vis-NIR spectrophotometer and were corrected for the baseline and the solvent.

Cell Culture.

Cervical carcinoma cells (HeLa) and normal human fibroblasts (MRC5) were procured from the Japanese Collection of Research Bioresources, Cell Bank, National Institute of Biomedical Innovation (Tokyo, Japan) and DS Pharma Biomedical Co. Ltd (Tokyo, Japan), respectively. Cells were cultured in Dulbecco's Modified Eagle's Medium (Gibco, Grand Island, NY, USA) containing 10% fetal bovine serum, 2 mM l-glutamine, 1 mM sodium pyruvate, gentamycin, penicillin-streptomycin (100 IU/ml[1]), and Hank's balanced salt solution (Life Technologies, Carlsbad, CA, USA). Cells were kept in a folate-free medium for at least 3 days before and during all treatments.

Cell viability assay.

Cell viability was assessed with Cell Counting Kit (CCK)-8 (Dojindo Laboratories, Kumamoto, Japan) following the manufacturer's instructions. Briefly, HeLa cells were seeded in a 96-well plate at a density of 5×10^3 cells/well and allowed to adhere to the substratum overnight. They were then exposed to mfG nanoconjugates as indicated. After washing with fresh medium, cells were incubated with CCK-8 solution for 3 h at 37°C. Absorbance at 450/690 nm was read on a microplate reader (Infinite M200 PRO; Tecan, Männedorf, Switzerland).

Fluorescence microscopy imaging.

HeLa cells were seeded in imaging dishes and allowed to adhere overnight. The attached cells were treated with mf-G/PEG-FA/ICG/Dox for 4 h at 37 °C, followed by nuclear staining with Hoechst 33342 (1 µg/ml; Thermo Fisher Scientific, Waltham, MA, USA) for 10 min. After washing with PBS, the cells maintained in RPMI 1640 phenol red-free medium (Thermo Fisher Scientific) result in live-cell imaging (Axiovert 200 M; Carl Zeiss, Tokyo, Japan).

Laser-induced cytotoxicity.

To assess cell viability after laser irradiation, HeLa cells were pre-seeded in 96-well plates (5×10^3 cells/well) and were incubated with culture medium containing samples as indicated. After 4 h incubation, cells were taken out from incubator to return to room temperature, followed by 10 min irradiation with a fiber-coupled continuous-wave laser at 785 nm at maximum power (1 W, ~8 W/cm^2). Viability was determined using the CCK-8 kit at 0 h- or 24 h-post-irradiation.

Blood tests.

Haematological and biochemical parameters in blood were measured by Japan SLC and Oriental Yeast Co. (Tokyo, Japan). Briefly, 10-week-old female BALB/cSlc mice (n = 5; average weight = 21 g; Japan SLC) were injected with 100 µL of mf-G dispersed BSA solution (2.5 mg/kg) or 100 µL of PBS buffer via the tail vein. Blood samples were collected from the inferior vena cava of the mouse after 1 and 7 days.

Statistical analysis

Results are presented as mean ± standard deviation of at least three independent experiments. The numbers of samples per group in each experiment are indicated in the corresponding figure legends as "n". Differences between groups were evaluated with the Student's t-test for two groups. *, ** and *** denote the p-values less than 0.05, 0.01 and 0.001, respectively.

Synthesis of model compound N-benzyl-N-(prop-2-yn-1-yl) prop-2-yn-1-amine (ML146)

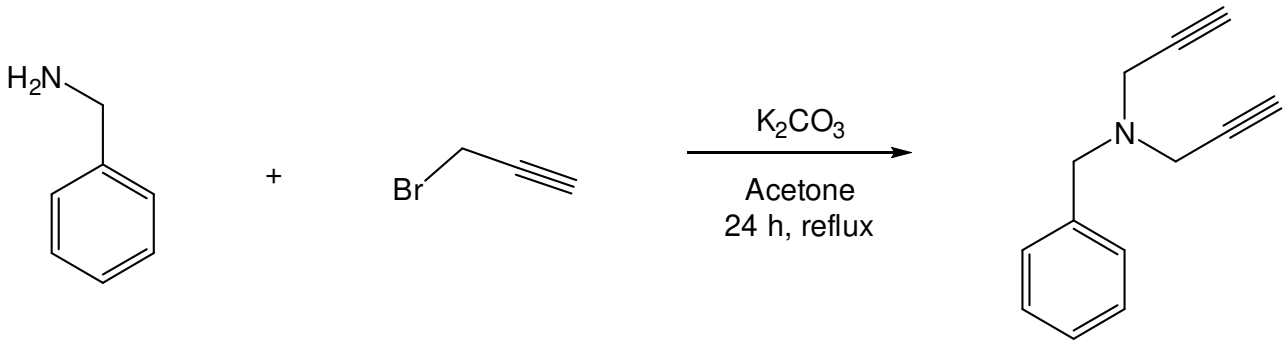

Benzylamine (1 eq., 0.5 g) was dissolved in acetone (40 mL), K_2CO_3 (1.2 eq., 0.77 g) was added and the mixture stirred for 15 min at room temperature. Propargyl bromide (4 eq., 2.2 g) dissolved in acetone (10 mL) was added, the flask equipped with a cooling system and the reaction stirred at reflux for 24 h. The evolving of the reaction was controlled by TLC (EtOAc/Cyclohexane 1:1). After the complete consumption of benzylamine, the reaction mixture was cooled to r.t. and acetone removed by rotavapor. The solid was dissolved in DCM (100 mL) and washed with H_2O (2x30 mL). The organic solvent, after drying with Na_2SO_4 and filtration was removed *in vacuo* to give a yellow/brown oil. The crude mixture was purified by flash chromatography column (cyclohexane/acetone from 90:10 to 75:25) giving a pale-yellow oil as final pure compound.

^{1}H NMR (400 MHz, $CDCl_3$) δ= 7.40 – 7.19 (m, 1H), 3.64 (s, 0H), 3.36 (d, *J*= 2.5 Hz, 1H), 2.21 (t, *J*= 2.5 Hz, 0H).

Synthesis of model compound N-benzyl-3-(2,5-dioxo-2,5-dihydro-1H-pyrrol-1-yl) propanamide (ML150)

a) Synthesis of precursor N-Succinimidyl 3-maleimidopropionate (ML149)

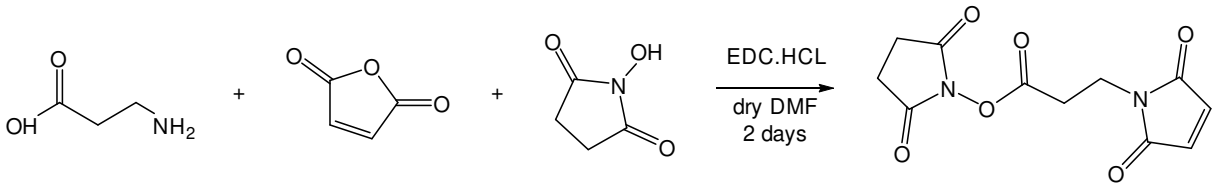

In a 250 mL round flask bottom, *beta*-alanine (1 eq., 1 g) and maleic acid (1 eq., 1.12 g) were dissolved in dry DMF (200 mL) and stirred for 2 hours. After this time, NHS (1.2 eq., 1.6 g) and EDC·HCl (2 eq., 4.64 g) were added and stirred for 2 days at room temperature. The mixture colour change from transparent to brown during the reaction time. The organic solvent was then evaporated in vacuo and the solid residue dissolved in DCM (100 mL) and washed with water (2x50 mL). Flash chromatography column was performed to purify the compound (DCM/Acetone 9:1).

^{1}H NMR (300 MHz, $CDCl_3$) δ= 6.71 (s, 2H), 3.91 (t, *J*= 7.0 Hz, 2H), 3.00 (t, *J*= 7.0 Hz, 2H), 2.80 (s, 4H)

b) Synthesis of ML150

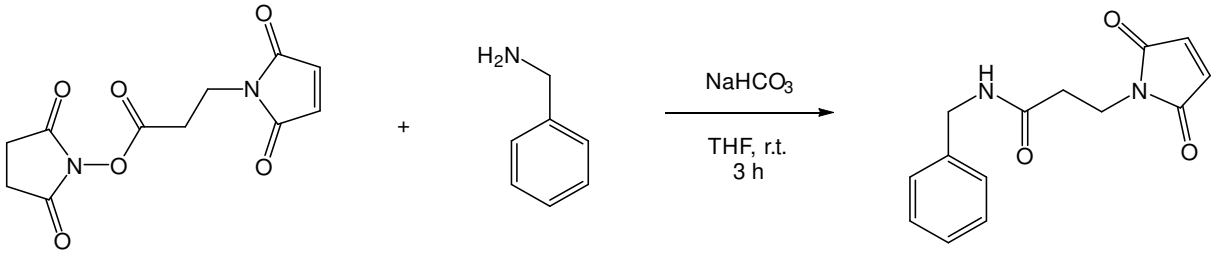

Benzylamine (1eq., 200 mg) was dissolved in THF (10 mL). $NaHCO_3$ (1 eq., 60 mg) was added and the mixture stirred at r.t. for 20 min. ML149 (1 eq., 80 mg) was added and the mixture stirred at r.t. for 3 h. The reaction was followed by TLC (DCM/Acetone 9:1) until complete consumption of the reagents. The organic solvent was then removed *in vacuo*. The crude mixture was dissolved in DCM (50mL) and washed with water (50 mL x 3), dried with Na_2SO_4 anhydrous, filtered and the solvent evaporated in vacuum, to get the final pure compound as a white powder.

^{1}H NMR (400 MHz, $CDCl_3$) δ= 7.25 (m, 5), 6.60 (s, 2H), 4.34 (d, *J*= 5.6 Hz, 2H), 3.80 (t, *J*= 7.2 Hz, 2H), 2.49 (t, *J*= 7.2 Hz, 2H).

Synthesis of mf-G/PEG-FA/ICG/Dox

a) ***Pht deprotection[2] (1) - mf-G$_1$***

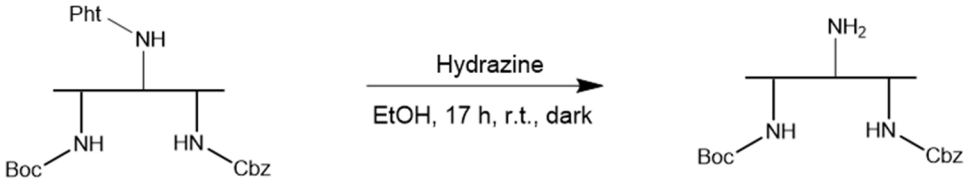

mf-G **mf-G$_1$**

mf-G (50 mg) was suspended (concentration 1 mg/mL) in a solution of hydrazine hydrate in ethanol (1:25 *v/v)*. The mixture was sonicated for 5 min in a bath sonicator to disperse the graphene and stirred for 17 h at r.t. in the dark. After this time, the dispersion was filtered and washed with 20 mL of dichloromethane (DCM), EtOH and water. The resulting solid was dried under vacuum. Kaiser test was performed on dispersion of the obtained powder to evaluate the amount of free amines, compared to mf-G protected (46 µmol/g of primary amines).
Kaiser test of mf-G_1 (Pht deprotected): ~65 µmol/g

b) ***Synthesis of mf-G-alkyne (2) – mf-G$_2$***

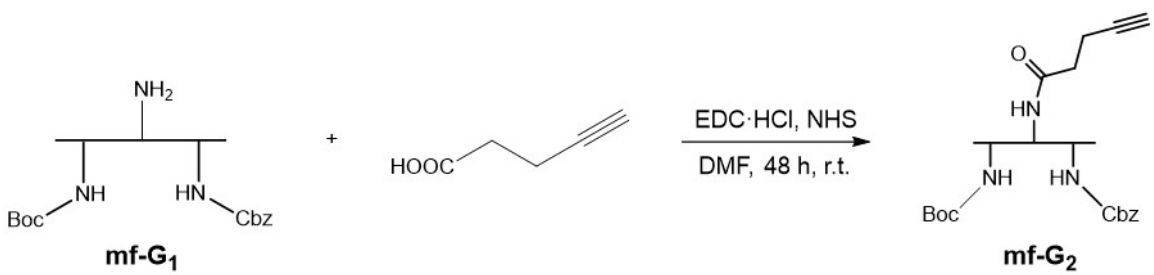

mf-G$_1$ **mf-G$_2$**

4-pentynoic acid was dissolved in anhydrous DMF (3mL), DIEA (30 µL, 1.5 eq) and EDC (1.7 eq) were added and the mixture stirred for 1 h at 4°C in Ar atmosphere. NHS was added and the mixture kept under stirring for 1 h at 4 °C. mf-G-Pht deprotected (49 mg, 1 eq.) was dispersed by bath sonication in anhydrous DMF (10 mL) in presence of DIEA (40 µL). The dispersion was added to the activated acid solution and stirred at 4°C for 2 days. After this time, the dispersion was filtered over Millipore filters and washed with DMF, EtOH and DCM (30 mL x 2). The filter was dried *in vacuo* and graphene recovered from the filter.
Kaiser test of mf-G_2: ~14 µmol/g. ~65 % yield

c) ***Boc deprotection (3), (5)***

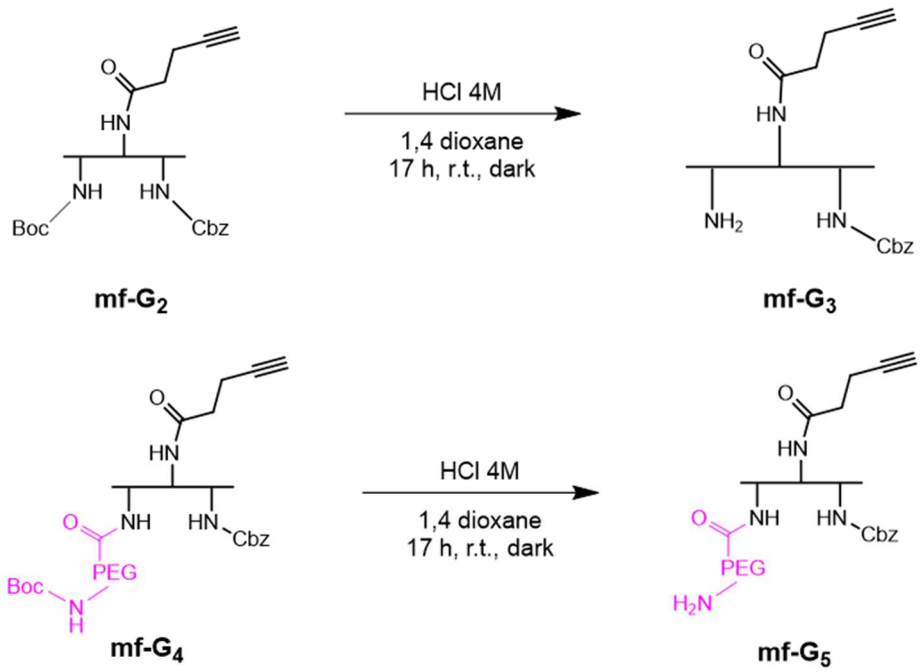

mf-G was suspended (concentration 1 mg/mL) in a solution of HCl 4 M in 1,4-dioxane (purchased Sigma Aldrich). The suspension was sonicated for 5 min in bath sonicator and stirred for 17 h at r.t. in the dark. After this time, the dispersion was filtered and washed with 20 mL of dichloromethane (DCM), EtOH and water. The resulting solid was dried under vacuum. Kaiser test was performed on dispersion of the obtained powder to evaluate the amount of free amines, compared to mf-G protected (76 µmol/g of primary amines).
Kaiser test mf-G_3: ~33 µmol/g
Kaiser test mf-G_5 (mf-G/PEG-NH_2): ~30 µmol/g

d) ***Synthesis of mf-G/PEG-Boc (4) – mf-G_4***

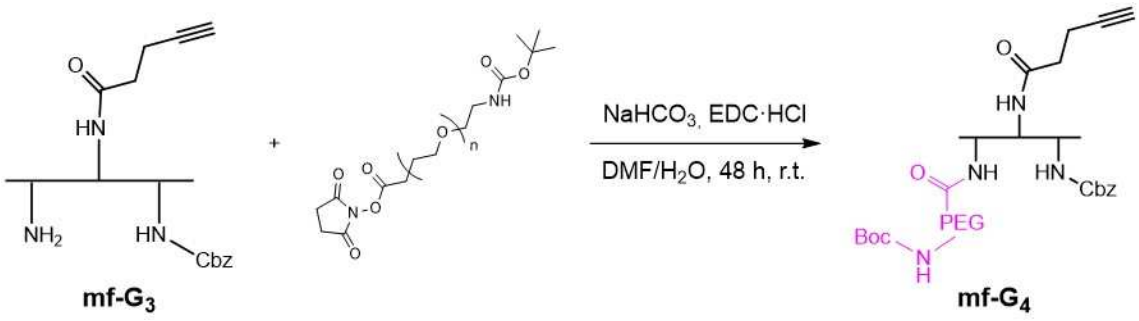

mf-G_3 (Boc deprotected) (47 mg) was dispersed in DMF/H_2O 8:2 (mixture (40 mL), $NaHCO_3$ (20 mg) was added and the mixture stirred for 10 minutes. After that, Boc-PEG-NHS (3000 Da) salt dissolved in DMF and EDC·HCl (20 mg, 4 eq. respect NHS-PEG-Boc) were added and the mixture stirred at r.t. for 2 days in the dark. After the reaction time, the dispersion was filtered over Millipore filters and washed with DMF, EtOH and DCM (30 mL x 2). The filter was dried *in vacuo* and graphene recovered from the filter.
Kaiser test mf-G_4: ~0 µmol/g. ~100% yield.

e) ***Synthesis of NHS-FA salt***

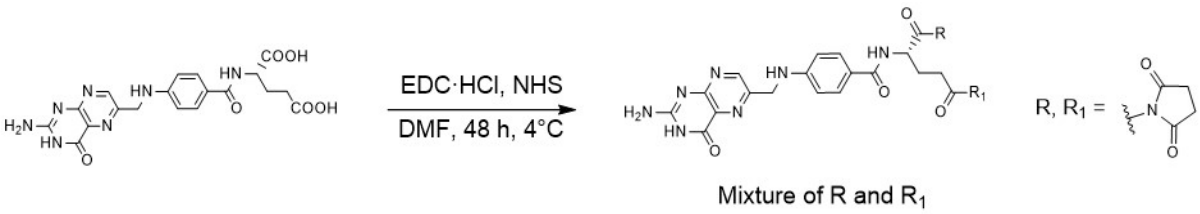

Folic acid (102 mg, 1 eq.) was dissolved in DMF/DMSO 4:1 (3 mL) and the solution stirred at 4 °C for 15 h (a yellow gel is forming). Under vigorous stirring at 4 °C, TEA (1 eq.), EDC·HCl (1.5 eq.) and NHS (1.3 eq.) were added and the mixture stirred over the night. After this time, FA-NHS was precipitated under strong stirring through the addition of DCM (6 mL) to the mixture. The yellow solid was filtered, washed with DCM and dried. The yellow powder obtained (100 mg) was used for further reaction without other purification and characterization.

f) ***Synthesis of mf-G/PEG-FA (6) – mf-G_6***

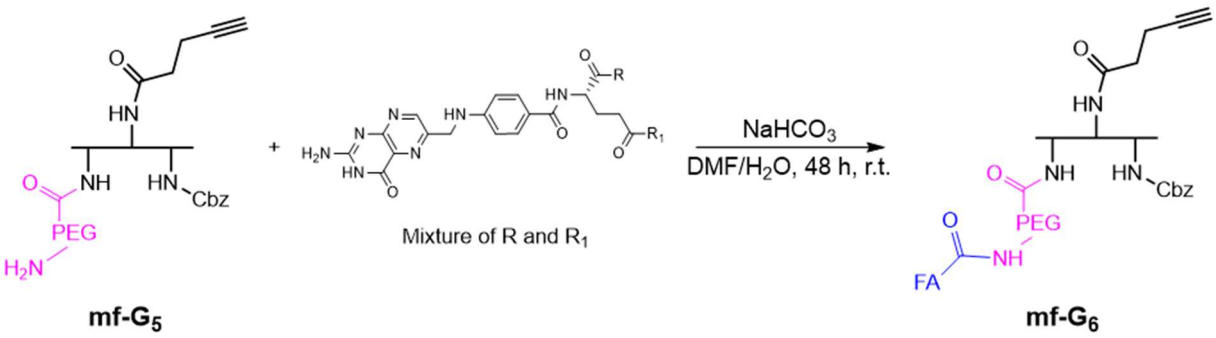

mf-G_4 (46 mg) was dispersed in DMF/H_2O 8:2 (40 mL), $NaHCO_3$ (20 mg) added and the mixture stirred for 20 minutes. FA-NHS salt (40 mg) was added at r.t. and the reaction stirred for 1 day. After this time FA-NHS (40 mg) was added again and the mixture stirred for 1 day at r.t. After the reaction time the dispersion was filtered over Millipore filters and washed with DMF, EtOH and DCM (30 mL x 2). The filter was dried *in vacuo* and graphene recovered from the filter.
Kaiser test mf-G_6: ~0 µmol/g. ~100% yield.

g) ***Cbz deprotection (7)***

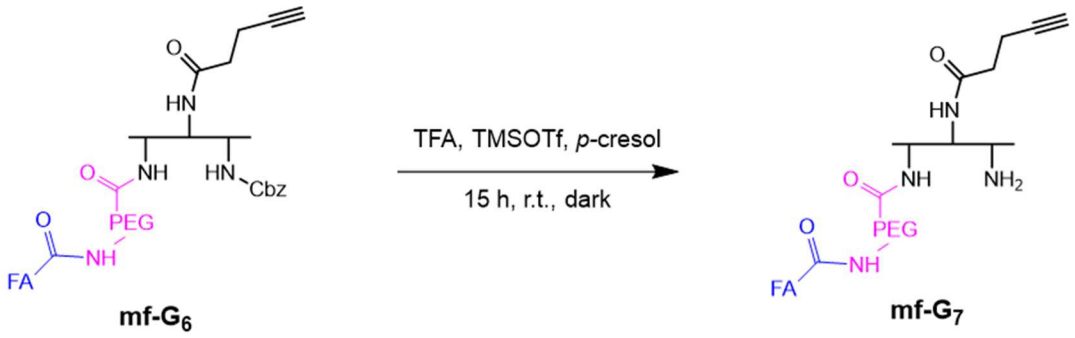

A solution of trifluoroacetic acid (TFA), TMSOTf and *p*-cresol (ratio 3.8:1 *v/v* and 10 mg *p*-cresol) was prepared. mf-G_6 (45 mg) was dispersed in the solution and sonicated for 5 min in bath sonicator and stirred for 15 h at r.t. in the dark. After this time the dispersion was filtered and washed with 20 mL of dichloromethane (DCM), EtOH and water. The resulting solid was dried under vacuum. To evaluate the amount of amines deprotected from Cbz protecting group, the deprotection was performed on the mf-G Boc deprotected. The amount of Cbz deprotected amines was evaluated subtracting the amount of Boc deprotected amines from the values obtained through the Kaiser test on the contemporary Boc and Cbz deprotected graphene (118 µmol/g of primary amines total, 46 µmol/g of Cbz protected amines).
Kaiser test mf-G_7: ~30 µmol/g

h) ***Synthesis of mf-G/PEG-FA/ICG (8) – mf-G8***

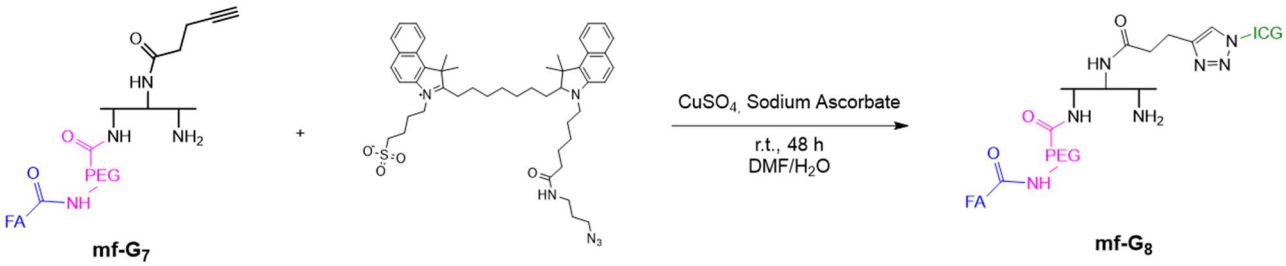

mf-G_7 (40 mg) was dispersed in DMF/H_2O 6:2 mL (5 mL). $CuSO_4$ (0.05 eq.) was dissolved in water with sodium ascorbate (0.08 eq.), stirred for 15 minutes at r.t. until the color of the solution pass from blue to orange and then added to the graphene mixture. After 10 minutes, ICG-N_3 salt (6 mg, 1 eq.) in DMF (3 mL) was added to the dispersion and the mixture stirred at r.t. for 48 hours in the dark. After 2 days the mixture reaction was filtered, washed with DMF, EtOH and DCM (20 mL x 2) and the filter dried *in vacuo*.
The presence of ICG residue was analyzed into the DMF washing solutions by fluorescence spectroscopy, showing the absence of ICG residue after the second washing.
Control reaction: The reaction control was carried out in parallel to the above-described reaction on mf-G_7 (5 mg) in the absence of $CuSO_4$ and sodium ascorbate.
Fluorescence spectra were collected on 0.1 mg/mL mfG dispersion in DMF.
Ex: 750 nm. Em: 780-900 nm.

i) ***Synthesis of mf-G/PEG-FA/ICG/Dox (9) – mfG/PEG-FA/ICG/Dox (mf-G9)***

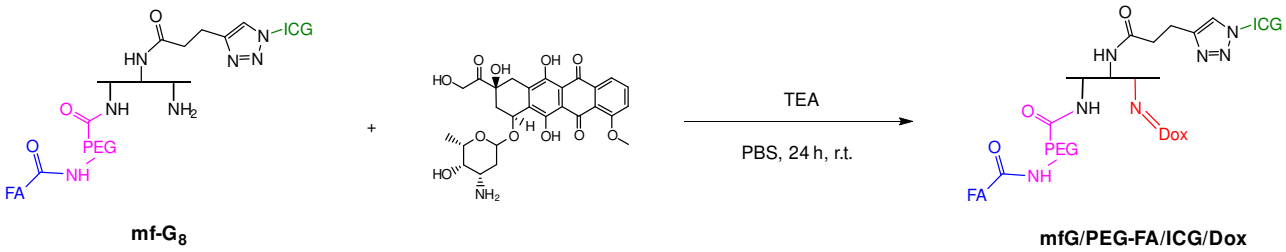

mf-G_8 **mfG/PEG-FA/ICG/Dox**

20 mg of mf-G_8 was dispersed by bath sonication (30 minutes) in PBS solution (35 mL) in presence on 243 µL of triethylamine and stirred at room temperature for 30 minutes. Doxorubicin (1 mg, 0.05 *w/w* ratio G/Dox) was dissolved in 5 mL PBS solution was added to graphene dispersion and the mixture stirred for 24 h at room temperature in the dark. After 24 h the mixture was centrifuged, the solution recovered to analyzes the quantity of Dox unreacted (by UV-Vis spectroscopy). mfG/PEG-FA/ICG/Dox was dispersed and centrifuged twice in 5 mL PBS solution to remove the adsorbed Dox and the washing solution analyzed by UV-Vis spectroscopy to evaluate the total amount of unreacted Dox.

j) ***Dispersion of mf-G/PEG-FA/ICG/Dox in BSA solution and Dox absorption.***

mf-G/PEG-FA/ICG/Dox was dispersed in BSA solution in water (1 mg/mL BSA, 0.5 mg/mL mfG) containing doxorubicin (mfG/Dox ratio 0.25 *w/w*). The mixture was sonicated for 30 minutes and stirred at 4 °C for 24 h. After this time the supernatant was collected and mfG dispersed and centrifuged twice in the same amount of BSA solution. The collected solutions were analyzed by UV-Vis spectroscopy to quantify the quantity of doxorubicin adsorbed on graphene.

4.6. Literature

1. Liu, Z., Robinson, J. T., Sun, X. & Dai, H. PEGylated nanographene oxide for delivery of water-insoluble cancer drugs. *J. Am. Chem. Soc.* **130**, 10876–10877 (2008).

2. Jiang, W. *et al.* Tumor targeting dual stimuli responsive controllable release nanoplatform based on DNA-conjugated reduced graphene oxide for chemo-photothermal synergetic cancer therapy. *J. Mater. Chem. B* **6**, 4360–4367 (2018).

3. Jasim, D. A., Ménard-Moyon, C., Bégin, D., Bianco, A. & Kostarelos, K. Tissue distribution and urinary excretion of intravenously administered chemically functionalized graphene oxide sheets. *Chem. Sci.* **6**, 3952–3964 (2015).

4. Li, Y. *et al.* Graphene microsheets enter cells through spontaneous membrane penetration at edge asperities and corner sites. *Proc. Natl. Acad. Sci. U. S. A.* **110**, 12295–12300 (2013).

5. Li, B. *et al.* Influence of polyethylene glycol coating on biodistribution and toxicity of nanoscale graphene oxide in mice after intravenous injection. *Int. J. Nanomedicine* **9**, 4697–4707 (2014).

6. Ménard-Moyon, C. *et al.* Controlled Chemical Derivatisation of Carbon Nanotubes with Imaging, Targeting, and Therapeutic Capabilities. *Chem. - A Eur. J.* **21**, 14886–14892 (2015).

7. Shim, G., Kim, M. G., Park, J. Y. & Oh, Y. K. Graphene-based nanosheets for delivery of chemotherapeutics and biological drugs. *Adv. Drug Deliv. Rev.* **105**, 205–227 (2016).

8. Xu, S., Luo, Y. & Haag, R. Water-soluble pH-responsive dendritic core-shell nanocarriers for polar dyes based on poly(ethylene imine). *Macromol. Biosci.* **7**, 968–974 (2007).

9. Paredes, J. I. & Villar-Rodil, S. Biomolecule-assisted exfoliation and dispersion of graphene and other two-dimensional materials: A review of recent progress and applications. *Nanoscale* **8**, 15389–15413 (2016).

10. Ledermann, J. A., Canevari, S. & Thigpen, T. Targeting the folate receptor: Diagnostic and therapeutic approaches to personalize cancer treatments. *Ann. Oncol.* **26**, 2034–2043 (2015).

CHAPTER 5. CONCLUSION AND PERSPECTIVES

5.1. **Conclusion**

In this work, the production of graphene and boron nitride to investigate their biocompatibility and the multifunctionalization of graphene for the development of a drug delivery platform have been pursued.

With this purpose, I investigated the production of graphene in water employing biocompatible surfactants as exfoliating agents. I explored the direct exfoliation in water through bath sonication, to avoid contaminations from organic solvents adsorbed on graphene surface. Few-layer graphene was obtained using riboflavin-5'-phosphate sodium salt (G-Rib), characterized by a high stability in water and cell culture media at concentration up to 2 mg/mL. The *in vitro* and *in* vivo toxicity of G-Rib was investigated, showing very low cytotoxicity in HeLa cells and RAW macrophages at high doses of FLG (300 µg/mL). Similarly, G-Rib showed 100% of survival and no sign of toxicity after a single intravenous injection in mice (100 and 300 µg/mouse), confirming its low toxicity and the possible biomedical applications of this material. In addition, applying ultra-centrifugation techniques for sheet size-selection, I obtained dispersions of G-Rib with different lateral size distribution. The so-prepared dispersions are currently under study in mice for the assessment of the impact of graphene with different sizes in lungs after inhalation. Stable dispersions of FLG were also obtained employing Rhodamine b base (G-R_{bb}) and a bodipy derivative (G-GIG100). These dispersions are characterized by surprising fluorescence properties, contrary to previous studies performed until now on graphene materials. Moreover, the direct observation of the fluorescent sheets was performed through confocal microscope, opening the doors to a wide range of applications of this material, from live tracking inside cells to fluorescent composites. Analogously to graphene, the production of hexagonal boron nitride in water was investigated. The combination of two different exfoliation techniques, dry ball milling followed by bath sonication in water in the presence of sodium cholate as surfactant allowed to obtain hBN sheets. The use of different sources of bulk BN led to the production of hBN dispersions with different shape and size, yielding round (r-hBN) and sharp (c-hBN, with graphene-like morphology) hBN. The materials were investigated for their cytotoxicity in H460 lungs epithelial cells, showing lower cytotoxicity in the case of r-hBN respect to s-hBN.

The development of a multifunctional platform for drug delivery applications started with the study of the functionalization of FLG. 1,3-Dipolar cycloaddition and diazonium compound reactions were tested. My research was focused on the bulk functionalization of graphene, to obtain high quantity of material for further advancement in the biomedical applications. With this aim, I compared the yield and quality of the materials obtained after reaction of FLG or graphene intercalated compound (GICs, KC_8 species) with diazonium compounds. As expected, I confirmed the high reactivity of KC_8 respect to FLG, obtaining high degree of functionalization, with sheets presenting great homogeneity on the functionalized surface. The use of three diazonium compounds, characterized by the presence of an amino group functionalized with three quasi-orthogonal protecting groups, led to the generation of a multifunctional graphene (mfG), suitable for specific strategy of subsequent derivatization. The characterization of the conjugate was performed employing different analytic techniques, to confirm the presence of the protected amines grafted onto graphene.

This mf-G is the first generation of a multifunctional material, in which I based the functionalization strategy to obtain the second generation of mf-G, constituted of various functionalities suitable for the development of an anticancer material. Following a specific step-by-step deprotection and functionalization strategy, I performed the synthesis of mf-G/PEG-FA/ICG/Dox (mfG-Dox). This material, characterized by the presence

of folic acid (FA) as targeting agent for cancer cells, indocyanine green (ICG) as fluorophore for the localization of mf-G in cells, and doxorubicin (Dox) as anti-cancer drug, was investigated for its drug delivery properties. The *in vitro* studies performed on HeLa cells showed great targeting activity of the mf-G platform, with good selectivity and cytotoxicity for cancer cells. The platform itself, without Dox present very low cytotoxicity for the cells, confirming the potential as drug delivery carrier. The combination of photothermal properties and drug release was explored, showing an important improvement of the therapy in terms of time and cytotoxicity, confirming the promising biomedical application of graphene-based material.

5.2. **Perspectives**

After the promising results showing the low cytotoxicity of hBN sheets, the *in vivo* investigation of its effect is desirable, to understand the potential of this material for biomedical applications.

Regarding the FLG exfoliated with fluorescent molecules, theoretical and experimental investigation on the interactions between the material and the surfactant are necessary to understand the observed phenomena and exploit this new possible field of applications of graphene. The characterization of the direct functionalization of KC_8 with alkyne derivatives would be important to understand the fate of the functional group introduced and develop new strategy for one-pot multifunctionalization of graphene with different functionalities. This could open the doors for easily scalable production of multifunctional graphene and to many different commercial applications of this material.

Regarding the obtaining of a flexible second generation of multifunctional graphene, the promising studies performed on the drug delivery properties of mfG-Dox suggest future direction in this research field. The wide opportunities of functionalization given by the flexibility of the proposed platform are desirable for the advancement of graphene biological research. The possibility of the use of one platform as base for the development of different therapies is a great ambition and could promote further the graphene biomedical applications. Moreover, *in vivo* studies on the anti-cancer properties of mfG-Dox are desirable to assess the real potential of this platform. For this purpose, the increase of the amount of fluorophore linked is also needed, to intensify the fluorescence of the platform and allow a better tracking into the organism.

LIST OF PUBLICATIONS AND COMMUNICATIONS

Publications

Lucherelli, M. A.; Raya, J.; Edelthalhammer, K. F.; Hauke, F.; Hirsch, A.; Abellán, G.; Bianco, A. A Straightforward Approach to Multifunctional Graphene. *Chem. – A Eur. J.* **2019**, chem.201903165.

Communications

Multifunctional graphene for drug delivery application, M. A. Lucherelli, J. Raya, G. Abellan, A. Bianco, 47th IUPAC chemistry conference, Paris, 7-12 July 2019. Oral Presentation

Multifunctionalization of graphene for drug delivery applications, M. A. Lucherelli, A. Bianco, "Journée des Doctorants de l'Ecole Doctorale des Sciences Chimiques", Strasbourg, 23 November 2018. Oral presentation

Exfoliation and functionalization of 2D materials, M.A. Lucherelli, A. Bianco, *Frontier Research in 2D Materials school*, Cargese, 2-14 April 2017. Poster

Exfoliation of graphene in organic solvents and water, M.A. Lucherelli, R. Kurapati, A. Bianco, Chem2Dmat, Strasbourg, 22-26 August 2016. Poster

Exfoliation and size selection of graphene, M.A. Lucherelli, R. Kurapati, A. Bianco, Sardinia Nano-biomed Workshop, Alghero, 24-27 June 2016. Poster